Hydrodynamic assessment of graptolite morphotypes

Lesley Rantell

Doctor of Philosophy
University of Edinburgh

2001

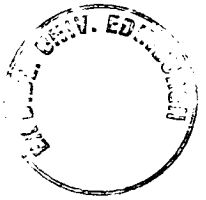

Preface and Declaration

Since October 1997 I have been engaged in a period of full time research (except for a three month suspended period) under the supervision of Dr. Sue Rigby, of the University of Edinburgh, and Dr. Barrie Rickards, of the University of Cambridge.

I declare that the work and results embodied in this thesis are my own except where otherwise stated or acknowledged. No part of this thesis has been submitted for any other degree or qualification at any other university.

Abstract

Physical and mathematical modelling techniques have been used to investigate the hydrodynamic significance of some aspects of the morphology of graptoloids. Functional structures are identified which could have had an impact on interpretations of graptolite taxonomy, oceanography and evolution.

Experiments, testing isolated specimens in seawater and scale models in oil, show that the nema, cauda and virgula had a profound effect on the orientation of scandent graptoloids. These structures acted as trailing stabilisers, enforcing a stable orientation on the rest of the colony. Isolated monograptids with hooked and simple thecae have their orientation controlled by the nema, and would have presented their rhabdosomes to water sicula aperture first. This orientation control function was particularly marked in experiments on immature specimens, probably because these early growth stages are preserved with full length nemas. Oil tank modelling highlighted the importance of mass distribution for colony orientation, and observations of flow patterns over detailed models in a wind tunnel indicated that the increased surface area provided by secondary structures (e.g. vanes) further enforced this function. Mathematical modelling of distal structures such as the nema suggested that they would have functioned as stabilisers for all scandent graptoloids if they were of sufficient length or surface area (i.e. were thickened or bore vanes). The rate at which they would have acted to stabilise the colony was a function of this length or width and the distribution of colony mass, with longer or wider structures responding faster to changes in current orientation. The graptolite fossil record contains numerous examples of specimens bearing long virgulae and vane structures.

Spines are a common feature of the proximal ends of biserial and uniserial scandent graptoloids. The virgella is evolutionarily conserved, while other processes have evolved more than once. Spines appear on the sicular aperture or on the first one or two thecae. These spines would have been the first element of the graptoloid colony to have encountered a mass of sea water. Their importance is implied by the

resource implications of their construction. Imaging of graptolite models in wind tunnels shows that these spines modified flow over the entire colony, and must have had a hydrodynamic role during life. Spines had two critical functions for the graptolite; firstly, they captured flow from a wide area and directed it to the surface of the rhabdosome, where it moved along this complex surface and into the apertures of the thecae. Food particles would have been entrained, by this process, from a wide cross-sectional area of water. Secondly, spines at the proximal end might have contributed to stabilising the rhabdosome, preventing separation of the flow over the sharp leading edges of the colony, contributing to the maintenance of orientation in changing regimes of flow. Mathematical modelling of the effects of proximal spines on the energy budget of a juvenile colony suggested a narrow range of spine angles for optimal feeding efficiency. Comparison with specimens of spinose species reveals two groups of spine arrays, one of which is consistent with the predictions of the mathematical model. The geological distribution of spinose scandent species throughout the Ordovician indicates that these forms were particularly dominant in the Caradoc. This was also a time of high productivity and food availability, which would have provided the necessary energy budget to experiment with these costly structures.

Physical experiments provide evidence for the life orientations of simple two-stipe dichograptids (dicellograptids, dicranograptids and didymograptids). These colonies would all have presented themselves to a prevailing current with the sicula aperture facing up-flow, this orientation may have changed with astogeny. The distribution of the colony weight is a controlling factor of this orientation. Twisted dicellograptids would have rotated as they sank.

The spines of scandent graptloids (nema, virgula, virgella anti-virgellar spines and thecal spines) were functional. These structures should be used with care for taxonomic analysis. Although spine origins vary many served a similar, universal, purpose (feeding efficiency and stability) and cannot easily be used to distinguish ocean environments.

Acknowledgements

I would like to thank above all Dr. Sue Rigby and Professor Barrie Rickards, my supervisors, for all their help, support, enthusiasm and good ideas over the past three years. I would also like to thank the late Dr. Jerry Rickards, whose initial observations of graptolite models provided the inspiration for a hydrodynamic study of fine scale graptolite morphology.

My wind tunnel experiments would not have been possible without technical support. I must thank Richard Eustace and Matt Crompton (Aerospace Engineering, University of Bristol) who ran the L.D.A. system. I also received invaluable assistance from the technicians of the Aerodynamics Laboratory (Engineering department, University of Cambridge), particularly Bunny, David and Ben, who were very patient even when I broke the machine.

Other valuable input has been provided by: Dr. David Loydell (University of Portsmouth), who sent me isolatable specimens; Dr. Michael Manga (University of Oregon), who checked the mathematics of my virgula model; Dr. Don Glass (Engineering department, University of Edinburgh), who provided viscosity data; and Dr. Harry Leach (University of Liverpool) and Profesor Tjeerd van Andel (University of Cambridge) for their suggestions of suitable ocean current velocities.

I would also like to thank my family for their support, especially my parents for proof reading my thesis over Christmas. My many friends in the department have provided invaluable encouragement, friendship and entertainment throughout my time here. I would particularly like to mention my office mates, Lisa Morfi, Nicola Cayzer, Julie Hollis and Amanda Voase, along with Conor Snowden and Guy Hall, who have listened to so many practise talks and discussed ideas, and who probably know my project almost as well as I do by now. A special thankyou to Emily Good who looked after me so well when I was ill or depressed.

1. Introduction

1.1. Introducing the graptoloids

Graptoloids were amongst the first macro-zooplankton to inhabit the oceans. These large, colonial, planktonic organisms, which ranged from the early Ordovician to the Devonian, are believed to have been hemichordates. This belief is based on similarities of colony construction, both in morphology and material (the protein collagen), with the extant hemichordates *Rhabdopleura* and *Cephalodiscus* (Dilly 1993).

The planktonic graptoloids evolved from benthic ancestors, the dendroids, early in the Ordovician, moving from the seabed to the open oceans. Coincident with this dramatic change in life-habit, graptolite morphology underwent rapid evolution. It is likely that many of these changes were adaptations to life in the open water and that they might have been driven by hydrodynamic considerations.

This PhD project investigates some of these morphologies, apparently evolved for an open water habitat, in order to determine whether the hydrodynamics of these structures could have been significant and beneficial to a graptolite colony.

Graptolites provide an unrivalled tool for precision dating and correlation of the Lower Palaeozoic (Ordovician and Silurian). Their prevalence is due to a number of key factors:

- Abundance and marine habitat – The combination of these two factors guarantees a good preservation potential. Marine deposits are preferentially preserved over terrestrial sediments due to the lower rates of erosion and weathering, and for this reason marine fossils tend to form the basis of dating systems. Due to their

abundance there is a good chance of finding graptolite fossils, although not necessarily with any diversity or abundance, in any marine sediment preserved from this period.

- Planktonic habit – Specimens of some species have been found in sediments from all continents (except Antarctica). Many species have similarly wide distributions allowing global correlation of individual rock units and dating systems.
- Rapid evolution – The graptolites underwent rapid evolution between species with recognisably different morphologies. The resultant combinations can be used to divide, and identify, units of geological time down to 0.2 Ma in parts of the Silurian.

These dating systems rely on good phylogeny, linking the taxonomy and evolution of the identified species. Identification of functional structures allows these to be reassessed in the light of convergent evolution, which might confuse phylogenetic analysis.

1.2. Aims of this project

The basic aims of this project were to investigate the impact of graptolite structures and morphologies on the hydrodynamics of the colony, considering both their impact on the flow patterns over the rhabdosome and on the overall movement of the colony. Structures are investigated in the light of published functional suggestions, and in some cases new functions are proposed.

Aims in brief:

- Investigate and image the fluid flow patterns produced upon interaction with graptolite structures.
- Investigate the effect of graptolite mophologies (and structures) on the orientation and motion of the colony on interaction with a fluid.

- Explore the key factors governing these affects.
- Speculate on potential functions. What benefit might these affects have had for the colony?

The identification of hydrodynamic structures, and their potential functions, could induce refinement of current ideas regarding taxonomy, evolution and identification of ocean environments.

1.3. Previous work on graptolite functional morphology

Most of the early work on the mode of life and ecology of graptolites was largely speculative. Graptolites and their structures were compared with those of living organisms but very little reliable information was available or could be tested.

1.3.1. Speculative investigations

At first it was speculated that graptolites might have moved from benthos to plankton by becoming epiplanktonic, using the nema to attach to already floating algae or debris (Lapworth 1897). A comparable condition may be seen today in the Sargasso Sea where the ocean circulation isolates an area of quiet water allowing the growth of large algae. These initially grow attached to rocks but are able to survive floating for some time after they become detached. However, Bulman (1964) demonstrated that, even when present, the nema was often too short or thin to be a suitable point of attachment for some graptolites. Due to the shape of certain colony forms, either the rhabdosome or the nema would have been forced to distort considerably were the graptolite to hang pendant.

Subsequently researchers have largely agreed that graptolites were more likely to have been holoplanktonic as no preserved structure is suitable for forming such an

attachment. Instead the nema has been proposed as an attachment site for floatation devices.

Various possible flotation devices have been identified. A number of secondary structures, built on the virgula of scandent colonies, were initially identified as flotation vesicles (Ruedemann 1947, Kozlowski 1971). These were later re-interpreted as three-part vane structures which may have aided the flotation of the colony either as a support structure for vaccuolated tissues (Bulman 1964 and Rickards 1975) or as a naked vane (Mitchell and Carle 1986). Finney (1978) also proposed the nema as an attachment site for floats when he described a floatation 'bubble' attached to the nema of a juvenile specimen of *Dicellograptus*. This is the only known specimen featuring such an attached structure, which implies that it was not a feature common to all graptolites.

Bulman (1964) first introduced the idea that the graptolite shape would have caused it to react passively with ocean currents, when he compared the form of *Cyrtograptus* to the 'umbrella sponge', *Axoniderma*, which has been observed to spiral upwards in response to quite gentle water movement. *Axoniderma* has an irregular shape in comparison with the highly organised form of a graptolite colony, and it might be expected that the graptolite would have been capable of a much more precise hydrodynamic response to accidental currents. He believed that graptolites would have also reacted passively to ocean currents, with the colony controlling its buoyancy through vacuolated tissues.

Kirk (1969) envisioned graptolites actively swimming, propelled by the feeding currents of the zooids within the colony. This theory led to hydrodynamic interpretations of various graptolite structures; the nema and virgula, vanes and proximal spines (Kirk 1972). Kirk also proposed that the feeding currents of the zooids would have led to rotation of the colony as it rose through the water column. Kirk's theories were not accepted by all. This is discussed in more detail in section 2.4.3.

1.3.2. Experimental Hydrodynamics

Recently these theoretical speculations have been tested through experimental studies. These focus on the hydrodynamics of the graptolite form, and rely largely on physical modelling, allowing a more objective investigation, which is to some extent testable.

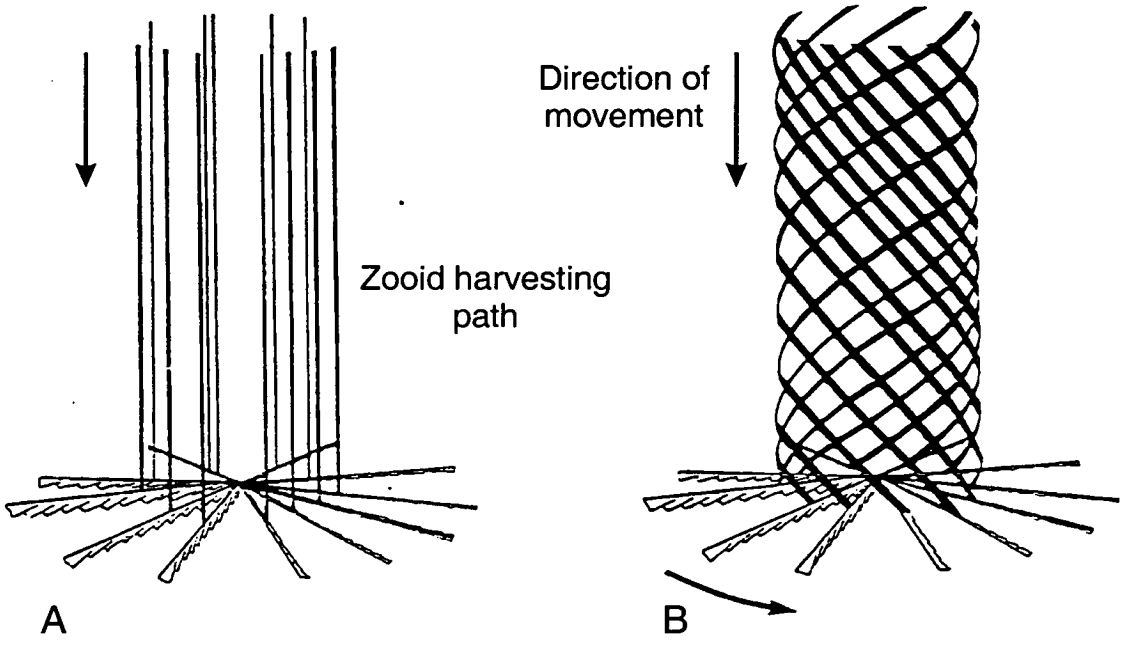

Figure 1.1: How the feeding paths of individual zooids on *Loganograptus* could be lengthened without overlapping one another if the colony rotated as it moved through the water. A. straight fall; B. rotating fall. From Rigby & Rickards 1989.

Rigby's PhD thesis (1990) represents the first experimental look at the hydrodynamics of graptolites. Real scale models of graptolites (the majority of these large, dichograptid, horizontal, many-stiped forms), with a realistic colony density, were tested in still water. These models were allowed to sink in order to simulate diurnal sinking. The experiments investigated the influence of gross colony morphology on the motion of the sinking colony interacting with a fluid. Many forms were observed to rotate, which would lead to more efficient feeding (Rigby &

Rickards 1989). The path of motion described by a zooid in a colony which rotated as it sank would have been considerably longer than that of a zooid in a colony which sank vertically without rotation (figure 1.1).

Jenkins (1997) investigated graptolite hydrodynamics through a combination of theoretical mathematical modelling and physical experiments. His work focused on the effects of small-scale turbulence on passive planktonic graptolites. Jenkins' paper criticised Rigby's use of still water, asserting that it is unrealistic to ignore the turbulent nature of the real ocean. However the majority of the models tested by Rigby (Rigby and Rickards1989, Rigby 1990) were large multiramous forms which Jenkins predicted would be little affected by small-scale currents. Jenkins' work suggested that smaller 'rod-like' colonies would have been strongly affected by small-scale flows, and that the relaxation time (the rate at which a particle introduced into a flow exponentially approaches the fluid velocity) calculated for these is so small that they may be considered to react instantaneously. Jenkins' tank experiments, using models of graptolites, indicated that the flow tended to run along the length of the rod-like colonies indicating some preferential orientation to a flow.

Melchin and Doucet (1996) used flume tank experiments to hydrodynamically test models of dendroid graptolites. These experiments demonstrated that a current flow across the top of a conical colony would have caused a pressure difference, drawing water up and out of the cone. This effect reinforces a useful feeding pattern, with incoming water passing into the colony through the conical walls, and the filtered water then passing out of the cone through it's open end. These experiments considered the effects of cone shape, current velocities and changes due to astogeny on this flow pattern (figure 1.2).

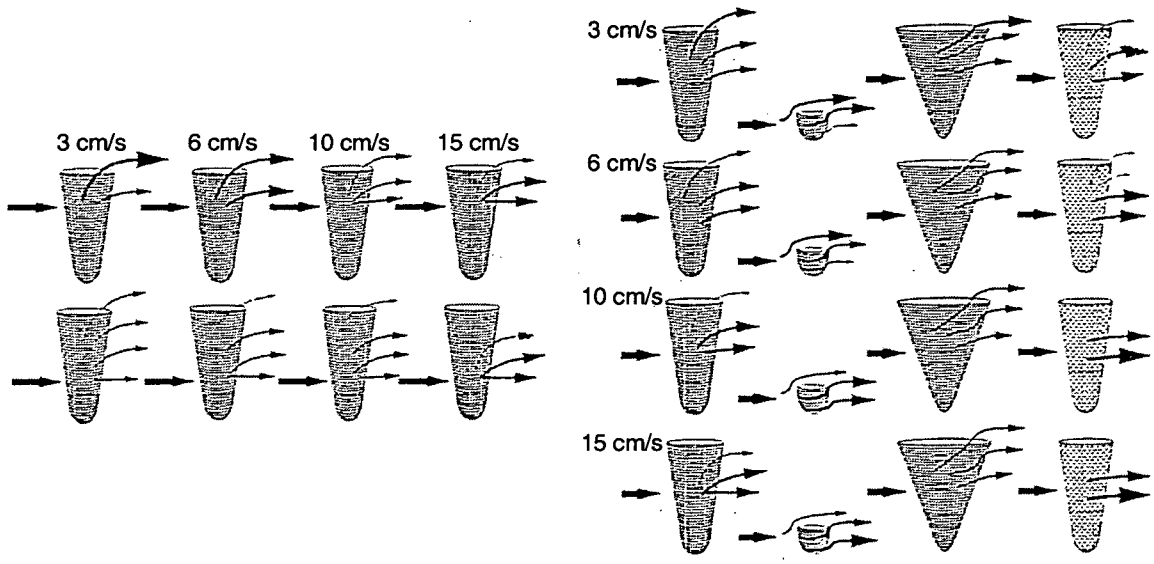

Figure 1.2: Schematic diagram showing directions and proportions of dye movement through dendroid models. The left set represents the introduction of dye near the top (upper diagrams) or near the base (lower diagrams) of the same model at different flow velocities (3 to 15 cms^{-1}). The right set illustrates the flow of dye through different dendroid models (the original model, a juvenile model, a widely flaring model and a coarser mesh model) at different flow velocities (3 to 15 cms^{-1}). The width of arrows, and size of arrowheads, of 'exhalent' currents are indicative of the relative proportions of dye that observed. Taken from Melchin & Doucet (1996).

Initial wind tunnel modelling was carried out by Rickards *et al* (1998), using a wind tunnel and LDA system, based in the University of Bristol, also used during this study. Models of *Saetograptus chimera* and *Amplexograptus maxwelli* were tested aligned with the virgella directed up-flow. This investigation indicated that the paired thecal spines of *S. chimera* produced a corresponding pair of trailing vortices. Impact with each successive pair of spines increased the turbulence and disorder of the flow, which would have entrained fresh food-bearing flow bringing it into the rhabdosome (figure 1.3).

The flow pattern images produced indicated that the virgella deflected flow from the thecal aperture, a suggestion supported by the theoretical investigations of Melchin (1998). These first experiments demonstrated that credible and useful data could be gained from this technique.

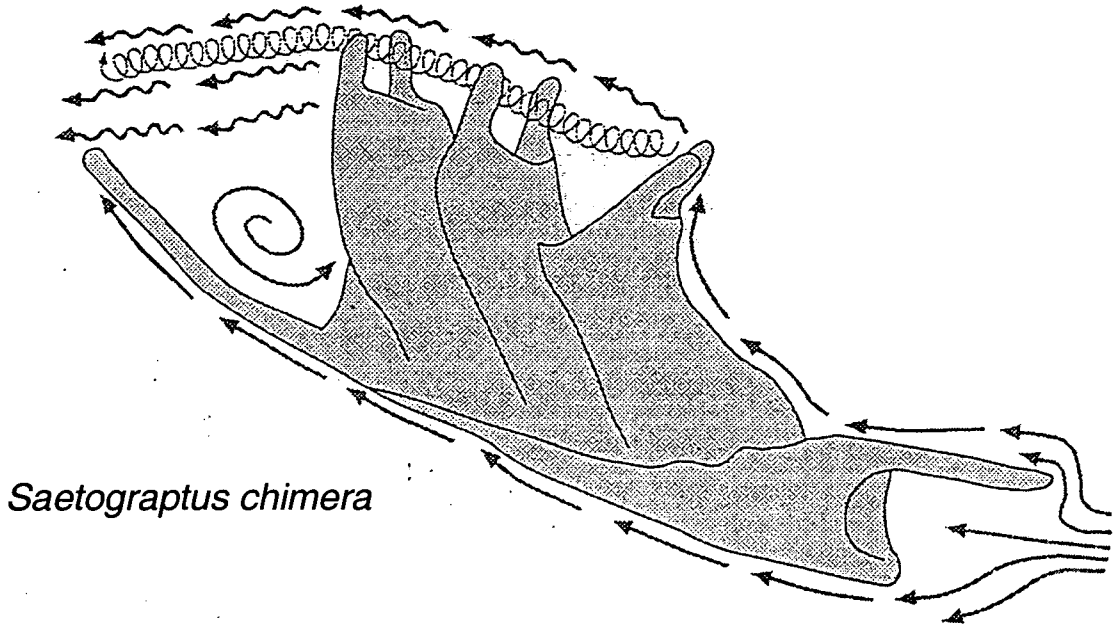

Figure 1.3: Pattern of flow observed over a model of *Saetograptus chimera*. Taken from Rickards *et al* 1998.

1.4. My approach to this investigation

1.4.1. Focus of the Project

This project concentrated on scandent species, some of the most abundant and simple morphologies, which dominated the mid-Ordovician to Devonian fauna. The investigation focused primarily on the spinose structures of the proximal and distal end; the virgella, thecal and anti-virgella spines, and the universal virgula and associated structures. There was some limited expansion of the project into the multi-branched dichograptids. Some two-stiped colonies (dicellograptids, dicranograptids and didymograptids) were modelled in order to initiate a link between this work and that of Rigby on many-branched dichograptids (Rigby and Rickards 1989, Rigby 1990 and 1992).

1.4.2. Brief outline of the experimental work

The hydrodynamic properties of fluids and their significance regarding an experimental study of graptolites are discussed in chapter 2. This includes the Reynolds number, which determines how a fluid flow behaves on interaction with an object (section 2.3). A reasonable estimate of the range of Reynolds numbers that would have been experienced by a living graptolite colony is essential for any hydrodynamic study. However a fluid flow produces consistent flow patterns for a range of Reynolds numbers (section 2.3.2). This range is tested using graptolite models, and provides a margin for model scaling accuracy.

This experimental study has used a combination of complementary techniques to investigate the hydrodynamics of graptolite morphologies. The study has relied largely on physical modelling techniques (described in chapter 3) using wind tunnels and fluid tanks, but some attempt has been made to extend these studies through mathematical and computer modelling. The majority of these techniques relied on physical or theoretical models of graptolite rhabdosomes. The methods used to construct these, and the limitations of accuracy required are discussed in chapter 4.

The wind tunnels (Bristol and Cambridge: sections 3.2.1 and 3.2.2) were used to investigate how the shape of the colony might have affected the pattern of flow over the graptolite. Accurate scale models of graptolites were constructed (chapter 4.4) for this purpose, such that patterns of air flow observed in the wind tunnel would be comparable to the patterns of seawater flow that would have been formed by a real colony under the influence of ocean currents. The theory behind such scaling and flow similarity is described in section 2.3.1. In these wind tunnel experiments the models were fixed such that they were not free to move in reaction to the flow. The fluid must take up all resultant movement.

The tank experiments (both in seawater and oil) considered the effect that interaction with a fluid might have had on the orientation and motion of a free moving colony. The seawater tank experiments relied on the use of real isolated fossil specimens to give the correct scaling factors of colony and fluid (chapter 2 and section 3.3.1). These observations were used in conjunction with those from simple models (section 4.5) tested in the oil tank. In the tank experiments the models were free to move, providing a more realistic situation than the wind tunnel, but the details of the fluid flow could not be observed.

The wind tunnel and tank experiments were used to identify, and gain understanding of, the key factors controlling colony orientation and the hydrodynamic effects of graptolite structures. Construction of a mathematical model was then attempted (section 5.6.2 and 6.4.2), picking out these key influencing factors, in order to gain further understanding of these potential hydrodynamic structures, and extend the predictions of the physical models. The predictions of these models are then compared with fossil evidence (section 5.10 and 6.11).

A smaller investigation of the hydrodynamics of two-stipe dichograptid morphologies was included (chapter 7) in order to extend this work beyond the scandent species. This focussed largely on the likely orientation of these species.

Finally the hydrodynamic principles identified through this study are applied to untested graptolite morphologies (section 8.2), to demonstrate how these principles might be applied to the hydrodynamic analysis of a wide range of species. The wider implications of these results are discussed with regards to taxonomy, oceanography and graptolite evolution (section 8.3).

2. Hydrodynamic constraints on assessing fossil functional morphology

2.1. Introduction

Any organism that lives in water is exposed to an array of fluid dynamic properties, from the velocity of the fluid to its dynamic viscosity or drag. Different sizes of organism experience different properties in the same fluid, and different fluid velocities also result in different hydrodynamic effects. A wide range of morphological innovations of modern organisms can be convincingly linked to evolution that accommodates these fluid properties (Vogel 1981). It is reasonable to assume that morphological adaptations related to fluid dynamics also occurred in past organisms. In order to investigate this, two arguments need to be made; one for the likely range of properties of the fluid as experienced by the fossil organism, and a second for the specific conditions that were probably encountered by an organism of the fossil's size and velocity within that fluid.

2.2. Basic hydrodynamics of water

The lithologies and location of graptolite specimens worldwide indicates that they were marine organisms. Consequently it is the properties of Palaeozoic seawater that must be determined and quantified to enable an experimental study of graptolite hydrodynamics. The Palaeozoic oceans would have been subject to the same forces, and similar inputs, as the modern ocean. As a first approximation the properties of modern seawater will be considered.

2.2.1. Density, dynamic viscosity etc.

The nature of a fluid, and how it might react as a flow, is described by a series of properties, the two most important of which are density and dynamic viscosity.

The **density** of a fluid describes the relationship between mass and volume. The concept of mass alone is of little use when studying fluid dynamics as the boundaries of the fluid under analysis can be ambiguous and, in many cases, the fluid may be moving through the area of interest.

Density is defined as the mass of a unit cube of fluid, and consequently has S.I. units of kg m^{-3}. It is traditionally given the symbol ρ in equations and this convention will be used throughout this thesis.

Dynamic viscosity is often referred to as simply viscosity, although correctly it should be distinguished from kinematic viscosity, a fluid property not utilised in this thesis. The dynamic viscosity is a measure of how much a fluid resists a shear rate, i.e. the resistance put up against an object moving through a fluid, at a particular velocity, and forcing it to shear and deform at a rate which would allow its passage.

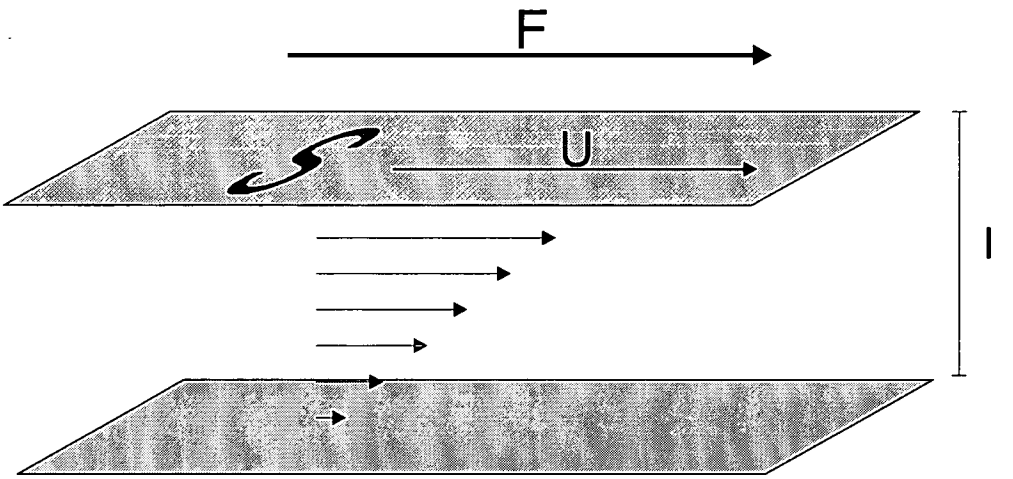

Figure 2.1: The simple viscosity model. The fluid is modelled as a stack of sheets between a plate, of area S, at distance l from a flat surface. The upper plate is pushed at velocity U, and the force F required to maintain this velocity is determined by the 'friction' between the fluid sheets (the viscosity of the fluid).

To calculate the viscous forces experienced within a flowing fluid, the fluid is modelled as a stack of sheets lying between two plates (Fig 2.1). If the plates were to move relative to each other, this movement must be accommodated by the stack of fluid sheets sliding over each other, and a form of friction will act between the

sliding sheets. This is the dynamic viscosity. If the upper plate is pushed with force F, causing it to move with velocity U, then the force must overcome viscosity of a stack of sheets l (distance between the two plates) thick, over the area S of the plate. When considering friction between two solid objects the coefficient of friction is considered: Frictional force = area of contact x velocity of movement x coefficient of friction. For a fluid the dynamic viscosity (μ) is used, representing the coefficient of friction per infinitely thin theoretical 'sheet' of fluid. Hence:

$$F_v = \frac{\mu US}{l} \quad (1)$$

Dynamic viscosity has the S.I. units Pa S (or Pascal second). It is given the symbol μ, which is used throughout this thesis.

2.2.2. Variations with temperature, salinity

Both the viscosity and density of a fluid are altered with changes in temperature and salinity.

Fluid	Temperature	Dynamic viscosity (PaS)	Density ($kg\ m^{-3}$)
Air	0°	17.09×10^{-6}	1.293
	20°	18.08×10^{-6}	1.205
	40°	19.04×10^{-6}	1.128
Fresh water	0°	1.787×10^{-3}	1.000×10^{3}
	20°	1.002×10^{-3}	0.998×10^{3}
	40°	0.653×10^{-3}	0.992×10^{3}
Seawater	0°	1.890×10^{-3}	1.028×10^{3}
	20°	1.072×10^{-3}	1.024×10^{3}
	30°	0.870×10^{-3}	1.022×10^{3}

Table 2.1: Dynamic viscosity and density values for air, freshwater and seawater at a range of temperatures. The seawater values presume a salinity of 35‰ (parts per thousand). Data taken from Vogel (1981).

The density of both air and water drops as the temperature increases. In the case of air, this density reduction is considerable: a density decrease of approximately 7% (1.293 kg m^{-3} to 1.205 kg m^{-3}) with a temperature increase from 0° to 20° (see table 2.1). The same temperature change produces only a 0.4% drop (1.028 $x10^3$ to 1.024 $x10^3$) in the density of seawater. Despite this it appears that the density differences of seawater with temperature have been significant to some biological organisms (Vogel 1981).

The viscosity of air increases slightly with temperature, with a 6% rise (17.09 x 10^{-6} to 18.08 x 10^{-6}) from 0° to 20°. In comparison the viscosity of water decreases with increasing temperature. The viscosity of seawater drops considerably, with a 43% reduction (1.890 $x10^{-3}$ to 1.072 $x10^{-3}$) over the same temperature change (table 2.1).

The data gathered in table 2.1 also show that density and viscosity both increase with increasing salinity with comparison of the fresh water and seawater data.

For this study, one set of values (seawater at 20°, table 2.1) is chosen which represents a reasonable description of modern, warm, tropical shelf seawaters. This is not inconsistent with a graptolite biotope living in early Ordovician low latitude (30°S to 30°N) shelf seas such as the pandemic species and those of the Pacific province as described by Cooper *et al* (1991).

2.2.3. Variations near to a boundary

One of the fundamental rules of solid / fluid interactions is the no-slip condition. This states that the fluid directly in contact with any solid is stationary with respect to the solid surface, regardless of the relative free-stream velocity of the fluid. This has been shown to be true of all fluids except for some very extreme examples not considered here.

The formation of a boundary layer is a direct response to the no-slip condition. The boundary layer represents the 'layer' of fluid through which the velocity changes from stationary at the solid surface to the free-stream velocity U. Since the velocity approaches U asymptotically it is impossible to define the point at which it reaches it, and the boundary layer has no discrete limits. In order to avoid this problem the upper limit of the boundary layer is defined as the distance at which the fluid reaches 99% of the free-stream velocity U.

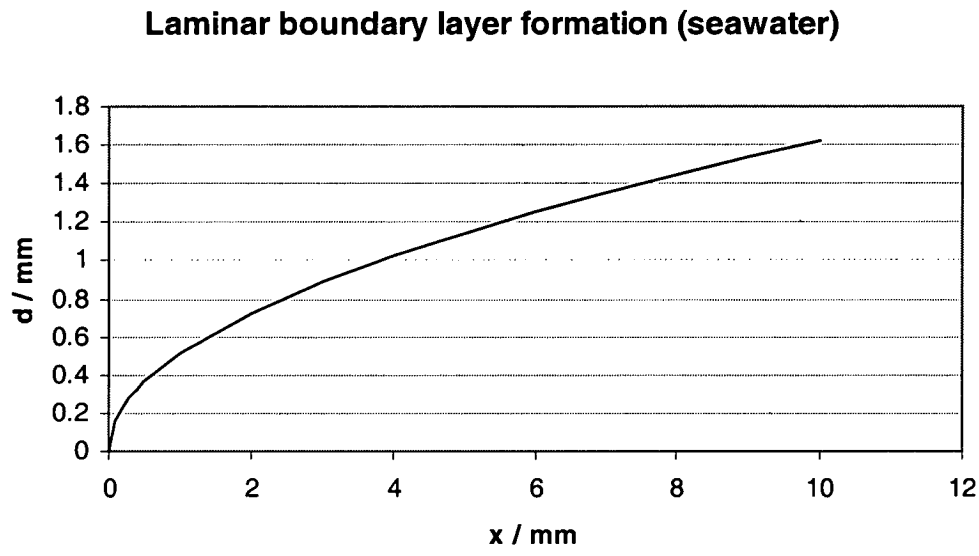

Figure 2.2: Evolution of a laminar boundary layer thickness (d), with distance along a surface (x), in seawater. Boundary layer thickness is calculated using equation (2).

A fluid impacting with an object will form a boundary layer around it. As the fluid travels along the object the boundary layer thickens and develops, the depth of the boundary layer can be calculated from this equation:

$$\frac{\delta}{x} = 5\mathrm{Re}^{-\frac{1}{2}} \qquad (2)$$

Where δ represents the thickness of the boundary layer, x the distance along the surface from the leading edge, and Re is the Reynolds number at the particular point (figure 2.2). The Reynolds number is a key concept in fluid dynamics. The value of this term provides a guide to how a fluid will react to interaction with an object and

will be discussed in more detail in the next section. Note low Reynolds numbers will lead to thicker boundary layers than high Reynolds numbers. This equation only provides crude estimates below Reynolds number values of 600. This boundary layer is a purely laminar one, with sheets of fluid taking up the velocity gradient of the boundary layer through simple shearing. In reality this laminar boundary layer might convert to a turbulent boundary layer at a point determined by the local Reynolds number. A turbulent boundary layer contains a laminar sub-layer close to the surface, but the majority of the velocity gradient is taken up through the turbulent, random motion of the fluid. The turbulent boundary layer thickens at a greater rate than the laminar boundary layer.

2.2.4. What effect does the boundary layer have on organisms?

The fluid forming a laminar boundary layer flows entirely parallel to the surface and has no movement perpendicular to this. This lack of mixing leads to a stagnant region through which particles cannot travel. The laminar boundary layer provides a barrier to transport of heat or matter. Any organism living on a surface within such a boundary layer will have difficulties getting rid of waste matter and bringing in new food particles. A turbulent boundary layer does not bring these problems as the turbulent flow allows free mixing across the boundary layer. Living in a boundary layer also affords the organism some protection form the higher velocities and consequent drag forces of the free-stream flow. However the boundary layer velocity gradient will produce shear forces.

The texture of a surface may have a significant effect on the nature of the boundary layer. A rough surface will tend to initiate a turbulent boundary layer at lower Reynolds numbers and the associated loss of drag may be critical to an organism.

The planktonic graptolites are believed to have lived in the open ocean. Far above the seabed, or other solid interfaces, the graptolites were unlikely to have encountered the effects of any such boundary layers. Boundary layers could have had a significant effect on the life of the graptolite zooids however, since a boundary layer would also

have formed at the interface between rhabdosome and seawater. The small size of a graptolite colony would limit the thickness of such a boundary layer but the zooids would have had to reach through the velocity gradient, to reach fresh food particles and eject waste products, unless a turbulent boundary layer formed allowing mixing.

2.3. Reynolds number

The key to studies of fluid dynamics is the dimensionless **Reynolds number**, which describes the balance of viscous and inertial forces and provides information on the expected behaviour of a flow. The importance and effects of these internal forces are described here and the equation used to calculate the Reynolds number is derived.

The Reynolds number represents a ratio of the forces acting on and within a flowing fluid body, and governs how it will behave upon impact with an object. Essentially these are the viscous fluid forces, that resist turbulence, and the inertial fluid forces, which encourage turbulence (Vogel 1981). A highly viscous fluid will maintain a laminar flow, and stop rather than overcome the high shearing forces required for turbulence. In comparison a fluid with a low viscosity, travelling at the same velocity, will present less resistance to shearing and is likely to become turbulent. A fluid with high inertial forces (fast flow velocity) will be carried forwards at pace by its momentum, regardless of shearing, leading to a turbulent flow, whereas a slow moving fluid will lack the momentum required to overcome these shear forces and will remain in laminar flow.

The forces due to viscosity are calculated using equation (1), derived from the model of a fluid as a stack of sheets (section 2.2.1).

The inertial force is determined by considering the momentum of the flow. Momentum is always conserved. A flow might impact with an object, a force will act between them to produce momentum change of both the fluid and the object, but the total momentum, of both together, will be unchanged. Newton's second law states that force (F) is equal to mass times acceleration, or the rate of momentum change (equation 3).

$$F = m\frac{dU}{dt} \tag{3}$$

Where U is the velocity of an object and m is its mass (Here it is assumed that the mass remains constant). However mass is not a useful concept when considering a fluid flow, consider instead the mass flux in a small stream-tube. Fluid flows through the tube at velocity U. The tube has cross-sectional area S, which allows a mass of fluid ρSU to pass through it per second (ρ is the fluid density). The mass flux is given by m/t (equation 4).

$$\frac{m}{t} = \rho SU \tag{4}$$

Momentum is given by the product of an object's mass and velocity (momentum = mU), for a fluid we consider the momentum flux (equation 5), the product of mass flux and velocity.

$$\frac{mU}{t} = \rho SU^2 \tag{5}$$

Using Newton's second law, momentum flux gives us the inertial force (equation 6).

$$F_I = \rho SU^2 \tag{6}$$

The Reynolds number is the ratio of these two forces:

$$Re = \frac{F_I}{F_V} \tag{7}$$

Inertial fluid force $F_I = \rho SU^2$

Viscous fluid force $F_V = \frac{\mu SU}{l}$

U = free fluid velocity.
l = characteristic length of object.
ρ = density of fluid.
μ = dynamic viscosity of fluid.

$$Re = \frac{\rho l U}{\mu} \qquad (8)$$

Note (as previously stated) that the Reynolds number is dimensionless, merely a ratio of the forces acting on a flowing fluid.

2.3.1. Dynamic similarity

In order to successfully investigate flow around an object using models, it is vital to understand how to ensure valid results. This relies on correct scaling such that the motion of the experimental fluid around the model will produce exactly the same patterns of flow as the motion of the real fluid around the real object. This is called dynamic similarity and relies on use of the Reynolds number. In this section the effect of scale and Reynolds numbers on the patterns of flow are described, and the correct model scaling for modelling the flow of seawater around an object using a wind tunnel is calculated.

The most frequently illustrated example of the relationship between Reynolds number and flow pattern, is that of a long cylinder with its axis lying perpendicular to the flow direction (figure 2.3). This shows that the flow behaviours observed can be grouped into behaviour types (creeping flow, attached vortices, von Karmen trail and turbulent), which are linked to broad Reynolds number bands. Within each behavioural band there is little significant difference with changing Reynolds number, a wake may change in width or length, but the essential pattern is constant. The patterns of flow become increasingly chaotic as the Reynolds number increases.

There is no scale given in this example, the size of the cylinder or the fluid properties are not given, and they are not relevant. As previously stated, the Reynolds number is dimensionless and is independent of scale. This means that the same pattern of flow would be expected around two cylinders of very different sizes if the fluid properties and flow velocity were scaled such that the resultant Reynolds number was the same in both cases.

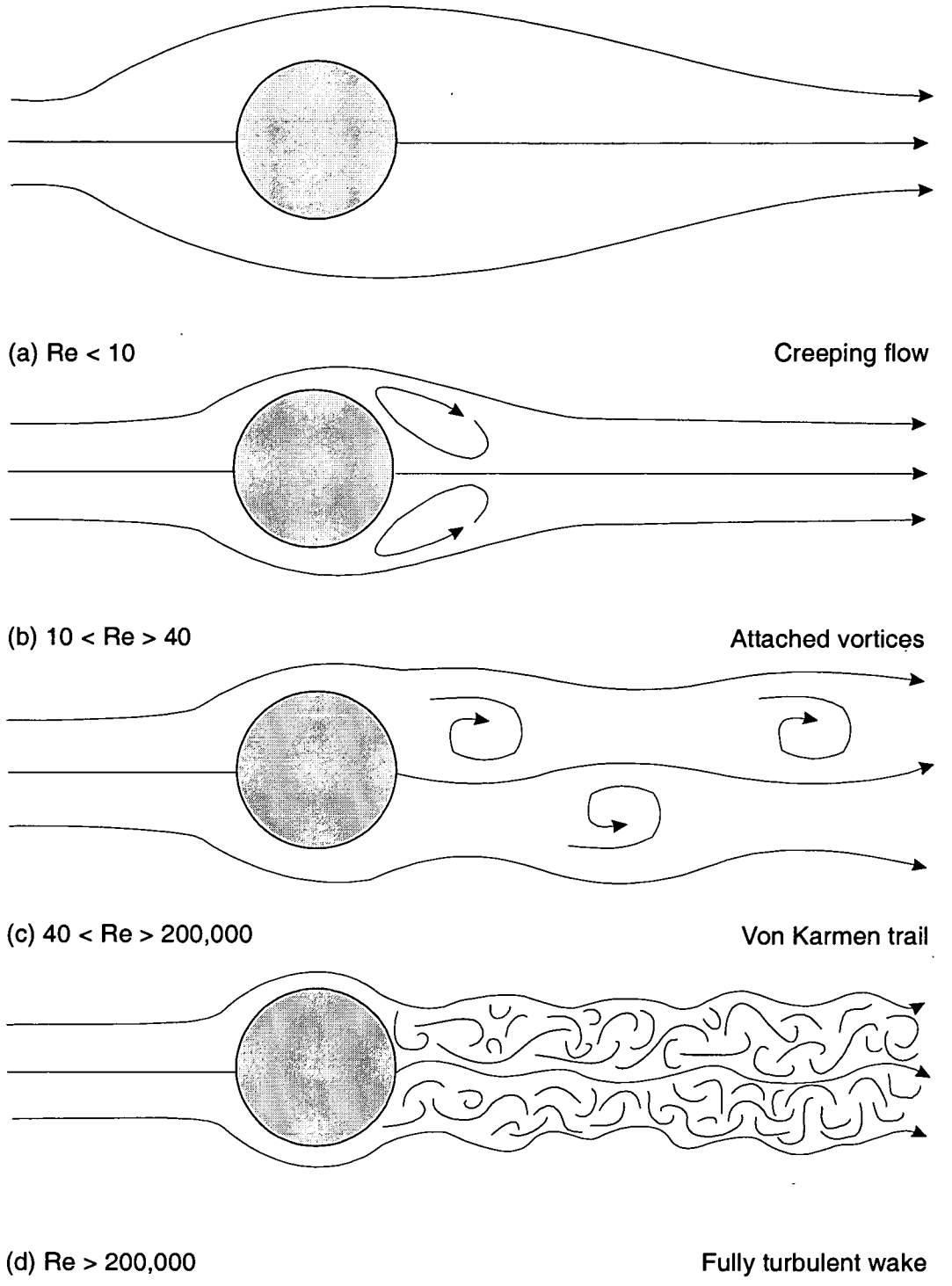

Figure 2.3: The patterns of flow around an infinitely long cylinder with it's axis aligned perpendicular to the current. The pattern becomes increasingly chaotic with increasing Reynolds number. Based on Vogel (1981).

'Equality of Re does not mean that forces are unchanged, but patterns of flow will be the same even if one fluid is a gas and the other a liquid' (Vogel 1981).

Thus a comparison of effects produced by different fluids on different sizes of object is appropriate if parity of Reynolds number can be achieved. The dimensionless quality of Reynolds numbers, and the scale tolerance of flow, allows the study of flow around objects in water by observing the flow around models of fluids with very different properties, such as oil or air (table 2.2). For example, air has a low density such that a model scaled up fourteen times, from the original size, will give the same Reynolds number (and hence flow pattern) as a smaller object in water, when the same fluid velocities are used. Physical experiments observing scale models of graptolites in a wind tunnel form the basis of much of this study so this relationship is particularly important here.

(All at 20°C)	Dynamic Viscosity μ / $kgm^{-1}s^{-1}$	Density ρ / kgm-3
Air	18.08×10^{5}	1.205
Seawater	1.072×10^{-3}	1.024×10^{3}

Table 2.2:Values for the density and dynamic viscosity, taken from table 2.1, for direct comparison of the properties of seawater (in which the graptolites lived) with air (in which models are observed in the wind tunnels).

The Reynolds number ($Re = \rho lU/\mu$) is proportional to ρ/μ.

Air: $$\frac{\rho}{\mu} = 6.7x10^{4}$$

Seawater: $$\frac{\rho}{\mu} = 9.6x10^{5}$$

$$\frac{Re_{seawater}}{Re_{air}} \propto \frac{9.6x10^{5}}{6.7x10^{4}} \approx 14 \qquad (6)$$

This translates to a scale change of fourteen times to produce the same Reynolds number for an object in air, as another in water at the same flow velocity, U. This means that graptolite models should correctly be constructed at a scale of x fourteen for observation in wind tunnels at velocities it is estimated that living graptolites might have experienced in seawater.

The illustrated example of the infinite cylinder, perpendicular to the flow, (figure 2.3) shows that flow behaviour falls within broad bands of Reynolds numbers (e.g. von Karmen trail 40 – 200 000) (Vogel 1981). The same pattern has been observed for different shaped objects in a flow, with broad Reynolds number bands of flow behaviour, although the Reynolds numbers acting as boundaries to the behaviour types will vary from shape to shape. Within one of these bands small details of flow may change with Reynolds number, but the overall pattern is maintained.

2.3.2. Limitations of dynamic similarity

This project assumes that a precise Reynolds number, and consequently the scale of models or fluid, is not required in order for these experiments to be valid. As described previously in section 2.3.1 the flow patterns around any object are robust to some variation of the Reynolds number. This expectation was confirmed by two experiments running the Cambridge wind tunnel at velocities from sub 0.5 ms^{-1} to 2 ms^{-1} on the same model (figures 2.4 and 2.5).

This experiment can be extended by considering the results obtained from the Bristol wind tunnel, which ran at 0.1ms^{-1}. Tests using the *A. maxwelli* models picked up the same pattern of flow along the thecal spine (see section 6 for more details).

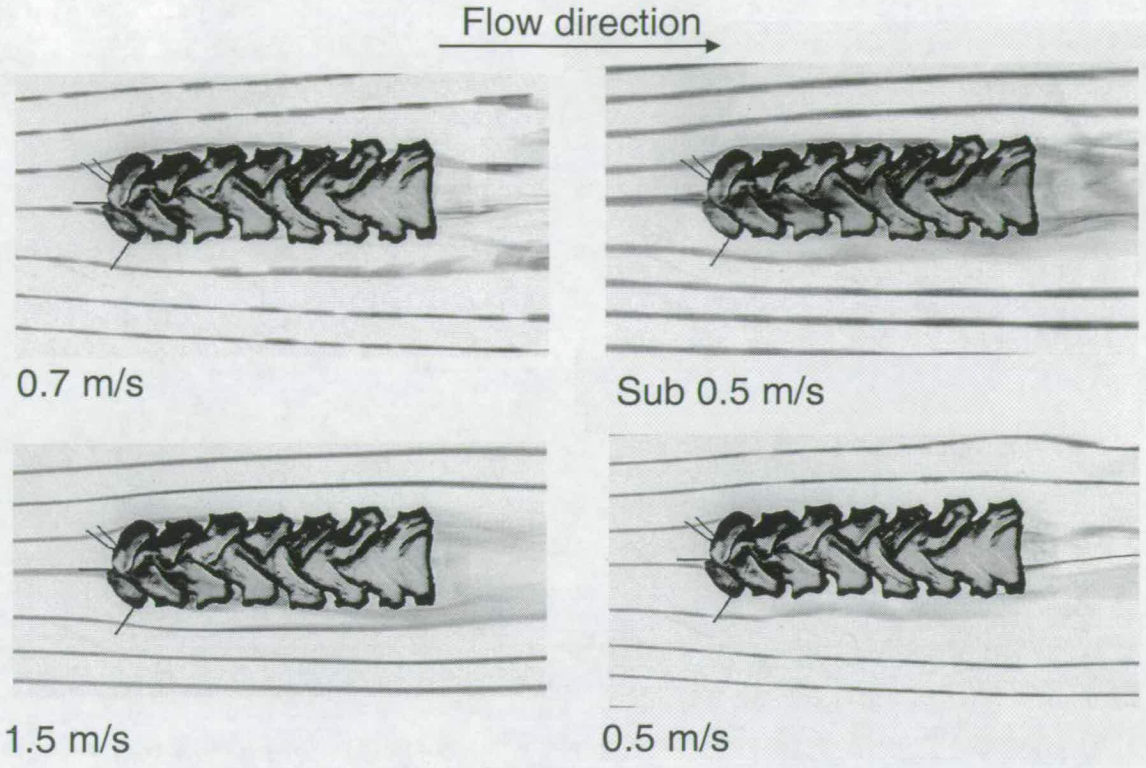

Figure 2.4: A series of digital pictures of a model of *A. maxwelli* run at a range of free airspeeds (less than 0.5 ms^{-1} to 1.5 ms^{-1}). The flow pattern observed changes very little between images. As the flow velocity increases the smoke streams become smoother and the flow pattern narrows, because the flow is deflected less on impact with the model. The same flare of smoke is observed running up the thecal spine, and smoke runs into the dorsal thecal openings at all velocities (see section 6 for more details).

These tests, combined with tests from the slower Bristol wind tunnel, have shown that the pattern of flow is not sensitive to changes in flow velocity (and hence Reynolds number) between 0.1-2.0 ms^{-1}. This result was further supported by running the Cambridge wind tunnel with four models, of the same graptolite *(C. schaeferi)*, built at different scales (figure 2.6). The model scales ranged from times fourteen (the scale at which models should be built to re-produce the same Reynolds number: see section 2.3.1) to times fifty.

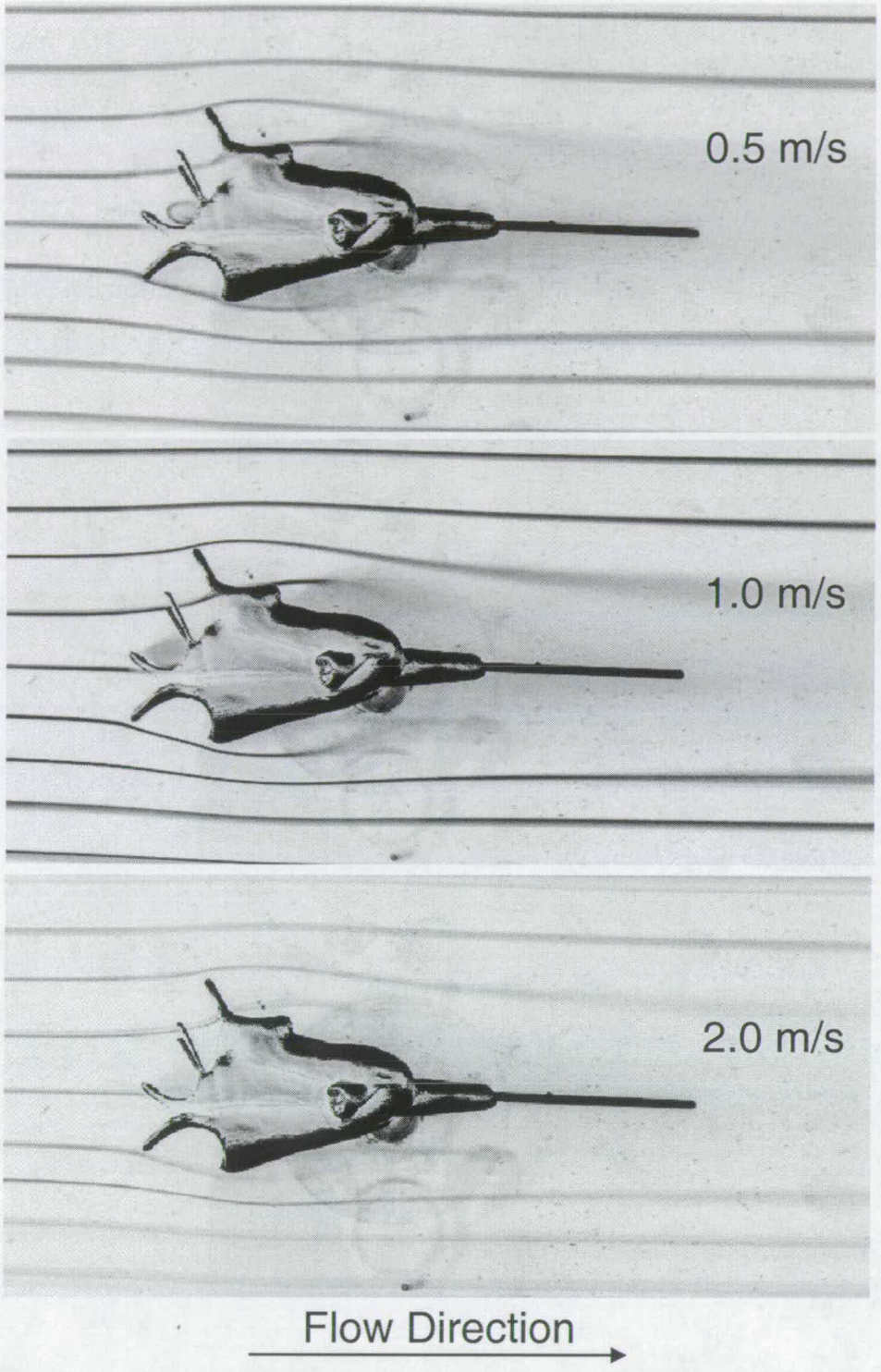

Figure 2.5: Another series of digital pictures, this time depicting the same model of *C. schaeferi* which was also run in the Cambridge wind tunnel at a range of flow velocities (0.5 ms^{-1} to 2.0 ms^{-1}). Once again the flow patterns observed at all velocities are very similar (see section 6 for more details).

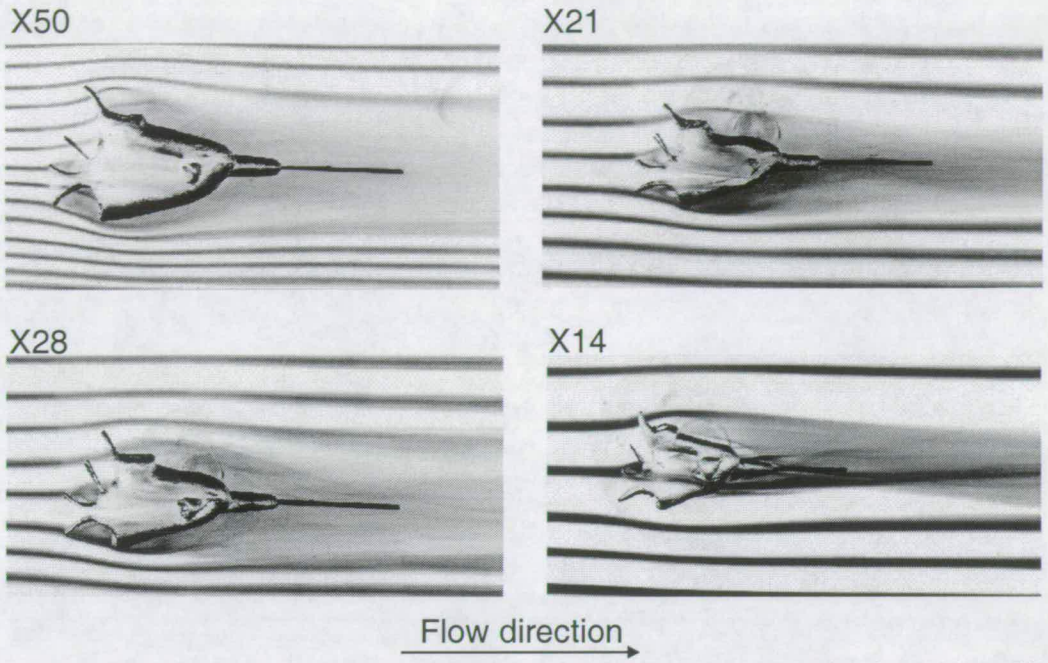

Figure 2.6: Digital images of a series models of *C. schaeferi* built at a range of scales (x14 to x50). The pattern of flow is broadly the same over all the models. As the model size becomes smaller fewer smoke-streams impact with it, and the flow pattern is less clearly seen.

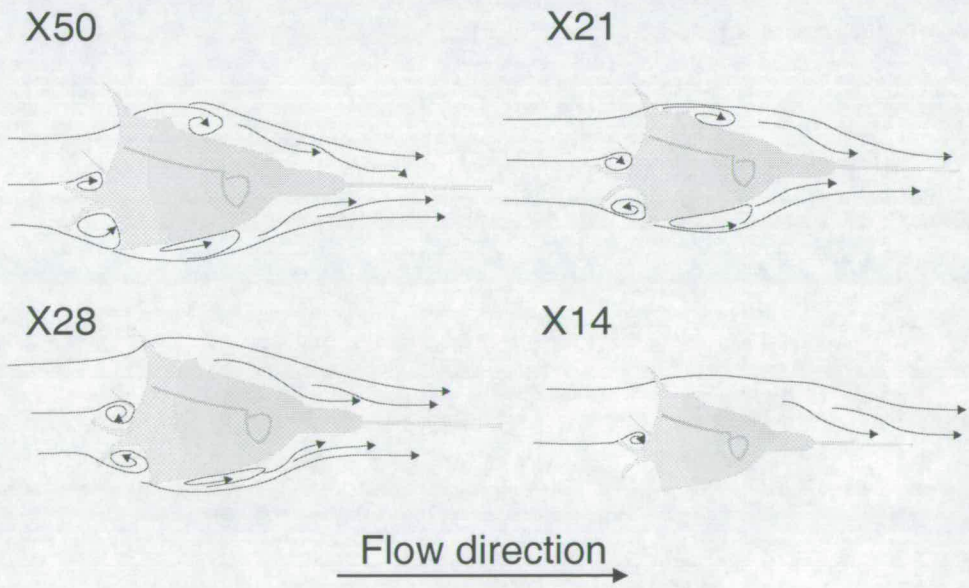

Figure 2.7: An interpretation of the flow observed around models of *C. schaeferi* in figure 2.6. Note the standing eddies forming in the apertures of the sicula and th1[1]. Standing eddies are also observed behind th1[2] and along the ventral surface of th1[1]. These features are common to the flow around the models of different scales although they may not all be visible in a single photograph (particularly of the smaller scale models) due to the limitations of the fixed smoke-streamer spacing and model size.

These simple tests confirm that flow patterns are not very sensitive to Reynolds number. The Reynolds number is easily changed in these experiments, either by building models at a different scale or varying the free air velocity in the wind tunnels. Models built at times fifty will produce very similar results to those built at times fourteen. The airflow velocity is also flexible; it has been shown that these experiments are robust over range 0.1-2.0 ms^{-1} (Re 1000-2000), and probably over a much greater range than this. Hence Reynolds number assumptions specific to graptolites only need to be 'ballpark' figures.

2.4. Graptolites in water

In order to investigate experimentally the hydrodynamics of graptolite shapes the likely Reynolds numbers which the living organisms might have experienced must first be calculated (using equation (8), section 2.3). The fluid properties (of seawater and the experimental fluids), the flow-parallel length of the graptolite specimen, and an estimate of the original relative flow-rate that graptolites might have experienced are required.

The problems of estimating graptolite colony size must be considered, and suitable values for relative flow-rate, and variation within these parameters, are discussed in the light of graptolite mode of life and in comparison with living organisms and other experimental studies.

2.4.1. The size of a graptolite

It is reasonably easy to estimate the size of a graptolite colony if it is assumed that the preserved rhabdosome represents the true external surface that a graptolite might have presented to the flow. This study assumes the absence of extra-thecal tissues that might have altered the colonies external dimensions (this assumption is discussed in detail in section 4.3.1).

Well-preserved specimens might be directly measured. Three-dimensional isolated specimens provide additional information allowing any distortion effects due to

flattening to be accounted for. This study largely considers the hydrodynamic interaction of relatively juvenile graptolite colonies (with less than six thecae), although a model of a more mature graptolite (with fifteen thecae) is also used. These juvenile specimens are more readily isolated complete. The delicate virgula spine is often broken, but this breakage is less common with very juvenile specimens. The relative completeness of the specimens on which this experimental study is based allows reasonable estimates of the original colony dimensions.

The isolated specimens used in seawater tank tests (section 5.3.1) were of the order of 1.5 – 7.0mm long. The specimens on which models were based for wind tunnel observation ranges from approximately 2.0 – 10.0mm in length.

The characteristic length of the colony, required to calculate the Reynolds number, is defined as the length parallel to the flow direction. Thus the orientation of the colony to a flow must also be known (or estimated). In order to estimate likely values for a graptolite Reynolds number in this chapter it is assumed that a scandent colony would have aligned parallel to the flow following the work of Jenkins (1997) and Rickards *et al* (1998).

2.4.2. Graptolite orientation

Traditionally biserial graptolites have always been illustrated vertically with the nema or virgula pointing upwards, and in most cases this has been accepted as their life orientation. Kirk's paper (1969) reversed this orientation and caused considerable controversy. She postulated that the zooid's feeding current would have projected in the same general orientation as the thecal openings, and that these currents would have buoyantly supported the colony.

Bulman pointed to bulb-like structures attached to the nema or virgula. These provided evidence for a traditional orientation when the bulb-like structures were interpreted as floats (Bulman - discussion following Kirk 1969). However the vast

majority of these structures have proved to be vanes, with no evidence of associated vacuolated soft tissue. Typically these vanes had three parts, which were set at approximately 120° (Rickards 1975). Kirk predicted that these vanes would have stabilised the colony as it moved vertically, and prevented rotation (Kirk 1972). This suggests that a vane would indicate an alignment of the long colony axis with the flow, but the polarity is not implied.

Jenkins (1997) argues that scandent, and few-stiped forms, could not have maintained a constant orientation in a turbulent environment. It would be unreasonable to assign them with a 'way up', as they would be constantly changing direction in response to even small-scale currents and turbulence. However in tank tests (using dye markers) Jenkins notes that the dye streams tended to run along the stipes of the 'blade like' forms. This implies that the graptolites were consistently aligned lengthways with respect to these small flows, and that an instantaneous preferred orientation with respect to the current might be expected. The relaxation time calculated for such colonies, (Jenkins 1997) which corresponds to speed at which a particle reacts to a new flow, is very small. This implies that a colony would have reacted almost instantaneously to a new flow and realigned.

In the present study we assume that the usual orientation of a colony was with the sicular aperture facing in the direction of relative motion (into the flow) following the work of Rickards *et al.* (1998). The aeronautical engineers working on the project advised this alignment. They believed this to be the only reasonable orientation based on their knowledge of shape and flow (C. Swales and J. Rickards: personal communication). Likely orientations of free-falling graptoloids have been independently investigated during this study (section 5.3.1 and 5.7) to broadly confirm this suggestion.

This orientation is further supported by a number of examples of current aligned graptolites (Gentile *et al.* 1984, Schleiger 1968) in which the alignment is typically

with the sicula directed up-current. The rapid re-alignment of blade-like colony shapes, as indicated by the experiments of Jenkins (1997), would imply that graptolites would have spent most of the time in a relatively consistent alignment to the prevailing flow. Most of the models tested in the Cambridge wind tunnel were run in several orientations in order to assess the most stable.

2.4.3. The velocities experienced by a graptoloid

Assessing the likely Reynolds numbers experienced by a graptolite is difficult, but can be done within moderate error bars (Rigby and Rickards 1989, Rickards *et al* 1998). Dynamic viscosity and density are known for air, oil and water, as are the lengths of both models and graptolites. The unknown in this equation is the velocity of graptolites in water.

Active or passive?

Estimates for the velocity of graptolites in water are hindered by the lack of information about the graptolite mode of life, particularly the question of passive response or active swimming. Most workers in the field have fallen into one of two camps, those who argue that graptolites responded passively to ocean currents (Bulman 1964, Kozlowski 1971 & Rickards 1975) and those believing graptolites to have been automotive, actively able to direct their movement (Kirk 1969, 1972).

Kirk (1969), further developed Bulman's idea of passive hydrodynamic response to water currents (1964), postulating that graptolites could have used directed feeding currents to actively propel themselves. Kirk (1972) also suggested that these directed feeding currents might also have been used to produce a controlled rotation of the colony.

Those opposing Kirk's ideas argued that the geometry of thecae in many colonies implies that any directional currents would have opposed and negated each other. For example currents projected from the thecal apertures along the two stipes of *Dicellograptus* or *Didymograptus* would have directly opposed each other. Perhaps

more importantly, it was argued that such small zooids would have been unable to produce currents large enough to move the colony (Bulman & Rickards - discussion following Kirk 1969). Further problems arise from the thecal apertures of cucullograptids which became almost entirely closed as the colony developed, and would have prevented these enclosed zooids from directing their feeding currents (Rickards discussion following Kirk 1969) (figure 2.8). Consequently it would seem unlikely that graptolite zooids could have had any active control on their motion in this way.

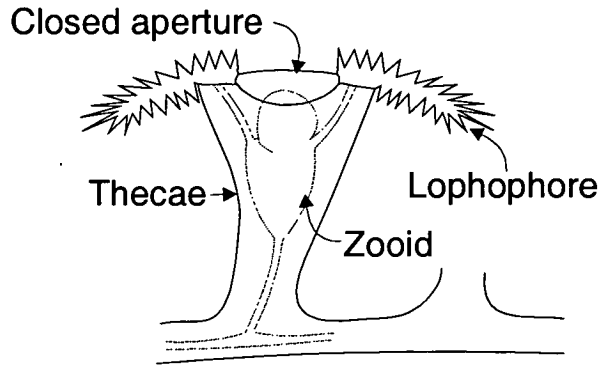

Figure 2.8: The thecal apertures of cucullograptids almost close over once the zooid has finished building. The remaining small holes are only large enough for the lophophores to project in a fixed position.

Through comparison with modern zooplankton, other active propulsion methods have been considered and largely rejected by Melchin and DeMont (1995), mostly on morphological grounds. They concluded that the only possible method of active swimming was through the use of specially adapted, cephalic shield 'wings'. These are soft tissue structures, and unobserved in fossil specimens, but the living hemichordates (*Cepaholodiscus* and *Rhabdopleura*) show that the cephalic shield can be flexible and highly adaptable.

In contrast Bulman (1964) and Rickards (1975) proposed that graptolites were entirely passive, their only active motion control through density changes, causing the colony to move vertically through the water column.

Ocean currents and turbulence, at all scales, are important to organisms living in the ocean, particularly those that are planktonic. Turbulence brings oxygen and food particles to the plankton, provides movement in place of active swimming and disperses offspring (Jenkins 1997). A graptolite colony was too large to gain particulate food through diffusion processes alone. It is clear that graptolites did move in the ocean (and must have moved with respect to the water around them) otherwise the colony would soon have depleted the surrounding food supply and starved (Kirk 1969).

A combination of the two methods (active swimming and passive response) may have also been possible, had the zooids used their feeding currents to provide additional buoyancy. However ocean turbulence and flows would have affected graptolites, automobile or passive, and their effect would have been stronger than any feeding currents produced by the zooids. Kirk's theory saw graptolites controlling their buoyancy, and hence positions in the water column, rather than actively swimming with any speed or precision. Therefore it makes little difference to this project if the graptolites are considered to be automobile or passive.

Consequently this study will focus on the effect of flow produced by ocean currents interacting with graptolite shape.

Likely velocities of ocean currents:

It is reasonable to assume that Palaeozoic ocean currents were produced by the same natural forces and processes as those in the oceans today: wind, tidal forces, gravity, temperature and salinity stratification. The overall pattern of flows, controlled largely by the arrangement of continental landmasses and the shape of the ocean floor, would have been very different, but the magnitude of these currents would have been similar.

The exact habitat of graptolite species is hard to determine, since distributions by depth or shelf location can be hard to distinguish, and the habitats of different genera or species may have been very different. Various controlling factors of graptolite

distribution have been suggested since 1934 when Keble and Harris (1934) started pointing out clear regional differences (Cooper *et al* 1980). These include: oceanic currents (i.e. Gulf Stream), latitudinal surface temperature (Atlantic and Pacific provinces), depth distribution and the partitioning of shelf and oceanic waters.

Cooper *et al* (1991) compared these controlling factors with the distribution of preserved species. Their study divided the Ordovican graptolite species into number of biotopes. These included a pandemic biotope of species which could be found in all sediments worldwide, and appeared to be unaffected by latitude (temperature), which was further divided into epipelagic (top 200m), deep water and inshore biotopes. The epipelagic biotope was identified by an apparent indifference to water depth. Other species were divided into Pacific and Atlantic Provinces, and also further divided by shelf location. The majority of Ordovician species fell into the pandemic biotopes, and all biserial species were part of the epipelagic biotope.

Graptolites are believed to have been too delicate to live within the wave influenced ocean surface waters, and are more commonly presumed to have lived in the relative calm of the deep oceans. However, they are found largely in shelf sediments seas and Cooper *et al* (1980) showed that many species must have lived at depths less than 200m, particularly the biserial species which are the focus of this study.

Finney and Berry (1997) refined this model through more detailed analysis of the precise location of graptolite-rich beds. Their studies revealed that graptolite preservation was concentrated at the palaeo-shelf edge where there would have been a rich supply of nutrients (and consequently phytoplankton) supplied by an upwelling zone. They compare this distribution, where planktonic diversity is concentrated along the shelf edges, with the ocean distribution of modern plankton. The upward movement of the upwelling oceanic waters could also have provided bouyancy to the graptolite colonies living in these regions.

The size of currents and scale of turbulence is given in table 2.3 for a variety of modern ocean depths and environments. These values are used to provide similar estimates for the velocity and turbulence of flow in the Palaeozoic oceans.

Environment	Scale of turbulence	Rot'n rate (rad/s)	Speeds at small scale (m/s)	Flow Re at small scale
Shelf waters				
0-200m	6mm-20m	3.2	0.1	1000
Open ocean				
0-100m	10mm-11m	1.0	0.05	500
100-300	19mm-2m	0.2	0.02	200
300-600m	61mm-0.21m	0.03	0.005	50

Table 2.3: The scale and rates of currents and turbulence within different ocean environments. Data taken from Jenkins (1997).

That ocean currents should provide the dominant effect on graptolites is supported by the physical experiments of Rigby and Rickards (1989). These experiments were largely performed in still water, based on a study of diurnal sinking and rising in comparison with modern zooplankton. When the 1:1 scale models were put into nearshore, wave influenced, ocean waters; the models (multiramous planar forms) were observed to align themselves with the current and spiral horizontally (Barrie Rickards, personal communication). It can be concluded that both diurnal movement (through passive density changes) and prevailing currents would have affected the rhabdosome but observation of alignment into these larger flows suggests that they may have been more influential and may give a reasonable estimation of rates of flow for modelling purposes.

This study assumes the simplest case scenario of a passive graptolite reacting to the action of ocean currents. It is envisioned that graptolites would have been caught into a turbulent flow and would have rapidly re-aligned to the flow (Jenkins 1997) and then have accelerated towards the flow velocity, before being caught by another

turbulent whorl. The scale of shelf turbulence is 6mm-20mm (table 2.3); larger than typical juvenile colony length (4-5mm) but of a similar scale to that of more mature biserial graptolites (Jenkins 1997).

How broad was the range of velocities to which graptolites were exposed?
It seems inevitable that graptolites would have been exposed to environments producing a range of Reynolds numbers as water conditions changed, as their own velocity varied and even as growth changed the colony size and shape. Stormy conditions may have increased the current velocities, within the top 200m of ocean waters, by as much as ten times.

Functional structures would have needed to be robust to quite extensive changes in Reynolds number, and would have operated at several size scales.

Supporting evidence for the broad Reynolds number tolerance of graptolite shapes, can be obtained from the range of scales at which apparently identical structures are observed in graptolites. For example, *C. inuiti* and *O. gracilis* both have the same pattern of proximal spines (medial spine on th1[1] and a pair of anti-virgella spines), but vary in size by a factor of two. A more extreme example of this is the thecal hooks of *Monograptus flemingi* and *Monograptus limatulus*, exhibiting the same shape at times ten scale difference. This assumes that a structure built on two species of graptolite, having the same shape and in the same relative location, would have had the same function in both cases, such that the thecal hooks of *Monograptus flemingi* and *Monograptus limatulus* acted on a fluid flow in the same way over a Reynolds number variation of at least times fifty.

2.5. Estimated Reynolds numbers

An estimated value of the range of Reynolds numbers that would have been experienced by living graptolite is required. Using ocean environment data from section 2.4.3, sinking rates from previous experimental studies and swimming rates of modern organisms a variety of possible Reynolds number estimates are calculated and discussed.

For these Reynolds number estimates the density and viscosity of Palaeozoic seawater is assumed to be the same as the modern ocean, and is therefore known. It is the flow velocity, U, and Characteristic length, l (figure 2.9), which are unknown values and must be assessed. The flow velocity might be predicted using a number of comparisons: sinking rates of models and specimens, swimming rates of modern zooplankton and ocean current velocities. Characteristic length (l) will be dependent on the graptolite shape and orientation.

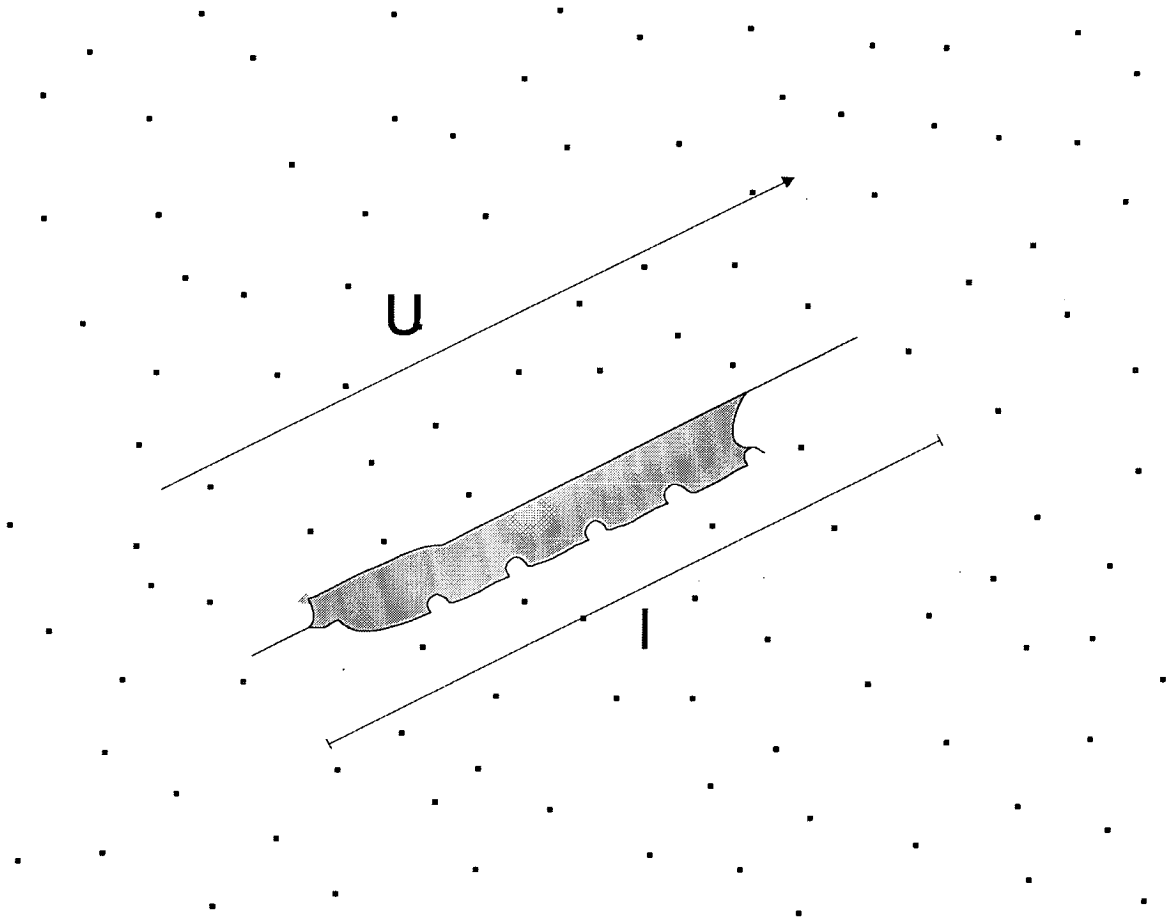

Figure 2.9: A diagram showing the characteristic length (l), along the direction of flow (U), of a graptolite colony, which is used to calculate the Reynolds number.

The 'real density' scale models built and tested by Rigby (1990) all sank at rates around $0.08ms^{-1}$ through still water. However even active modern swimming plankton cannot achieve this speed for diurnal migration (diurnal migration: 0.004 -

0.055 m/s). The water used in Rigby's experiments was still. Observations of isolated specimens have shown small turbulence, as would be expected in a real ocean, prevents sinking. Prof. Van Andel (Department of Earth Sciences, University of Cambridge) and Dr Leach (Oceanography Department, University of Liverpool) both recommended an experimental flow velocity of 0.1 m/s, based on shelf currents of 1m/s (largely tide influenced) with turbulence at 0.1 m/s. This also agrees well with Jenkins' small scale current velocities (Section 2.4.3).

Reynolds numbers are calculated using these flow-rate values for a scandent graptolite. The graptolite is assumed to align with the flow such that the colony length corresponds to the characteristic length l in the Reynolds equation. Scandent colonies are typically 1-100mm long.

Calculations for a scandent colony of length 1-100mm.	Flow velocity, U (m/s)	Reynolds Number
Diurnal migration	0.004-0.055	4-5000
Test model sinking velocities	0.08	80-7000
Small scale ocean current	0.1	100-10000

Table 2.5: A range of possible flow velocity estimates and corresponding Reynolds numbers for a scandent colony of length 1-100mm.

The average size of specimens considered in this investigation was approximately 4 mm. Assuming that small scale ocean currents (0.1 ms^{-1}) provided the dominant flows acting on the colony, or in rare still conditions sinking or fast migration velocities (0.055 - 0.08 ms^{-1}), a scandent colony of this length (aligned to the flow) would have experienced a Reynolds number of 200 - 400. This represents the middle ground of Reynolds number estimates, ignoring the end members predicted by slow diurnal migration rates and stormy (high turbulence) ocean conditions.

2.6. Conclusions

Any two fluid / object interactions working at the same Re (with an object of the same shape although at a different scale) will produce the same fluid flow pattern independent of scale. As a result scaled models, tested in air or oil, are a valid means to investigate flow patterns around graptolites in water. In order to do this the range of Reynolds numbers that living graptolites might have experienced must be estimated.

This Reynolds number is calculated using equation (8), where U is the free-stream velocity, l is the characteristic length of the graptolite parallel to the flow, and ρ and μ represent the density and dynamic viscosity of the fluid.

$$\mathrm{Re} = \frac{\rho l U}{\mu} \tag{8}$$

These calculations have assumed that the Palaeozoic ocean would have had very similar fluid properties (density and dynamic viscosity as a result of salinity) to the modern ocean. Values for a warm, tropical ocean at 20°C are used. It has also been assumed that ocean currents (small-scale currents ~0.1m/s) would have provided the dominant flow velocity (U) influencing graptolite reactions and motion, and that these would have been of a similar scale to small-scale currents in the modern ocean. This lead to a predicted Reynolds number range 200 to 400 for a 4 mm scandent graptolite.

The broad bands of Reynolds numbers, corresponding to essentially similar flow patterns, were investigated in section 2.3.2. This has indicated that the flow patterns are consistent within a range of wind tunnel velocities from 0.1 to 2.0 ms^{-1}, corresponding to a Reynolds number range from 1000 to 20,000, and probably over a greater range than this. It is not clear that the flow patterns will remain consistent down to the lower Reynolds numbers estimated to have been the typical experience of a graptolite (Re 200 to 400). Values of 1000 are within the greater estimated Reynolds number range experienced by a graptolite under the influence of small-scale ocean currents (section 2.5: Re 100 to10000).

Experiments carried out at the higher Reynolds numbers (Re 1000 to 20,000) are valid for modelling graptolites under the influence of small-scale ocean currents, as is assumed by this study. It is not clear that flow patterns predicted would have also occurred at the lower Reynolds number estimates, but these experiments may still provide valuable insight.

3. Experimental techniques:

3.1. Introduction:

This study involved a variety of techniques for investigating and viewing flow patterns. The majority of methods used were qualitative, including the Cambridge wind tunnel and tests in tanks of oil and seawater; some were more quantitative, including laser Doppler anemometry (LDA) work using the Bristol wind tunnel and computational fluid dynamics (CFD).

The Bristol wind tunnel, and LDA system, was the original investigation point of the project, following work by Rickards *et al* (1998), and this work was extended further using another wind tunnel in Cambridge. This second tunnel allowed more direct visualisation of the airflow using smoke streamers.

The wind tunnel work focuses on the effect of an object on the flow. The orientation of a model was fixed, and without more information about the density distribution and natural centre of rotation of a living graptolite it would not be realistic to allow the model to move freely in the airflow. Consequently a realistic alignment was required for testing, and in many cases a model was observed with the airflow impacting from several orientations. This static work was complemented by tank experiments (seawater tank and oil tank) which focus on the effect of a flow on the object. These experiments allowed the object to move freely, providing clues to the natural life orientations of the graptolite when alive.

3.2. Wind tunnels:

Although it is counter-intuitive, it was demonstrated in section 2.3.1 that a model of an object naturally found in seawater should be fourteen times larger when testing in a wind tunnel. This is a result of the change in density and dynamic viscosity from water to air, and allows reasonably accurate models of tiny organisms to be constructed for testing.

The times fourteen scaling factor only applies if the same flow velocity (ocean current to wind tunnel free airstream) is maintained. Wind tunnels are more commonly used to test the fluid dynamics of vehicles, or buildings in strong winds, and consequently are normally run with a high flow rate. The flow velocities required to investigate graptolite dynamics are considerably lower, of the order of 0.1 – 1 m/s, and there are few wind tunnels that are capable of maintaining a stable laminar flow at these low speeds. Although a laminar flow is obviously not a natural condition, this simplified case is used to observe object-flow interactions. If a faster free-airflow is used, then in order to reproduce the 'correct' Reynolds number a smaller scale model must be used (given that the fluid properties within a wind tunnel cannot be varied significantly).

The modelling materials and complexity of the graptolite limit model scales. However an exactly 'correct' Reynolds number is not a significant concept with regards to these experiments, where it has been shown that flow behaviour falls into broad bands (section 2.3.2). A high wind tunnel flow speed will only represent a problem if it is several orders of magnitude greater than predicted small-scale ocean currents.

3.2.1. Bristol wind tunnel and LDA.

The Bristol wind tunnel is capable of producing a stable airflow down to 0.1 m/s, and the flow velocities within the tunnel are observed using LDA (laser Doppler anemometry). This technique is very accurate and is also non-invasive; i.e. measuring the velocities does not affect the flow in any way, unlike methods which introduce probes or instruments into the tunnel.

Approximate Reynolds number

(for models of length 0.15–0.2 m)

$$\mathrm{Re} = \frac{\rho l U}{\mu} = \frac{1.205 \times 0.15 \times 0.1}{18.08 \times 10^{-6}}$$

Re ≈ 1000

Air 20°C:

Density = 1.205 kg/m^3

Viscosity = 18.08 x10^{-6} PaS

Freestream velocity = 0.1m/s

A Reynolds number of 1000 lies within the estimated Re range calculated for graptolite specimens under the influence of small-scale ocean currents (Re 100 to 10,000: section 2.5). These values lie outside the range predicted as that which might have been more typically experienced by a graptolite colony (Re 200 to 400). However it has been shown that these experiments are robust over a large range of Reynolds numbers (section 2.3.2: Re 1000 to 20,000) and consequently the Cambridge wind tunnel experiments are also valid for investigating graptolites (section 2.6).

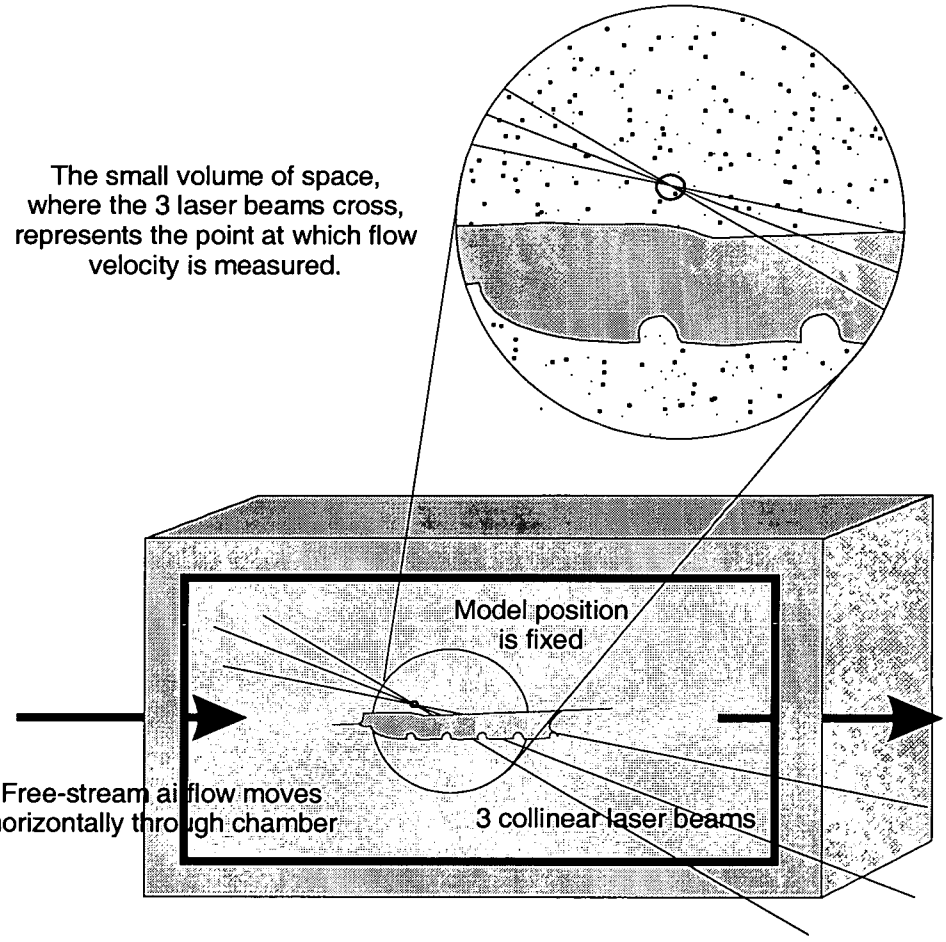

Figure 3.1: A schematic diagram of the Bristol wind tunnel and LDA system. Three colinear laser beams measure the flow at the point at which they all intersect.

The LDA system uses the differential Doppler technique (Drain 1980). Smoke particles (vaporised mineral oil) are introduced to the airflow over the object, and

three non-colinear laser beams (three-component Dantec system) are directed to a point in space where the flow velocity is measured (figure 3.1).

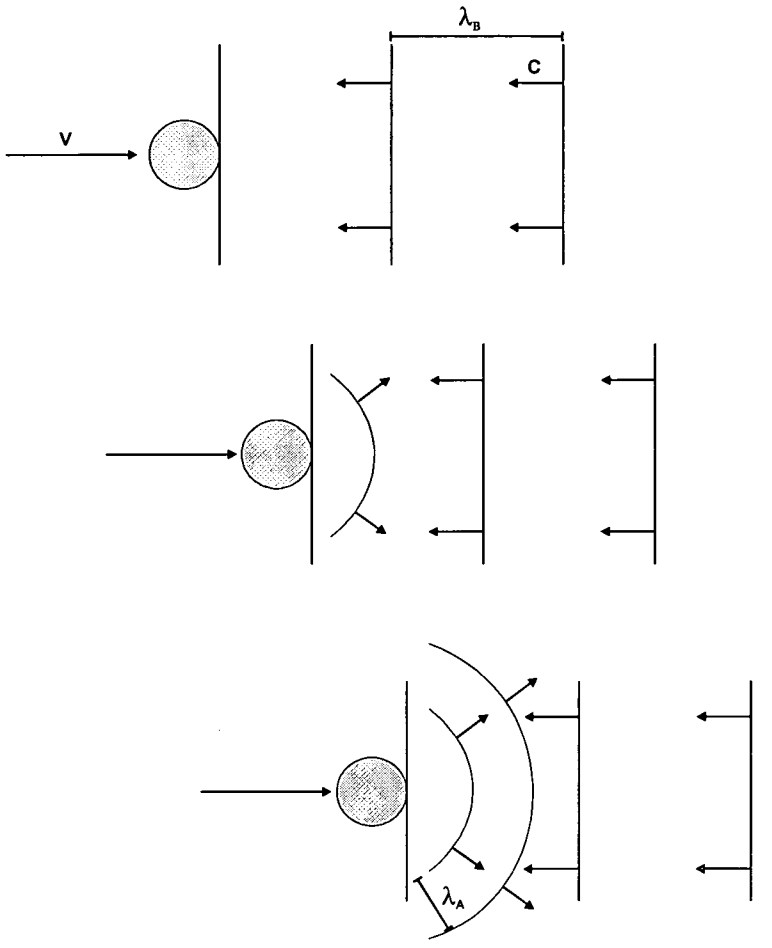

Figure 3.2: The Doppler effect.

a.Wave fronts, at separation λ_B and moving at velcoity c, approach a particle also moving towards them at velocity v.

b. When a wavefront reaches the particle it is reflected.

c. By the time the next wavefront reaches the particle and is reflected, the particle has moved closer to the waves and consequently the distance between the reflected wavefronts (λ_A) is smaller than that between the impacting wavefronts (λ_B). This represents an increase in frequency that can be detected and measured.

The velocity of the particle is given by: $v = c\left(1 - \frac{\lambda_A}{\lambda_B}\right)$

As particles cut the beams (all three beams must be cut simultaneously to ensure the particle is moving through the precise point observed) the Doppler shift of the

reflected beam is detected. This Doppler shift can be used to calculate the component of particle velocity along the laser beam, and hence that of the airflow (figure 3.2). The values from the three beams are combined to give a three-dimensional airflow velocity. The system calculates the average velocity calculated from a large number of particle detections, and the stability of the flow can be assessed from the variation. This increases the accuracy of this technique, but also slows the gathering process; each plane of data takes one to two hours to collect.

The LDA produces quantified 2D images of flow within, and through, any plane intersecting the model, provided that all three lasers have a clear path to all points in the plane. Data were then processed using TECPLOT.

The Bristol tunnel was able to run at low velocities (down to 0.1 m s^{-1}) which made it ideally suited to the purposes of the project, but the system is very expensive and complex, an experienced operator was required. The LDA is limited to looking at only the flow through (and within) a few planes, and it is difficult to visualise the overall pattern of flow over the graptolite from these isolated pieces of data.

3.2.2. Cambridge Wind tunnel

The quantitative results from Bristol were extended by more qualitative wind tunnel work in Cambridge. The University of Cambridge, Department of Engineering, provided access to a smaller wind tunnel. During this study the wind tunnel was run at velocities between 0.5 and 2.0 m s^{-1}.

Approximate Reynolds number

(for models of length 0.15–0.2 m)

$$\mathrm{Re} = \frac{\rho l U}{\mu} = \frac{1.205 \times 0.15 \times 0.5}{18.08 \times 10^{-6}}$$

Re ≈ 5000

Air 20°C:

Density = 1.205 kg/m^3

Viscosity = 18.08 x10^{-6} PaS

Freestream velocity = 0.5m/s

A Reynolds number of 5,000 lies within the estimated Re range calculated for graptolite specimens under the influence of small-scale ocean currents (Re 100 to 10,000: section 2.5). These values lie outside the range predicted as that which might have been more typically experienced by a graptolite colony (Re 200 to 400). However it has been shown that these experiments are robust over a large range of Reynolds numbers (section 2.3.2: Re 1000 to 20,000) and consequently the Cambridge wind tunnel experiments are also valid for investigating graptolites (section 2.6).

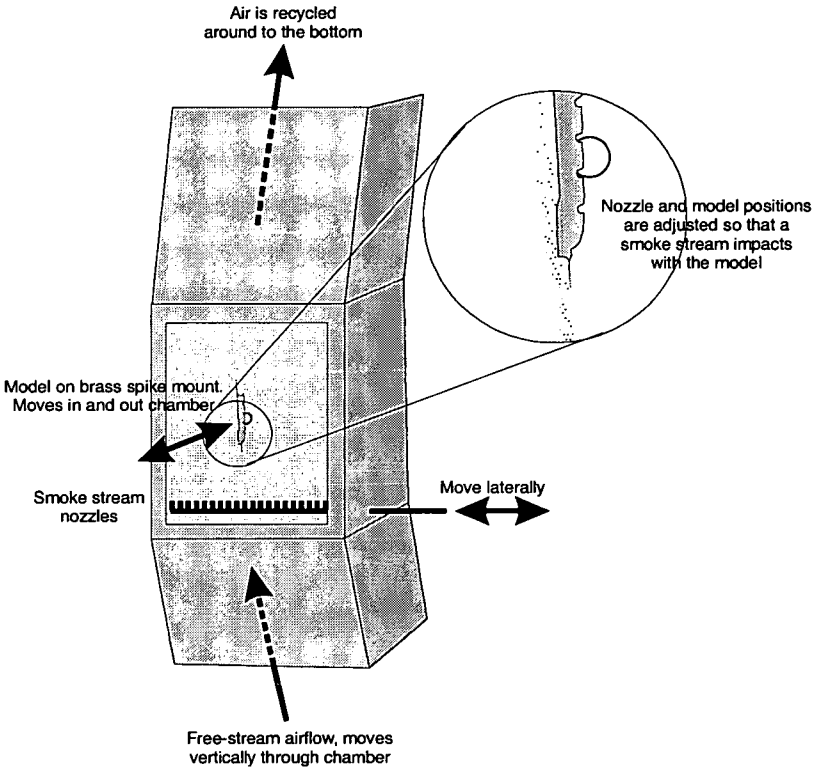

Figure 3.3: A schematic diagram of the Cambridge wind tunnel. The nozzles that release smoke into the chamber can be moved laterally. The model is mounted on a spike through the back of the chamber and can be moved further in or out. Using a combination of these two movements a model is positioned such that a smoke stream impacts with a structure of interest allowing the flow over the structure to be observed.

Airflow patterns are visualised using smoke streams and these are photographed using a digital camera and processed to disc. Similar to the LDA system, the smoke stream method is non-invasive and has no effect on the flow. Using this method the

entire pattern of flow can be seen in three dimensions, but this is not a precise technique, and accurate velocities cannot be measured.

A line of small nozzles, along the bottom of the viewing box, release paraffin smoke into the airflow. The nozzles are aligned with the vertical airflow and are shaped to disturb the laminar flow as little as possible. The test model is fixed to a brass spike mounting which passes through the back of the wind tunnel chamber. The nozzles can be moved laterally across the box to move the smoke-streams, and the brass mounting spike can be rotated or moved further in or out of the box to alter the position and orientation of the test model. The affect of the graptolite on the flow is investigated by moving the model, and the smoke streamers, so that a smoke stream impacts with a structure, or part of the graptolite, which is being observed (figure 3.3).

The Cambridge wind tunnel is easily operated, without additional help, making this method much simpler, cheaper and quicker than using the LDA. Visualising the broad pattern of flow over the graptolite shape, rather than focussing on the flow through a particular point or plane, is more useful for a general investigation of hydrodynamics, prior to focussing on a particular structure.

3.3. Tank experiments:

The tank experiments complement those using the wind tunnels. In the wind tunnel the models were always held in a fixed orientation, and the effect of the graptolite on the flow was observed. In contrast, graptolites and models are entirely free to move within the tank, and it is the effect of flow on the graptolite that is observed. The tank experiments also support the wind tunnel experiments by confirming likely life orientations to flow. The wind tunnel can be used to further investigate what causes motion observed in the tank experiments.

When experimenting with fluids in a tank, it is important to be aware of edge effects. Shear forces within the boundary layer, forming as a result of the tank walls, tend to hold an object close to the wall surface. These forces will also affect orientation and movement as the object is no longer free to move as it would be in the open ocean, where such edge effects are rare. The majority of tank experiments were carried out under still conditions, quite different from the turbulent environment in the ocean. The experimental work of Rigby and Rickards (Rigby and Rickards 1989, Rigby 1990, 1991 & 1992) was criticised by Jenkins (1997) for this disregard of ocean turbulence. The still tank experiments observe the simplified case of a laminar flow acting on an object, where sinking under gravity acts as a proxy to a simple flow. Experiments were also carried out in moving fluids to 'ground-truth' the still-water experiments.

The velocity of a sinking object cannot easily be controlled in order to produce a reasonable Reynolds number (within a broad band of flow pattern behaviour). However the tank experiments were relatively simple, consequently they can be adjusted and repeated many times until a valid balance of fluid properties and sinking rates could be achieved.

3.3.1. Seawater tank

The seawater tank was used to test chemically isolated graptolite specimens. The use of real, unflattened, specimens and seawater ensured that the scaling of the graptolites and fluid properties were as close to a realistic situation as possible. Similar tests were carried out by Rickards and Crowther (1979) using pieces of broken graptolite stipe dropped through a column of water. This work focuses on complete specimens of juvenile colonies.

The graptolite specimens were isolated from Cornwallis Island (Arctic Canada) concretions by dissolving the limestone overnight in 40% hydrochloric acid. All the specimens isolated were late *riccartonensis* Biozone monograptids (except for a

single diplograptid specimen). Other isolated specimens (diplograptids and dichograptids) were borrowed from the Sedgwick Museum, Cambridge.

These experiments have assumed that the original colony density, and mass distribution, was not greatly different from that of the isolated specimens. The density of an isolated graptolite is approximately 1.2 kgm^{-3} (Rigby & Rickards, 1989), which is consistent with that of living relatives, *Cephalodiscus* and *Rhabdopleura* (Dilly 1993). Typically the soft tissue of modern plankton has approximately unit density, and consequently it is unlikely that the addition of graptolite soft tissues would have had much effect on the density distribution of the colony.

Approximate Reynolds number

(for specimens of length 1.5–7mm

$$\mathrm{Re} = \frac{\rho l U}{\mu} = \frac{1.024\mathrm{x}10^{3}\,\mathrm{x}0.005\mathrm{x}0.05}{1.072\mathrm{x}10^{-3}})$$

Re ≈ 250

Seawater 20°C:

Density = 1.024×10^{3} kg/m^3

Viscosity = 1.072×10^{-3} PaS

Sinking velocity ≈ 0.05m/s

This lies well within the estimated range of Reynolds numbers for living graptolites under the influence of small-scale ocean currents (section 2.5: Re 100 to10000), and is compatible with the middle range values chosen to represent more typical graptolite Reynolds numbers (section 2.5: Re 200 to 400).

The specimens used were photographed and drawn, then washed thoroughly in seawater before testing. The washing of test specimens is an important stage of these experiments; reactions between any residual acid (or glycerine) and the tank seawater causes micro-turbulence around the specimen and leads to very erratic, and rapid, falls.

The orientations of these isolated specimens were observed as they sank freely through a tank of seawater (figure 3.4) at room temperature (approximately 20°). These experiments used a cylindrical tank; diameter 16cm, depth 9cm; large enough to avoid any edge effects with specimens up to 5mm long. The specimens sink under gravity, causing the fluid to move upward relative to the graptolite. The tank was backlit by a powerful light to aid observation of orientation. Each specimen was dropped several times until three consistent falls were observed, or it was clear that orientation was erratic and would not be repeated. Observations made by eye included; the orientation of the specimen (ϕ), the relative positions of the virgella, virgula and thecae, the stability of the graptolite in this orientation and how rapidly the alignment occurred. These observations were all subjective such that the error of recorded angles is of the order ±5°.

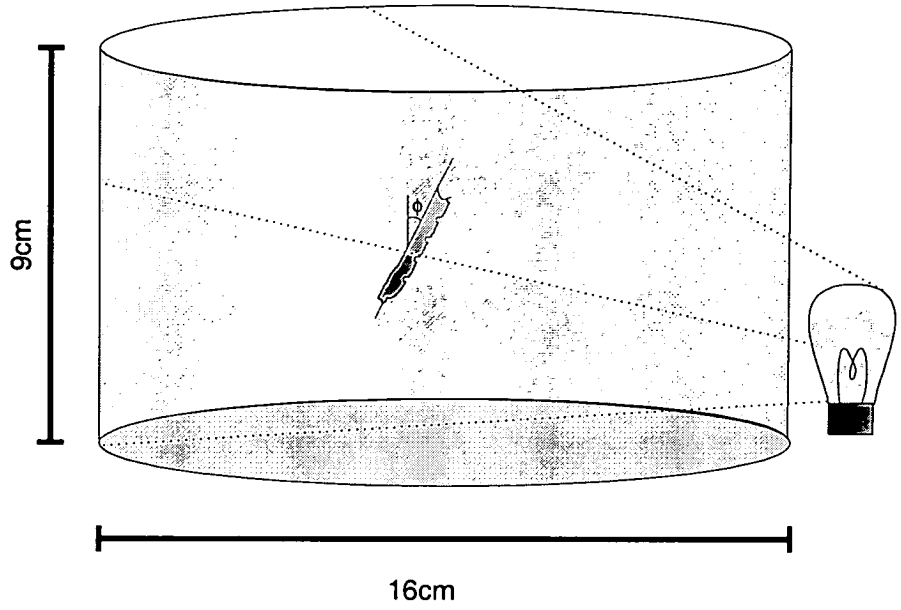

Figure 3.4: The seawater tank experiments. Isolated specimens are allowed to sink through a tank of seawater (16cm diameter, 9cm depth), large enough to avoid edge effects. The angle of the specimen from vertical (ϕ) is measured as it sinks.

The seawater tank experiments were valuable as they allowed observation of real specimens in a relatively realistic environment. This method was limited by the low numbers and variation of specimens, and a lack of genuine turbulence.

3.3.2. Oil Tank

The oil tank experiments greatly extended the seawater tank experiments. Not many species are available as isolated specimens. Those that can be isolated are only preserved in small numbers and individual specimens are often incomplete. Graptolite models were tested in order to gain information about the orientations, and movement under flow, of a wider range of graptolite colony shapes.

It is unrealistic to attempt to build models at the scale of real specimens, and early attempts to experiment using larger models in water were unsuccessful. The models were too flat and light, acting as aerofoils and producing lift, and consequently they all sank like a sheet of paper through air. More three-dimensional models fell too rapidly. The orientation of sinking monograptids, which was known from the

seawater tank experiments, acted as a sort of benchmark. The tank experiments using models could only have validity if they agreed with the tests using real graptolite specimens.

The water was exchanged for rapeseed oil. Oil has a much greater viscosity than seawater, but lower density, allowing larger models to be tested at approximately the same Reynolds numbers the living graptolites might have experienced. The higher viscosity also led to a slower sinking rate allowing model size to be increased further.

Approximate Reynolds number

(for models of length 0.05-0.1m)

$$\mathrm{Re} = \frac{\rho l U}{\mu} = \frac{0.97\mathrm{x}10^3\,\mathrm{x}0.05\mathrm{x}0.5}{0.16}$$

Re ≈200

Rapeseed oil:

Density = $0.97\mathrm{x}10^3$ kg/m^3

Viscosity = 0.16 PaS

Sinking velocity = ~0.5m/s

This lies well within the estimated range of Reynolds numbers for living graptolites under the influence of small-scale ocean currents (section 2.5: Re 100 to10000), and is compatible with the middle range values chosen to represent more typical graptolite Reynolds numbers (section 2.5: Re 200 to 400).

Because the density distribution along real graptolite specimens (and hence living graptolites) is unknown, it is impossible to produce accurate free-moving models. These experiments were limited to very simplified models, but these can still provide valuable insight. Observations were made largely by eye and little attempt was made to quantify anything, since these experiments are too crude and purely qualitative.

The models were allowed to sink through a large cylindrical tank of vegetable oil: diameter 20 cm, depth 28 cm. This was sufficiently large to avoid edge effects using models 5-10cm long (provided the long models did not sink horizontally). If a model sank too close to the tank walls the test was discounted and repeated. Observations were made of; the re-alignment of the model as it sank, rapidity of alignment, any stable orientation chosen, and any additional motion resulting from the fluid moving

over the model (for example rotation). Specifically the final orientation of the model was noted in comparison with a protractor fixed to the side of the tank. The sinking time for each model was also measured, as was the time taken for the model to re-align to its final orientation where appropriate. The tests were repeated a number of times to ensure that results were consistent.

The oil tank allowed experimentation over a much wider range of graptolite shapes than the seawater tank, however these tests were of limited accuracy due to the crude nature of the models.

3.4. Computer modelling

Some attempts were made to model flow around graptolites using CFD (computational fluid dynamics). A temporary license was obtained for INCA (a CFD package which links into TECPLOT) to assess the suitability of these packages for obtaining realistic results.

CFD programmes are complex, even working in only two dimensions as was attempted initially. These programmes use a large amount of processing power, such that each computation runs very slowly. In order to calculate the predicted flow around an object, the object must first be mathematically described to the programme, and boundary conditions given. In order to test this package the graptolite shape was simplified to a series of rectangles. Even working with such a simplified case, it was difficult and time consuming. In the limited time available on the licence no realistic results were produced.

This method was rejected as too complex and time consuming, resulting in unhelpful, oversimplified results.

3.5. Simple mathematical models

This study includes a couple of simple mathematical models (section 5.6.2 and section 6.4.2) intended to enhance understanding of functional structures highlighted by other experimental techniques.

The results of the tank experiments and wind tunnel observations were used to identify possible key factors affecting (or controlling) the function of a structure. These factors were then written into a simple model in which the graptolite colony is typically reduced to a combination of cylinders or rectangular boxes, and may be only two-dimensional (section 6.4.2). The equations were basic, ignoring other environmental factors and the detail of the graptolite shape, focussing only on those that appear to be most important. Assumptions were required to simplify the problem and the effects of these should be properly considered when applying the results.

The numbers produced by these models have purely relative, rather than absolute meaning. The detailed input required for these models (for example: the energy cost of building a graptolite structure, energy gain from consumption of particles or the drag coefficient of a graptolite shape) is not available. Rather the relative values produced by different morphologies (lengths, widths and angles), allowed within the confines of the model, should be compared in order to determine what makes a structure more efficient or beneficial to the model colony. In this way predictions can be made about optimal morphologies (optimal spine lengths or angles; section 6.4.2), or linking particular morphologies to structures (robust colonies and vanes: section 5.6.2). Looking for these relationships and optimal value in the fossil record can then potentially test the model.

3.6. Summary:

The techniques used to investigate hydrodynamics were all limited by common problems of scale. In order to reproduce the correct Reynolds numbers, models had to be built on a small scale, and exposed to low flow velocities of air or water. This

limitation was relieved by an investigation into the sensitivity of flow patterns around an object to Reynolds number. A simple test demonstrated that the experimental methods used, as part of this project, need not be accurate to a precise Reynolds number; a value within an order of magnitude was sufficiently accurate (section 2.3.2).

A variety of experimental techniques were used to investigate the interactions of graptolites and flow. Each method complemented, and built on, work produced by another.

Work with the two wind tunnels was concerned purely with the effect of a graptolite colony (and its structures) on the flow passing over it. The Cambridge wind tunnel provided a general overview of the entire pattern of flow, visualised using smoke streams. The majority of the work was carried out using this tunnel which was cheap and simple to use. More quantitative data were provided by the Bristol wind tunnel, but this data was limited to flow through (and within) only a few isolated planes. The Bristol tunnel was also expensive and slow, and required an experienced operator. This greatly restricted the work that could be done on this machine.

The tank experiments allowed the graptolites to move freely, and were concerned with the effect of the flow on the colonies' movement and orientation. These experiments were all simple, cheap and repeatable. The seawater tank experiments were particularly valuable to this project. Experimentation with real specimens in a relatively realistic environment provided a benchmark for further tests using models. The low numbers and lack of variation of specimens available limited this method. The oil tank extended the free-graptolite tests over a much wider range of graptolite species. The accuracy of the oil tank method was limited by the crude nature of the models, and unknown weight distribution along a living graptolite colony.

The physical modelling was supported by simple mathematical models, constructed using information gained from the tank and wind tunnel investigations. The major strength of these models lie in their ability to make predictions beyond the scope of

the physical experiments. These predictions could then potentially be tested through fossil evidence providing a checking system for the experimental results and suggested functions. These models are very simplified and the results must be used only in consideration of the assumptions used to construct the model.

The use of computational fluid dynamics (CFD) was rejected. The programmes were complex to use, time consuming, and produced only very simple results.

4. Making Models:

4.1. Introduction:

This largely experimental project has relied on the use of reasonably realistic graptolite models for testing in wind tunnels and fluid tanks. As little is known about the living form of a graptolite, assumptions must be made based on extant relatives (*Cephalodiscus and Rhabdopleura*) and evidence from colony construction.
The degree of model accuracy required varies with the experimental method; what constitutes a reasonably realistic model must be determined, and modelling techniques devised to achieve this.

4.2. Limitations of accuracy:

Observations of graptolite hydrodynamics made through physical experiments using models and fluids other than seawater are valid provided the models are scaled such that dynamic similarity is achieved (section 2.3.1), given the experimental fluid properties and flow velocities available. Highly accurate models, which reproduce a precise Reynolds number, are not required, or realistic, as dynamic similarity is robust within broad bands of Reynolds numbers. Natural limitations are also imposed on the achievable accuracy of the experimental data by the nature of the experimental techniques used.

A precise Reynolds number is an unrealistic concept here; living graptolites would have encountered a range of Reynolds numbers within their lifetime due to growth and changing ocean conditions (section 2.4.3). Wind tunnel experiments (using a range of fluid flow velocities and model scales) have shown that the scale of a graptolite test model is not critical. The same flow patterns were observed, around a model graptolite, between Reynolds numbers of 1000 to 20,000 (section 2.3.2). The illustrated example of flow patterns around an infinite cylinder (Section 2.3.1 and figure 2.3) indicates that this range is probably a lot greater. This flexibility allows

the model scale to be determined by other factors such as complexity of the structures to be modelled, and the limitations on the techniques used. The models used in this study were all built to within an order of magnitude of the 'correct' scale.

A precise graptolite shape is also an unrealistic concept. Real graptolite specimens show natural variation within a species population, as would be expected from any living organism. Specimens of *A. maxwelli*, as illustrated by Walker (1953), exhibit a standard deviation of 10 – 30% from the mean lengths of spines and rhabdosome dimensions (figure 4.1). A percentage of this irregularity may be a function of preservation, but given that some must be a result of natural variation, it also confirms that a certain amount of deviation would not have detracted from the function of a structure. The models produced represented a possible graptolite, often an idealised case.

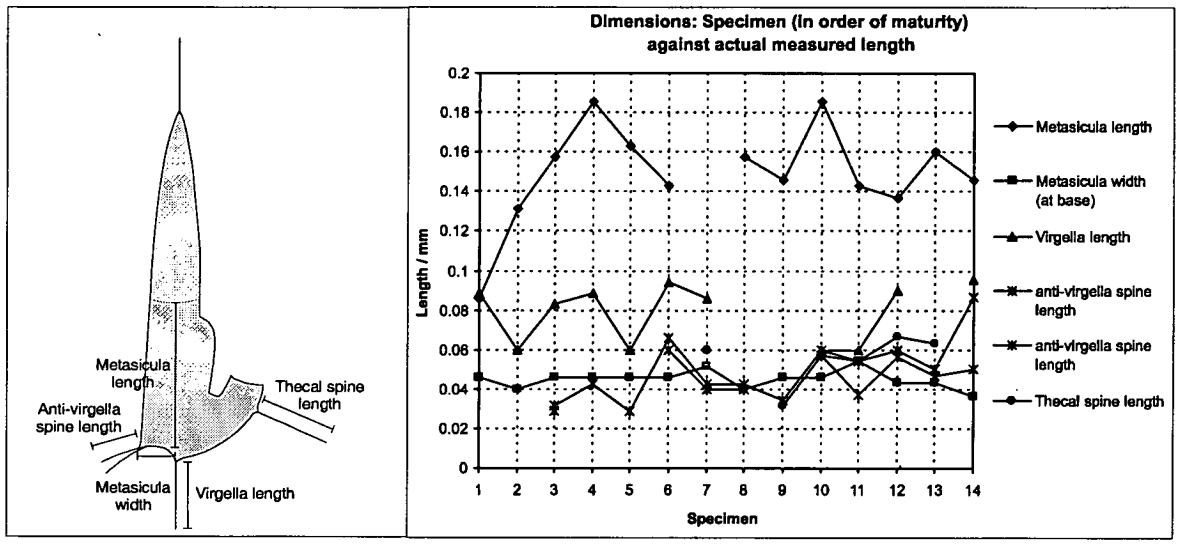

Figure 4.1: The dimensions (defined by the left-hand diagram) of a number of isolated specimens illustrated by Walker (1953) are measured and plotted in order of increasing maturity of the graptolite. Some of the early variability of these values may be due to continued growth, but the majority is due to the natural variation of specimens.

When making models it was important to consider the limitations of the experimental techniques used. Only models that could fit inside the oil tank or wind tunnel, with enough space to avoid the problems of edge effects, were valid for hydrodynamic

testing. This provided a natural upper size limit. The LDA system had a minimum model size limit below which the laser array was not effective (4cm). A minimum size was also considered for techniques in which observations were made by eye (the seawater and oil tank experiments) where orientation must be observable. The accuracy required of the models must be consistent with the accuracy of the experimental technique. The oil tank experiments were very crude, similarly crude models were appropriate, and time spent producing more accurate models would have been redundant.

A combination broad band Reynolds number variation, natural variation of specimens and the accuracy of the techniques used, limited the requirement to construct precise models. Models within an order of magnitude of the 'correct' scale, and representing an idealised specimen were deemed sufficiently accurate.

4.3. Soft Tissue:

Very little soft tissue has ever been found preserved in association with a graptolite fossil, and as a result little can be said about its living form. The addition of soft tissue could potentially have considerably altered the shape of a living graptolite, and models based only on the preserved skeletal remains might be very misleading. The evidence regarding the extent of soft tissue, and the possible effect such tissue might have on the hydrodynamics, must be considered.

Graptolite soft tissue could be divided into two types: extrathecal, which would have covered parts of the rhabdosome surface; and intrathecal, the zooids and any additional tissue within the rhabdosome. The two will be discussed separately here.

4.3.1. Extrathecal tissue:

Many graptolite workers have at some point postulated that the graptolite rhabdosome may have been entirely, or at least partially, covered with a thin layer of

extrathecal tissue (Rickards - discussion following Kirk 1969 and Bates and Kirk 1985). Such an external covering could clearly have significantly altered the external shape of the colony, and hence its hydrodynamic response.

Today there is little support for the concept of graptolite extrathecal tissue. Studies of the fine structure of the rhabdosome have shown that it is constructed from a number of layers, the outer one of which is built from large numbers of collagen bandages apparently plastered onto the external surface (figure 4.2). The presence of a soft tissue layer covering this external surface would have made access for secreting zooids impossible (Crowther & Rickards, 1977).

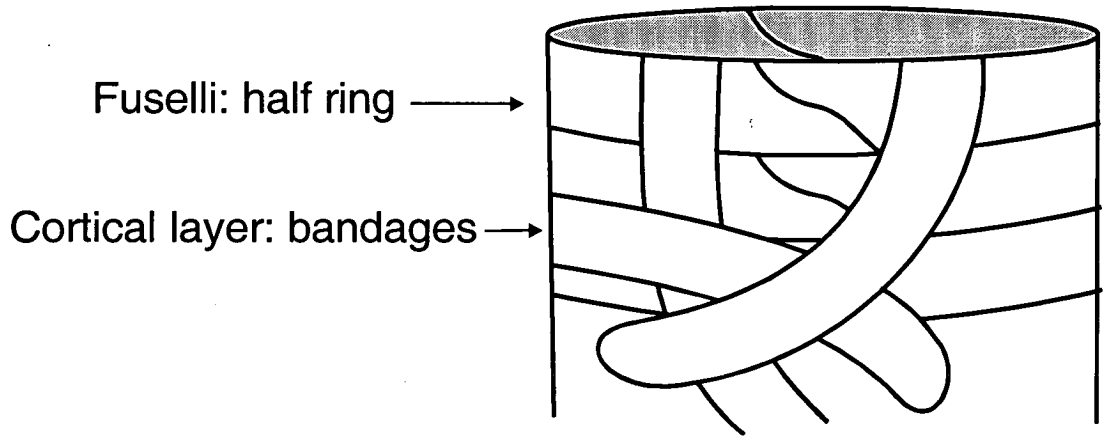

Figure 4.2: The rhabdosome is constructed in two stages. The colony shape is built up incrementally of collagen half-rings. Collagen bandages are then plastered over the external surface (and part of the internal surface).

Sue Rigby ignored the presence of extrathecal tissue for the purpose of her modelling experiments (PhD thesis 1990, Rigby and Rickards 1989). She argued that since the models without extrathecal tissue reacted in the water in a stable and consistent manner then the addition of such material was unnecessary; the colony form 'worked' without it (Rigby & Rickards 1989).

Extrathecal tissue will be ignored for the purposes of this project and the preserved skeletal form is assumed to represent the external shape of the living organism.

4.3.2. Intrathecal tissue:

The internal soft tissue of the zooids is more problematic. It must be assumed that zooids were present in a living colony but little is known about their shape, size or anatomy. It is generally excepted that graptolites have strong affinities with the extant *Rhabdopleura* and *Cephalodiscus* (Dilly 1993), due to the close similarities of their skeletal construction and colony organisation. Consequently the graptolite zooid is assumed to have been very similar in size and appearance to those of these living relatives (figure 4.3).

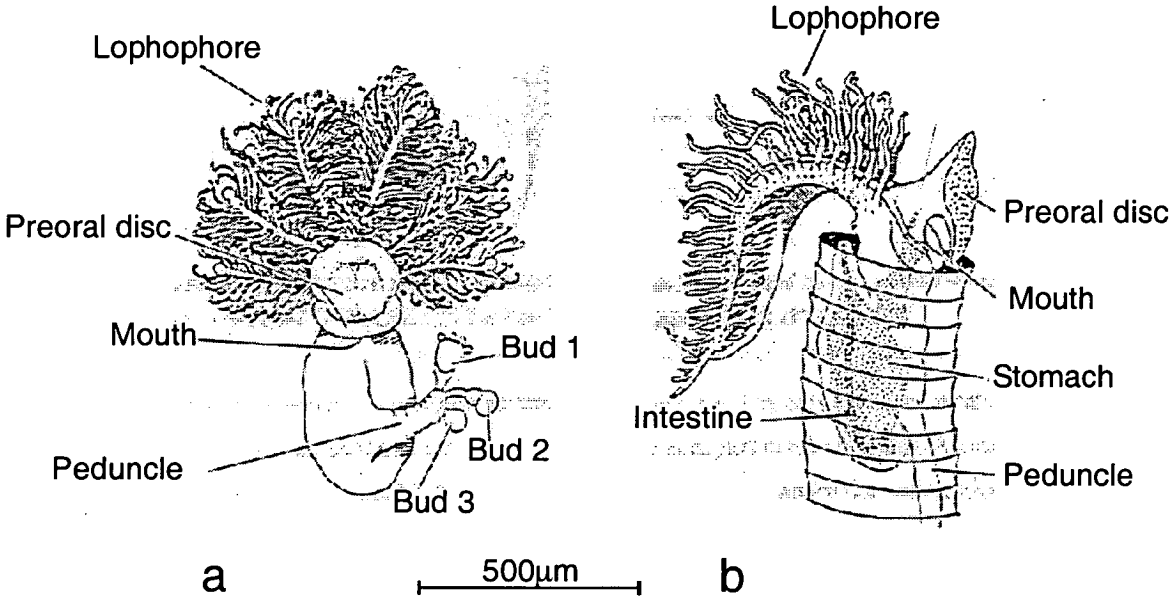

Figure 4.3: The zooids of living relatives of the graptolites, a. *Cephalodiscus* and b. *Rhabdopleura*, are the major source of information with regard to the possible nature of the graptolite zooid. Illustration taken from Rickards 1979.

The size of the living graptolite zooid is significant to this study. Clearly zooids retracted within the thecal tubes will have little effect on the external shape, and consequently the hydrodynamic response of the colony. It is not known how much zooid soft tissue would have projected beyond the thecal tube during feeding, and whether this, or zooids wandering the external surface to build, would have had a

significant effect on the hydrodynamics. The only direct fossil evidence for zooid size and shape is provided by preserved blobs of organic matter within the thecae. These are very rare and limited to dendroid specimens and *Psigraptus* only (Rickards and Stait 1984), the best preserved example of which (seen only as a nondescript black 'blob') is 700μm long (figure 4.4). Rigby and Sudbury (1995) attempted to predict the size of the graptolite zooid through a comparison of fossil graptolite fusellar increments and bandage widths to those of living *Rhabdopleura.* This data predicted a range of potential zooid size, which are consistent with that of the fossilised specimens (table 4.1).

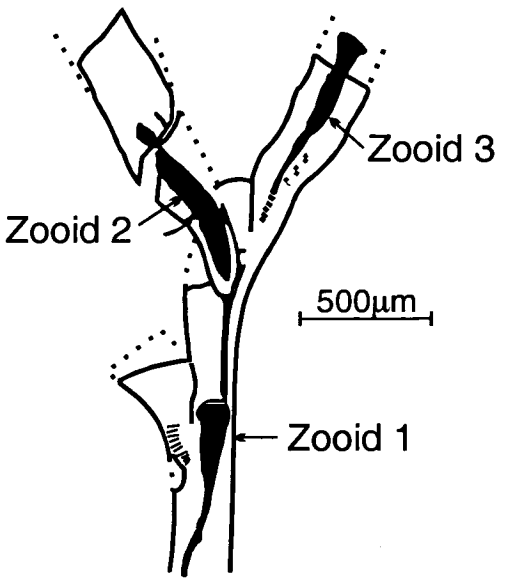

Figure 4.4: Sketch of a specimen of an early planktonic graptolite, *Psigraptus*. This fossil is one of the few examples where graptolite zooids have been preserved as 'black blobs'. Taken from Rickards and Stait 1984.

Zooid size calculated from bandage widths.	125 - 500μm
Zooid size calculated from fusellar increments.	400 - 1650μm
Observed fossilised zooid size	700μm

Table 4.1: The size of a graptolite zooid as suggested by different lines of evidence. Calculations from the bandage widths and fusellar increments carried out by Rigby and Sudbury (1995). Fossilised zooids of *Pristograptus* described by Rickards and Stait (1984).

The potential zooids (125-1650μm: table 4.1) are small enough that they would have had little effect on the colony hydrodynamics. Observations of flow round simple thecal shapes (Sue Rigby, *pers. com.*) shows the flow detaching from the thecal lip. Anything directly behind the aperture, in the quiet zone produced, would have had no effect on the flow; i.e. the zooid, or the thickness of the thecal walls (figure 4.5). A roaming graptolite would have had more of an impact on the flow but this would be variable and unpredictable dependent on the location of the zooid. Studies of extant *Rhabdopleura* and *Cephalodiscus* indicate that they only feed for a small percentage of the time (Noel Dilly, *pers. com.*), and are otherwise retracted into the thecal tube, or occupied in tube building. It is clear that the colony must 'work' hydrodynamically whether the zooids are retracted, feeding or building, the presence of zooids on the colony surface cannot disrupt this significantly.

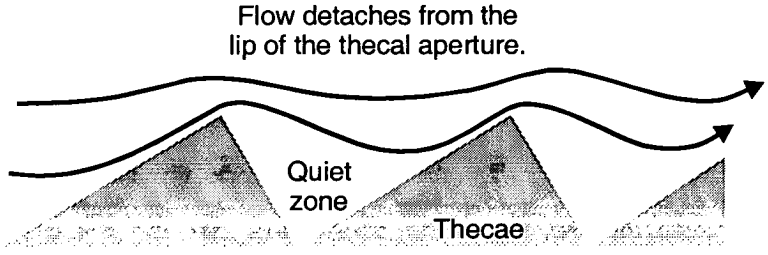

Figure 4.5: Schematic diagram of a flow running over a series of thecae. The flow runs up the ventral surface of the thecae and then detaches at the lip of the thecal aperture leaving a quiet zone directly in front of the aperture.

Intrathecal tissue (zooids) is not believed to have significantly altered the hydrodynamics of the colony and will also be largely ignored for the purposes of this project.

4.4. Wind tunnel models:

The majority of testing using models was done in the two wind tunnels (Cambridge and Bristol). Both tunnels observed the flow over the model; the Bristol wind tunnel providing a very accurate view of the flow through an isolated plane, the Cambridge tunnel giving a more general view of the overall flow pattern. Small-scale flow detail can be observed in both cases, as a result the models used must reproduce the graptolite shape accurately to a similar scale. The precision and scale of the models was affected by the experimental methods used, and modelling techniques were developed to ensure a sufficient degree of accuracy.

As previously discussed (section 2.3.1), models for testing in the wind tunnels (where fluid velocities similar to those which graptolites might have experienced in the oceans are used) should correctly be scaled at approximately fourteen times actual. However it has been shown that the scale of the test models is not critical, and the size restrictions imposed by the wind tunnels and modelling techniques were more significant. The upper size of models was limited by the size of the wind tunnel chamber. The viewing box of the Cambridge wind tunnel was 50cm by 65cm by 25cm. A model larger than this would not fit into the tunnel, and ideally a model should lie within the central third of the chamber to avoid any interactions with the tunnel sides (i.e. models for the Cambridge tunnel should be no wider than 16cm by 8cm). Models for the Bristol tunnel must be larger than 4cm in order for the LDA system to work effectively. A minimum model length of approximately 8-10cm (dependant of the complexity of the graptolite shape) was chosen as an appropriate and reasonable scale for modelling. This disparity did not cause a significantly large increase in Reynolds number, which would be increased by a maximum factor of 4 (this varies with the species and growth stage modelled).

Building the models on top of good line drawings, and photographs of real specimens, ensured accuracy. The drawings were photocopied to the scale required. Ideally pictures were required showing a number of different views of specimens (preferably including a cross section of the rhabdosome), in order to build an accurate three-dimensional model from flat images. Some distortion due to flattening

and poor preservation was inevitable, but well drawn, well preserved, specimens which had been chemically isolated from unflattened concretions were used whenever possible. Producing an idealised, composite, graptolite model from a number of different specimens and images reduced preservation effects.

The model graptolites were largely constructed from 'super sculpy', a professional sculptor's material that can be moulded like plasticine and then cured in a domestic oven. In some cases these were constructed around a wire frame to provide support.

All the graptolite species tested featured spines: nema, virgula, virgella and possibly further proximal or thecal spines. These spines could not be constructed accurately using super-sculpy, which was not strong enough to support such a thin structure. Instead copper, solder and fuse wire was used (these can be obtained in a variety of diameters) which was able support any spine length. This provided the models with additional flexibility where spine length could be easily altered, or the spine removed entirely, allowing a single base model to represent several species with different combinations and dimensions of spines. The wire produced a much more even and smooth spine than those built by real graptolites, however the model is an idealised one representing a reasonable approximation to reality.

The collagen rhabdosome is a remarkably thin-walled structure. This was impossible to recreate using super-sculpy. Instead the graptolite was modelled as a solid shape, with strong indentations representing the thecal apertures. The thickness of the thecal walls would not have affected the flow over a living graptolite as it would have detached from the lip of the thecal aperture (Sue Rigby, *pers. com.*), and would not have interacted with structures directly behind it. Very little flow would have entered the aperture. Modelling a graptolite as a solid shape was not a problem for the wind tunnel experiments where the models were fixed. In these cases the accuracy of the shape is significant but, as the model will not move in response to the flow, the weight distribution is not.

A model constructed from a combination of materials will exhibit a variation in surface textures, this could affect the hydrodynamics but this was not expected to be significant. Surface texture has a major effect only at Reynolds numbers close to the turbulent transition point. The majority of models were painted to produce a consistent surface, and this also reduced reflection interference when using the LDA array. Real graptolites were probably quite smooth; the external rhabdosome surface is constructed by means of a series of bandages secreted by the zooids. The collagen is extruded chemically from the pre-oral disk (comparison with *Rhabdopleura* and *Cephalodiscus*) and as a result of this process the molecules in the collagen 'bandage' are all aligned along its length.

The wind tunnel models represented an idealised graptolite built to a scale within an order of magnitude of times fourteen, such that the final model was 8-10cm long. The observation techniques used provided a detailed view of the flow patterns, consequently the models needed to be equally detailed, but the natural variation of a species population provided a natural limit to the degree of accuracy required. Correctly scaled line drawings were used to ensure accuracy, and only the external shape of the model was considered during construction.

4.5. Oil tank models:

The oil tank experiments were very simple. The movement of model graptolites was observed as they were acted on by a fluid, moving past the models as they sank under gravity. These tests did not provide a detailed view of the fluid reaction, or fine scale details of the model movement; only alignment to the flow, and simple rotation could be observed. Correspondingly simple models were appropriate, the detailed shape of the model was not significant, but rather the tests looked at the motion of a range of simple shapes that form the basis of a graptolite rhabdosome. In these tests the model was free to move as the fluid acted on it, and the weight distribution along the colony must be considered as it would have a significant affect on the motion.

The weight distribution along the model colonies had a significant effect on the motion within a fluid. It has commonly been observed that isolated graptolite specimens vary in colour along the rhabdosome length. The colour changes from black, or dark brown, to a translucent honey colour at the distal end, and serial sections through fossil specimens show that this is caused by a variation in collagen thickness. The periderm was considerably thicker towards the proximal where it was re-enforced by many layers of cortical bandages, as the colony was extended the number of these layers reduced and the structure became more delicate. Although the colony often became broader distally, the change in collagen thickness was such that the concentration of mass was located closer to the proximal end. Consequently the models were weighted towards the proximal end and the results compared with those from the seawater tank.

The 'correct' orientation of a monograptid colony sinking through seawater was known for the seawater tank tests, which used isolated specimens believed to have had a very similar weight distribution to that which would have been found in a living colony. In order for the oil tank models to represent credible graptolite colony responses, the scandent colony models tested in the oil tank were required to reproduce the orientations observed in the seawater tank.

Early attempts to build models demonstrated that the weight distribution was critical and that the models must also be realistically three-dimensional. Flattened models with an even weight distribution all sank horizontally regardless of shape. The final models tested were simple shape and mass representations of graptolite forms built from wire (solder and fuse wire of different diameters) and plasticine (or occasionally lead fishing weights). For example a simple scandent colony might be modelled as a plasticine weight with a projecting wire spine, representing the mass concentration of the colony and virgular spine projecting beyond.

The effects of different degrees of proximal end weighting, and variations in the precise distribution of this weight, were tested (section 5.4) in order to determine

how robust the oil tank experiments were, and how significant this might have been to a living graptolite.

Given that the majority of the models tested sank at approximately 0.5 ms^{-1} (and the density and viscosity of the rapeseed oil used) the models should be built at lengths 6 – 13cm in order to reproduce the predicted graptolite Reynolds numbers 200 - 400 for a 4mm length colony (section 2.5).

Approximate model length

(for Re values 200-400)

$$\mathrm{Re} = \frac{\rho l U}{\mu} \Rightarrow l = \frac{\mathrm{Re}\,\mu}{\rho U}$$

$$l \approx \frac{\mathrm{Re\,x0.16}}{0.97\mathrm{x}10^{3}\,\mathrm{x0.5}}$$

Rapeseed oil:

Density = 0.97×10^3 kg/m^3

Viscosity = 0.16 PaS

Sinking velocity = ~0.5m/s

$l \approx 6$ - 13cm

The crude nature of these experiments and the broad Re band behaviour of flow requires the models to be within an order of magnitude of this range only. The majority of models were built at approximately 6cm long.

The crude observations that were provided by the oil tank experiments warranted only simple test models. These concentrated rather on the study of simple shapes that provided the basis of graptolite colony forms. The distribution of weight along the colony would have had a significant affect on the motion of a graptolite in a fluid. The weight was believed to have been concentrated towards the proximal end of a living colony, and the distribution and degree of mass disparity was recreated and investigated using these models.

4.6. Theoretical models:

Two types of theoretical modelling were attempted within this thesis. One using sophisticated computational fluid dynamics (CFD), the other using a simple mathematical model. In both cases the model graptolite constructed was very basic.

4.6.1. Computer models:

The computer modelling program (INCA) included complex fluid dynamic equations and powerful mathematical solving capabilities. The program was limited to two-dimensional problems so the corresponding graptolite models were also two-dimensional. Potentially this program could have predicted the flow around a complex graptolite shape in some detail, however this would have taken considerable calculation time and computer memory. The CFD method was limited partially by this, and rather more by my ability to describe the details of a graptolite shape mathematically.

The model was constructed within the program as a series of defined points, with mathematically defined lines between them. These lines were combined to describe areas that were then gridded using a mathematical spacing rule defined by the user. The program predicted the flow through these grids given boundary conditions for each area. The process of constructing such a model is a long and complex process that is easily subject to small mistakes which then block the whole process. These problems led me to initially attempt a very simplified graptolite model in which the thecal-bearing colony was described as a rectangle with a long centrally located thin rectangle attached at one end (the virgula), and another thin rectangle attached offset from centre at the other (the virgella). The limited time provided by the licence did not allow the construction of more detailed models.

4.6.2. Mathematical models:

Two mathematical models were created for this thesis (sections 5.6.2 and 6.4.2). In both cases the equations used were very basic, ignoring many factors in order to simplify the situation such that it could be modelled. Consequently only a very simple model graptolite was constructed.

In order to input a realistic graptolite shape into the model it must first be described mathematically. This would have greatly complicated the equations within the model, making them impossible to solve by hand. Instead the graptolite is modelled as a combination of simple shapes which might easily be mathematically described. In both cases the model is reduced to two dimensions for simplicity.

The nema model (section 5.6.2) describes a graptolite colony as two rectangles. One for the thecal-bearing colony joined to another representing the nema. These rectangles are defined by their length and width, relative to each other, such that a range of graptolite morphologies can easily be modelled by varying these relationships. It is assumed that the details of thecal shape did not have any substantial impact on the role of the nema.

The proximal spine model (section 6.4.2) describes a spine in isolation. The colony shape is assumed to have had little impact on the function of the spine, given that it does not lie between the spine and the incoming flow. Although it is known that graptolite spines taper distally this was ignored for simplicity, and the spine was modelled as a rectangular rather than a triangular shape. It was assumed that the additional area provided by this blunt spine would not have a significant affect on the model predictions, given the simplicity of the equations used.

Both the theoretical models were very simple, reducing the graptolite morphology to a series of basic geometrical shapes. This was necessary in order to simplify the problem so that it could be solved mathematically, or within a reasonable length of

computor processing time. With a more powerful machine, and more time to construct a model, the model could approach the complexity of a real graptolite.

4.7. Summary:

Both extrathecal and intrathecal tissue was ignored for the purposes of this project. There is no convincing evidence for the presence of extrathecal tissue, and the zooids are not believed to have been of a size to affect the flow pattern significantly. Although they may have had very small-scale affects on the flow, the hydrodynamics of the colony must also have 'worked' when all the zooids were retracted into the thecae. Models were consequently constructed on the assumption that the preserved skeletal form represented the external shape of the living organism

The precision of models built for this study need only be appropriate to the accuracy of the techniques used. This varied greatly between the wind tunnel investigation and oil tank experiments.

The wind tunnel experiments, which observed the flow over the graptolite shape, revealed finer scale details of the fluid motion than the oil tank experiments, consequently much more accurate models were required. Models were built to within an order of magnitude of the 'correct' scale (times fourteen: section 2.3.1) at a convenient size for the wind tunnel used and modelling techniques; approximately 8-10cm long. These models represented an idealised composite specimen. A combination broad band Reynolds number variation and the natural variation of specimens limited the precision required, but models were built as accurately as possible. This was achieved through the use of correctly scaled line drawings of specimens in several views, and the use of appropriate modelling materials (super-sculpy and wire of various diameters).

The oil tank experiments provided only a general idea of the affect of flow on the graptolite shape. The flow itself was not visualised and the movement of the model in reaction to the fluid was observed instead. Only simple models were required representing simple colony shapes, but as these models were free to move the weight

distribution must be realistic. Observations of isolated specimens show that the greater mass of collagen is concentrated towards the proximal end, which is reinforced by many cortical layers. This mass distribution was modelled using plasticine weights on wire frames, and the degree of mass disparity (and distribution) required to reproduce observations from tests using real isolated specimens (seawater tank section 5.3.1) was investigated in order to test the validity of this method.

Both types of theoretical model (computational and mathematical) involved a very simplified representation of a graptolite constructed from basic geometric shapes. The mathematical models provide only a simplified view of the problem in order to be solvable, in which only the most important factors are considered. In this situation a simplification of the graptolite shape is appropriate. The time available and the processing power of the computer limited the complexity of the computational model. Theoretically much more detailed modelling should be possible.

5. The possible hydrodynamic function of distal structures on scandent graptolites

5.1. Introduction

The nema (*sensu lato*), a spine projecting from the distal end of a scandent colony, is a defining feature of the planktonic graptoloids. Common to nearly all species (Fortey and Cooper, 1986), the nema evolved from the benthic holdfast when graptolites moved into the open water early in the Ordovician (Rickards 1975). The free-living graptolites evolved through a wide range of colony morphologies. The initial planktonic species were cone-shaped, as were their benthic ancestors; through successive stipe (branch) loss they evolved rapidly through a series of morphologies to the simple, stick-like, scandent colonies (monograptids and diplograpids). As the nema was overgrown by the colony, it apparently re-evolved and was replaced and extended as the virgula (figure 5.1). In the Silurian the scandent spiralled forms evolved, producing large sub-horizontal colonies once more (Rickards 1975). The free nema (or virgula) persisted through all these changes in rhabdosome morphology, only rarely incorporated into the thecal wall, for example of *Dicranograptus* and *Oncograptus* (Rickards, 1996).

The virgulae of several diplograptid species are embellished by the addition of a vane. Biserial species with these structures were not abundant but examples can be found in a broad distribution of genera. The presence of a vane is not consistent; specimens of the same species might sometimes exhibit a vane, however such a vane would not typically be found on all specimens of the same species, many might have a simple nema only. Only a few species are always observed with a vane (Bulman 1964), for example *Orthograptus vesiculosus.* This may be an artefact due to the late development of vanes in the astogeny of some species.

This investigation focused on the function of the nema, and other distal spines and structures, through the experimental study of their hydrodynamics. The nature of these spines and structures and previous theories as to their purpose must first be considered.

5.1.1. Nema, virgula and cauda

The nema is a thin, collagenous tube that projects from the apex of the sicular cone. Despite differences of internal structure and secretion, the nema is often confused with other spinose structures; the virgula and the cauda (figure 5.1). The cone-shaped larval stage (prosicula) was secreted as one piece. This cone featured a pointed extension at the apex (the cauda or nema prosicula), which for some species was relatively long and spine-like (Hutt, 1973). The nema was built as a hollow tube extending from the tip of the cauda as the sicula lengthened incrementally (Hutt, 1973).

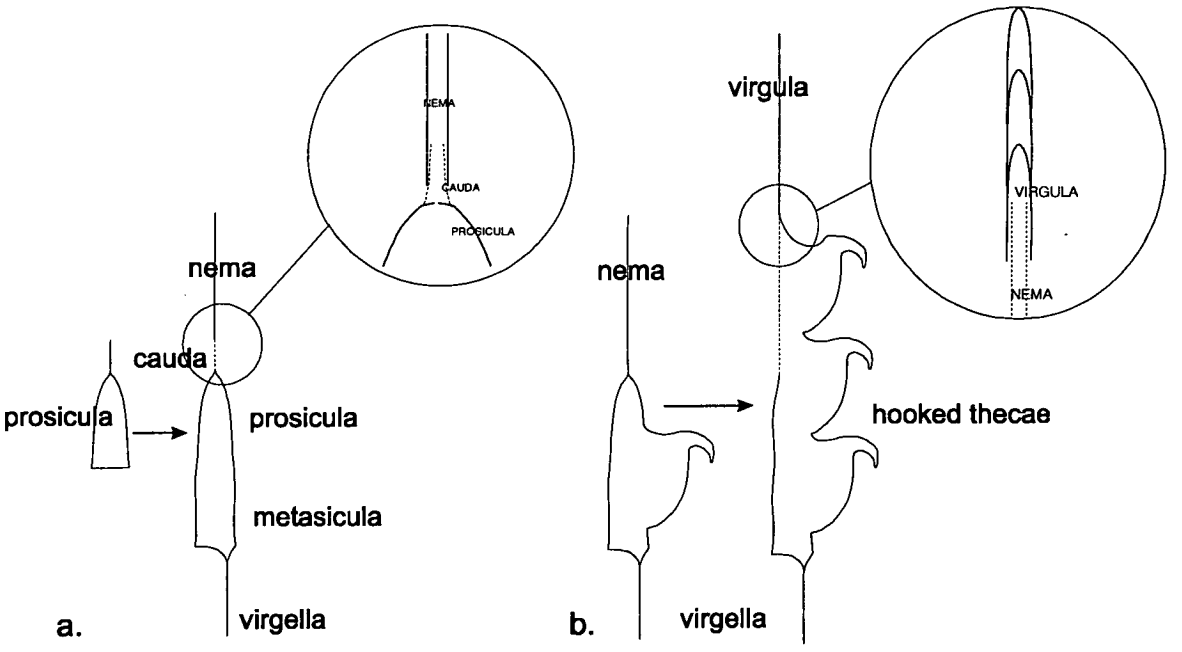

Figure 5.1: Cauda, nema and virgula.

a. The nema extends the cauda as the sicula increases length with the addition of the metasicula. Note the cauda and nema are hollow tubes.

b. The virgula extends the nema as the thecae overgrow it. The virgula is solid and built incrementally.

When graptolites became scandent the thecae were constructed back along the sicula towards the apex of the cone and eventually overgrew the nema. A freestanding spine was maintained in this position, even as the nema was overgrown, by the addition of a spike on the dorsal edge of the fusellar rings building the thecae. This spine, extending the nema, is the virgula, built incrementally from a series of these spikes (figure 5.1). The increments were added such that the nema/virgula maintained a free projected length beyond the distal end of the colony, construction would have begun as the thecae started to grow along the nema.

Despite these constructional differences the cauda, nema and virgula might be expected to act hydrodynamically in the same way; the nema extending the cauda as the sicula increases length, the virgula acting as an extension to the nema as it is overgrown by the scandent thecae. Assuming this, the nema, virgula and the cauda will be referred to as the *nema* throughout the rest of this chapter, for simplicity.

5.1.2. Functional morphology

There has been much speculation about the possible function of the *nema*. This speculation has fallen into three main ideas; suggestions that the *nema* was a point of attachment for the colony to an external object, that it was a tether for a float, or that it served a hydrodynamic function.

Lapworth (1897) believed that the graptolites were epiplanktonic; he suggested that the *nema* was a means of attachment to large floating algae. However there is no evidence of actual attachment (Bulman, 1964), and the geometry of some species makes attachment impossible without distortion of the *nema* or rhabdosome. This led Bulman (1964) to propose that the *nema* was a means of attachment to algae for the juvenile stages only. Perhaps influenced by the belief that many virgular structures were vesicles, Bulman (1964) further suggested that the vanes could act as attachment sites and support structures for vaccuolated soft tissues, a suggestion

supported by Rickards (1975). It was believed that these vaccuolated tissues, or vesicles, would provide buoyancy, maintaining the colony at the required depth and orientation.

The majority of vanes are preserved in a flattened form and it is difficult to be sure of the original three-dimensional shape. Initially structures built on the virgula were believed to be two or three-part, vanes or floatation bubbles (Bulman 1964), but the majority of these have now been re-interpreted as three-part vanes (Rickards 1975). Nearly all graptolite vanes are currently believed to have had a three-part structure, comparable to the flights of a dart, but a few species exhibited twisted vanes (for example, *C. parvus*).

Finney (1978) also proposed the nema as an attachment site for floats when he discovered a juvenile specimen of *Dicellograptus* that appeared to have a floatation 'bubble' attached to the *nema*. He also described a more mature dicellograptid with an identical, but detached, 'float' preserved adjacent to it. The 'float' was formed from the same material as the *nema* and was unlikely to be an artefact. However, this is the only known specimen featuring such an attached structure, which implies that it is not a feature common to all graptolites.

Kirk (1969), who envisioned graptolites actively swimming with the *nema* directed backwards, predicted that the *nema* was a hydrodynamic feature. She suggested that the *nema* might have helped to stabilise early, asymmetrical, growth stages; and that the virgular and proximal structures of more adult colonies would have emphasised the polarity of the colony, stabilising it and preventing rotation. Kirk (1972) expanded on this idea suggesting that a three-part vane was the 'most economical device for ensuring smooth up-and-down movement', and that such vanes would have 'prevented any tendency of the rhabdosome to rotate about the sicula axis'.

Rigby and Rickards (1989) investigated possible hydrodynamic functions through physical modelling. They proposed the opposite function to Kirk, concluding that

'*Pseudoclimacograptus scharenbergi*, and presumably other vaned forms, rotate if twisted vanes are added'. Rickards (1996) also suggested that a simple *nema* might also have aided rotation, particularly of early growth stages.

More recent experimental work by Rickards *et al* (1998) involved the use of a wind tunnel with scaled up graptolite models. These experiments have highlighted the hydrodynamic importance of graptolite orientation to flow and the degree to which rhabdosome features could control this. However, their report did not include an analysis of the *nema*, which could clearly operate to this end.

5.1.3. The focus of this investigation

Despite speculation the *nema* remains a functional enigma. This evolutionary conservation, and the repeated evolution of similar structures, points to the *nema* having a critical function for the planktonic habit, and it seems a reasonable assumption that it is likely to be of hydrodynamic significance. It is believed that understanding the function of the *nema* would be a key to the understanding of graptolite ecology (Rickards, 1996).

Investigations into the hydrodynamic function of an element of the graptolite rhabdosome can be undertaken using physical or mathematical models, or real specimens. Each method has different limitations due to necessary assumptions, scaling or detail (see section 3), however a combination of complementary methods may be used to reduce these, and approach the problem from different directions.

The *nema*, and associated structures, are well documented, simple and may be modelled relatively easily. However, even in dealing with such common features care must be taken to ensure that any interpretation of results allows for possible taphonomic factors, such as breakage or bending of delicate structures.

5.2. Experimental aims and methods

The following experiments attempt to investigate a number of the functional interpretations that have been put forwards for the *nema* and related structures (vanes etc.). They have focussed on the suggestions that the *nema* might affect stability and polarity (Kirk 1969 and 1972) and any effect of secondary structures on the rotation of the colony (Kirk 1972, Rigby and Rickards 1989). The *nema,* and associated structures, as a support for a floatation device (Finney 1978) or vaccuolated tissue (Bulman 1964) are not considered here as these are not hydrodynamic functions and require modelling of unpreserved (and consequently unknown) structures.

Real specimens, tested in seawater, were the starting point for this investigation because few assumptions are required (section 3.3.1). As the nema, virgula and cauda are so widespread, they frequently occur in isolated specimens and are amenable to such an investigation. Further investigation was carried out through oil tank modelling, simple mathematical modelling, and the use of the Cambridge wind tunnel (section 3).

The experiments investigate particular questions as follows:

- Does the *nema* affect / control orientation?
- How significant to this orientation is the colony mass distribution?
- What affect does the addition of secondary features have on orientation and motion?
- What impact has relative *nema* / colony length?
- Do different thecal shapes have any impact on the function of the *nema*?
- What was the nature of water flow patterns over the *nema* and related structures in light of their probable orientations?

5.3. Investigating the role of the *nema* in controlling colony orientation

The question of the role of the *nema* in controlling colony orientation, and enforcing polarity, was investigated initially through testing chemically isolated specimens in seawater, and later through oil tank modelling.

5.3.1. Isolated specimens in seawater

Method: The seawater tank experiments were carried out as described in section 3.3.1.

The specimens used were isolated by dissolving limestone concretions from Cornwallis Island (Arctic Canada) in 40% hydrochloric acid. The assemblage is from the late *riccartonensis* Biozone (early Wenlock) and all the isolated specimens were monograptids; *M. flumendosae* (Gortoni), *M. priodon* (Bronn), *?M. riccartonensis* (Lapworth) and small cyrtograptids (figure 5.2). The monograptid specimens with simple, straight thecae (*M. flumendosae* and *?M. riccartonensis*), and early growth stages of all species, were tested initially. This consisted of 41 specimens of early growth stages (31 complete specimens and 10 lacking a *nema*), and 42 more mature specimens (24 complete, 16 lacking a *nema* and 2 lacking a virgella). The more mature specimens included those with up to five complete thecae, although the majority featured one to three complete thecae. It was not clear that the more mature specimens (with four to five thecae) were truly complete specimens, the nemata of these specimens was likely to be incomplete due to taphonomic breakage. Illustrated examples of many biserial (Elles and Wood 1901-1918) and uniserial (Palmer 1986) species has shown that the *nema* may have grown to a length comparable to the colony. This is investigated later in section 5.10.1.

Observations were made of the orientation of the specimen as it fell through seawater, noting the relative positions of the virgella, *nema* and thecae. The stability of the graptolite in this orientation and how rapidly the alignment occurred were also recorded.

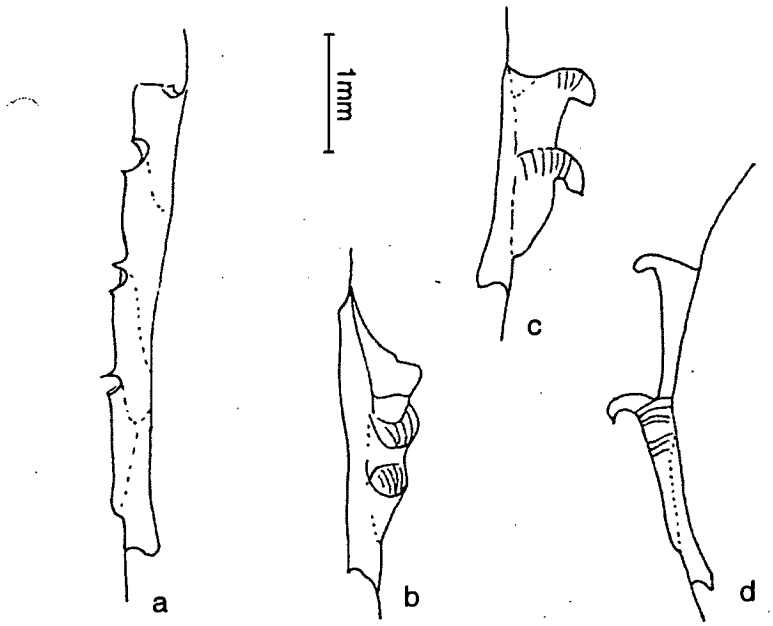

Figure 5.2: Test specimens. Examples of the specimens isolated and tested from the Cornwallis material, drawn using a camera lucida. a. and b. *Monoclimacus flumendosae* (Gortoni) c. *Monograptus priodon* (Bronn) d. *Cyrtograptus* sp.

Results: The approximate angle of the falling specimens (angle of *nema* from vertical) was plotted against the number of thecae. The data were divided into two morphological groups; straight monograptids (with a minimum of one complete theca), and early growth stages (before the first theca is complete and the final shape of the thecae is undetermined).

In each case the presence of a *nema* had a profound effect on the orientation of the colony (figures 5.3 and 5.4). Complete specimens fell with the *nema* pointed upwards, those lacking a *nema* fell with the virgella upwards regardless of growth stage or thecal morphology.

All the complete early growth stage specimens fell with the *nema* directed vertically upwards (i.e. fluid running from proximal to distal end), more mature specimens with over three thecae (straight or hooked) fell with orientations tending closer to horizontal (figures 5.3 and 5.4) although the *nema*, if present, is raised. Hence a change from a broadly vertical to a more angled alignment has been observed with increasing colony length (maturity). The early growth stage plot shows that some specimens fell vertically with the sicular cone orientated apex upwards despite the lack of a *nema* (figure 5.4). This anomaly is due to the narrow cone of the sicula acting like the *nema* and controlling orientation.

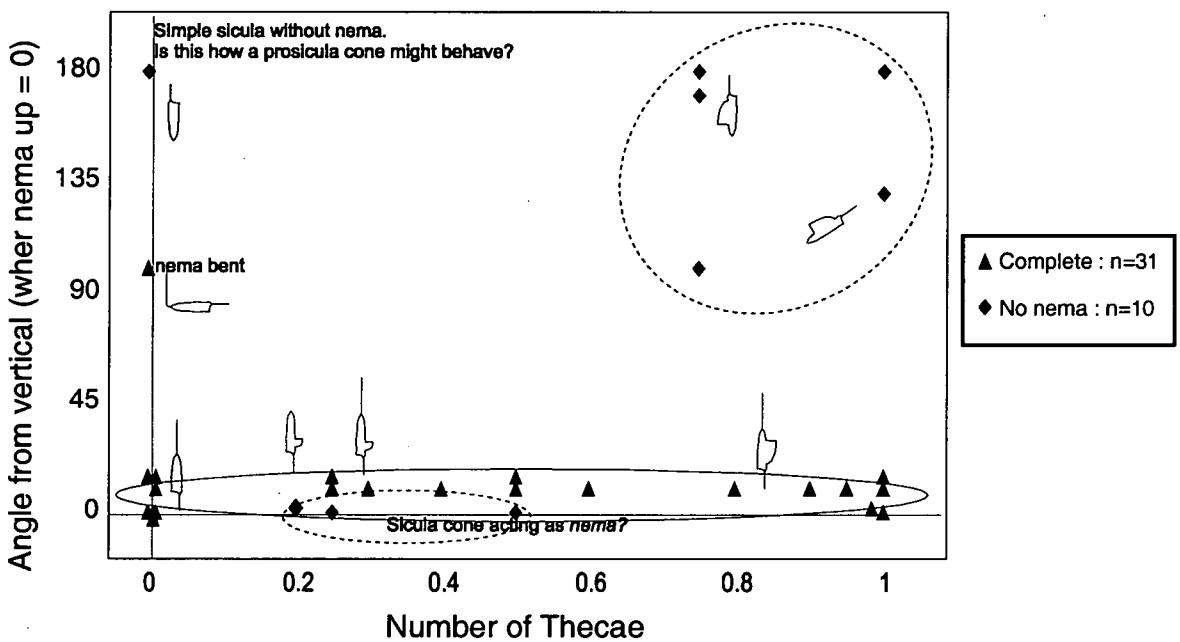

Figure 5.3: Early growth stages. Complete specimens produced very consistent results. The outlying point was produced by a specimen with a bent *nema*. This specimen fell with the *nema* orientated vertically rather than the sicula.

Those lacking a *nema* were less consistent falling into three groups: sicula stage, initial growth of first theca and those with this theca nearly completed.

Complete data tabulated in appendix A.

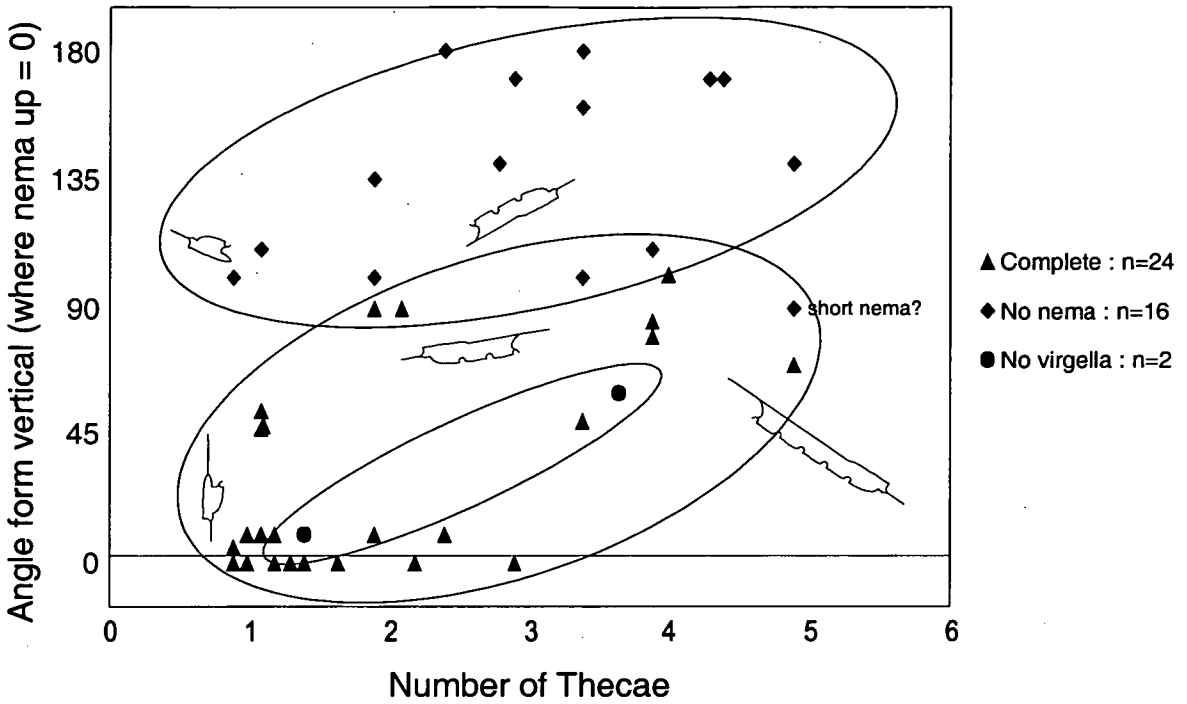

Figure 5.4: Straight monograptids. Points broadly fall into two groups dependant on the presence or absence of the *nema*. Specimens with a *nema* but lacking a virgella appear to plot within the same area as specimens with both a *nema* and virgella.
Complete data tabulated in appendix A.

In later growth stages, especially of graptoloids with simple thecae, it was observed that if the *nema* was particularly long with respect to the colony, the orientation during a fall was with the *nema* approximately vertical. The effect of the *nema* was strong enough that a specimen with a *nema* bent almost at right angles (by taphonomic processes) to the rest of the colony fell with the *nema* vertical rather than the colony vertical (Plotted in figure 5.3, an enlarged diagram is given in figure 5.5). A few well-preserved specimens have indicated that the *nema* was normally much longer than those commonly observed. In contrast, specimens with a less pronounced *nema* fell with the *nema*-virgellar line vertical (figure 5.5), and the colony orientated at an angle to vertical dependant on the width of the sicular aperture and length of the colony. Longer specimens (more than three thecae) which sank with a near horizontal orientation tended to have a rather short *nema*. It was clear that many of these specimens had incomplete nemata, which are more likely to have been lost through taphonomic breakage as *nema* length increased with maturity.

The broken termination of these nemata could be observed under the microscope in direct comparison to the tapered points terminating the complete *nemata* of more juvenile colonies. As the specimens become more mature (four to five thecae) the seawater tank results become increasingly unreliable. The change in orientation as specimens become more mature is probably an artefact.

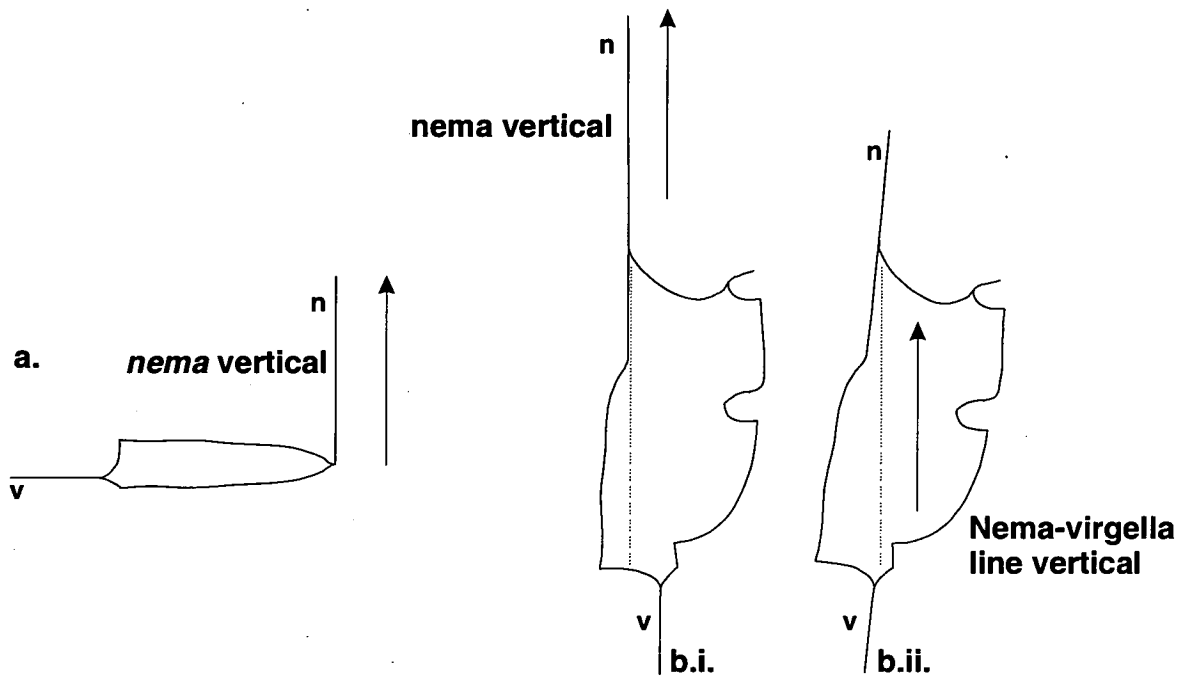

Figure 5.5: Nema determined orientations. n: *nema*. v: virgella.

a. A specimen with *nema* bent at right angles to the sicula cone fell with the *nema* vertical and the remainder of the colony horizontal despite it's greater mass.

b. i. Specimens with a long *nema* relative to the complete colony length fell with the *nema* vertical.

ii. Those with a shorter *nema* tended to fall with the *nema*-virgella line vertical.

A few specimens lacking a virgella were also tested. When plotted these fell into same areas as complete specimens; the *nema* directed upwards regardless of the presence or absence of the virgella. This may reflect the fact that the virgella is usually much shorter than the *nema*.

Conclusions:

- The *nema* did act as a stabiliser, enforcing a broadly vertical orientation (*nema* upwards) on colonies with three thecae or less.
- The narrow sicula cone may have been enough to enforce orientation on very early growth stages.
- The virgella does not strongly effect the colony orientation and is likely to have had other hydrodynamic functions.
- Specimens of more mature colonies tested tended towards a more horizontal position although the *nema* was still raised. These specimens were probably incomplete and lacking the full length *nema,* observed on a minority of specimens, through taphonomic breakage. This experiment concentrated on juvenile specimens and is not a reliable indicator of the orientation of more mature colonies.
- The longer the length of the nema, relative to the thecal-bearing colony, the greater the apparent control on orientation.

5.3.2. Simple models tested in oil

Method: The oil tank experiments were carried out as described in section 3.3.2. All the models tested in the oil tank throughout this chapter (sections 5.3.2, 5.4, 5.5 and 5.6.1) would maintain a vertical orientation if initially dropped vertically. These experiments focus on the changing alignment of models dropped with an initially horizontal orientation.

The weight distribution of a living scandent colony is assumed to have been similar to that of the collagen rhabdosome, i.e. it is assumed that the soft tissues (which are entirely unknown and cannot be modelled) would have had no significant affect on the mass distribution as they are likely to have been close to unit density. It is unlikely that the weight of a graptolite rhabdosome would have been distributed entirely evenly over the colony. Specimens of scandent graptolites, which have been

chemically isolated, are commonly black / dark brown and opaque at the proximal end, and grade to a transparent honey colour towards the distal end. This is due to a variation in the thickness of collagen forming the colony walls, where the proximal end is reinforced with additional cortical layers of collagen bandages resulting in a concentration of colony mass. Following this line of reasoning it is appropriate that the models are preferentially weighted at the proximal end.

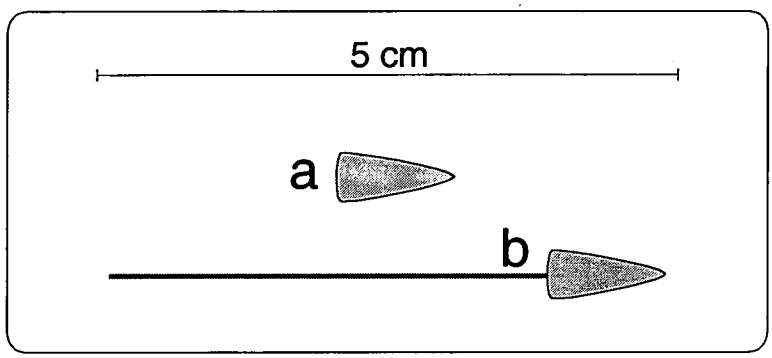

Figure 5.6: Model set A. The graptolite colony modelled as a cone-shaped Plasticine weight with a wire *nema*. a. Model without a *nema*. b. Model with a *nema*.

The mass of the thecal-bearing colony is far greater than that of the *nema*; the colony section is constructed from a larger volume of collagen material, and the density of this material is greater than that of the surrounding seawater. At its simplest a graptolite rhabdosome may be compared to a spine (*nema*) with a weight attached to one end (thecal-bearing colony). The oil tank was used to test the *nema* by modelling the graptolite colony as a simple wire spine attached to a plasticine weight (figure 5.6).

The weight was given a cone shape in response to the broadly conical shape of a mature colony, which is produced as successive thecae are constructed wider, and larger, distally. The cone shape also models the tapered proximal end of a colony. As the first thecae ($th1^1$ and $th1^2$) grow upwards from the sicula cone they form a roughly cone-shaped proximal end, lacking the pointed apex where the sicula aperture lies. The rate of expansion of this cone-shape can vary considerably with species; *Glyptograptus brevis* has a narrow, tapered, proximal end in contrast to the rapidly flaring, blunt, proximal end of *Orthograptus austiodentatus oelandicus*. Some species, for example *Paraclimacograptus innutatus obesus*, have a strikingly

triangular proximal end in cross section. The cone shape was built into the simple models as a generalisation of the colony shape, although the finer details of this shape were ignored as the method will not allow observation of comparably detailed patterns flow (section 4.5).

The initial experiment dropped a cone-shaped plasticine weight into the oil tank. This model was re-tested until a consistent sinking orientation was observed. A wire spine (*nema*) was then added and the weight re-tested until a consistent sinking orientation was observed for this modified model. This experiment was designed solely to consider the absence or presence of the *nema* spine. Spines of different length were not tested in the experiment described in this section but are considered in a later experiment (section 5.6).

Results: The cone-shaped Plasticine weight, without a *nema* wire, fell horizontally. Adding a wire *nema* changed this orientation, causing it to sink with the *nema* trailing upwards, in an orientation close to vertical (table 5.1).

No *nema* Sinking time / s	*Nema* (6.3cm) Sinking time / s	*Nema* (6.3cm) Rotation time / s
0.83	0.64	0.49
0.8	0.86	0.49
0.84	0.72	0.37
0.76	0.70	0.55
0.6	0.64	0.61
0.71	0.64	
0.69	0.49	
0.64	0.61	
0.71	0.63	
0.77	0.66	
Ave:0.74	**Ave:0.66**	**Ave:0.50**
Final angle 0°	Final angle 65°	
	Rotation rate 129°/s	

Table 5.1: Oil tank test results using model set A (figure 5.6). Final angle represents the stable sinking angle of the model where the *nema* wire is directed vertically upwards at 0°. Rotation time is measured from release (horizontal orientation) until stable sinking orientation is achieved. Rotation rate calculated from average sinking times / rotation times and angles.

Conclusions:

- The presence of a wire *(nema)* has an obvious effect on orientation of the model, enforcing a vertical alignment with the *nema* trailing.
- This result is in broad agreement with those produced testing real isolated specimens in seawater (section 5.3.1) which also suggested that a complete *nema* would have enforced a sinking orientation with the *nema* directed vertically upwards.

5.4. Investigating the role of weight distribution on *nema* efficiency

These experiments focus on the significance of the colony's mass distribution on orientation. A factor which was briefly considered in the previous experiment (section 5.3.2). As previously these experiments look at the changing alignment of models dropped with an initially horizontal orientation.

i. The first experiment used the same length of wire (*nema*) and varied the size of the weight in order to investigate the scale of density variation along the colony required to enforce orientation.

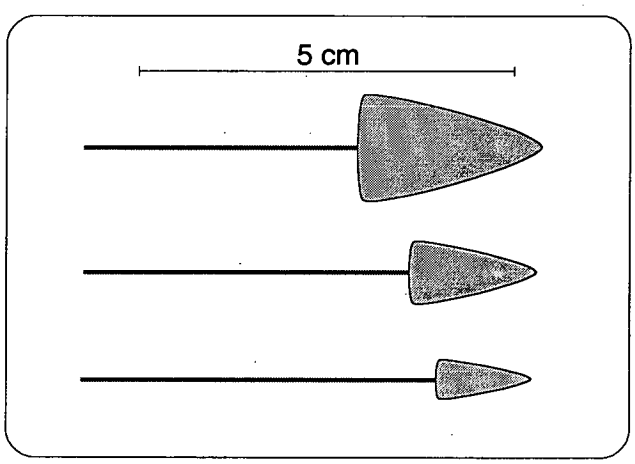

Figure 5.7: Model set B. Four models with an identical wire length (6.3 cm). The first model has no Plasticine weighting, the remaining three have increasing Plasticine weights attached to one end. The diagram is drawn to scale. The weights were cone-shaped.

For this model set B, illustrated in figure 5.7, were tested. The models were re-tested to ensure that the results were consistent. The time taken by the model to re-align, from horizontal to vertical, as it sinks was measured.

ii. The second experiment used the same total weight of plasticine, but varied the mass distribution along the wire to investigate the degree to which this distribution controls orientation. For this experiment model set C, illustrated in figure 5.8, was used.

Although model d. (figure 5.8) superficially appears most like a graptolite the mass-distribution along this model is strikingly different than would have been expected along a real rhabdosome. The proximal end of a graptolite colony is reinforced with additional layers of cortical fabric as the colony matures. This leads to a concentration of mass at the very proximal end despite the expansion of the external colony shape distally, which was constructed with correspondingly increasingly thin collagen walls. The long-cone shaped model d. depicts most realistically the external shape of such a graptolite, however the model d colony mass is concentrated towards the distal end where the cone is widest. This model is consequently not a realistic representation of a graptolite.

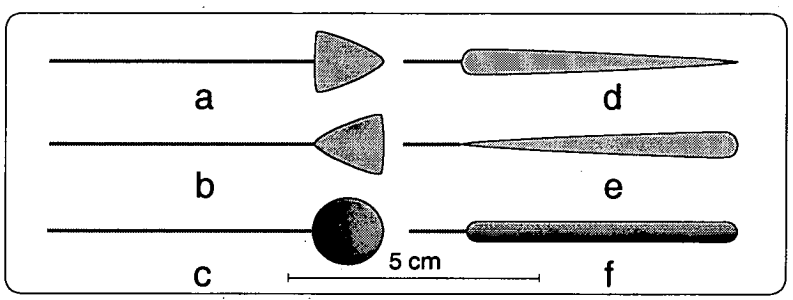

Figure 5.8: Model set C. Six models with an identical initial wire length (6.3 cm), carrying an identical weight of Plasticine. The distribution of Plasticine is different for each model. Model a, b, d, and e have cone-shaped weights; model c has a spherical weight and model f has a cylindrical weight.

The re-orientation time of the models (from horizontal to vertical) and their orientations were observed. The models were re-tested to ensure that results were consistent.

Results:

i. The size of plasticine weight had a significant effect on the stable sinking orientation of the models. An unweighted wire sank with a horizontal orientation, but with only a small plasticine weight added to one end, the model would fall with the *nema* raised. Larger weights produced increasingly vertical sinking orientations and rapid reaction times (table 5.2 and figure 5.9).

Weight (g)	Stable sinking angle (degrees)	Rotation rate (degrees s^{-1})
0.94	65	129.48
0.68	60	99.34
0.26	25	28.34

Table 5.2: Oil tank test results using model set B (figure 5.7). The stable sinking angle of the model is relative to a position where the *nema* wire is directed vertically upwards at 0°. Rotation rate calculated from average sinking times / rotation times and angles. Complete data in appendix B.

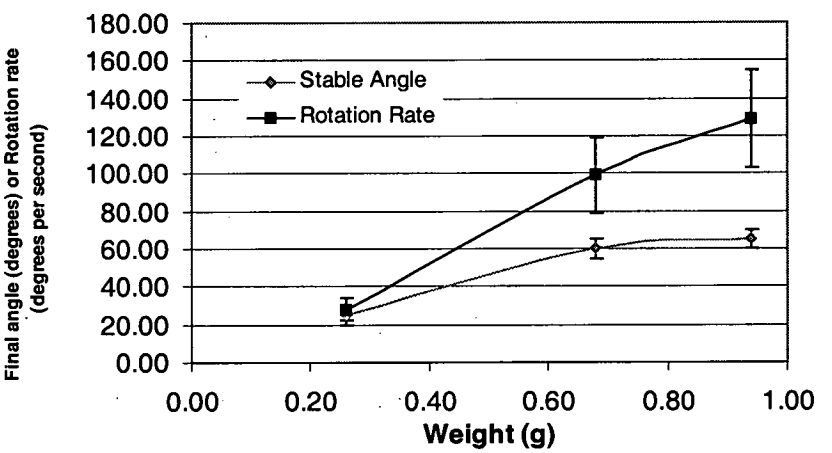

Figure 5.9: A graph illustrating the relationship between stable sinking angle, rotation rate and model weighting. As the weighting increases both the rotation rate and the stable sinking angle also increase. Data given in table 5.2 and appendix B.

ii. The distribution of the plasticine weight, along the wire frame of the model, also had a marked effect on the sinking orientation. The models with the majority of

the weight concentrated at one end of the wire (Figure 5.8. Set C: models a, b, c and e) sank with a vertical alignment (table 5.3 and figure 5.10); the models with a mass distribution centering more on the middle of the wire (figure 5.8. Set C: models d and f) sank with an alignment tending towards horizontal (table 5.3 and figure 5.10).

Weight shape	Stable sinking angle (degrees)	Rotation rate (degrees s^{-1})
Fat cone (fig 5.8a)	65	129
Fat reverse cone (fig 5.8b)	---	116
Sphere (fig 5.8c)	---	111
Long cone (fig 5.8d)	10	---
Long reverse cone (fig 5.8e)	40	69
Cylinder (fig 5.8f)	30	60

Table 5.3: Oil tank test results using model set C (figure 5.8). The stable sinking angle of the model is relative to a position with the *nema* wire directed vertically upwards at 0°. An angle is not given if the model was not observed to reach a stable orientation within the confines of the tank. Rotation rate calculated from average sinking times / rotation times and angles. Complete data in appendix B.

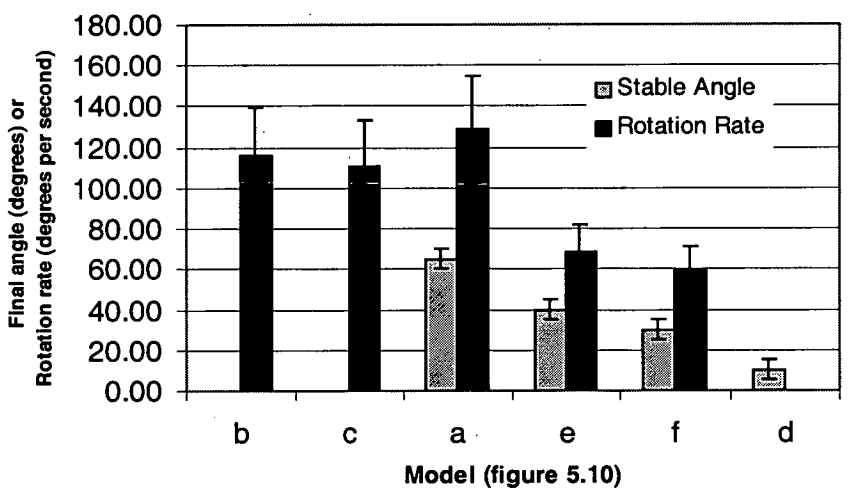

Figure 5.10: Bar chart comparing the stable sinking angles and rotation rates of model set C (figure 5.8). Typically the rotation rate and stable sinking angle decreased as the model centre of mass became more central.

Conclusions: These experiments suggest that it is the distribution of mass along the colony that is key to the function of the *nema*.

- An uneven distribution of mass is required to produce a vertical alignment, with the heavier end leading.
- The *nema* provides the required uneven mass distribution as it has a reduced mass per length in comparison to the colony, which acts as the weight.
- Any weight / colony at one end of the wire / *nema* will not necessarily be sufficient. The finer details of mass distribution can be significant, as was shown in experiment ii.

The models in experiment ii. show that the centre of mass must but be located close to the proximal end of the colony for the *nema* to function as a stabiliser. A conical colony shape, flaring rapidly towards the distal end (c.f. model a: figure 5.8. Set C) may still align vertically provided the *nema* is long in comparison to the colony (e.g. *P. scharenbergi*). Model d (figure 5.8 Set C) depicts another conical colony form, in this case the plasticine weight extends along the majority of the model length; the *nema* wire is short in comparison to the colony weight length. Model d sank with a horizontal alignment. Similarly model f, which features a cylindrical weight running along the majority of the model leaving only a short projecting free *nema* wire, sank with a horizontal alignment. In both cases the centre of mass was located near the centre of the model length. Models a-c show that the shape of the plasticine weight (colony) is not significant when the mass is all concentrated at one end of the wire.

These results also have some overlap with the issue of *nema* length. The *nema* spine of colony models a-c was relatively long compared to the plasticine weight length, whereas the *nema* spine of models d-e was relatively short. It appears that to some extent a longer *nema* is more efficient for controlling colony orientation. However model e, which had a relatively short *nema* wire and long weight, sank with a vertical orientation. Model e was different from models d and f in that its centre of mass was located close to the proximal end. The effects of *nema* length are investigated later in section 5.6.

5.5. Investigating the role of secondary features on the nema

The oil tank experiment (section 5.3.2) was expanded to consider the additional affect of secondary features (vanes etc.) built onto the *nema* on the orientation and movement of the colony. A number of vane types (flat, twisted and three-part vanes) were modelled in addition to multiple *nema*-like threads projecting from the distal end of the colony.

The vane models represented; *Climacograptus parvus,* bearing a twisted vane, *Glyptograptus nobilis* (and many other species) bearing a three-part vane, and a model with a flat vane which is not actually observed as a real graptolite structure. The model with multiple *nema*-like threads represented *Petalolithus* cf. *ovatoelongatus.*

In particular this experiment hoped to address the question of whether vanes caused (Rigby and Rickards 1989) or prevented rotation (Kirk 1969).

Method: In section 5.3.2 a simple *nema* was modelled as a wire projecting form a Plasticine weight. In order to model secondary structures silver foil 'vanes' are added to the wire *nema.* The multiple *nema*-like threads of *Petalolithus cf. ovatoelongatus* was modelled with many pieces of fine wire.
The vanes were also tested with different sized plasticine weights in order to investigate the density variation needed to enforce orientation in the presence of a vane. The models tested are illustrated in figure 5.11 (Model set D) and figure 5.12 (Model set E).

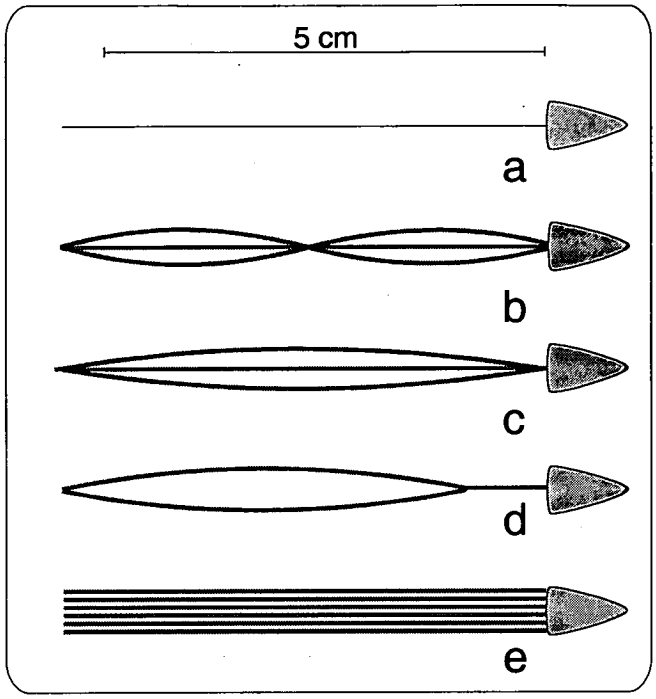

Figure 5.11: Model set D. Five models with identical length (6.3cm) and identical Plasticine weights. The models have a variety of different vane structures: a. no vane. b. twisted vane. c. three-part vane. d. flat vane. e. a number of finer wire threads.

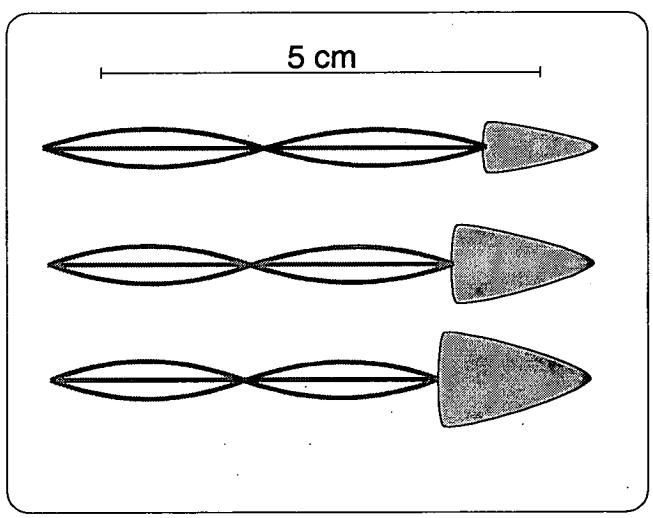

Figure 5.12: Model set E. Three models with identical length (6.3cm) and twisted vane structure. The size of Plasticine weight is increased with each model. Models are drawn to scale. The weights are cone-shaped.

Results: The addition of a vane had a dramatic effect on the model. The re-alignment of the vaned models was significantly more rapid in comparison to a

model with the same *nema* length and weight, without a vane (table 5.4 and figure 5.13). A model with a vane also settled into a more vertical sinking orientation. With the addition of a vane less weight variation along the model was required to enforce orientation (table 5.5 and figure 5.14).

Vane structure	Stable sinking angle (degrees)	Rotation rate (degrees s^{-1})
No vane	60	99
Twisted vane	70	191
3-part vane	75	140
Flat vane	65	138
Threads	85	145

Table 5.4: Oil tank test results from model set D (figure 5.11). The stable sinking angle of the model is relative to a position with the *nema* wire directed vertically upwards at 0°. Rotation rate calculated from average sinking times / rotation times and angles. Complete data in appendix B.

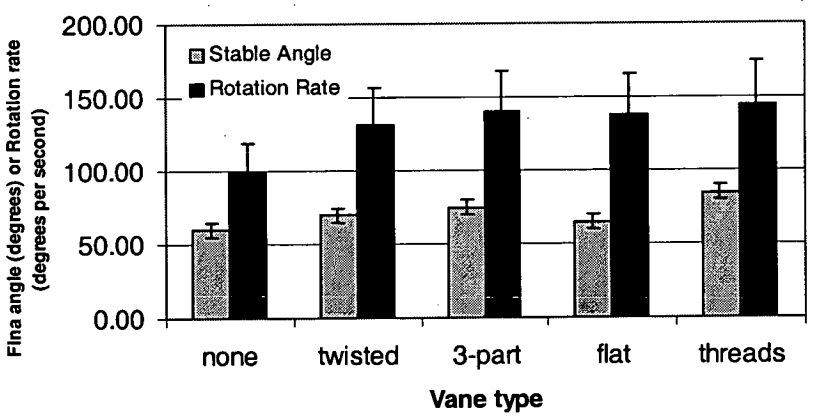

Figure 5.13: Bar chart comparing the stable sinking angles and rotation rates of model set D (figure 5.11). All vane bearing-models sink with more vertical orientations and rotate to these orientations at a greater rate than the model with a simple wire.

No strong rotation was observed as a reaction to any of the vanes tested. The models bearing the flat vane, and three-part vane, did undergo a slight rotation in order to obtain a preferred orientation of the vane as the model moved towards vertical alignment. During the colony rotation from a horizontal to vertical orientation, the

model with a flat vane twisted about its axis such that the flat plane of the vane was vertical. Similarly the model with a three-part vane rotated about its axis to an orientation with one of the vane flukes directed vertically upwards. Even with a very enlarged vane the oil tank models did not rotate. This is in contradiction to the experimental modelling results of Rigby and Rickards (1989), whose vaned model of *Pseudoclimacograptus scharenbergi* did rotate as it sank. The model tested by Rigby and Rickards (1989) bore a twisted three-part vane, unlike the untwisted vane tested in these experiments (as illustrated by Mitchell and Carle (1986) *C. scharenbergi*), which might account for this difference.

The model with many *'nema'* threads also exhibited a slower fall and stronger influence on the colony orientation than a single *nema*, resulting in more rapid alignment to a more vertical position.

Weight (g)	Stable sinking angle (degrees)	Rotation rate (degrees s^{-1})
0.94	75	108
0.68	70	131
0.26	65	96

Table 5.5: Oil tank data for model set E (figure 5.12). The stable sinking angle of the model is relative to an orientation with the *nema* wire directed vertically upwards at 0°. Rotation rate is calculated from average sinking times / rotation times and angles. Complete data in appendix B.

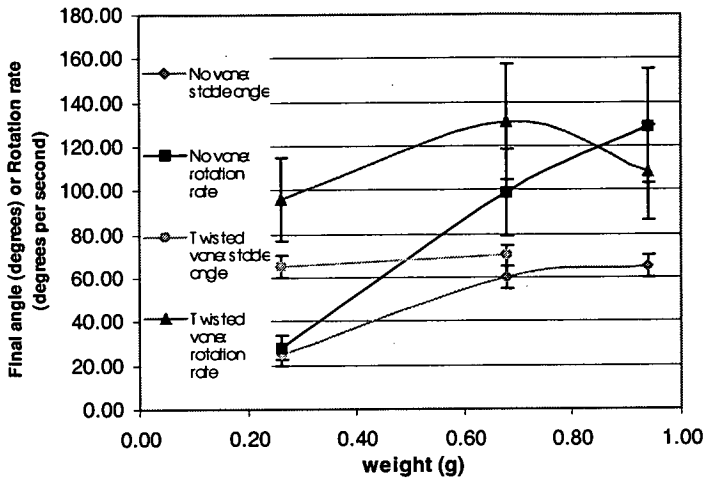

Figure 5.14: A graph comparing the relationship between rotation rate, stable sinking angle and weighting for models with and without a vane. The stable sinking angles of the vaned model is consistently more upright than that of the simple wire model. The rotation rate initially increases with increasing weight. The apparent reduction of rotation rate with the heaviest weight is probably due to experimental error.

Conclusions:

- Vanes would have enforced *nema* function.
- Vanes would not have caused significant rotation.
- Multiple *nemata* (*Petalolithus cf. ovatoelongatus*) would also have enforced *nema* function.

5.6. Investigating the relationship between nema and colony length

5.6.1. Simple models tested in oil

A simple oil tank experiment was used initially to investigate the significance to colony orientation of the relationship between *nema* length and colony length.

Method: The oil tank experiments were carried out as described in section 3.3.2.

The colony was modelled as a weight with a projecting *nema* spine. This wire spine was changed for successively longer spines and re-dropped through the oil. The orientations and reaction times were observed. Model set F (figure 5.15).

All the models would maintain a vertical orientation if initially dropped vertically. These experiments focus on the changing alignment of models dropped with an initially horizontal orientation.

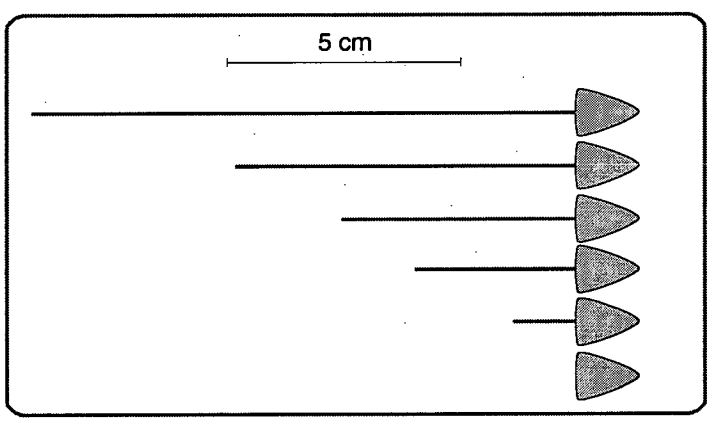

Figure 5.15: Model set F. Five models with identical, cone-shaped, plasticine weights. The length of the model free-wire varies from 0-12.8 cm.

Results: All models (except the model with no wire) rotated towards an orientation with the wire spine directed vertically upwards. Increasingly long *nema*

wires slowed the reaction time of the model, i.e. it took longer to rotate into a stable orientation, but the model consequently tended to continue rotating towards a more vertical orientation (table 5.6 and figure 5.16).

Length (cm)	Stable sinking angle (degrees)	Rotation rate (degrees s^{-1})
0.0	0	---
2.6	30	---
4.5	60	207
6.3	65	129
9.2	---	79
12.8	---	64

Table 5.6: Oil tank results for model set F (figure 5.15). The stable sinking angle of the model is relative to a position with the *nema* wire directed vertically upwards at 0°. An angle is not given if the model was not observed to reach a stable orientation within the confines of the tank. Rotation rate calculated from average sinking times / rotation times and angles. Complete data in appendix B.

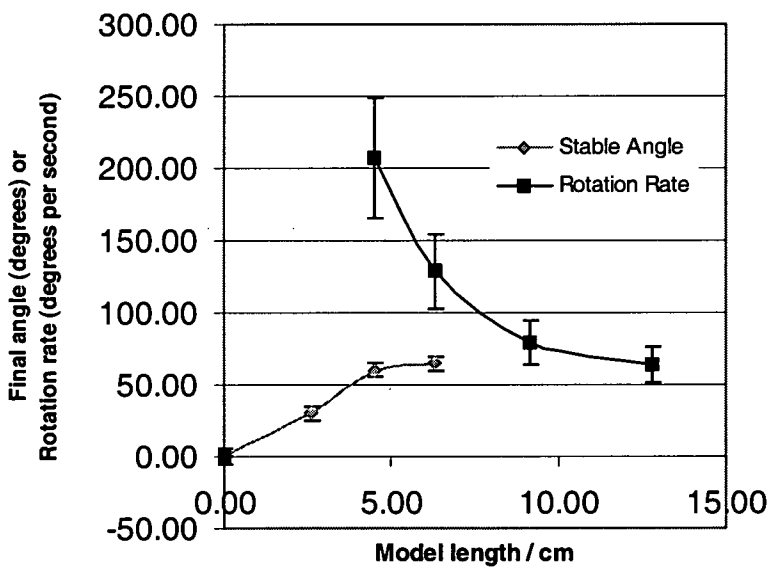

Figure 5.16: A graph illustrating the relationship between the stable sinking angle and rotation rate and model free wire length. As the free wire length increases the stable sinking angle becomes more vertical (approaches 90°) and the rotation rate decreases.

Conclusions: These experiments also confirm that the length of the *nema* / wire controls the reaction time and final alignment of the colony / model.

- A longer *nema* would have been more effective for controlling orientation.
- A long total rhabdosome length (colony plus *nema*) would have slowed the reaction time.

5.6.2. Mathematical model

Two very simple mathematical models were constructed to attempt to model the *nema* function. These models consider the effects of drag and gravity forces on the orientation and motion of a graptolite in a flowing fluid.

Method: Only the forces of gravity and drag, as a result of a simple laminar flow, are considered here. The drag forces acting on an object in a flow is estimated using this equation:

$$Drag = \frac{1}{2} C_d \rho S U^2 \qquad (9)$$

Where U is the relative velocity of the fluid to the object, ρ is the density of the fluid and S is the object are presented to the flow. C_d is the drag coefficient; a number determined by the Reynolds number and shape of the object, which combines the effect of all types of drag (both skin friction and momentum drag). Both skin friction and momentum drag are determined by the surface area presented to the flow. The coefficient of the drag equation C_D is valid for a particular shape for a particular range of Reynolds numbers, corresponding to the relative importance and values of these two drag types. This coefficient is unknown in this case and all calculations are given relative to this value, consequently which type of drag dominates is not important.

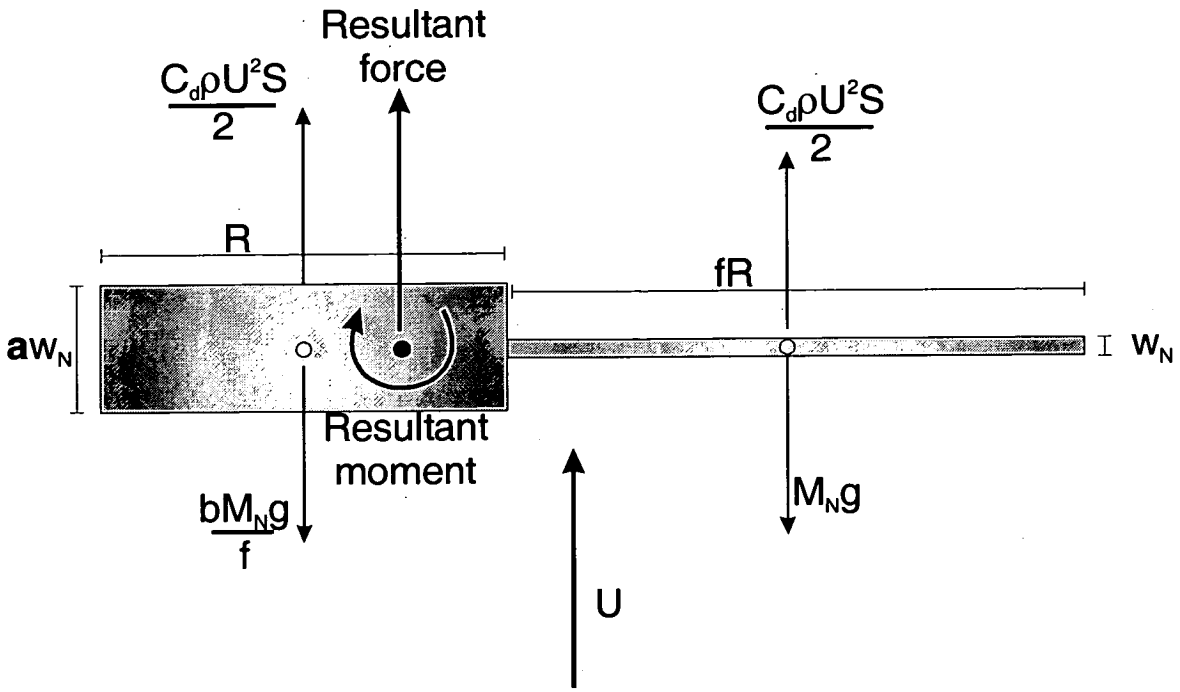

Figure 5.17: A graptolite colony is modelled as two simple boxes (colony and *nema*). The only forces acting on the model, in a flow of velocity U, are drag and weight. These forces can be resolved to a single resultant force and resultant moment acting on the centre of rotation (marked by a black dot). M_Ng is the force acting due to the mass of the *nema* (M_N). $\mathbf{b}M_Ng/f$ is the force acting due to the mass of the colony as explained in the text.

This model (figure 5.17) considers a graptolite with colony length R, and *nema* length fR. The colony lies such that it's long axis is perpendicular to a flow, velocity U. The colony is defined to be **a** times wider (in the dimension perpendicular to the flow) than the *nema*. The drag force produced by an object is directly proportional to the surface area it projects to the flow; consequently the colony **a** times wider than the *nema* produces drag forces (per unit length) that are **a** times greater than the drag forces (per unit length) of the *nema*. The colony is also **b** times heavier per unit length than the *nema*, such that the mass of the colony is $\mathbf{b}M_N/f$ where M_N is the total mass of the *nema*.

Relationship between *nema* length (N) and colony length (R): $N = fR$

Relationship between width of *nema* (w_N) and width of colony (w_R):

$w_R = \mathbf{a}w_N$

Relationship between unit length mass of *nema* (m_N)

and unit length mass of colony (m_R): $m_R = \mathbf{b}m_N$

The total mass of the thecal-bearing colony is $M_R = Rm_R$,

where $R = \frac{N}{f}$ and $m_R = \mathbf{b}m_N$

Substituting these give: $M_R = \frac{\mathbf{b}Nm_N}{f}$

But $Nm_N = M_N$ the total mass of the *nema*.

Hence the total mass of the theacal-bearing colony is $M_R = \frac{\mathbf{b}M_N}{f}$

Newtonian physics states that the majority of force systems acting on a rigid body can be resolved to a single resultant force and a moment acting on, and around, the centre of gravity (figure 5.17). However this is only the case for a mass dominated system. A graptolite would have had a similar density to the seawater in which it was living (graptolite collagen ~1.2 $x10^3$ kg m^{-3} (Rigby and Rickards 1989), seawater ~ 1.02 $x10^3$ kg m^{-3}) as a result the buoyancy and gravity forces acting on the colony may cancel and mass will have a negligible effect. In this case the drag forces would not resolve to a single resultant force and moment acting on the colony's centre of gravity, but around some other point governed by the surface area determining the magnitude drag forces. The system would be area dominated rather than mass dominated.

Both a mass-dominated and an area-dominated model are created and compared here.

Mass dominated model:

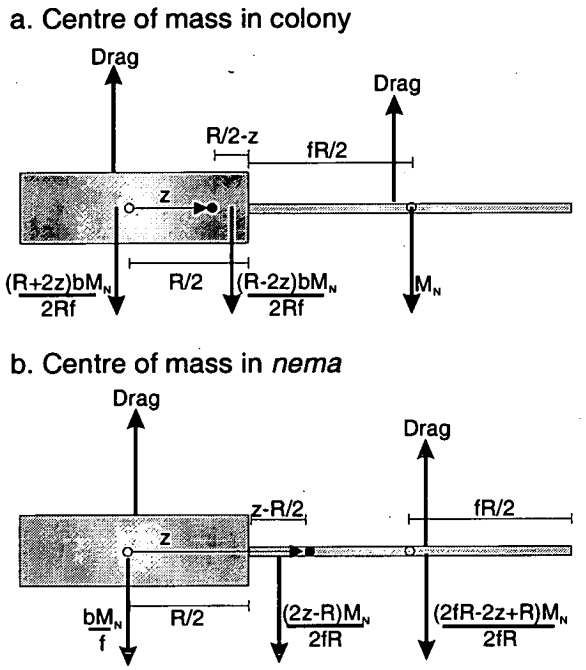

Figure 5.18: The mass dominated model. Both drag and weight forces are considered. Two situations are modelled: a. the rotation point (black dot) lies in the colony, b. the rotation point lies in the *nema*.

In this model (figure 5.18) it is assumed that an unconstrained graptolite will rotate around its centre of gravity. This is determined by calculating the point at which the moments resulting from the mass forces are balanced; the point (z) on which the graptolite would balance if it were to rest on a pivot.

$$z = \frac{(f+1)}{2\left(1+\left(\frac{b}{f}\right)\right)} \qquad (10)$$

When considering moments about this point (centre of gravity) the mass forces have no net effect by definition, however the drag forces (produced by the fluid flow moving relative to the graptolite) may result in a moment, and consequently rotation about the centre of gravity.

Again two sets of moment equations are required dependant on the location of the centre of gravity (figure 5.18). If the centre of gravity (point z) lies within the colony $z \leq R/2$, if the centre of gravity lies within the *nema* $z > R/2$.

Centre of gravity within the colony:

The moments are calculated using the same drag equation (1) with an unknown constant C_d and density ρ; the area S is replaced by $w_N dx$, along the *nema*, and $\mathbf{a}w_N dx$ along the colony (w_N represents the width of the *nema,* and the colony is defined to be **a** times wider (in the dimension perpendicular to the flow) than the *nema*). The resultant clockwise moment is given by:

$$\text{moment} = \frac{1}{2} C_d \rho U^2 \left\{ \int_0^{\frac{R}{2}+z} a w_N z dz - \int_0^{\frac{R}{2}-z} a w_N z dz - \int_{\frac{R}{2}-z}^{\frac{R}{2}+fR-z} w_N z dz \right\}$$

$$= \frac{1}{4} C_d \rho U^2 w_N \left(a\left(\frac{R}{2}+z\right)^2 + (1-a)\left(\frac{R}{2}-z\right)^2 - \left(fR+\frac{R}{2}-z\right)^2 \right) \qquad (11)$$

The terms in this equation (11) are all produced through integration of equation (9), the drag function, over different parts of the colony (the *nema* and colony either side of the centre of rotation).

Centre of gravity within the *nema*:

The resultant clockwise moment is given by:

$$\text{moment} = \frac{1}{2} C_d \rho U^2 \left\{ \int_0^{z-\frac{R}{2}} w_N z dz + \int_{z-\frac{R}{2}}^{z+\frac{R}{2}} a w_N z dz - \int_0^{fR+\frac{R}{2}-z} w_N z dz \right\}$$

$$= \frac{1}{4} C_d \rho U^2 w_N \left(\left(z - \frac{R}{2} \right)^2 + a\left(z + \frac{R}{2} \right)^2 - a\left(z - \frac{R}{2} \right)^2 - \left(fR + \frac{R}{2} - z \right)^2 \right) \quad (12)$$

Combined mass-dominated model:

The two halves of this model (z within the colony and the *nema*) are only valid for certain values of z, and must be combined to produce a complete model as the rotation point moves along the rhabdosome, with increasing *nema* length (increasing f). The resultant moments produced, and rotation points z, for a variety of values of **a** and **b** are plotted against f (the variable describing the length of the *nema* relative to the colony) (figure 5.19).

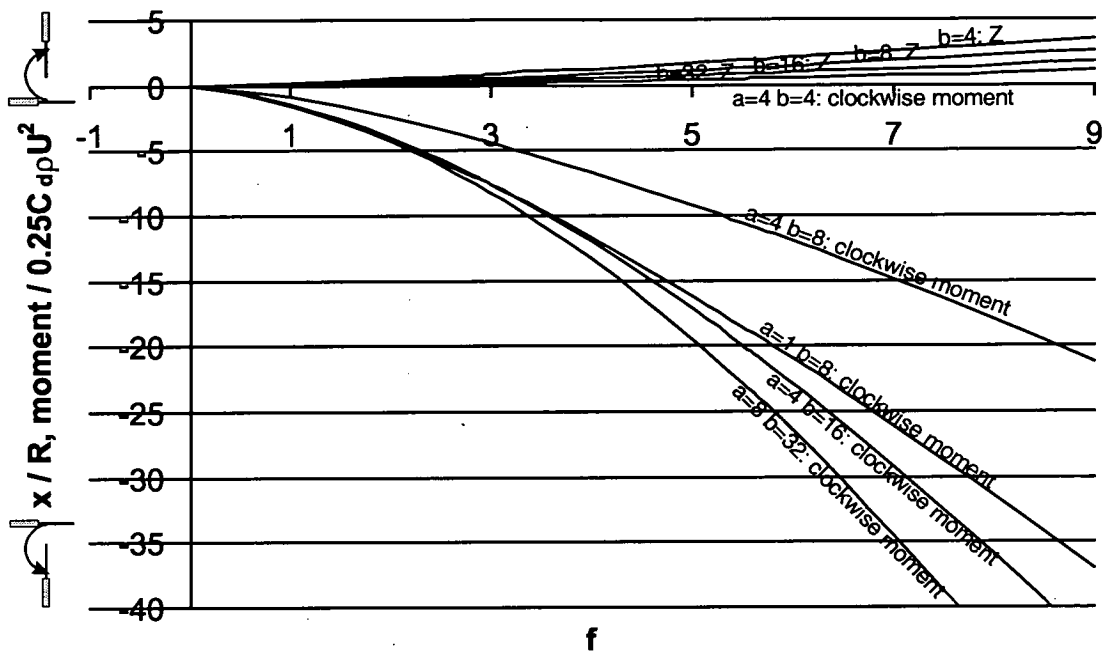

Figure 5.19: Mass-dominated model. The instantaneous clockwise moments predicted for various values of **a** (where the colony is **a** times as wide as the *nema*) and **b** (where the colony is **b** times as heavy per unit length than the *nema*) are plotted against relative *nema* length (f). The scale of the moment is only given meaning relative to the velocity (U) and density (ρ) of the fluid and the drag coefficient C_d, which are unknown, and hence the units are quoted as $x0.25C_d\rho U^2$. The location of the rotation point (z) is also plotted.

The position of the rotation point z (the centre of mass) is dependant only on **b** (the relative weight per unit length of the colony to the *nema*) and f. With increasing values of **b** the centre of mass remains closer to the proximal end of the rhabdosome as the *nema* length increases.

The resultant moment is dependant on **a** (the relative width of the colony compared to the *nema*), **b** and f. As the value of **b** increases, the colony is increasingly heavier than the *nema* and z closer to the proximal end, the resultant moment increases. As the value of **a** increases, the *nema* is thinner relative to the colony, and the resultant moment decreases. When **a=b** there is no resultant moment, the drag on either side of the centre of mass is equal.

When f=0, there is no *nema*, and the resultant moment is 0 for all values of **a** and **b**, consequently a colony without a *nema* would not experience a moment due to drag forces. The moment does not increase linearly as f increases, as it did with the area-dominated model, but becomes larger more rapidly with increasing f. The resultant clockwise moment is always negative, which would cause the colony to rotate anticlockwise (around point z), and the *nema* end of the rhabdosome would be raised (if a *nema* is present) in reaction to a flow acting upwards past an initially horizontal colony.

Area-dominated model:

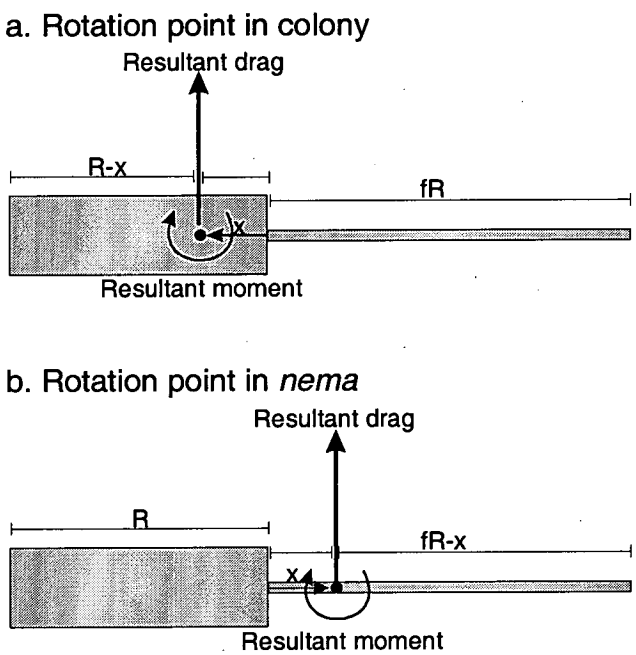

Figure 5.20: The area dominated models. Mass is not significant so drag forces only are considered. Two situations are modelled: a. the rotation point (black dot) lies in the colony, b. the rotation point lies in the *nema*.

In the area-dominated model (figure 5.20) the mass of the colony is considered negligible and gravity forces are ignored.

The drag forces acting on the colony will resolve to a single resultant force (equal to the sum of drag forces) and a balanced couple acting around the rotation point, x. The moment of forces acting around a variable point x are calculated. At the area-dominated rotation point the couple will be balanced such that the moment of forces acting on either side of this point will be equal; i.e. the clockwise moment from the left of point x plus the anticlockwise moment from the right of point x will cancel.

Initially the sum of drag forces is calculated. The area (S) is replaced by $w_N dx$ along the *nema*, and $aw_N dx$ along the colony (w_N represents the width of the *nema*).

$$\text{Resultant} = \frac{1}{2} C_d \rho U^2 \left(\int_{-R}^{0} a w_N dx + \int_{0}^{fR} w_N dx \right) = \frac{1}{2} C_d \rho U^2 \left(R a w_N + f R w_N \right) \tag{13}$$

The average of this resultant force is assumed to act at all points along the colony.

$$\text{Average Force} = \frac{1}{2} C_d \rho U^2 \frac{\left(R a w_N + f R w_N \right)}{\left(R + fR \right)} = \frac{1}{2} C_d \rho U^2 \frac{w_N (a + f)}{(1 + f)} \tag{14}$$

Additional drag force (or negatively lack of force) to this average, acting at each point along the colony, produces the moment. The sum of moments produced by these 'excess' forces, acting on either side of point x, is calculated.

As the position of the rotation point (x) is unknown two possible situations must be considered (figure 5:20): a. the rotation point lies within the colony (equations valid when $x \geq 0$) b. the rotation point lies within the *nema* (equations valid when $x < 0$).

Rotation point in the colony:

The moment produced by the 'excess' drag acting along the rhabdosome, on either side of point x are calculated.

The moment produced by the drag of the rhabdosome to the left of point x, clockwise moment:

$$\text{Left moment} = \frac{1}{2} C_d \rho U^2 \left\{ \int_0^{R-x} \left(a w_N - \frac{w_N(a+f)}{(1=f)} \right) x dx \right\} \tag{15}$$

The moment produced by the drag of the rhabdosome to the right of point x, anti-clockwise moment:

$$\text{Right moment} = \frac{1}{2} C_d \rho U^2 \left\{ \int_0^{x} \left(a w_N - \frac{w_N(a+f)}{(1=f)} \right) x dx + \int_x^{fR+x} \left(w_N - \frac{w_N(a+f)}{(1=f)} \right) x dx \right\} \tag{16}$$

When x lies at the area-dominated, free rotation, point the moments acting on either side of the rotation point will be equal such that:

Left side, clockwise moment + Right side, anti-clockwise moment = 0

$$\frac{1}{4} C_d \rho U^2 w_N \left\{ \left(\frac{(af-f)}{(f+1)} \right) (R-x)^2 + \left[\left(\frac{af-f}{f+1} \right) x^2 + \left(\frac{1-a}{f+1} \right) \left((fR+x)^2 - x^2 \right) \right] \right\} = 0 \tag{17}$$

This equation solves to:

$$x = \left(\frac{R}{2(af-f)} \right) \left[(2f(a-1)) \pm \sqrt{\left[(2f(1-a))^2 - 2(af-f)(af-f+f^2(1-a)) \right]} \right] \tag{18}$$

Rotation point in the *nema*:

Once again the moment produced by the 'excess' drag acting along the rhabdosome, on either side of point x are calculated.

Moment produced by drag forces to the left of point x, clockwise moment:

$$\text{Left moment} = \frac{1}{2} C_d \rho U^2 \left\{ \int_0^{x} \left(w_N - \frac{w_N(a+f)}{(1=f)} \right) x dx + \int_x^{R+x} \left(a w_N - \frac{w_N(a+f)}{(1=f)} \right) x dx \right\} \tag{19}$$

Moment produced by drag forces acting to the right of point x, anti-clockwise moment:

$$\text{Right moment} = \frac{1}{2} C_d \rho U^2 \left\{ \int_0^{fR-x} \left(w_N - \frac{w_N(a+f)}{(1+f)} \right) x dx \right\} \tag{20}$$

When x lies at the area-dominated, free rotation, point the moments acting on either side of the rotation point will be equal such that:

Left side, clockwise moment + Right side, anti-clockwise moment = 0

$$\frac{1}{4} C_d \rho U^2 w_N \left\{ \left[\left(\frac{1-a}{f+1} \right) x^2 + \left(\frac{af-f}{f+1} \right) \left[(R+x)^2 - x^2 \right] \right] + \left(\frac{(1-a)}{(f+1)} \right) (fR-x)^2 \right\} = 0 \tag{21}$$

This equation solves to:

$$x = \left(\frac{R}{(1-a)} \right) \left[(2f(1-a)) \pm \sqrt{\left[(2f(a-1))^2 - 2(1-a)(af+f+f^2(1-a)) \right]} \right] \tag{22}$$

Combined area-dominated model:

The two halves of this model (x within the colony and the *nema*) are only valid for certain values of x, and must be combined to produce a complete model as the rotation point moves along the rhabdosome, with increasing *nema* length (increasing f). The resultant moments produced, and rotation points x, for a variety of values of a are plotted against f (the variable describing the length of the *nema* relative to the colony) (figure 5:21).

The location of rotation point x does not vary with **a**, provided **a>1**. When **a=1** the *nema* presents the same surface area to the flow as the colony, as might be expected of a *nema* baring a broad vane. There is no net moment as the drag forces, acting at any point along the rhabdosome, encountering the same surface area, are equal. When **a<1** the *nema* presents a greater surface area than the colony and the resultant moment is anti-clockwise, which would move the *nema* towards a position trailing with the flow.

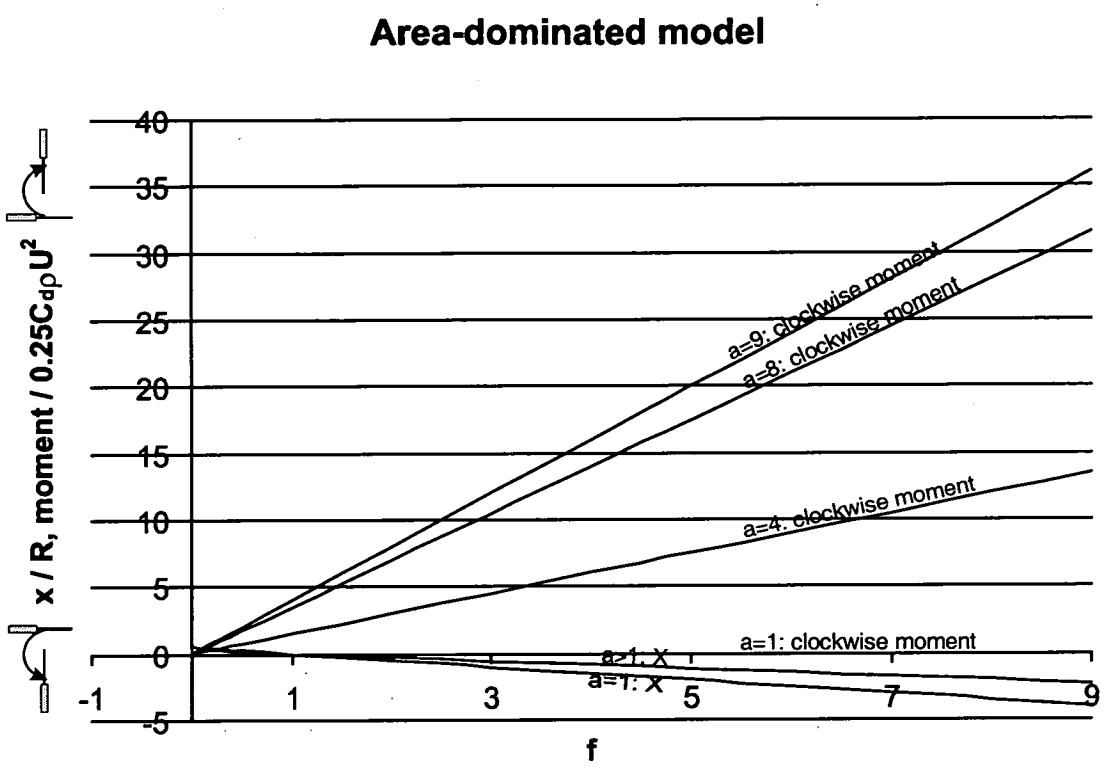

Figure 5.21: Area dominated model. The instantaneous clockwise moments predicted for various values of **a** (where the colony is **a** times as wide as the *nema*) and **b** (where the colony is **b** times as heavy per unit length than the *nema*) are plotted against relative *nema* length (f). The scale of the moment is only given meaning relative to the velocity (U) and density (ρ) of the fluid and the drag coefficient C_d, which are unknown, and hence the units are quoted as $x0.25C_d\rho U^2$. The location of the rotation point (x) is also plotted.

Increasing the value of **a** models a thinner *nema* relative to the colony. The resultant moment increases as a increases. Moment = $(0.25C_d\rho U^2)$ 0.5(**a**-1)f. When f=0, there is no nema, and the resultant moment is 0; the colony does not rotate. This resultant clockwise moment is always positive, which would cause the colony to rotate clockwise (around point x), and the colony end of the rhabdosome would be raised if a *nema* is present, in reaction to a flow acting upwards past an initially horizontal colony.

Discussion / Conclusions: In both models (area-dominated and mass-dominated) gravity forces are ignored with regards to the moment acting on the colony, and resultant rotation. The surface-dominated model considers the mass of the graptolite

to be negligible due to the similar densities of seawater and the rhabdosome. The mass-dominated model considers motion around the centre of gravity, the point at which by definition the moment of the gravity forces cancel out. Consequently these equations consider a flow from any direction. This enables us to consider gravity as proxy to a flow. The current is supplied by the graptolite sinking under gravity, as a result the centre of mass will sink vertically downwards in still water, and the colony will rotate due to the moment produced by the unequal drag along it.

The reaction of a linear graptolite to flow that is predicted by these models differs greatly if the system is considered to be area-dominated or mass-dominated. The area-dominated model predicts that a colony with a *nema*, upon encountering a current, will start to rotate such that the proximal end is directed with the flow, i.e. the proximal end will be raised when sinking under gravity. The mass-dominated model predicts the opposite: if a *nema* is present, the colony will start to rotate such that the distal end will be directed with the flow, i.e. the distal end will be raised when sinking under gravity.

The experimental data shows that typically it is the distal end that is raised when an isolated colony sinks under gravity. Consequently it can be claimed that, although small, the mass of a graptolite is significant. The mass-dominated model appears to be the more correct.

The mass-dominated model (figure 5.21) predicts that a longer *nema* would have been more effective, producing a stronger moment, but that the presence of any *nema* at all would have induced a small initial rotation. The *nema* length considered in the model is relative to the length of the colony; in order to maintain the same stabilising effect throughout astogeny the *nema* would have to have grown in proportion to the colony length. The addition of a vane gives **a**=1, **b**=8 in comparison with **a**=4, **b**=8: i.e. the nema has the same width as the thecal bearing colony (**a**=1) but the colony is eight times as heavy per unit length (**b**=8) as opposed to a graptolite with the same weight difference between nema and colony (**b**=8) but a much thinner *nema* spine

where the colony is four times as wide (**a**=4). This vane would have increased the drag of the *nema* without moving the centre of mass, and would consequently also have increased the moment experienced by the graptolite, causing the *nema* to function more rapidly and efficiently. The differing reaction of a monograptid and diplograptid might be predicted by assuming that a diplograptid would also have preferentially sank with the thecae lying in the flow (vertical) plane. Hence a monograptid colony would have been as wide in comparison to the *nema* as a diplograptid colony, but the diplograptid colony might have been as much as twice as heavy as the monograptid. A comparison of **a**=4 **b**=8, and **a**=4 **b**=16 illustrates such an example. The diplograptid (**a**=4 **b**=16) moment would have been much greater than that of the monograptid (**a**=4 **b**=8) for the same *nema* length (f).

These models are not accurate for a number of reasons. The model is not dynamic, providing instead an instantaneous view of the fluid acting on a 'stationary' graptolite. The resultant moment indicates the direction of initial rotation only, the size of moment and subsequent resistance to this motion are not properly considered.

The model is also limited because the graptolite is assumed to be initially perpendicular to the flow. However the drag forces acting a graptolite at an angle (θ) to the flow would have a similar effect; the impact area being reduced by a factor of $\cos\theta$, and $\sin\theta$ of the resulting force acting to produce a moment. All drag forces would be reduced by the same $\cos^2\theta$ factor, resulting in the same point of rotation (x,z) and sense of rotation, but a reduced moment. Hence as the graptolite approached alignment to the flow the moment causing the rotation would have dropped to zero.

The drag equation (9) used for this model is too simple. It uses a drag coefficient that collects all drag effects for a particular shape, at a specific range of Reynolds numbers, together. The drag coefficient cancels out of the calculation of x, and merely acts as a constant by which the entire moment equations are multiplied. The

moment produced by such a drag coefficient does not consider the distribution of drag over the shape, i.e. whether it is increased at the ends of the cylinder. However the mass-dominated model appears to fit the experimental data gathered. Although this is only a guide and a first approximation to the problem, the model can still be used to aid understanding of the *nema* and how it functioned.

5.7. Investigating possible changes in nema function with different thecal shapes

In order to investigate any significance thecal shape might have had to *nema* function more isolated specimens (with different thecal shapes) were tested in seawater and compared with the initial experiment described in section 5.3.1.

Method: The seawater tank experiments were carried out as described in section 3.3.1.

This experiment again used specimens isolated from Cornwallis Island (Arctic Canada) limestone concreations, as described in section 5.3.1. The assemblage is from the late *riccartonensis* Biozone (early Wenlock) and all the isolated specimens were monograptids; *M. flumendosae* (Gortoni), *M. priodon* (Bronn), *?M. riccartonensis* (Lapworth) and small *cyrtograptids* (figure 5.2). The monograptid specimens with hooked thecae (*M. priodon* and small *cyrtograptids*) were tested.

Observations were made of the orientation of the specimen, noting the relative positions of the virgella, *nema* and thecae. The stability of the graptolite in this orientation and how rapidly the alignment occurred were also recorded.

Results: The approximate angle of the falling specimens (angle of *nema* from vertical) was plotted against the number of thecae. Specimens with hooked thecae fall into two groups: complete specimens falling with the *nema* directed upwards, those lacking a *nema* falling with the virgella directed upward (figure 5.22). The data collected from specimens with hooked thecae also show a trend towards a more

horizontal orientation with increasing length (number of thecae). A larger test set of specimens would be required to confirm this. The extra weight of hooked thecae, adding to the extreme asymmetry of the smaller colonies, may be responsible for this.

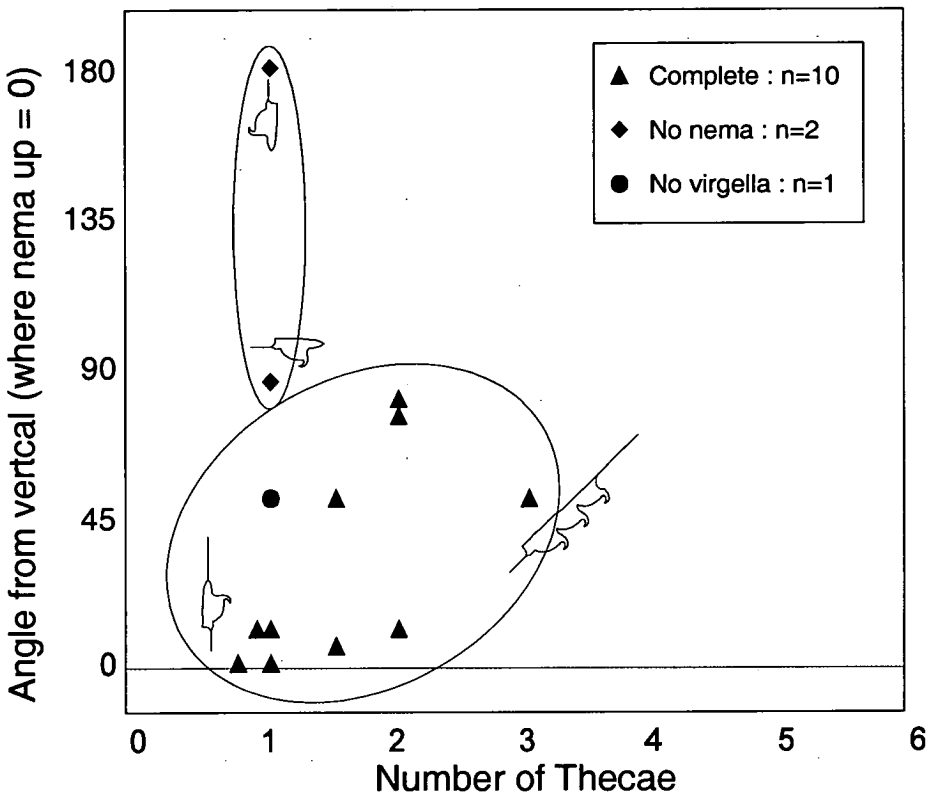

Figure 5.22: Hooked monograptids. Although fewer specimens were tested the hooked thecae data compares well with the straight thecae data. Points broadly fall into two groups dependant on the presence or absence of the *nema*.

Comparing these data with the results from section 5.3.1 (testing specimens with simple, straight thecae and early growth stages) it appears that differing thecal morphologies (straight or hooked thecae) had no effect on orientation of the specimens tested. This indicates that although thecal morphologies and structures are likely to be functional, their purpose was not related to orientation.

Discussion: These results do not agree with apparent relative flow orientations observed by Rickards (1975) who describes a bedding plane scattered with orientated monograptids. Two species are represented, one with straight thecae (*Pristograptus dubius*), and one with hooked thecae (*Monograptus flemingii*). The two species are

orientated in opposite directions, indicating that species with hooked thecae might have had a different natural alignment to flow. However it should be noted that these specimens were aligned due to currents experienced *post-mortem*. These currents were probably ocean bottom currents or turbidity currents and would have been strongly affected by shear forces due to interaction with the boundary layer. The flow orientation of these graptolites might also have been strongly affected by the presence of sediment carried by a turbidity current that would have increased the effective density of the fluid.

Schleiger (1968) studied a number of current orientated graptolite beds with associated primary directional flow structures in order to determine the relationships between graptolite and current orientation. His investigation revealed that the relative orientations of graptolite and current varied with sediment fraction and population densities, indicating that sediment interaction could influence graptolite orientation.

An attempt was made to look at the isolated specimens (figure 5.2) in moving water in order to ground truth the tank experiments. Specimens of early growth stages, and those with straight and hooked thecae were all observed in the same alignment when moving with the water. This test was not robust, as it is very difficult to produce a laminar water flow without a large and sophisticated flume tank. Consequently it is impossible to ensure that shear forces produced by interaction with the tank boundary layer did not affect the specimen orientation. Only gentle currents were used to reduce this problem.

Conclusions:

- The orientation of an isolated graptolite falling through seawater is *nema* up regardless of whether the thecae are hooked or straight.

5.8. Patterns of flow over distal structures

5.8.1. Detailed flow over a simple *nema* and the significance of nema length

This experiment used the Cambridge wind tunnel to observe the details of flow pattern over the colony and *nema.* The significance of *nema* length is also revisited.

Method: The model used was based on *Glyptograptus brevis*, although any other might have been used provided the same model was used throughout the experiment. *G. brevis* had a relatively simple, streamlined shape which would allow the affects of the *nema* to be concentrated on. The model was run in the Cambridge wind tunnel, aligned with the flow along the long axis. The same model was tested with a range of wire *nema* lengths; these ranged from no *nema* to a *nema* of 150mm.

The free airstream velocity was $0.7ms^{-1}$. The flow patterns were observed using smoke streamers (see section 3.2.2) and photographed using a digital camera.

Results: All results are shown as digital photographs, from which flow line interpretations have been drawn based on observations made during the wind tunnel runs.

A ring-shaped standing eddy (figure 5.24) formed around the *nema*, in the lee of the graptolite distal end. This eddy captured and recycled smoke particles, and can be observed as a smoke shadow around the model *nema* wire in figure 5.23. Small-scale turbulent mixing with air flowing past this region swept some of the smoke beyond the *nema* where this mixing continued freely. Beyond the nema the small-scale turbulence resulted in complete mixing of smoke-bearing and clear air such that the streams were no longer visible. Prior to this the *nema* prevented this complete mixing along its length; 'protecting' the eddies from the turbulence.

A longer *nema* provided protection for larger (longer) eddies and the smoke shadow can be seen extending along the increased spine length. As the *nema* length was

reduced the turbulence down-stream of the colony disrupted fewer smoke streams (figure 5.23), the graptolite model having less lateral influence on the flow, indicating a narrower turbulent wake.

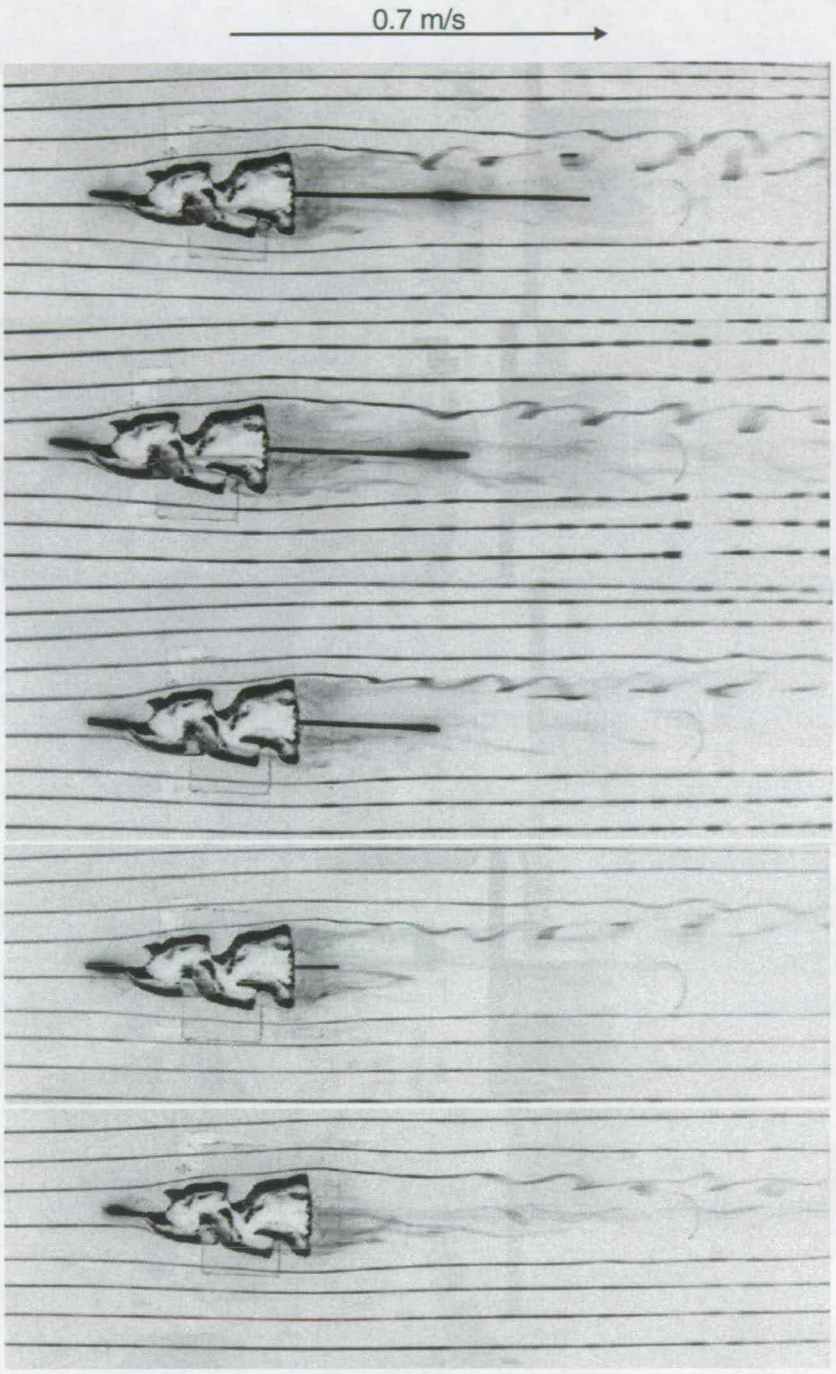

Figure 5.23: Four digital images of the same model in an identical position in the Cambridge wind tunnel. The wire *nema* length varies from 0cm to 15cm. The image is inverted such that white smoke streams appear black.

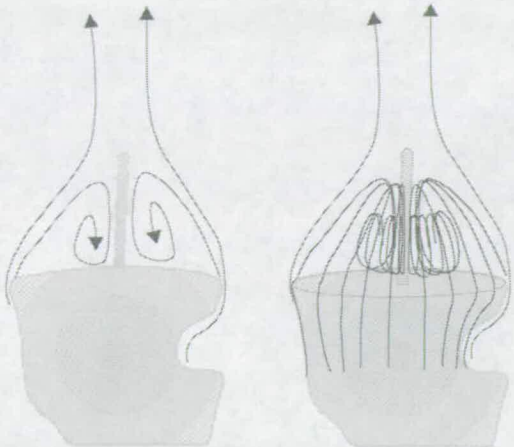

Figure 5.24: A three-dimensional interpretation of the ring-shaped eddy (right), forming in the lee of the thecae, with a cross-section of the same eddy (left).

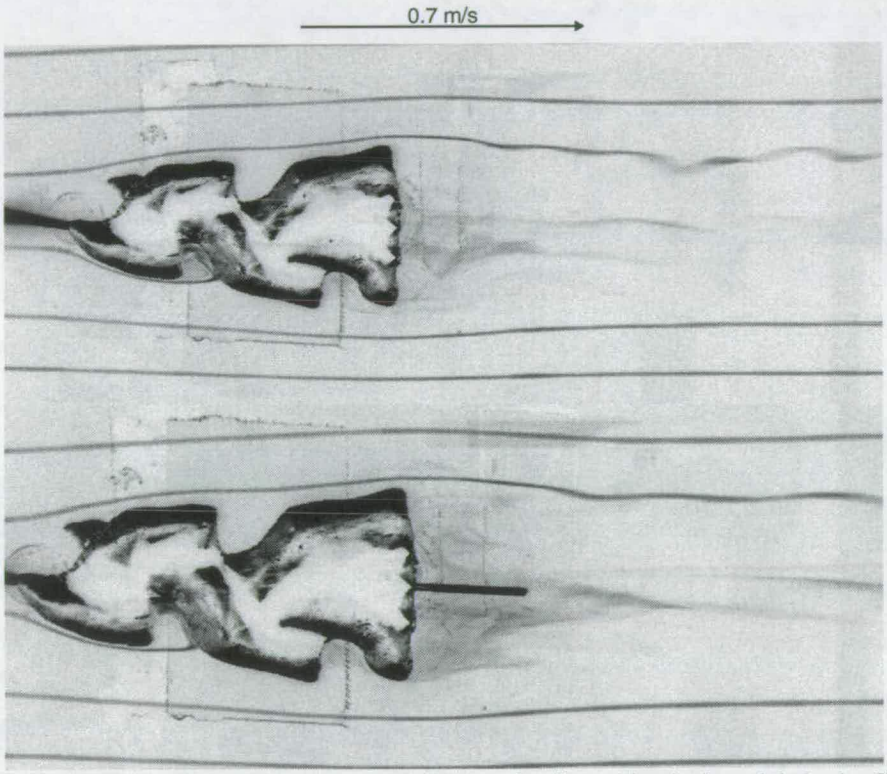

Figure 5.25: An enlarged digital image of the distal ends of two identical models in the Cambridge wind tunnel run with and without a *nema* wire. The image is inverted such that white smoke streams appear black. The ring-shaped eddy can be seen as a shadowy area in the lee of the thecal-bearing portion, where smoke particles are captured and recycled. The model with a *nema* forms a stronger eddy (larger and darker area) which is centred on the spine.

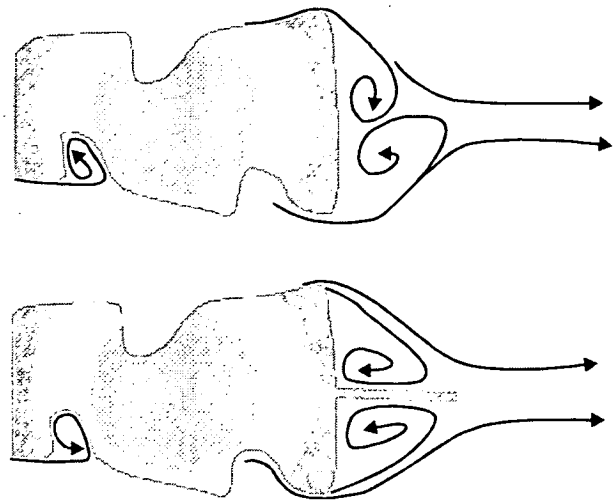

Figure 5.26: An interpretation of the flow imaged in figure 5.25 based on observations made during experimentation. The ring-shaped eddy is shown as a pair of standing vortices in the lee of the thecae. Note that the *nema* (lower diagram) fixes the centre of the ring.

Taking a closer look at the distal end of the thecal-bearing colony section (figure 5.25 and 5.26) it is observed that the standing eddies formed around the *nema* spine, which fixeed their location. Standing eddies also formed without the presence of a *nema* spine, but the centre of the eddy ring is not fixed. The eddies formed without *nema* protection were small. Air flow past the colony distal end and swept the smoke-bearing air downstream, only a small region was protected by the flow separation.

Conclusions:

- *Nema* length would have controlled turbulent wake width, and trailing attached vortex length.
- The *nema* prevented complete mixing of air in the wake of the colony model.

5.8.2. Flow over vane-bearing *nemata* and changes with orientation

The Cambridge wind tunnel was used to observe the different flow patterns produced by a colony with a simple *nema* compared to a vane-bearing *nemata*. Different vanes, and orientations, are investigated here.

Method: The basic *climacograptid* model (with a simple *nema*) was used for this experiment. This represents a very simple, and common, graptolite morphology and provides a reasonable approximation for the rhabdosome of a number of vane-bearing graptolites (*Climacograptus parvus*, *Orthograptus vesiculosus* and *Glyptograptus nobilis*) given that it is the flow over the vane which is of interest. Using the same base model allows direct comparison of the flow patterns over different vane structures.

The model was tested, in the Cambridge wind tunnel, with the long axis at a range of angles to the flow ranging from parallel to perpendicular alignment. The tests were repeated with a variety of vane structures, and flow patterns compared. This experiment was designed to confirm how the *nema* interacts with the flow to control orientation, and why a vane-bearing *nema* might be more effective.

Results: All results are shown as digital photographs, on some of which flow lines have been drawn from observations made during the wind tunnel runs. The results are divided by vane type.

Simple *nema*, no vane: The smaller model allows observation of the wake at a greater relative distance from the colony (figure 5.27 and 5.28). When the model is aligned with its long axis parallel to the flow the smoke can be observed deflecting around the proximal end of the colony, then drawn into the expanding conical wake behind it. Towards the end of the *nema* spine the smoke streams are drawn back together.

When the model is tilted from parallel alignment with the flow the *nema* is exposed to direct impact from the smoke streams. Impacting smoke is flared along the *nema*

towards the distal end. Behind the *nema* spine the smoke looses coherency as small scale turbulence mixes the smoke into the cleaner airflow.

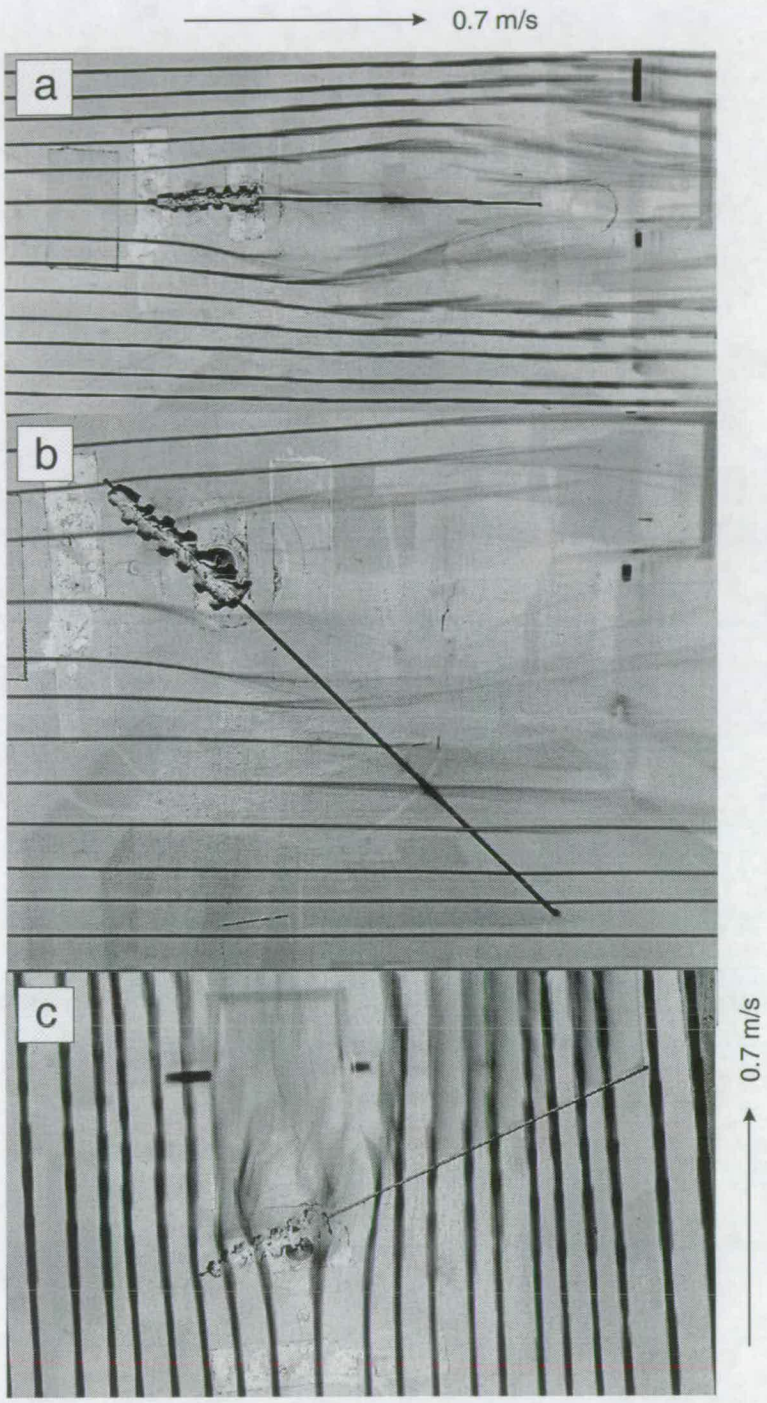

Figure 5.27: Simple *nema*. The same model is run in the Cambridge wind tunnel in different orientations to the free-stream airflow. As the angle to the flow increases the turbulent wake produced by the model broadens. The image is inverted such that white smoke streams appear black.

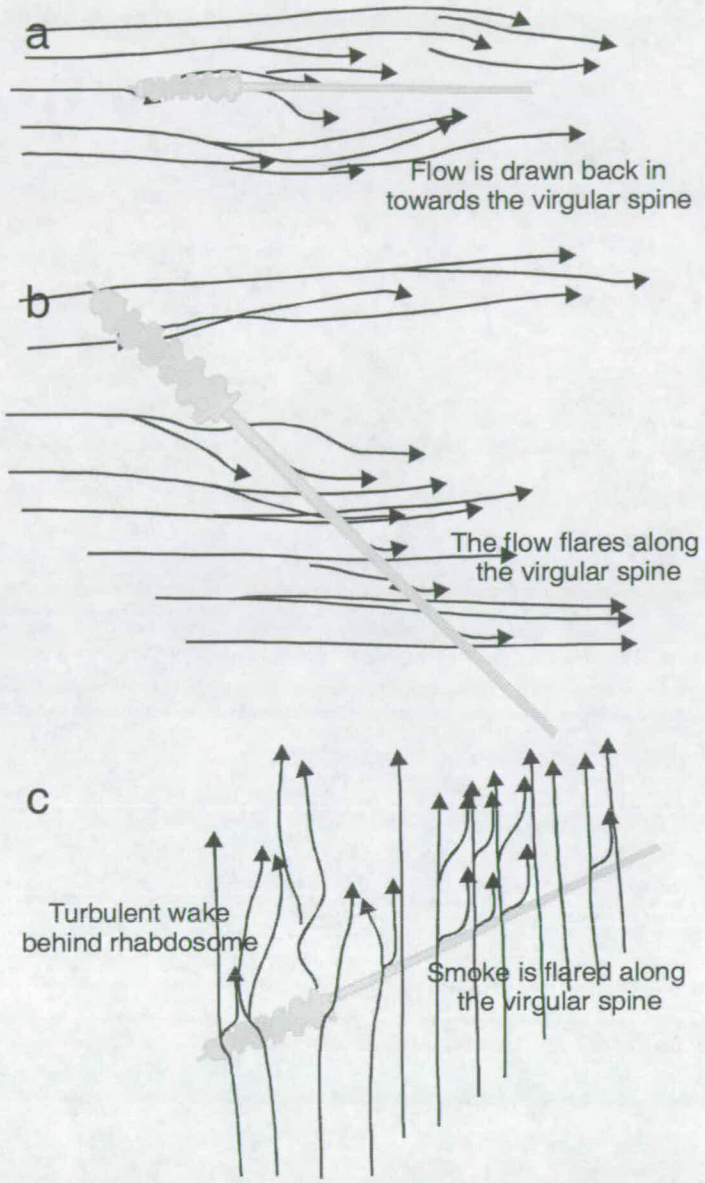

Figure 5.28: An interpretation of the flow patterns, imaged in figure 5.27, over the model with a simple *nema*. As the model is re-orientated from vertical towards horizontal the size of the turbulent wake increases.

Flat vane: When the model is orientated with the long axis parallel to the flow the vane appears to make little difference to flow, the overall pattern is very similar to that over the simple *nema* (figure 5.29 and 5.30). As the model is tilted away from this alignment, with the flat vane surface perpendicular to flow, the vane flares the impacting smoke streams creating a turbulent wake and a much bigger disturbance than behind the simple *nema*. During the oil tank experiments (section 5.5) it was

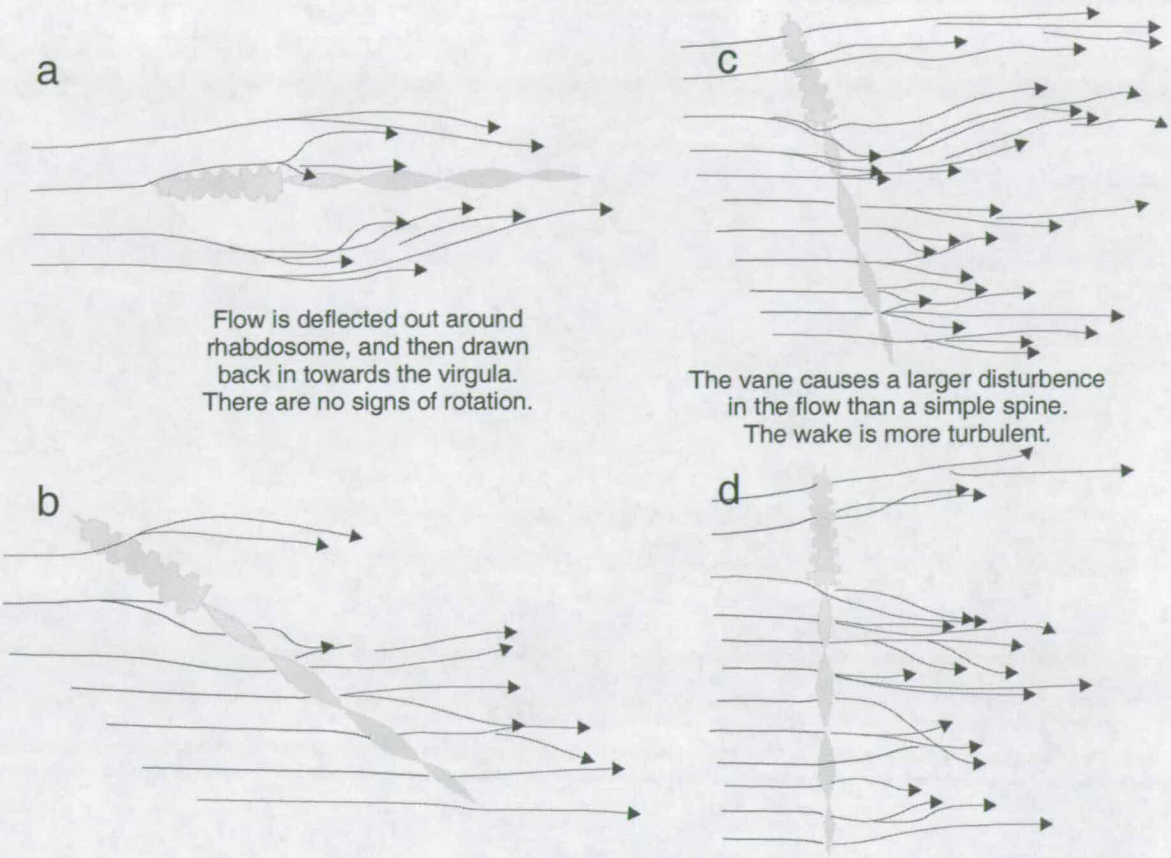

Figure 5.32: An interpretation of the flow patterns, imaged in figure 5.31, over the model bearing a twisted vane. This interpretation is based on observations made during experimentation. As the model is re-orientated from vertical towards horizontal the size of the turbulent wake increases. No additional rotation of the flow is observed as a result of the twisted vane.

The flow patterns over the model bearing the three-part vane are shown in figure 5.33 to 5.36. When the model was vertically aligned the presence of the three-part vane caused little more flow disturbance to the flow than was observed as a result of the model bearing a simple *nema* in the same orientation (figure 5.33 and 5.34). A smoke stream impacting the vane is drawn into a small flare running along the distal edge to the tapering point of the vane. As the model is tilted towards a horizontal alignment the smoke streams are stretched along the vane, and turbulent flow behind the vane increases. Close observation shows that the impacting smoke streams twist over the vane, always towards the most horizontal vane fluke, resulting in a rotation of the flow (figure 5.36). When the model is aligned perpendicular to the flow the wake is very large and turbulent.

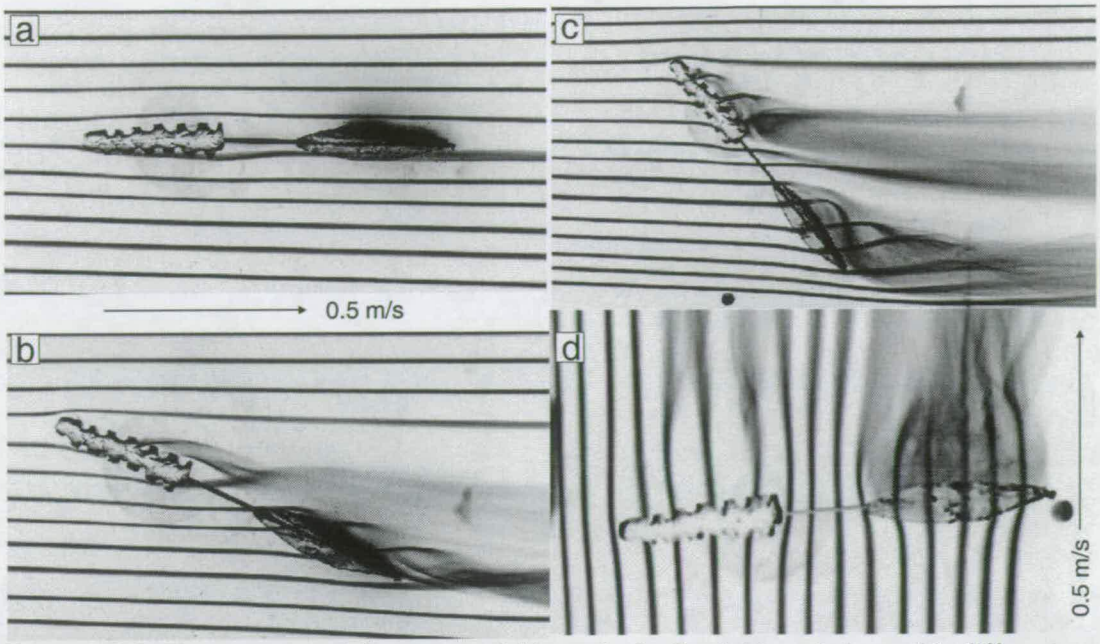

Figure (5.33): Three-part vane. The same model is run in the Cambridge wind tunnel in different orientations to the free-stream airflow. As the angle to the flow increases the turbulent wake produced by the model broadens. The flow is observed twisting around the vane. The image is inverted such that white smoke streams appear black.

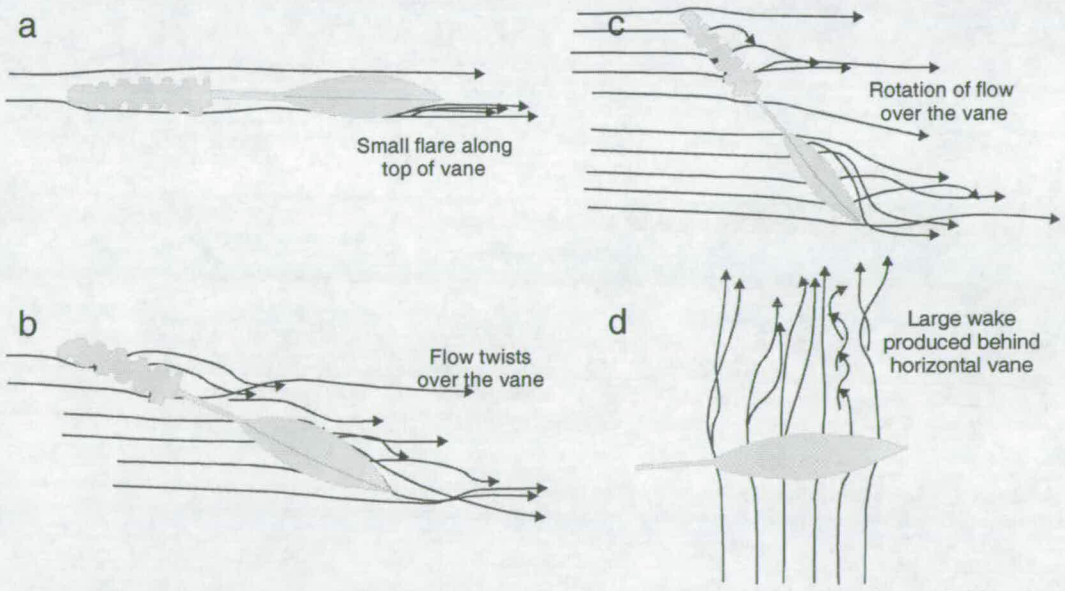

Figure 5.34: An interpretation of the flow patterns, imaged in figure 5.33, over the model bearing a three-part vane. This interpretation is based on observations made during experimentation. As the model is re-orientated from vertical towards horizontal the size of the turbulent wake increases. The flow was observed twisting over the angled vane.

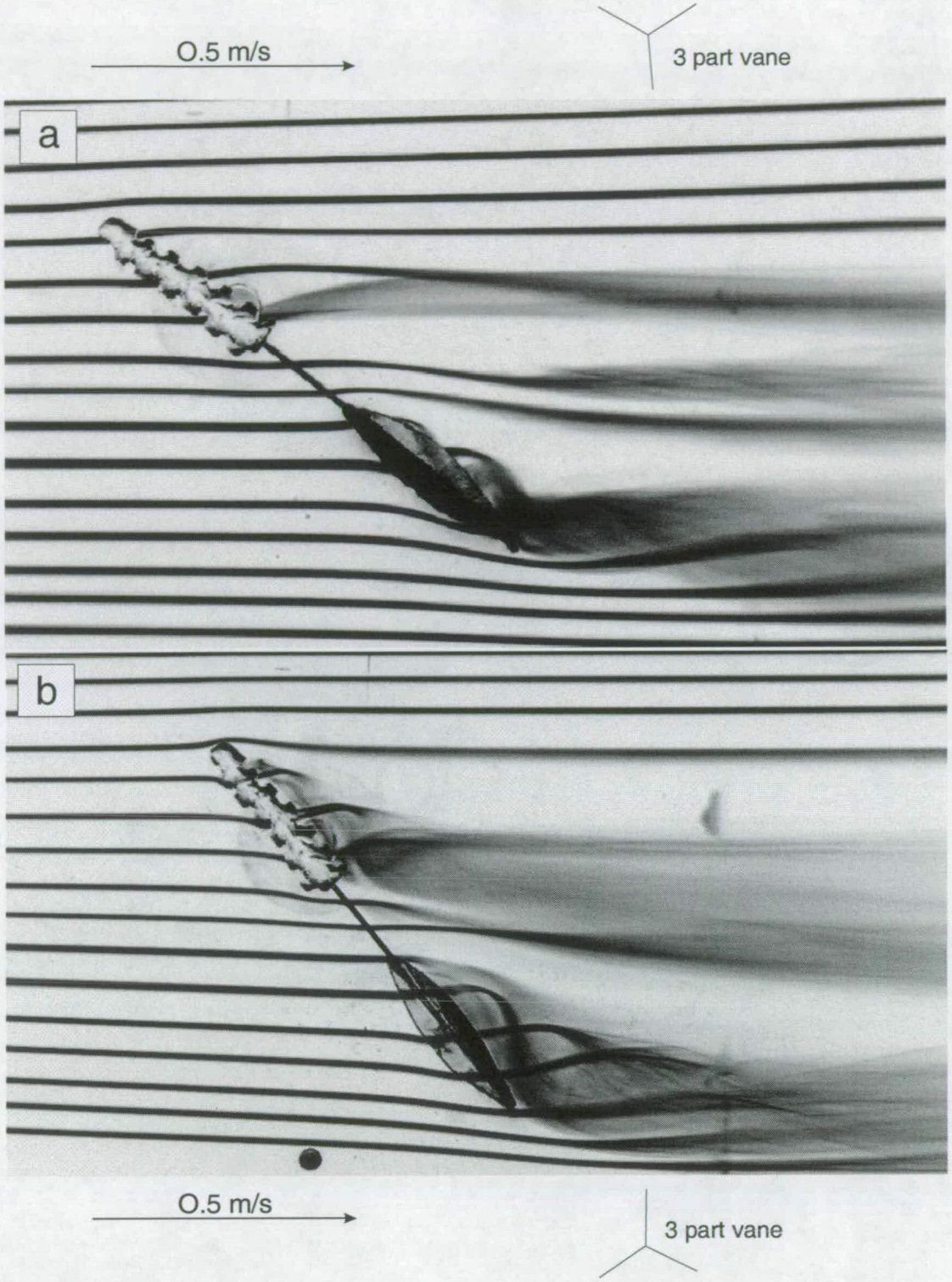

Figure 5.35: Three-part vane. The same model is run in the Cambridge wind tunnel in different orientations; with a single vane fluke directed horizontally towards the camera (upper image), with a single vane fluke directed horizontally away from the camera (lower image). The flow can be observed twisting over the vane towards the horizontal fluke. The image is inverted such that white smoke streams appear black.

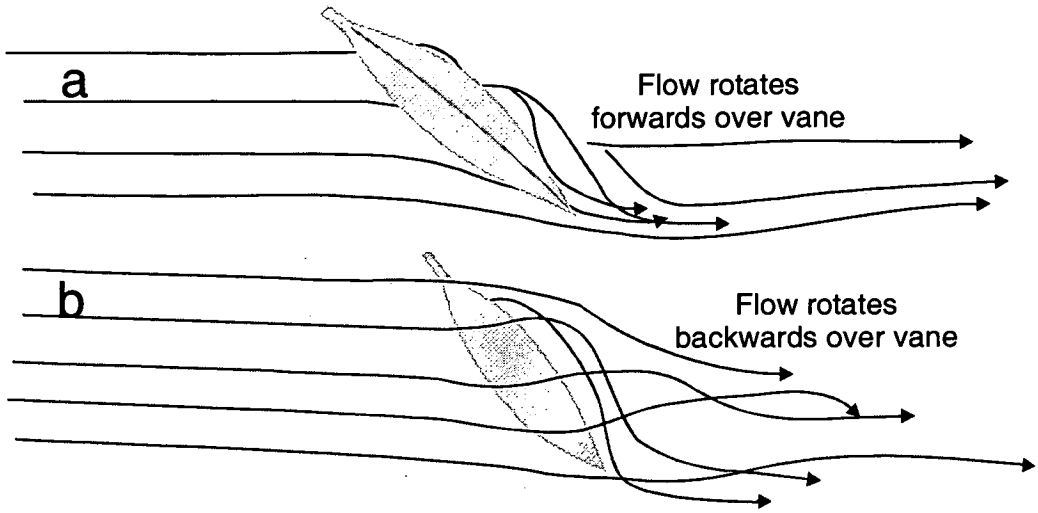

Figure 5.36: An interpretation of the flow patterns, imaged in figure 5.35, over the model bearing a three-part vane. This interpretation is based on observations made during experimentation. The flow twists towards the most horizontal vane fluke.

Discussion: The flat vane can present two very different aspects to the flow; the plane of the vane may be perpendicular to the flow, producing a lot of turbulence and drag, or the plane of the vane could lie parallel to the flow, producing a lot less turbulence and drag, although it is still greater than a simple *nema*. Tank experiments (section 5.5) indicate that as the graptolite sinks it finds the orientation with the least drag; moving to a parallel alignment though positions with the vane parallel to the flow. The twisted and three-part vanes would have always presented a large surface area to the flow, and been all the more effective.

Conclusion:

- As the relative angle between the free-stream flow and the model increases the turbulent wake area also increases.
- The vane structures produced significantly more turbulence than the simple *nema* spine.
- Only the three-part vane produced any resultant rotation of the flow which passed over it.

5.9. The likely range of hydrodynamic function for distal structures on scandent graptoloids

5.9.1. How the nema functioned

It has been observed in the tank experiments that the *nema* would have had a controlling effect on the orientation of the colony. The oil tank experiments (sections 5.4 to 5.6.1), observed flow patterns in the Cambridge wind tunnel (section 5.8) and mathematical modelling (section 5.6.2) have indicated that the weight distribution and relative surface areas of the *nema* spine and thecal-bearing colony were the keys to how the *nema* functioned.

The oil tank experiments have shown that the distribution of mass along the colony was key to the function of the *nema* (section 5.4). An uneven distribution of mass would have been required to produce a vertical alignment, typically with the heavier end leading. The models in section 5.4, experiment ii, show that the centre of mass must have been located close to the proximal end of the colony for the *nema* to function as a stabiliser.

The Cambridge wind tunnel provided images of the flow pattern over the colony at a variety of angles relative to a current. When the colony was aligned with the free-stream current the *nema* would have had little affect on the flow. The *nema* might have reduced the drag by acting as a splitter plate. (Adding a splitter plate to a sphere significantly reduces the drag forces experienced in a flow. The splitter plate maintains a separation of the flow deflected around the sides of the sphere, allowing it to come together beyond the plate when it has stabilised along the plate surface (figure 5.37)). However the increased width of the turbulent wake with increasing *nema* length would seem to indicate a slight increase in drag. In this orientation the drag forces acting on the colony would have been directed along its length.

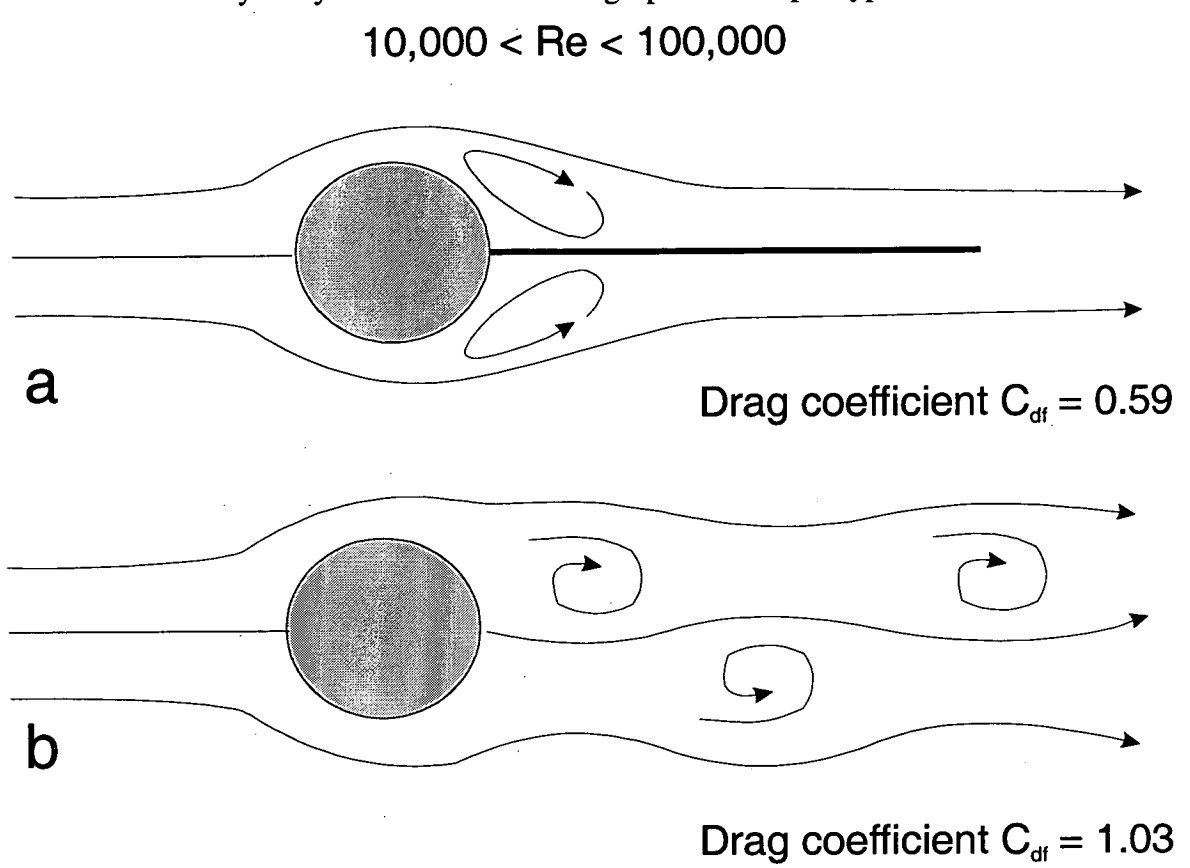

Figure 5.37: Drag reducing effects of a splitter plate attached to a cylinder. a. Cylinder with a splitter plate. b. Cylinder without a splitter plate. The splitter plate stabilises the wake beyond the cylinder in comparison to the more unstable flow pattern behind the simple cylinder. This has the effect of dramatically reducing the drag of the cylinder with the splitter plate. From Vogel (1981).

If the rhabdosome were to lie at an angle to the flow, the drag of the entire graptolite would be increased and can be observed as an increased area of turbulent flow behind the model colonies (figure 5.25). These drag forces would have pushed the graptolite around its centre of rotation until the forces were equal on either side of the rotation point (usually when it is aligned parallel to the flow). An uneven drag force on either side of the rotation point would have been required to cause the rotation, the side with the greatest drag forces acting upon it moving to a trailing position.

The mathematical model confirmed that it was the location of the centre of gravity (around which the colony would naturally rotate) and the relative surface areas of the colony and *nema* that were significant. Additional thickening of the collagen at the proximal end, and the lightweight construction of the *nema*, ensured that the rotation point was closer to the proximal end than the distal end of the colony. Consequently

the rhabdosome more distal of the rotation point would have presented a greater surface area to the flow than the rhabdosome more proximal of the rotation point. The end with the greater surface area, and therefore greater drag, would have rotated such that it trailed with the flow, leading to the observed *nema* downstream orientation.

A graptolite had dynamic stability in a position parallel to the flow, small perturbations would have resulted in a restoring force as greater surface area was presented to the flow.

5.9.2. Why was this of benefit to the graptolite?

During these experiments the *nema* maintained the orientation of the rhabdosome. Alignment to a fluid flow would have been consistent regardless of whether this flow was supplied by gravity or a current, and re-alignment to new flow was typically rapid. It is apparent that the *nema* was a functional structure and not just an evolutionary relic.

A consistent alignment to flow would have created a 'pseudo-stable' environment for the colony in which the fluid flow over the colony might be expected from the same direction. The flow impacting the colony would not have always come from the same direction, as the graptolite encountered a new flow it would have needed to re-align. However with rapid re-alignment to a current the colony would have spent the most of its time with the flow impacting from a uniform direction.

Having ensured a consistent orientation to flow, and consequently a uniform flow impact direction, any hydrodynamic structure could be 'designed' to act on this directed flow in preference to functioning with flows from any direction. This would have allowed graptolites to develop structures with a higher degree of functional complexity, specialised for unidirectional flow.

Jenkins (1997) suggested that the concept of a stable orientation is untenable with realistic ocean turbulence. He argues that the similarity of scale of graptolite colonies and turbulent whorls would have disallowed any stability. However the scales of turbulence he considers (50-100mm peak shear) are considerably longer than the juvenile specimens tested. A small specimen would react to a 100mm turbulent whorl as to any other current. Jenkins calculates the response time of scandent graptolites to a change in flow, and predicts that they would have reacted almost instantly. Jenkins' own experiments, using models in a turbulent environment, showed dye tracks tending to pass along the stipe of simple, stick-like species indicating a consistent alignment to the flow as observed with the isolated specimens.

Wind tunnel investigations of Rickards *et al.* (1998) indicated that thecal spines helped zooids feed from within the thecal apertures by creating vortices that entrained fresh food particles into the flow over the colony. These wind tunnel experiments held the model in constant orientation relative to the current flow. In another orientation particles might not have been entrained. The tank experiments have shown that a consistent (although not fixed) orientation was not unreasonable for living graptolites. The *nema* would have allowed thecal feeding structures to act efficiently by creating and maintaining an environment equivalent to a fixed position with consistent flow impact orientation.

The most likely function of the *nema* was to maintain the orientation of fluid flow over the colony such that thecal (and other) structures may have a consistent, and specific, effect on this flow. This would allow a graptolite to function at maximum feeding efficiency despite an environment of rapidly changing current directions.

5.9.3. Secondary structures

The function of secondary structures (vanes etc.) built on the *nema* was also investigated here through oil tank experiments (section 5.5) and visualisation of the flow in the Cambridge wind tunnel (section 5.8.2). What affect did the addition secondary structures have on the *nema* as a device for controlling orientation?

The oil tank experiments indicated that a vane-bearing *nema* could still have controlled the orientation of the colony, and that in fact alignment would have been more rapid. The addition of a vane appeared to strengthen the function of the *nema.* The observations made using the Cambridge wind tunnel showed that the addition of a vane would have greatly increased the turbulence behind the *nema*, and hence drag forces acting on it (compare figure 5.25 and 5.28).

The mathematical model indicated that the unbalanced drag forces (around the centre of gravity) produced by a colony disaligned with a flow would have provided the turning force to bring the colony parallel to the current. A vane-bearing *nema* would have presented an increased surface area to the flow (and consequently generated larger drag forces) than a simple *nema* spine, producing a greater turning force. The mathematical model (section 5.6.2) predicted that a *nema* with a vane would have reacted more rapidly, as was observed in the tank experiments (section 5.5).

No significant rotation of the vaned models was observed during the oil tank experiments. The model bearing the flat vane did undergo a slight rotation, during the oil tank tests (section 5.5), in order to obtain a preferred orientation of the vane as the model moved towards vertical alignment. During the colony rotation from a horizontal to vertical orientation, the model with a flat vane twisted about its axis such that the flat faces of the vane were vertical. This would have minimised the drag on the colony by minimising the surface area presented to the oncoming flow. However, it is suggested that the increased drag of the vane would have been required to enforce *nema* function. This might explain why flat vanes are not observed in the fossil record in favour of three-part or twisted vanes. These would have presented a large surface area to the flow regardless of their rotational orientation (when the colony was not aligned vertically).

The three-part vane appears to produce some rotation in the flow that runs over the vane when the model was angled to the flow (figure 5.35), but only a small rotation (to a preferred orientation) of the graptolite was observed during the oil tank testing. The rotation of the flow was not strong enough to carry the whole graptolite model

around. When the model bearing the three-part vane was aligned with the wind tunnel freestream current rotation of the flow was observed as a result of the vane (figure 5.33).

Multiple '*nema*' spines, also had a stronger effect on orientation than a single *nema* as a result of increased surface area at the distal end of the colony. This structure appears to have much the same functional implications as a vane, and merely represents another constructional solution.

5.10. Geological examples

The various experiments, modelling the *nema* both physically and theoretically, (sections 5.3 to 5.8) have shown that the presence of a *nema* would have had a strong controlling effect on the orientation of the colony. These tests have also indicated that a longer (or vaned) *nema* would have been more effective. The simple mathematical model (section 5.6.2) indicated that even a short *nema* would have affected the colony alignment to flow, and implied that a very robust colony (large in both cross-sectional dimensions) would require a longer or fatter/vaned *nema* for effective orientation control.

There are few apparent pre-conceptions regarding *nema* length, as this area has been little studied. This section looks at specimens of both diplograptid and monograptid species in an attempt to determine a rough value for the relative length of the *nema* (in comparison to the thecal-bearing colony), and to look for a real life test for the simple model.

5.10.1. Did real graptolites have long *nemata*?:

Method: The *nemata* and thecal-bearing colony sections of 440 specimens (350 diplograptids representing 186 species, and 90 monograptids representing 42 species) were measured from published illustrations. The ratio of *nema* length to thecal-bearing colony length was calculated. The maximum relative *nema* length observed

was taken for each species, these data were gathered together and assumed to represent minimum life values assuming that these represented *nemata* least reduced by taphonomic damage.

Results: The results are calculated as relative *nema* lengths. This is defined below:

$$\text{Relative length} = \frac{\text{length of nema / virgula}}{\text{length of thecal - bearing section}}$$

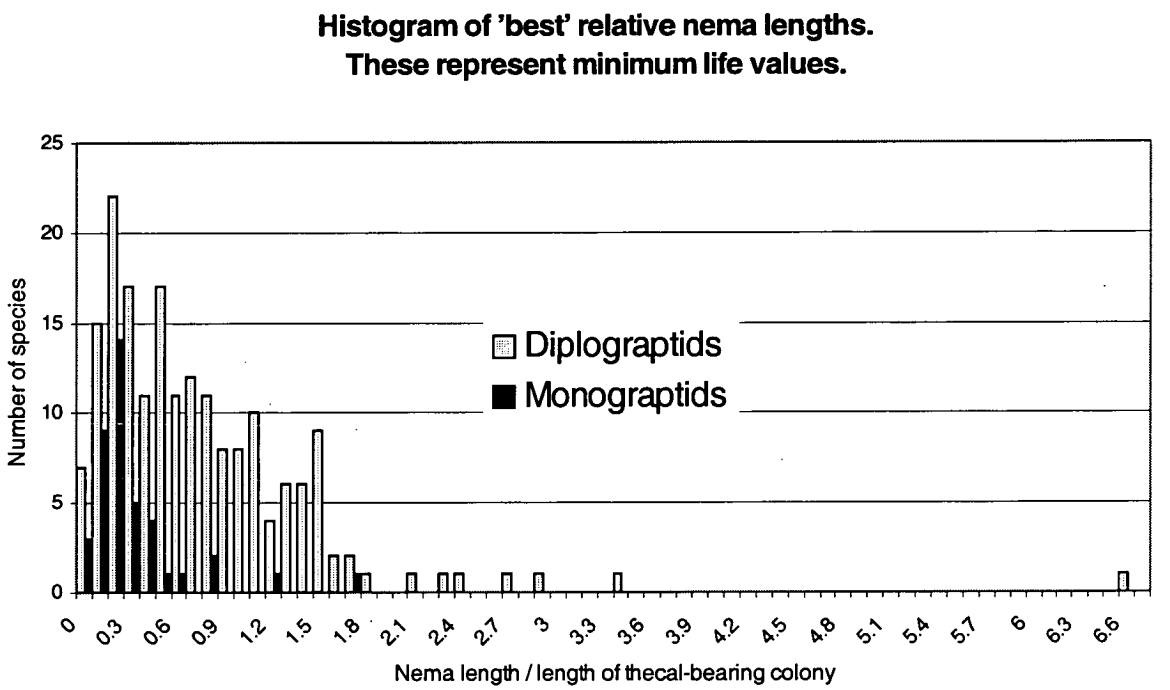

Figure 5.38: Histogram plot of the longest observed relative *nema* lengths (in comparison to that of the thecal-bearing colony) for each species. Data are divided into monograptid and diplograptid species. Original data given in appendix C.

The 'best' relative length values for each species (i.e. the maximum observed) are gathered together. In many cases only one specimen of a species was measured. These data are divided into two groups; monograptid and diplograptid species. As described below the maximum length observed represents a minimum life value, these are plotted as a histogram illustrating the abundance of species with these relative lengths (Figure 5.38).

- Diplograptid species relative *nema* length (*nema* length/thecal-bearing colony length):

  Average 0.70.

- Monograptid species relative *nema* length (*nema* length/thecal-bearing colony length):

  Average: 0.35.

Discussion: These data cannot provide reliable true nema lengths. A few fossil examples have shown that some species had relatively long *nemata* (up to x6.7 the thecal-bearing colony length: *Climacograptus spiniferus*) but their rare preserved occurrence most clearly illustrates that the *nemata* of most specimens are broken and incomplete. This delicate structure would have been easily damaged by events prior to burial (actions of seafloor currents etc.). Even the maximum values produced for each species can only be taken as representative of minimum life values, and no quantitative answers can realistically be gained. However the data collected have shown that many species certainly did have relatively long *nemata* such as would have been effective at maintaining colony orientation to a flow as described in chapters 5 & 7.

Typically the measured monograptid relative *nema* length values were consistently lower than the diplograptid ones. Does this imply that monograptids had shorter *nemata*?, or is this a bias in preservation. At first glance the mathematical model (section 5.6.2) may appear to suggest that monograptid colonies, being uniserial and therefore more narrow than a biserial diplograptid colony, would present a smaller surface area to the flow and might not require such a long *nema* for the same efficiency of function. However this is not what the model predicts. A biserial diplograptid colony would have had a more blade-like form than a uniserial monograptid colony, such that the diplograptid was twice as wide as the monograptid when measured across the scandent stipes (normal view) and both colonies exhibited a similar width across the thecal apertures (scalariform view). The oil tank experiments have shown that a colony will automatically realign itself to present the

least surface area to the flow. Even as they are re-aligning from a horizontal to vertical orientation a colony with a flat vane will twist about its axis such that the vane presents the least area to the flow while the colony is off-vertical. Consequently it would be expected that the real monograptid and diplograptid colonies would have presented the narrower scalariform colony face to the flow such that both types would have exposed a similar surface area. In addition the added weight of an additional line to thecae would have caused the diplograptid colony to have up to twice the weight per unit length along the thecal portion than the monograptid colony. The increase in weight discrepancy between the thecal-bearing colony and *nema* would have put the centre of gravity closer to the proximal end of a diplograptid colony, whilst the drag produced by the colony area would not have increased. In this case the model predicts that the monograptid (less exaggerated mass distribution and same surface area) would require a longer *nema* than the diplograptid (more less exaggerated mass distribution and same surface area) in order to have functioned as efficiently (section 5.6.2).

Monograptid *nemata* may have been more delicate than their diplograptid counterparts and consequently more easily broken. Another suggestion is that this length contrast is a result of an illustration bias; the monograptid specimens chosen for illustrations in papers are typically those with an absent *nema*, or the *nema* is not completely drawn.

Conclusions:

- It is observed that some diplograptid species (and fewer monograptid species) had relatively long *nemata*/virgulae that could have controlled orientation.
- The preserved relative *nemata*/virgulae lengths of monograptid species are typically much shorter than those of diplograptid species. (This is probably due to a preservation or illustration bias).

5.10.2. Supporting evidence for the mathematical model

Palmer (1986) examined a monotypic bedding plane assemblage of *Saetograptus varians* including specimens from a variety of growth stages (juvenile colonies with few thecae to mature colonies). He investigated the development of the *nema* with overall colony growth, and showed that the *nema* length had broadly increased in proportion with the thecal-bearing colony length maintaining a ratio of approximately 1:1. 'The nema tends to be twice as long as the thecal-bearing portion or the rhabdosome thus the length of the 'free' nema is roughly as long as the thecal portion'.

This finding supports a suggestion that monograptid species could also have borne long *nemata* and that their preserved absence may just be a weakness of the fossil record. This also provides a strong indication that the *nema* was required to keep growing with the colony to maintain function, as was predicted by the mathematical model for *nema* stabilisation (section 5.6.2), and other experimental evidence.

The model also predicted that robust colonies with a circular cross-section would require a longer or thicker *nema* or vane in order to function as efficiently as a thin *nema* spine on a slender or flat colony. The circular-cross section would have forced the colony to always present a large surface area to the flow, when not aligned parallel to it. The graptolite would be unable to twist about its axis to alter the exposed area as these experiments have shown that a blade-shaped colony would have done (in comparison with the flat vane, section 5.5).

It is very difficult to gain information about the cross-section shape of a graptolite colony from illustrations or flattened specimens, making this prediction of the model hard to test. A combination of both sclariform and normal views might provide some idea of the cross-sectional shape, but as flattened specimens both are distorted and unreliable. The illustrations of some species in Elles and Wood (1901-1918) show both sclariform and normal views.

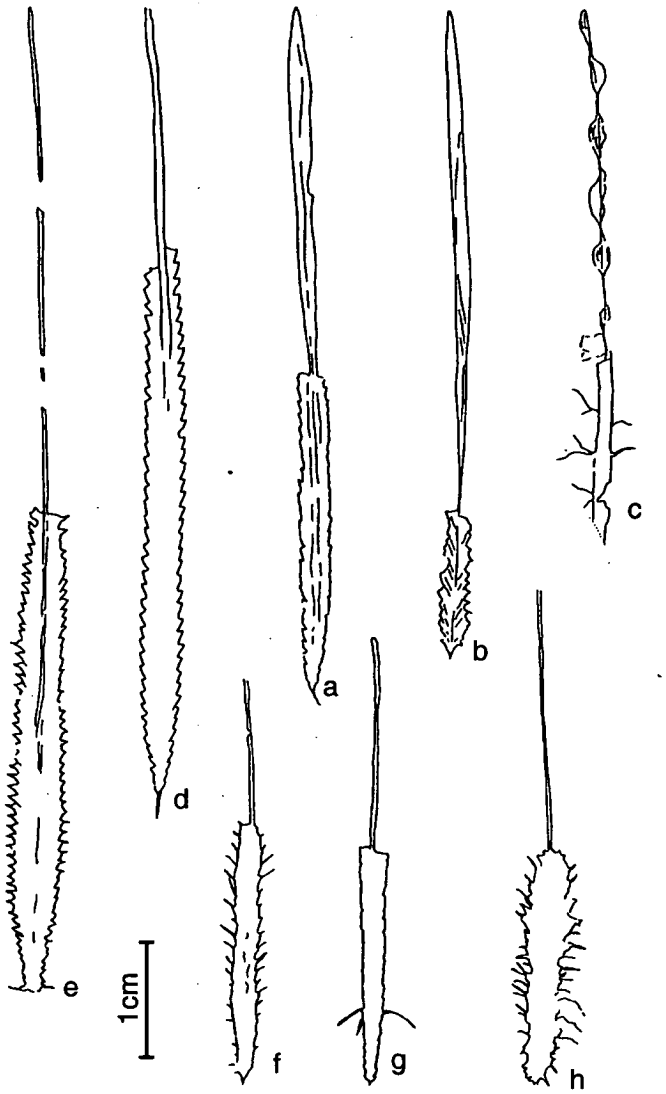

Figure 5.39: Camera lucida drawings of specimens form the Sedgwick Museum, Cambridge, illustrated in Elles and Wood (1901 - 1918). These species all have robust thecal-bearing portions which are balanced by long robust, or vane-bearing, virgulae. Plate and figure numbers are given as are museum catalogue numbers. GSE, Geological Survey, BIRUG or BU, Lapworth Museum, Birmingham.

Specimens a – c feature vane structures. a. *Orthograptus vesiculosus*, Plate XXVIII figure 8b. (BIRUG 1230). b. *Petalograptus palmeus*, Plate XXXII figure 1a (BU1302). c. *Hallograptus mucronatus,* Plate XXXIII figure 8a (SO55359).

Specimens d – h feature robust virgulae. d. *Orthograptus calcaratus vulgatus*, Plate XXX figure 5c (BU1263). e. *Orthograptus pageanus*, Plate XXVIII figure 3a (BU1222). f. *Orthograptus whitfieldi*, Plate XXVIII figure 6a (GSE5491). g. *Orthograptus pageanus abnormispinosus*, Plate XXVIII figure 5a (BU1227). h. *Glossograptus hincksii*, Plate XXXIII figure 2j (BU1332).

These would appear to suggest that vane-bearing species such as *Orthograptus vesiculosus* (figure 5.39) and *Climacograptus styloideus*, and those bearing a particularly robust *nemata* such as *Climacograptus antiquus var. lineatus* were robust in both orientations. Species bearing many spines along the thecal-bearing colony also commonly exhibited vanes and robust *nemata* such as *Hallograptus mucronatus nobilis*, *Glossograptus armatus* and *Glossograptus hinksii* (figure 5.39). These significant spines would have added to the drag producing area of these colonies that also appeared to have had an equant cross-section. Some of these specimens and other examples from Elles and Wood (1901-1918), depicting a combination of robust thecal-bearing colony section and robust (or vane-bearing) virgulae, are illustrated in figure 5.39.

Kirk (1972) suggested that vanes, built on the *nema*, were intended to prevent rotation of scandent colonies, an idea which is not supported by this investigation. However Kirk remarked that 'vane structures are commonly built onto biserial colonies with a circular, or square, cross section rather than onto blade-like biserial colonies'. This observation supports the predictions of the mathematical model (section 5.6.2) where colonies with an equant cross-section would require a longer or wider *nema* in order to function as efficiently as a smaller *nema* on a more blade-like colony, able to present a smaller surface area to the flow.

The obvious exception to this is *Petaloithus*, which has an exaggerated rectangular cross-section and may bear vane structures (e.g. *Petalograptus palmeus*, figure 5.39). Despite the predictions of the mathematical *nema* model (section 5.6.2), that a flat colony shape would have only required a narrow virgula, it could be argued that the substantial surface area of such a colony, even when orientated with the large surface parallel to the flow, would have added considerably to the drag of the thecal-bearing portion. The model oversimplifies the drag equations, using the same (shape dependant) drag coefficient for such a flattened shape as a cylindrical colony. The increased drag represented by the large surface area of *Petaloithus* would have been counterbalanced by the presence of the vane, reinforcing virgula function.

5.11. Further study

A proper study of fossil *nemata* dimensions and structures would provide more significant evidence for the possibility of the nema as an orientation control device. A similar study to that carried out by Palmer (1986) on *Saetograptus varians*, looking at the relative growth of the *nema* as the colony matured using mono-specific biserial specimens found on a single bedding plane, could provide valuable information. Provided such assemblages, rich in graptolites of variable stages of maturity, could be found this might then be extended to look at a number of species to test whether such balanced growth (thecal-bearing colony and *nema*) is typical.

6. The possible hydrodynamic function of proximal spines on scandent graptolites

6.1. Introduction

6.1.1. Proximal structures

Spinose proximal structures are commonest amongst scandent biserial graptolites. One of the most abundant of these are arrays of proximal spines, which can form at the aperture of the sicula or on the proximal thecae of the colony, and are the concern of this study.

Some spines appear as innovations in a single lineage, such as the two sets of paired antivirgellar spines in *Hustedograptus hystrix*. Others, such as the virgella are considered to be so morphologically conservative that Fortey and Cooper (1986) attempted to used it to identify a common single ancestor for the planktonic graptoloids. The importance of understanding any function that these spines might have served is highlighted by this suggestion; Fortey and Cooper (1986) postulated that such a constant feature is an evolutionary relic, without use and hence unlikely to have been either lost or gained multiple times during graptoloid evolution. However it has now been shown that the virgella has evolved more than once (Williams & Stevens 1998) indicating that it may indeed have served an essential purpose for the planktonic graptoloids.

Two observations suggest that there may be a flaw in the argument that proximal spines were highly conserved due to a lack of function. Firstly, many spines, including the virgella, continue to grow throughout the astogeny of the colony, suggesting that they had a lifelong utility for the rhabdosome. Secondly, graptoloids began to grow proximal spines early in their astogeny, when their energy budget must have been precarious. Assuming that immature graptolite zooids probably built

most of the fuselli of the rhabdosome (Rigby and Sudbury 1995), then a single immature zooid had to build the sicula, apertural spines and at least the first elements of th1 or th1^1. A pair or three zooids, only one of which was mature, had to build th2 or th1^1 and 2^1 at the same time as generating any ornaments to these thecae. Subsequent zooids experienced a progressively more favourable ratio of food gatherers to builders. This early allocation of scarce resources to structures suggests that they had a use, and so were 'worth' building in terms of the likely survival of the colony even though their construction was costly.

6.1.2. Brief evolutionary history of proximal spines

Among graptoloids thecal and rhabdosomal spines are very rare in dichograptids, which also typically had a ventral process rather than a virgellar spine. The virgella first appeared in the Arenig (Cooper and Fortey 1983) in the genus *Xiphograptus*, and is now also known in the genera *Didymograptus* (Rickards and Khashogii, 2000) and *Yutagraptus* (Riva 1994) respectively of Llanvirn and late Arenig age. In post - Llanvirn strata, graptolites with a virgella and proximal spines are increasingly common (*Dicranograptus*, *Dicellograptus*, *Leptograptus*) and in biserial diplograptids proximal rhabdosomal spines become almost universal. A very small number of biserial species lack proximal thecal spines before the late Caradoc. However, toward the end of the Ordovician, in the late Caradoc and Ashgill, the number of spineless biserial species increased (e.g. *Normalograptus* and the latest orthograptids) and in the early Silurian antivirgellar spines and proximal thecal spines were uncommon. This may be a chance factor deriving from the small number of end-Ordovician survivors.

6.1.3. Multiple thecal spines

The spines of graptolites were not always limited to the first pair of thecae, several graptolite species continued to build thecal spines on subsequent thecae. Although many species exhibited multiple spines along the colony the patterns were subtly different. In many cases these spines were rapidly reduced to thecal processes after

approximately three spine pairs (for example *Climacograptus haljalensis* and *Amplexograptus bekkeri*), and these processes may have been more like flanges than spines. These flanges typically projected from the geniculum of the thecae, and would have presented a greater obstacle to flow running over the colony.

The dicranograptids (for example *Dicranograptus nicholsoni longibasalis*) commonly built thecal spines along the whole biserial section length. A juvenile specimen of such a graptolite would have had the appearance of a spinose biserial species, with the spines on the geniculum of the thecae. The glossograptids (e.g. *Paraglossograptus holmi* and *Glossograptus hincksii fimbriatus*) included biserial species that also had a spine (or rutellum) on every thecae. These projected from the proximal edge of the thecal apertures.

Many monograptid species also feature multiple spines along the colony; these are commonly built on, or develop into, hoods over the thecal apertures. The paired thecal spines of the monograptid *S. chimera* were investigated by Rickards *et al* (1998) using the Bristol wind tunnel and LDA system. This species had pairs of thecal spines built on successive thecal apertures, which were shown to produce a set of trailing vortices. It was believed that these would entrain fresh food bearing water from beyond the rhabdosome path.

6.1.4. Previous suggestions of function for proximal spines.

Spines at the proximal end of a biserial rhabdosome might have had a local function, such as protecting the sicular zooid, and / or a general use affecting the whole colony. It has been suggested that spines were used by individual graptoloids for feeding (Rigby and Dilly 1993) and for defence against predation (Loydell and Zalasiewicz 1998). Sicular spines might have functioned in this way for the sicular zooid, though it is difficult to understand why multiple spines often developed in this area and on early thecae, but not on later thecae. Spines may also have acted to aid buoyancy through an increase of skin friction and drag on the colony (Mitchell and Carle 1986). It was proposed that the increased drag might hold the graptolite at the

required depth; for this to have been very effective, graptoloids would have been forced to exist at low Reynolds numbers where viscous forces and skin friction dominate, as suggested by Mitchell and Carle (1986). This seems unlikely in view of previous modelling work that has been done on graptoloid rhabdosomes (Rigby and Rickards 1989, Rickards *et al.* 1998).

In the standard orientation of graptolites, which is supported here by the conclusions of chapter 5, it seems likely that structures at the proximal end had a prolonged effect on water moving over the colony as a whole, as the proximal end encounters the flow first. It is possible that the small-scale turbulence which graptoloid colonies experienced might have meant that the idea of a stable orientation requires modification (Jenkins 1997). However, experiments with a variety of graptoloid forms suggest that blade or rod shaped colonies were most responsive to such changes in flow direction (Jenkins 1997) and might have orientated quickly enough to have spent the majority of their time in a relatively consistent orientation to the force being applied to them regardless of the varied directions from which this force was coming.

6.2. Experimental aims and methods of testing these aims

Eleven common designs of proximal end spines were identified (figure 6.1, table 6.1). These are all 'real' proximal end designs, found on biserial graptolites of Arenig to Llandovery age. Some are unique to a single lineage, whilst others are common and iteratively present.

These designs were chosen as they represented simple spine patterns formed from combinations of thecal and anti-virgellar spines only. Biserial graptolites also embellished the proximal end with a wide range of other structures: vanes, ancora etc. but these are beyond the scope of this study and are not commented on here.

		Species	Virgella	Paired anti-virgellar spines	Thecae 1^1 spine	Thecae 1^2 spine
Simple-sicula set		*Climacograptus pulchellus*-type	normal	---	---	---
		Pseudoclimacograptus scharenbergi-type	normal	---	Yes	---
		Climacograptid-type	normal	---	Yes	yes
		Amplexograptid bekkeri-type	normal	---	Spines on first six thecae.	
Anti-virgellar spine set		*Geniculograptus typicalis*-type	normal	yes	---	---
		Amplexograptus maxwelli-type	normal	yes	Yes	---
		Hustedograptus uplandicus-type	normal	yes	Yes	yes
		Hustedograptus teretiusculus-type	normal	Paired lappets	Yes	yes
		Hustedograptus. hystrix-type	normal	2 spine pairs	Multiple spines	multiple spines
		Pacificograptus pacificus-type	normal	yes	Spines on all thecae	
Deflected virgella		*Climacograptus brevis*-type	deflected	---	---	---
		Climacograptus (Diplacanthus) spiniferus-type	deflected	---	Yes	---

Table 6.1: The twelve common designs of proximal spines are divided into three sets here. The simple-sicula set which have a straight sicula cone, a 'normal' straight virgella and no anti-virgellar spines. The anti-virgellar set which have a straight sicula cone, a 'normal' straight virgella and at least one pair of anti-virgellar structures. The deflected-virgella set have a curved sicula and virgella deflected across the sicula opening.

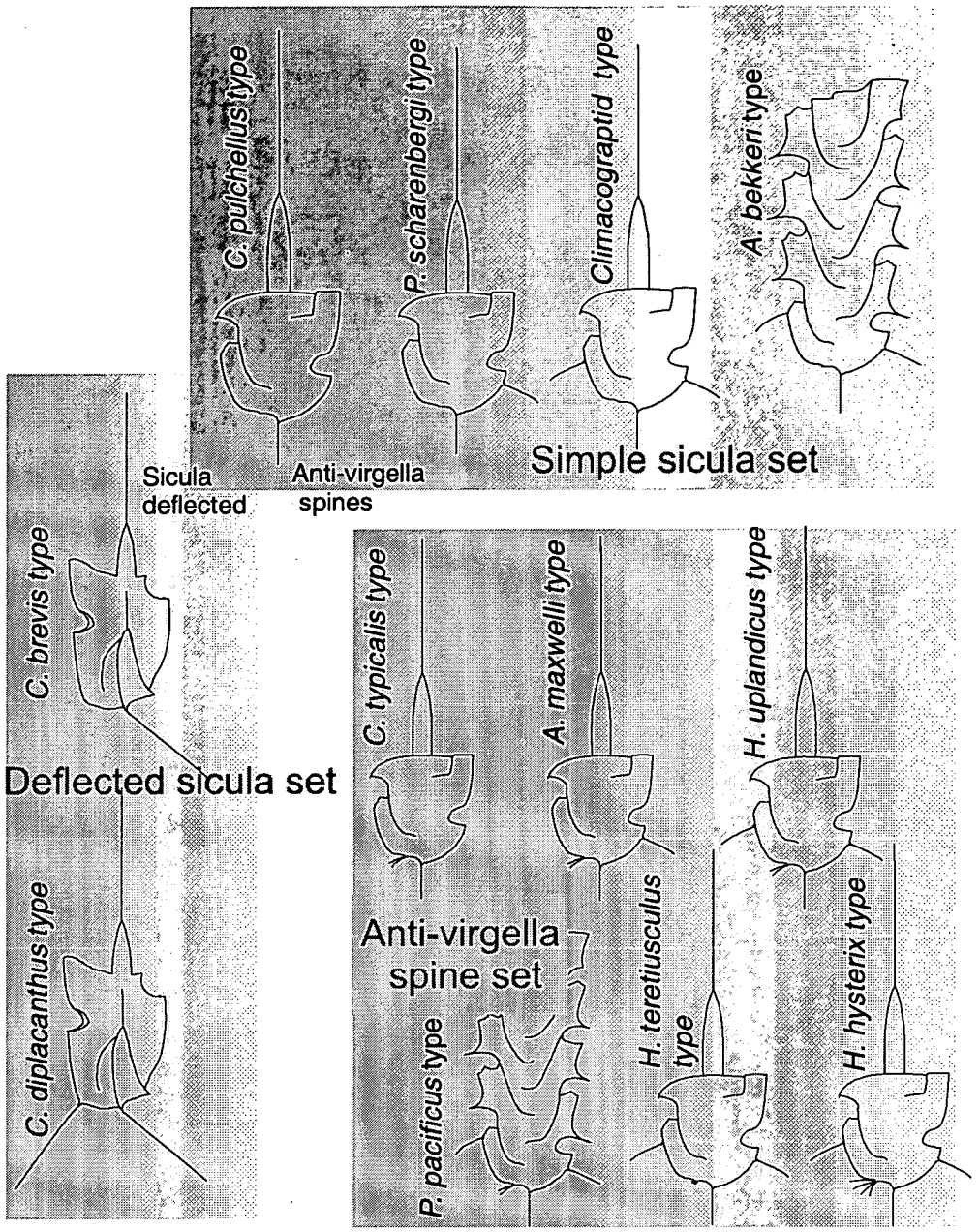

Figure 6.1: Twelve common designs of proximal end spines identified in this study. These are divided into three sets; three with a simple sicula (straight and without ventral spines), five with anti-virgellar spines, and two with a deflected sicula and virgella.

The experiments were designed to investigate the patterns of fluid flow over each proximal end 'design' and to compare these results with flow over proximal ends lacking spines. They were also intended to investigate changes in flow pattern which might occur during the early development of the colonies and to examine the importance of spine angle to any functions which might be identified.

These questions are addressed in the following sections:

- What hydrodynamic role might proximal thecal spines have had?
- What is the significance of spine angle?
- How might spines on successive thecae have interacted?
- What hydrodynamic role might anti-virgellar spines have had?
- What hydrodynamic role might a deflected virgella have had?
- How do the flow patterns/functions change through early astogeny?

6.3. Investigating the role of proximal thecal spines

Two model biserial rhabdosomes were constructed, one with a straight sicula (based on *Amplexograptus maxwelli*) and one with a deflected sicula (based on *Climacograptus (Diplocanthus) spiniferus*) (see section 4.4). These base models were constructed with removable spines so that different spine patterns could be modelled.

These models were tested in both the Cambridge wind tunnel, which provided a qualitative view of the flow patterns, and the Bristol wind tunnel which provided more quantitative data but only of the flow through a few limited planes. Additional information on the effect of proximal spines on orientation was gained from seawater tank experiments using isolated specimens.

6.3.1. Cambridge Wind tunnel

Method: The models were tested, with and without the $th1^1$ and $th1^2$ spines, in the Cambridge wind tunnel which was run at velocities between 0.5 and 0.7 m s^{-1} (Re's 5,000 - 8,000), which represent the minimum running velocities of the wind tunnel. Flow patterns were visualised using smoke streams, and these were photographed using a digital camera and processed to disc.

Results: The results are shown here as digital photographs of the smoke streams flowing over the models in the wind tunnel (figure 6.2). The pictures are negative images in which streams of white smoke against a black background appear as streams of black smoke against a white background. Flow line interpretations have been drawn on based on observations made during wind tunnel runs.

The *C. pulchellus*-type (figure 6.2 a and 6.3 a) spine array is the most simple case of all tested models, bearing no proximal spines except the virgella. If a smoke stream directly hits the colony it runs over the surface and into standing eddies in the thecal apertures. A smoke stream that just misses the colony is deflected further away, by the separation at the colony edge, and flows past the thecal apertures. A smoke stream hitting a thecal spine (*Climacograptus*-type and *Pseudoclimacograptus scharenbergi*-type, figure 6.2 b & c and 6.3 b & c) is cut by the spine and expands laterally along the spine, towards and onto the rhabdosome body. As the particle-bearing air runs up the spine, small–scale turbulence causes mixing with air flowing around the spine, and it is swept downstream. As a result, the concentration of smoke particles flowing along the spine attenuates with distance. This smoke, which would otherwise have bypassed the colony unaffected, now runs over the surface and into vortices in the thecal apertures along the rhabdosome. The flow over the two columns of scandent thecae appears to be largely independent, with only a little smoke flowing across the rhabdosome from one side to the other.

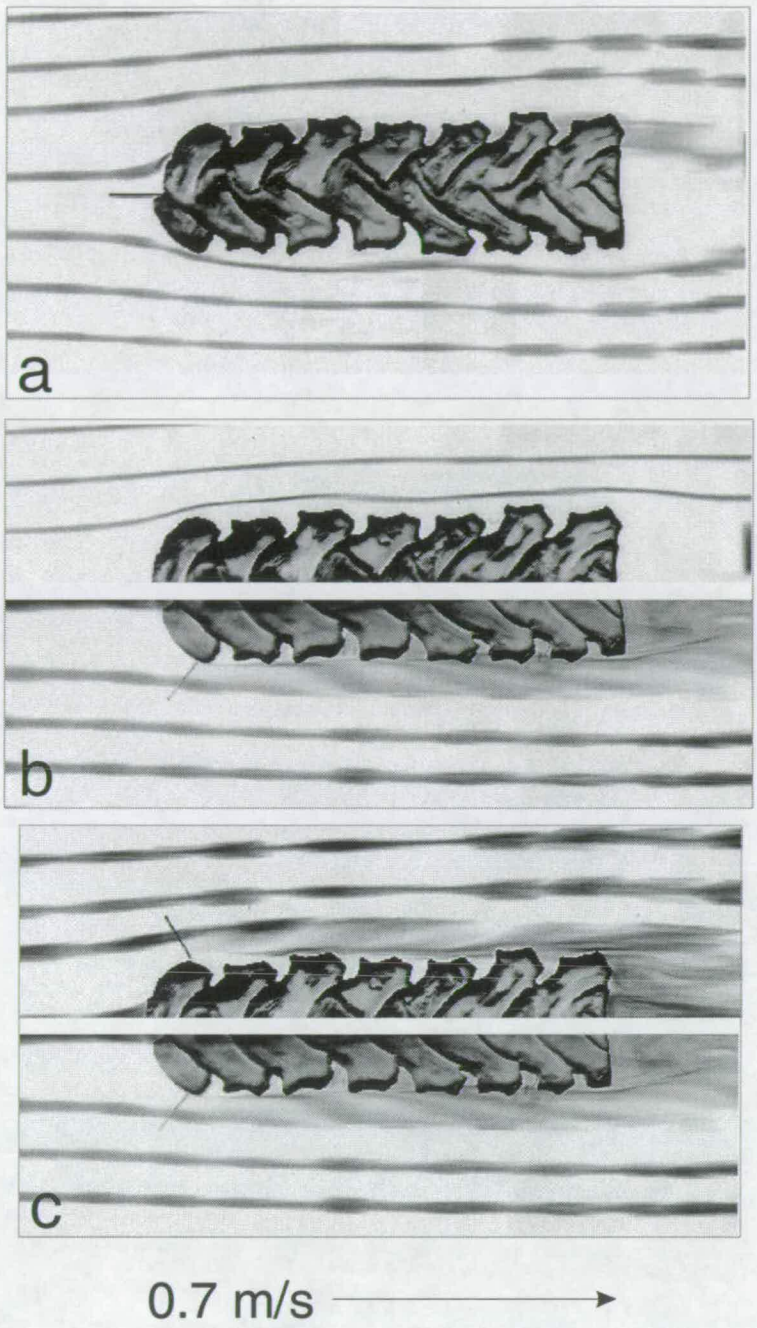

Figure 6.2: a. *Climacograptus pulchellus* lacks any proximal spines (except the ubiquitous virgella). A smoke stream directly hitting the rhabdosome flows over the surface and into the thecal apertures, otherwise it is deflected around the colony, and passes clear of the surface. The addition of thecal spines (b. *Pseudoclimacograptus schaerenbergi* and c. Climacograptid type) flares these smoke streams (which would otherwise have been deflected) along the spine and onto the colony surface, where it then flows into the thecal apertures.

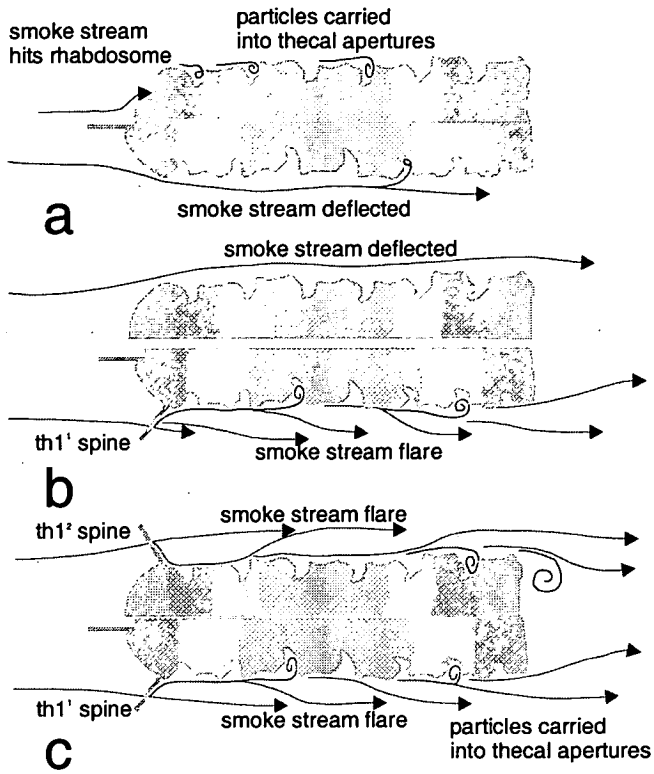

Figure 6.3: An interpretation of the flow over the simple sicula spine set observed in figure 6.2 based on observations made during testing.

Conclusions: Spines were functional. Thecal spines primarily increased feeding efficiency by bringing food to the surface from a wider capture area.

6.3.2. Bristol wind tunnel

Method: The *Amplexograptus maxwelli* body-type model was also run in the larger wind tunnel at the University of Bristol, which was able to run at low velocities (down to 0.1 m s^{-1}). Measurements were made using laser Doppler anemometry (LDA) (section 3.2.1). Data are processed using TECPLOT (version 7.0).

This investigation focused on the changing flow patterns in the absence or presence of a spine on $th1^1$. The thecal spine was investigated by observing the flow through a plane situated just behind each of the first three dorsal thecal apertures (figure 6.4), at

a growth stage consistent with the completion of that thecae, both with and without the spine

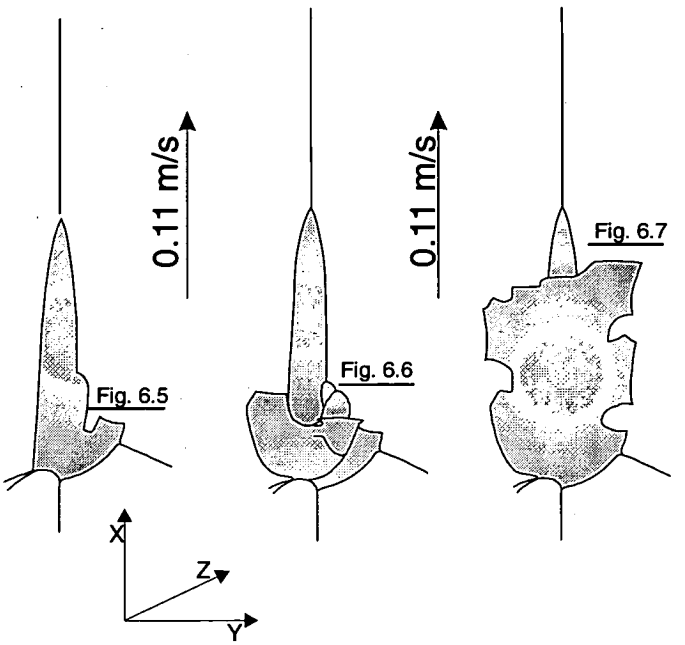

Figure 6.4: The *Amplexograptus maxwelli*-type body was modelled at three astogenetic stages. These were tested in the wind tunnel at the University of Bristol and flow through (and within) the marked planes was observed using LDA, and given here as figures 6.5 to 6.7.

Results: The results from this set of experiments are shown as contoured vector plots of a two-dimensional plane. The vectors represent the velocities of flow within the plane, and the contours represent velocity of flow through the plane. All the planes were measured perpendicular to the wind tunnel freestream flow (0.1 m/s), such that the major component of flow velocity is through the plane, and any within-plane velocities are disturbances caused by the presence of the model. The locations of the planes investigated are shown in figure 6.4.

The first dorsal plane (figure 6.5) clearly shows a low (through-plane) velocity shadow behind the spine, and in-plane velocities are observed running down the spine towards the rhabdosome into a very low velocity area directly behind the thecal aperture. When the spine is absent the size of the low velocity zone is reduced and a strong vortex is set up, in contrast to the much weaker vortex formed behind the

spine-bearing theca (figure 6.5). Further along the colony the effect of the spine can be seen in the other dorsal planes (figures 6.6 and 6.7) as a line of strong in-plane velocities lying in the lee of the spine, and running towards the rhabdosome.

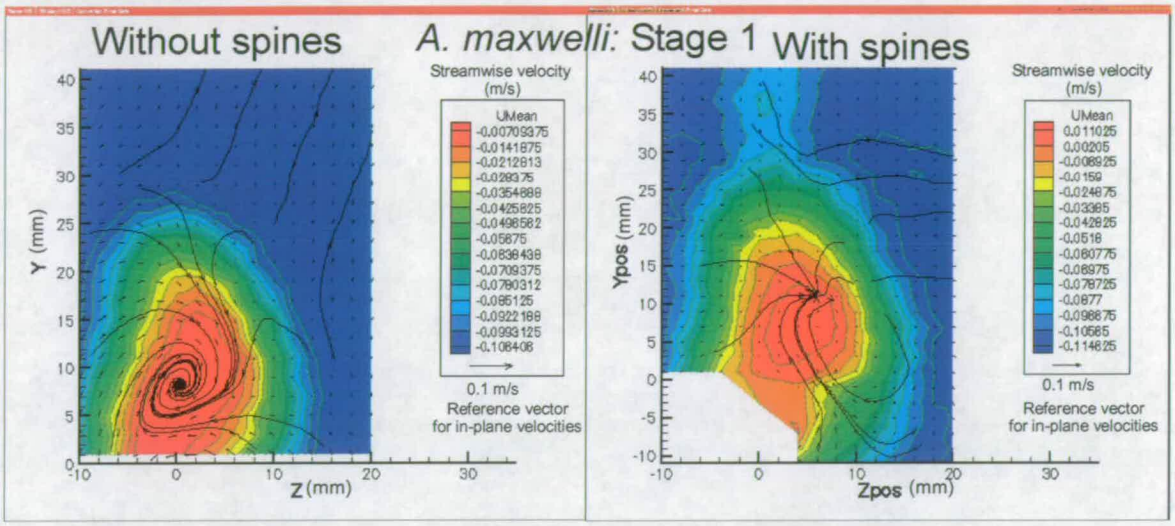

Figure 6.5: A vector plot of the flow through (and within) a plane behind th1[1], the position of which is shown in figure 6.4, using the most juvenile model. The two plots represent the flow in the presence and absence of the thecal spine. The vectors, direction and length, represent in-plane velocities, direction and speed. The colour represents through-plane velocities. Streamtraces have been added to show how a particle would move through the plane. The large low velocity area on both plots is behind the thecal aperture, and it is slightly larger in the presence of the thecal spine. Without this spine a vortex is set up in this area. In the presence of the thecal spine an elongate area of low through-plane velocities can be seen behind it, and in-plane velocities in this area run towards the graptolite.

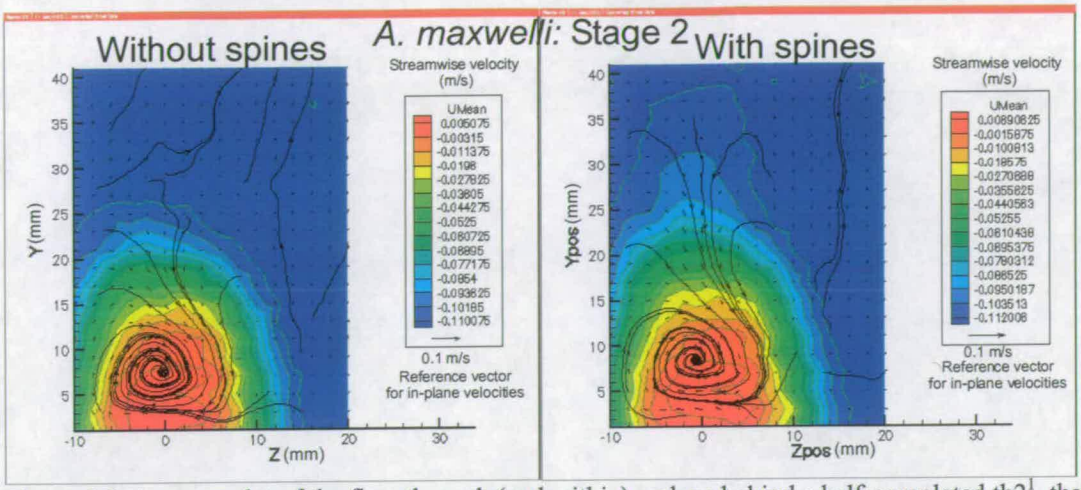

Figure 6.6: A vector plot of the flow through (and within) a plane behind a half-completed th2[1], the position of which is shown in figure 6.4. The two plots represent the flow in the presence and absence of the spine on th1[1]. The vectors, direction and length, represent in-plane velocities, direction and speed. The colour represents through-plane velocities. Streamtraces have been added to show how a particle would move through the plane. The second plot shows a small low (through-plane) velocity area behind the thecal spine, which is absent in the first plot when the spine is absent, in-plane velocities in this area run towards the graptolite. The presence of a thecal spine has little effect on the large low-velocity area behind the thecal aperture; a vortex is present in both cases.

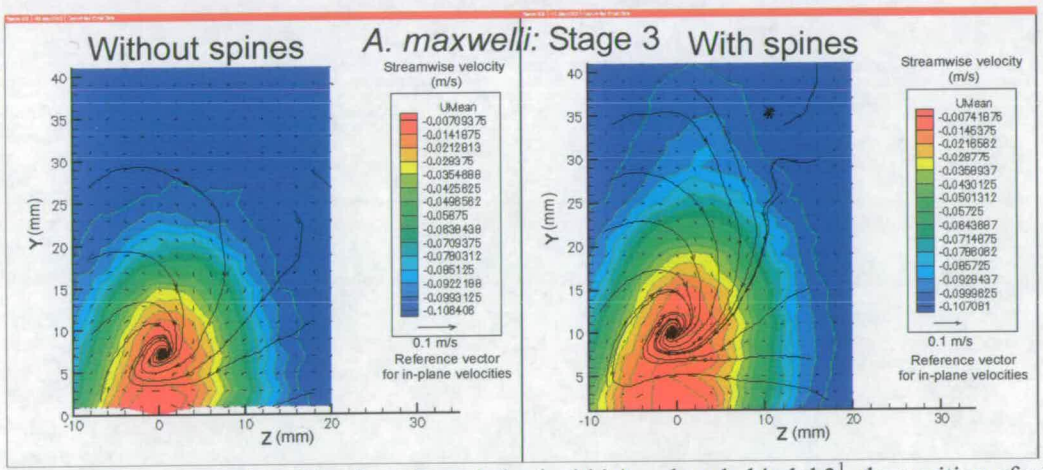

Figure 6.7: A vector plot of the flow through (and within) a plane behind th3[1], the position of which is shown in figure 6.4. The two plots represent the flow in the presence and absence of the spine on th1[1]. The vectors, direction and length, represent in-plane velocities, direction and speed. The colour represents through-plane velocities. Streamtraces have been added to show how a particle would move through the plane.

The second plot shows a small low (through-plane) velocity area behind the thecal spine, which is absent in the first plot when the spine is absent; in-plane velocities in this area run towards the graptolite. The presence of a thecal spine has little effect on the large low velocity area behind the thecal aperture; a vortex is present in both cases.

Conclusions:

- Through plane velocities are reduced directly behind the spine, as would be expected.
- In the lee of the thecal spine flow is drawn towards the colony.
- This increased flow towards the colony is detectable even beyond $th1^3$.

6.3.3. Isolated specimens tested in a tank of seawater

Simple seawater tank experiments (as described in section 3.3.1) were carried out using isolated specimens of juvenile biserial colonies (*A. leptotheca* and *C. typicalis*) borrowed from the Sedgwick Museum, Cambridge. These demonstrated that the proximal spines had a large effect on the stable sinking orientations of these juvenile colonies. As the sicula develops and the anti-virgellar spines are constructed these increase the drag of the ventral side of the colony, tilting the stable orientation up on the ventral side. Once the thecal spine has been added, this creates more drag on the dorsal side to tilt the colony back.

Conclusions: The proximal spines would have had a strong effect on the stability of the colony during early astogeny. This is particularly true of the anti-virgellar spines.

6.4. How significant is the angle of the spine?

6.4.1. Cambridge wind tunnel

Method: The mature *Amplexograptus maxwelli* base model was tested (in the same position in the wind tunnel) with the thecal spine ($th1^1$) projecting at a range of angles to the colony axis. This experiment was designed to test the significance of this angle to the processes observed drawing smoke-bearing airflow along the spine in section 6.3.1.

The Cambridge wind tunnel was run at velocities between 0.5 and 0.7 m s^{-1} (Re's 5,000 - 8,000), which represent the minimum running velocities of the wind tunnel. Flow patterns are visualised using smoke streams, and these were photographed using a digital camera and processed to disc.

Results: Regardless of angle, the thecal spines caused an impacting smoke stream to be extended laterally and drawn along the spine towards the graptolite rhabdosome (figure 6.8). The angle of the spine was significant to the efficiency of this process. The smaller the angle between the spine and direction of flow the greater the percentage of smoke from the streamer that extends along the spine, and is consequently carried into all the thecal apertures along the side of the colony.

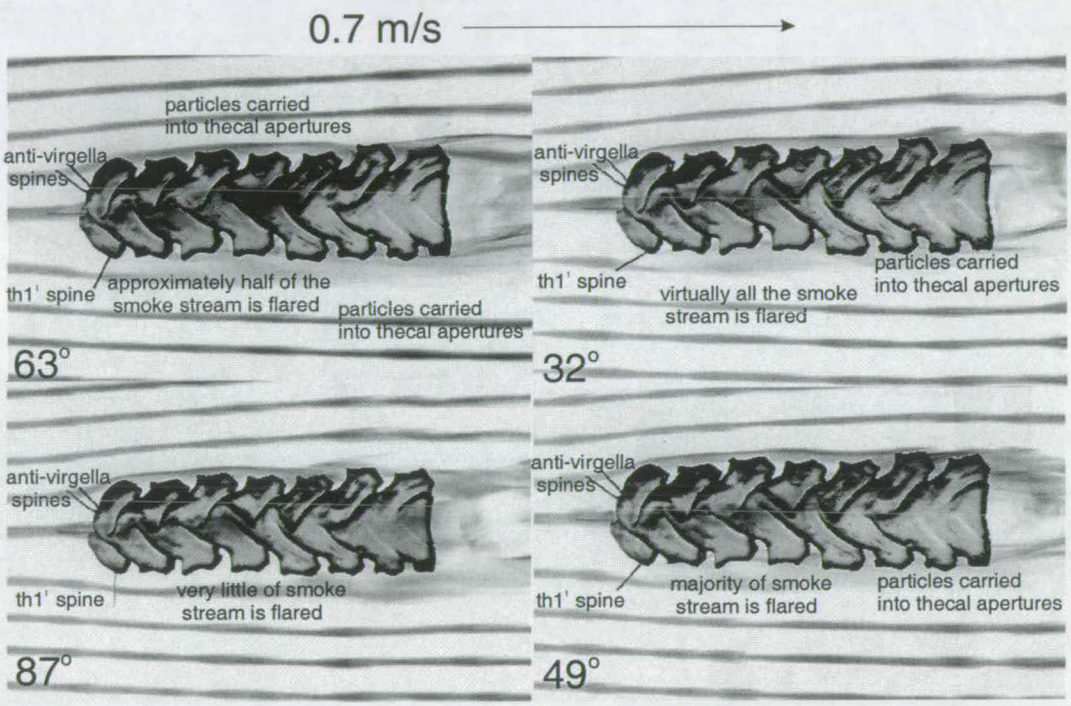

Figure 6.8: The *Amplexograptus maxwelli*-type model was run in the Cambridge wind tunnel, in the same position, with the $th1^1$ spine set at a range of angles to a line running along the length of the colony; 32°, 49°, 63° and 87°. At 32° the majority of the impacting smoke stream is flared onto the rhabdosome surface and very little smoke is visible running past the colony. As the spine angle increases more smoke is visible running past the colony, and a smaller percentage of the smoke stream is brought to the surface. At 87° virtually all the smoke runs past the colony without flaring towards the surface, or entering eddies in the thecal apertures.

The action of the spine was observed at a wide variety of different angles, all of which are not illustrated here. When the spine is nearly at right angles to the flow direction (87° as shown) barely any of the smoke streamer is drawn inwards, and no smoke is brought into the majority of the thecal apertures. A spine at 0° (i.e., parallel to the colony) naturally lies within an impacting smoke stream, as it lies along the flow direction. The smoke stream flows along the spine and onto the rhabdosome surface with a small amount of turbulent mixing with surrounding airflow. If the spine is directed with the flow (at angles greater than 90°), as opposed to into the flow, the smoke is drawn away from the graptolite.

Conclusions:

- The spine angle is significant to the effective function of the spine.
- At low angles flow is sampled from only a small area, but a greater percentage of the smoke-bearing flow is drawn along the spine. Using a spine at a larger angle flow is sampled from a greater area, but only a small percentage of the smoke bearing flow extends laterally along the spine.
- When the spine is at an angle greater than 90° to the colony axis impacting flow is drawn away from the colony.

6.4.2. Budget model

The proximal spines were clearly functional, and have implications for feeding efficiency. With smoke acting as a proxy for food particles, it can be seen that particles carried in a flow impacting a spine would be carried along it, and across the rhabdosome surface, into small vortices within the thecal apertures where it would be relatively easy for the zooids to filter them out.

In the very juvenile stages a graptolite would have had a limited energy budget, with very few zooids to support and build the colony. The production of proximal spines during these very early stages would have been relatively expensive to the colony,

and this cost must be balanced by an energy or survival gain, through an increased feeding efficiency or other functions.

This 'payback' is investigated here by theoretically calculating the time taken for a spine to pay for its construction through energy gain to the colony. Energy output (building the spine) is set against energy gain (particles drawn to the colony by the spine). A variety of spine lengths and angles are considered in order to consider the optimum geometry for spines. The spine is modelled as a rod of length x, projecting at angle ϕ from an imaginary line running along the length of the biserial colony (figure 6.9).

The budget calculation is approached through a series of steps. Firstly mathematical functions are assigned to approximate the experimentally observed relationships between percentage of extended smoke-streamer reaching the rhabdosome, angle and length of spine. A variety of different functions were used. The volume of particles brought to the graptolite by a spine of length x and angle ϕ is calculated, using combinations of these functions. The volume of particles brought to the graptolite is assumed to be proportional to the energy gained consuming them, and the cost of building the spine is then calculated (this is assumed to be proportional to the length of spine). The energy gain is given as a rate (particles per second) consequently the time in which a spine would have paid for itself may be calculated as building cost divided by energy gain rate. Each combination of functions will provide a different prediction of optimal spine geometry.

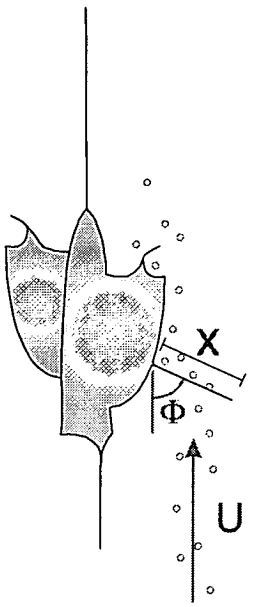

Figure 6.9: The simplified 2-dimensional model, used for the budget calculations, represents the proximal spine (here a thecal spine) as a simple stick of length x and at angle ϕ to a line running along the length of the colony. A concentration (P) of particles are carried in a flow at velocity U along the line of the colony, to impact with the spine.

These calculations are theoretical and oversimplified. The limitations and assumptions of this model must be fully considered before applying any results.

Assumptions and Limitations:

1. The spine was modelled as a rod, whereas in reality these spines taper away from the colony. This would have reduced the cost of building such a spine.

2. The energy gained from consuming food particles, and the energy cost for building a spine, are totally unknown. Consequently it is impossible to get real figures out of this model, however the model will still produce the same graphic distributions of energy against x and ϕ.

3. The relationships between attenuation and distance, and angle and percentage of smoke-stream extension, are also unknown in detail. Without an accurate picture

of these relationships it is hard to assign a mathematical function to them. Mathematical functions are used which are too simple to recreate the complexity of reality. Without reliable functions relating the variables it is impossible to make accurate predictions about optimal angles, rather it is intended that this model should provide a different perspective on the problem of proximal spines and provide some insight.

4. The model is only two-dimensional.

The model: For simplification this is a two-dimensional model (figure 6.9), such that the water has a concentration of particles P per metre^2. At point x along the spine, a very small increment of the spine, of length δx, will be hit by $PU\sin\phi\delta x$ particles. A percentage of an impacting smoke stream initially extends along the spine governed by $f(\phi)$ (a function relating the percentage of the smoke streamer extension to the angle of the spine ϕ), but small-scale turbulence mixed this smoke-bearing air with passing clear-air, and the percentage of smoke-particles attenuates along the spine. This means that when the extended smoke-streamer has stretched the distance to the rhabdosome 'body' the number of particles has been reduced to a percentage A(x) of the initial streamer.

$f(\phi)$ is a function giving the percentage of particles (smoke or food) hitting the spine which are extended along the spine. Observations from the smoke tunnel experiments have shown that this varies with the angle; going from 100% at $\phi = 0°$ to 0% at $\phi = 90°$ to flow direction (section 6.4). It is very unlikely that the true relationship between angle and streamer-extension would fit a mathematical equation of any simplicity, but this is only an elementary model so basic functions will be used to look at the possibilities (figure 6.10).

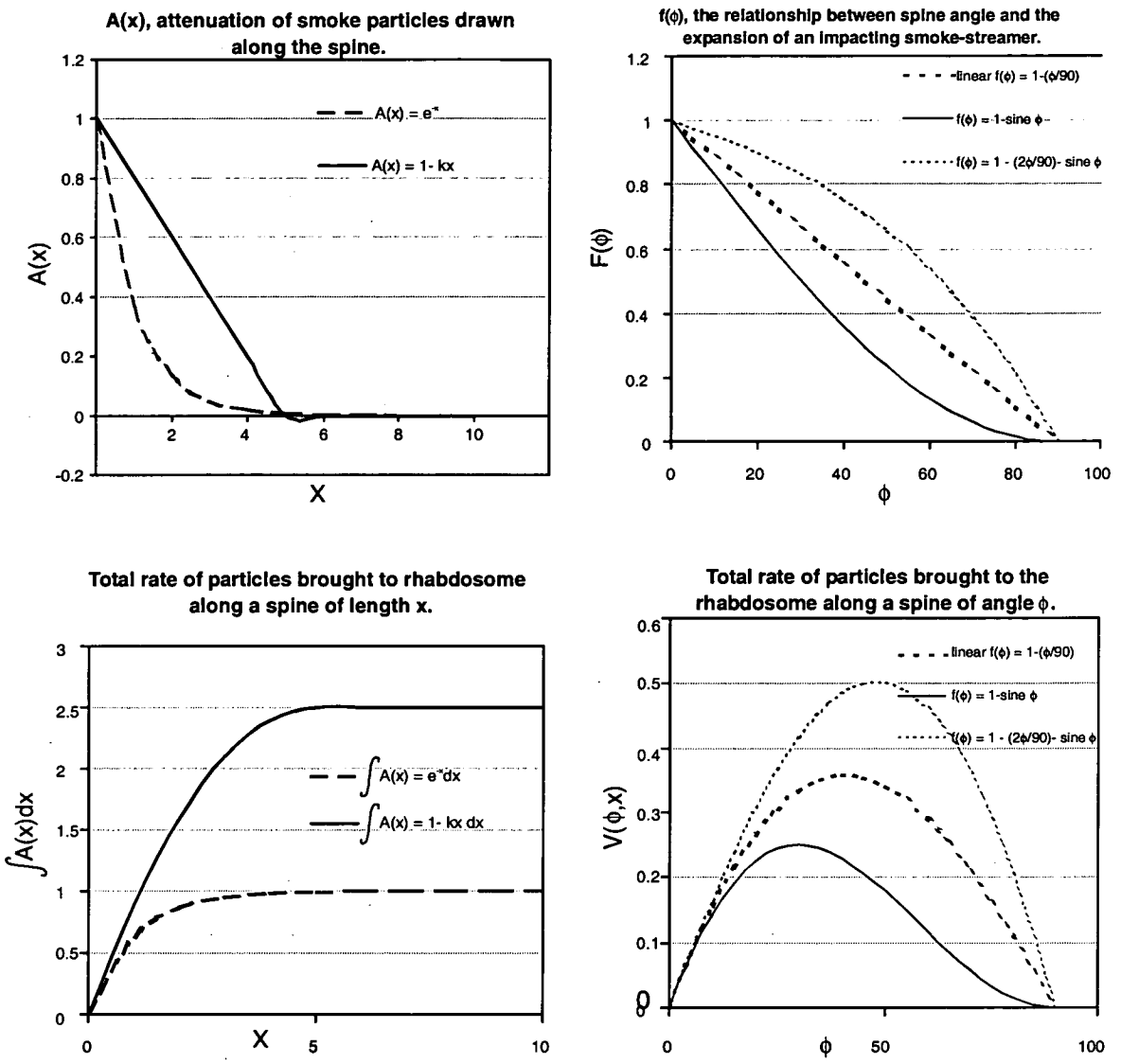

Figure 6.10: The upper plots represent the functions f(ϕ) and A(x) used for the 2-dimensional budget modelling. The two extremes of a linear and exponential relationship were used for A(x), the attenuation function. A variety of functions were used for f(ϕ), the percentage of impacting smoke flared along the spine dependant on spine angle. The lower plots show the effect of the different functions on V(ϕ,x), the rate at which particles brought to the rhabdosome (calculated from the integrals of A(x) and f(ϕ)) along: Lower left plot - A spine of fixed angle, and variable length x; Lower right plot - A spine of fixed length, and variable angle ϕ.

The simplest relationship would be a linear one. $f(\phi) = 1 - (\phi/90)$. Slightly more complex relationships would form curves either side of this linear line and are modelled here as functions built around partial sine waves $f(\phi) = 1\text{-sine}\phi$, and $f(\phi) = 1\text{-}(2\phi/90)\text{-sine}\phi$.

A(x) is a function giving the attenuation of the smoke-streamer as it mixes with freestream clear air along the spine.

We considered the two possible extremes as linear or exponential decay (Fig. 6.9).

Linear $A(x) = 1-kx$

Exponential $A(x) = e^{-x}$

(23)

Hence the total number of particles reaching the rhabdosome body from point x,

$$V(x) = A(x)f(\phi)UP \sin\phi\delta x. \quad (24)$$

The total number of particles brought in from the length of the spine can now be calculated as the sum of contributions from a series of increments, of length δx, making up the spine of total length X.

$$V(total) = \sum A(x)f(\phi)UP(\sin\phi)\delta x \quad (25)$$

Reducing the increment length, δx , until it tends to 0, increases the accuracy of the equation as it becomes an integral.

$$V(total) = \int A(x)f(\phi)UP(\sin\phi)\partial x$$

$$V(total) = PU(\sin\phi)f(\phi)\int A(x)\partial x \quad (26)$$

The gain in particles is balanced against the energy cost to the graptolite of building the spine. The cost (C(x)) increases only with length (x) as we assume the angle makes no difference to the zooids.

$$C(x) = gx \quad (27)$$

Where g is an unknown constant.

Hence the time ($T(x,\phi)$) in which the initial outlay for building the spine is recouped by the energy gained through particles brought to the colony is given by:

$$T(x,\phi) = \frac{gx}{UP(\sin\phi)f(\phi)\int A(x)\partial x} \qquad (28)$$

Results: Plotting the variation of T(x,ϕ) with length (x) and angle of spines (ϕ), using different combinations of the proposed functions f(ϕ) and A(x), produces a series of pictures with a remarkably similar shape, despite the differences between the functions used (figure 6.11). The increasingly blue colour towards the centre represents a spine that 'pays' for itself after an increasingly short period of time.

The values plotted for T1 and T2 (figure 6.11) use the same linear f(ϕ), but a different attenuation function A(x). These two plots show that it is the attenuation function that determines the optimal spine length. The most profitable length cannot be predicted without accurate energy figures.

The function f(ϕ) determines the shape of the plot; T1, T3 and T4 (figure 6.11) were produced using the same exponential A(x), but differing functions for f(ϕ). Although it is not possible to pin actual numbers to any of these equations each budget model predicted an optimal spine angle with a range over approximately 20°. The various models, using different combinations of functions f(ϕ) and A(x), predicted different 20°ranges from a minimum value of 20° (predicted by f(ϕ) = 1-sineϕ), to a maximum of 60° (predicted by f(ϕ) = 1-(2ϕ/90)-sineϕ) (figure 6.11).

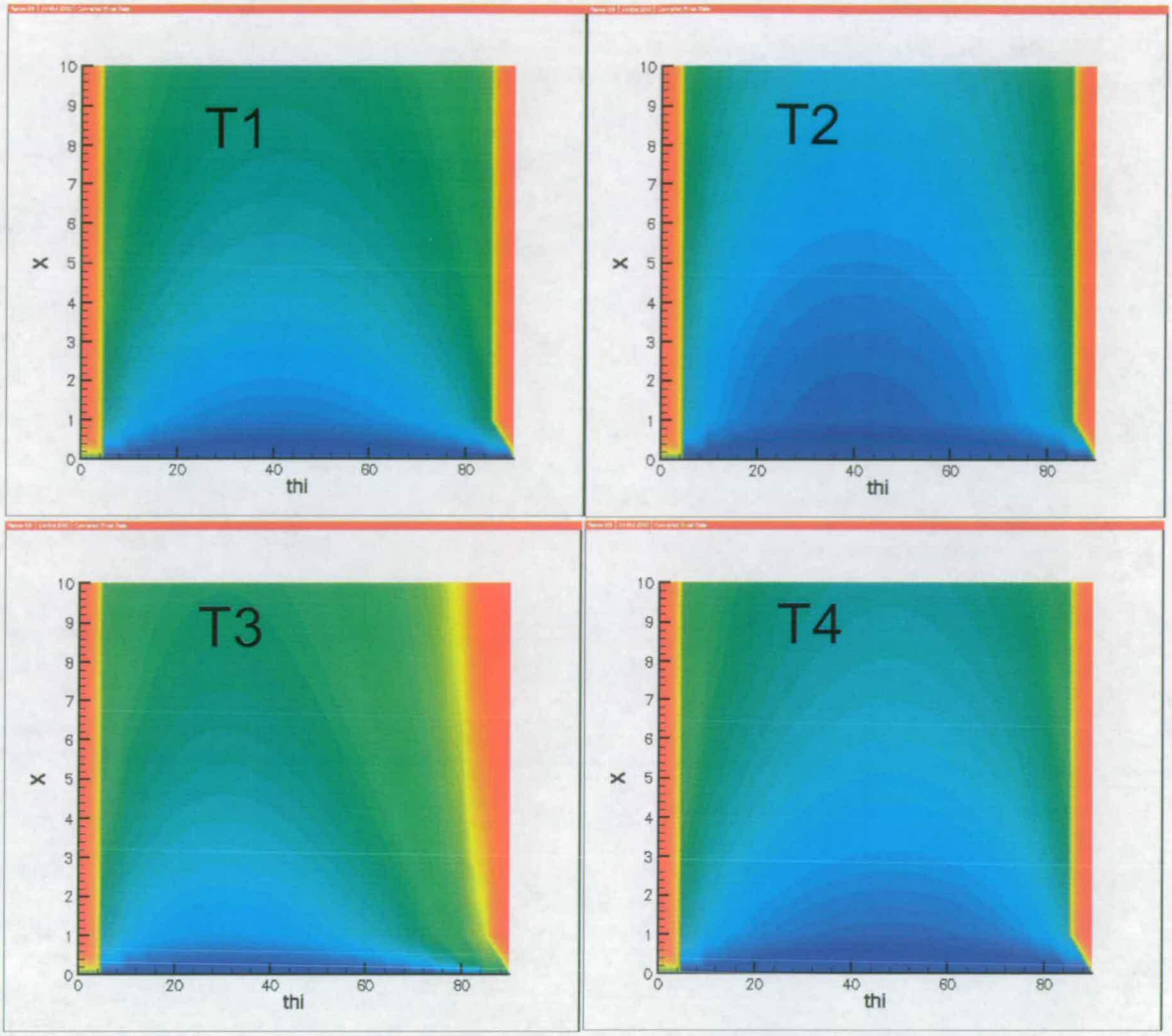

Figure 6.11: Budget plots. All graphs plot ϕ (the angle of the spine, in degrees) against x (the length of the spine, which has no meaningful units). The colour represents the time after which the energy outlay for building the spine has been repaid through energy gained from particles brought in by the spine. At angles of 0° and 90° a spine does not capture any additional particles for the graptolite and could never pay for its construction. The four plots are produced by different combinations of functions A(x) and F(ϕ). T1: $A(x) = e^{-x}$ $F(\phi) = 1 - (\phi/90)$. T2: $A(x) = 1-kx$ $F(\phi) = 1 - (\phi/90)$. T3: $A(x) = e^{-x}$ $F(\phi) = 1-\sin\phi$. T4: $A(x) = e^{-x}$ $F(\phi) = 1-(2\phi/90)-\sin\phi$.

Discussion: This model only provides a broad idea of which spines are likely to have been viable. There are many unknowns used in the calculations; P, the concentration of particles, the rate of attenuation and g, the cost of building the spine. The model does not properly consider the effect of different flow velocities. A higher velocity would increase the rate at which particles arrive at the spine and are drawn towards the rhabdosome body, but may be partially balanced by a reduction of the percentage of smoke-streamer extension and an increase in the rate of attenuation.

However it is clear that the average velocity would have had a net effect on profitability.

The longer a spine functioned, the more particles it would have gathered and building it would have been more 'profitable' for the graptolite. Hence spines which were quickly overshadowed by later construction of thecae (which projected further laterally into the flow) and other structures were less likely to have been 'profitable' for increased feeding efficiency.

Building these modifications into the model would be unlikely to greatly affect the broad pattern of the 'profit' plots, and although they might have a significant effect on the optimal length of spine, the optimal angle is still valid.

Conclusions: The budget modelling has shown that, given thecal spines functioned mainly to increase feeding efficiency, a small range (over approximately 20°) of optimal spine angles would be expected. The model was unable to predict this range, as the controls governing the expansion of an impacting smoke-streamer with increasing spine angle are not known.

6.5. Investigating the interactions of multiple thecal spines

Method: The mature *A. maxwelli* model was modified to investigate how a line of single thecal spines might interact. Sequential spines in two locations were considered: a. spines at the lip of the thecal aperture (c.f. *glossograptids*), and b. those projecting from the geniculum of thecae (c.f. *dicranograptids* and *A. bekkeri*).

Two sets of holes were drilled so that the same base model could be used to investigate spines in both locations. This represents a major approximation, as the thecal shapes and development of *Dicranograptus nicholsoni* and *Paraglossograptus holmi* are quite different from that of *A. maxwelli*. However it is the interaction of the spines which is being investigated, and all the species involved can be approximated as a simple biserial colony. The spines of *A. bekkeri* and *C. haljalensis* developed into flanges, which are modelled here as simple spines. A flange should produce a

similar flow pattern to a spine, but would block flow along the colony more effectively, and set up a series of vortices in front of the successive flanges. The *A. maxwelli* body model has small processes on the geniculum of the thecae.

A model of *Dicranograptus nicholsoni* was also tested to investigate the spinose biserial section. Further wind tunnel experiments with this model are discussed in section 7.6.1.

These models were tested in the Cambridge wind tunnel using smoke streamers to observe the flow. The free airflow velocity was 0.5 ms^{-1}.

Results:

a. Spines at the thecal aperture (figure 6.12 a and 6.13 a):

The flow over a projecting spine did interact with the flow over following spines. A smoke streamer, impacting with a spine, was extended laterally along the spine towards the rhabdosome. Small-scale turbulence caused some mixing between the streamer and surrounding airflow producing a visual 'flaring' of the streamer. This wider streamer would then impact with the following spine and 'flare' again.

No other smoke streams, beyond the initial impact width of $th1^1$ and $th1^2$, were drawn into the spines. However these smoke streams, deflected around the colony, were drawn in closer as they flowed around the rhabdosome, indicating that air may be being brought weakly in along the whole colony length.

Small vortices were set up in the slight dip just in front of the thecal spines. Smoke was observed in thecal apertures but no clear vortices were set up. This smoke appeared to be passing laterally though the apertures.

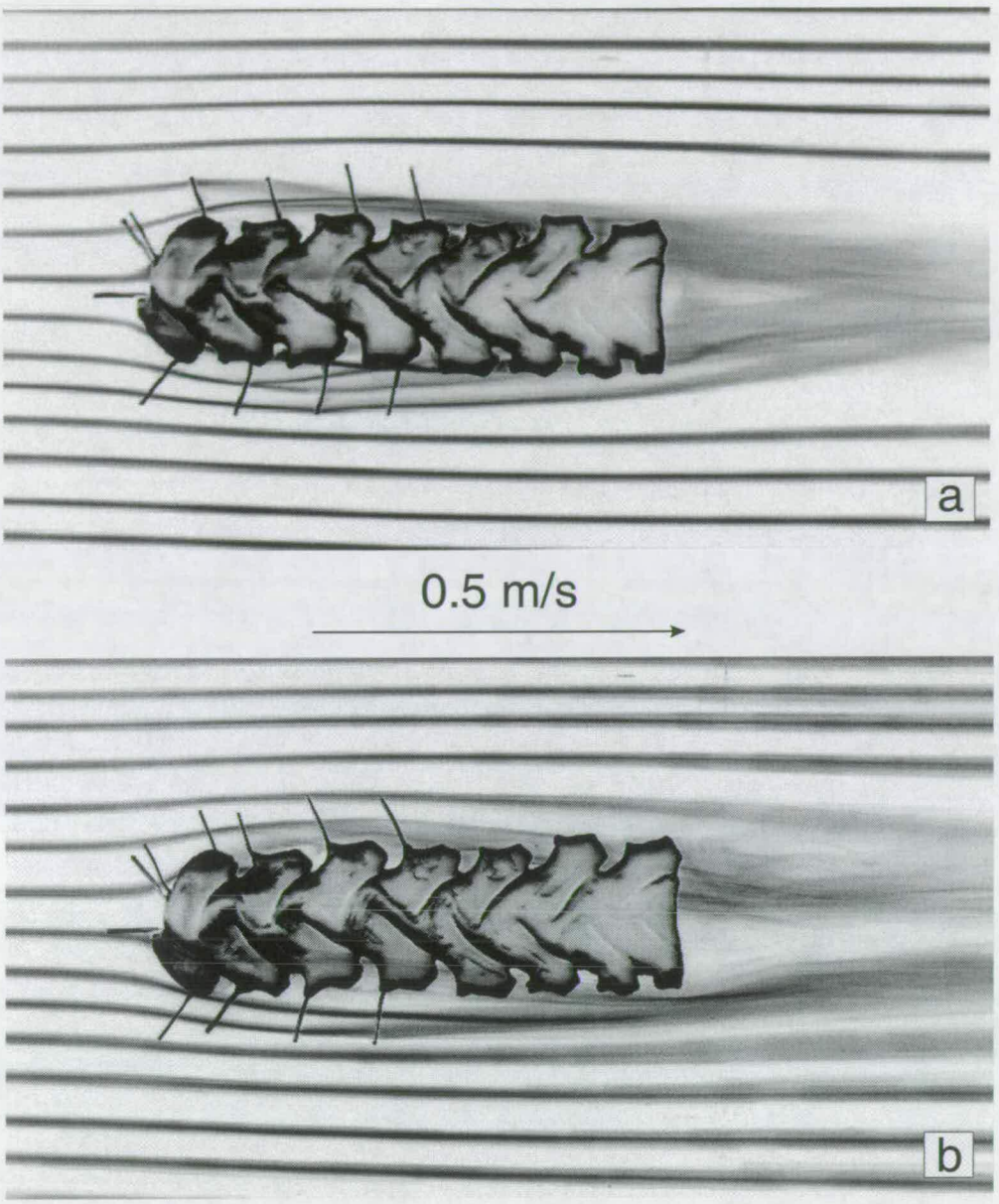

Figure 6.12: The *Amplexograptus maxwelli* body-type model was run in the Cambridge wind tunnel with multiple spines in two locations. Free-stream velocity is 0.5 ms^{-1}.

a The spines project from the thecal apertures. Smoke-streamers are drawn and extended towards the colony but few vortices are observed.

b The spines project from the geniculum of the thecae. The smoke-streamers are extended and drawn into large vortices between the spines.

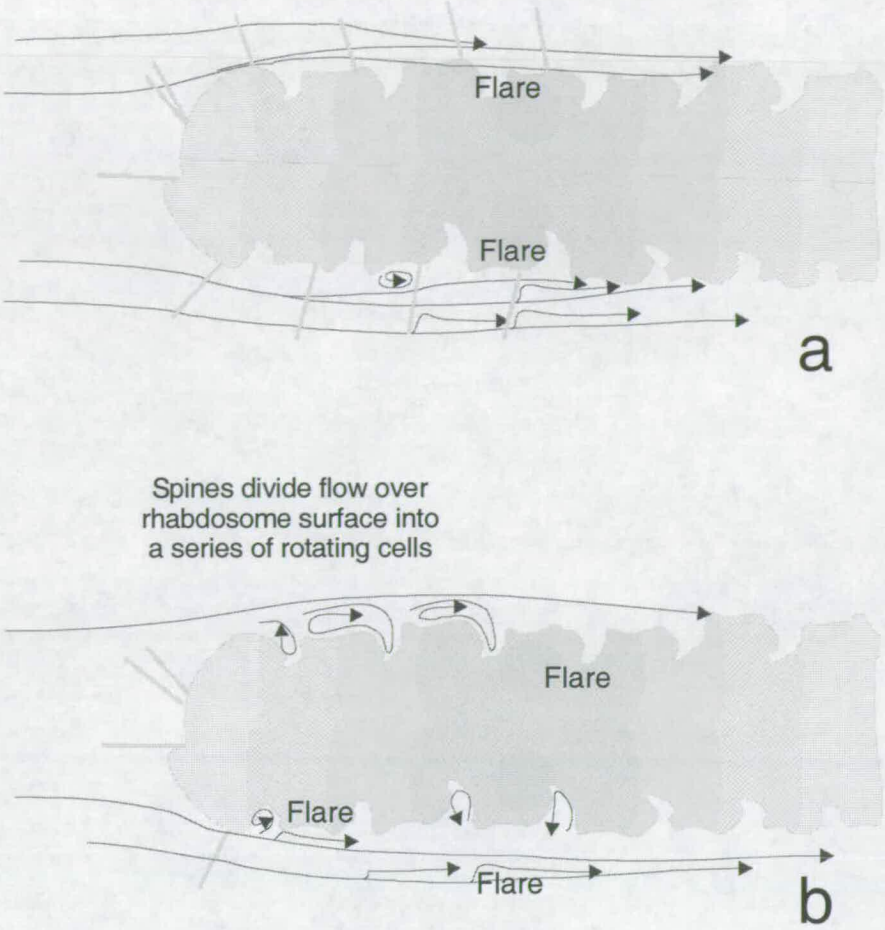

Figure 6.13: An interpretation of the flow over the simple sicula spine set observed in figure 6.12 based on observations made during testing.

b. Spines on the geniculum (figure 6.12 b and 6.13 b):

Interaction was observed between the sequential projecting spines. The smoke 'flared' by one spine, 'flares' again upon impact with a second spine. The major flow pattern difference with the spines in this location, are the large whorls set up between the spines which pass into the thecal apertures.

With this example it can be observed that if a spine projects further beyond the rhabdosome than more proximal spines, new smoke streams may be drawn in. Again it can be observed that the smoke streams deflected around the rhabdosome are drawn closer to the spinose model than to one without these spines.

c. *Dicranograptus nicholsoni* (figure 6.14 and 6.15)

A series of vortices were set up along either side of the biserial section. The vortices formed directly upstream of the thecal spines and flowed back into the thecal apertures. Impacting smoke streamers could be observed extending along the successive spines, bringing the flow onto the rhabdsome surface where it was drawn into the whorls in the thecal apertures.

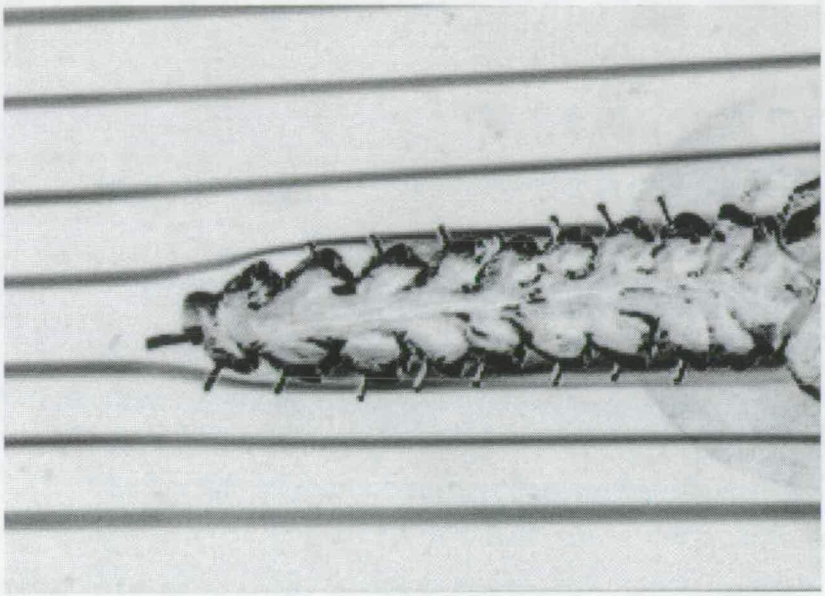

Figure 6.14: The model of *Dicranograptus nicholsoni* was run in the Cambridge wind tunnel. Free-stream velocity was 0.5 ms^{-1}. The focus of this investigation was on the spinose biserial section. Standing eddies are observed forming between the spines and in the thecal apertures.

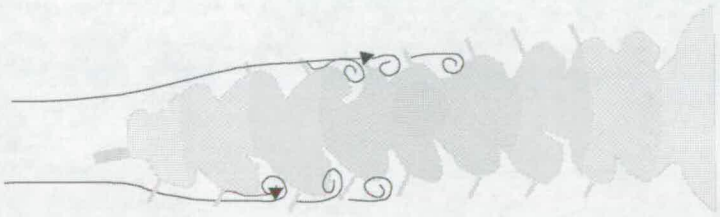

Figure 6.15: An interpretation of the flow over the *Dicranograptus nicholsoni* observed in figure 6.14 based on observations made during testing.

Discussion: The spines on the geniculum appeared to be more effective than spines in other locations at bringing the flow into the thecal apertures of the *A. maxwelli* model base. The genicular spines set up a series of large vortices that passed into the thecal apertures, and would have brought particles directly to a zooid sitting in the thecae. The apertural spines tended to break up these vortices, forming smaller ones directly upstream of the spines in a natural dip of the thecal wall, defined by the genicular process. It is in the detail of vortex formation that the thecal shape becomes significant.

The thecae of *A. maxwelli*, *D. nicholsoni* and *P. holmi* were all different (figure 6.16). *A. maxwelli* represents one extreme where the thecae are strongly sigmoidal (s-shaped), with a distinct process on the geniculum. The biserial section of *D. nicholsoni* has more gently sigmoidal thecae, and the thecae of *P. holmi* are relatively straight tubes (beyond the complex initial thecal development). Vortices would have formed directly upstream of the thecal spines. If the theca were straight or gently curved, a vortex forming in front of an apertural spine might have extended back along the thecae and into the thecal aperture, bringing food directly to the zooid (figure 6.16). If the thecae were strongly curved, or had a geniculum process, this vortex would have only extended back as far as the geniculum, and would not have entered the thecal aperture (figure 6.16). A genicular spine would have been far more effective for a strongly curved thecal shape, forming a vortex back along the sloping thecal wall into the previous thecal aperture.

Thecal spines and processes were typically located at the geniculum of diplograptid species (*A. bekkeri* and *C. haljalensis)* which often have curved or sigmoidal thecae. The dicranograptids (*D. nicholsoni*) have more gently curved thecae, and the thecal spines are located at the point at which the thecal wall becomes parallel to the stipe. Vortices would have been set up between successive spines and into thecal apertures (see section 7.6.1). The thecae of the paraglossograptids (*P. holmi*) are very gently curved, the thecae project at a fairly consistent angle from the stipe.

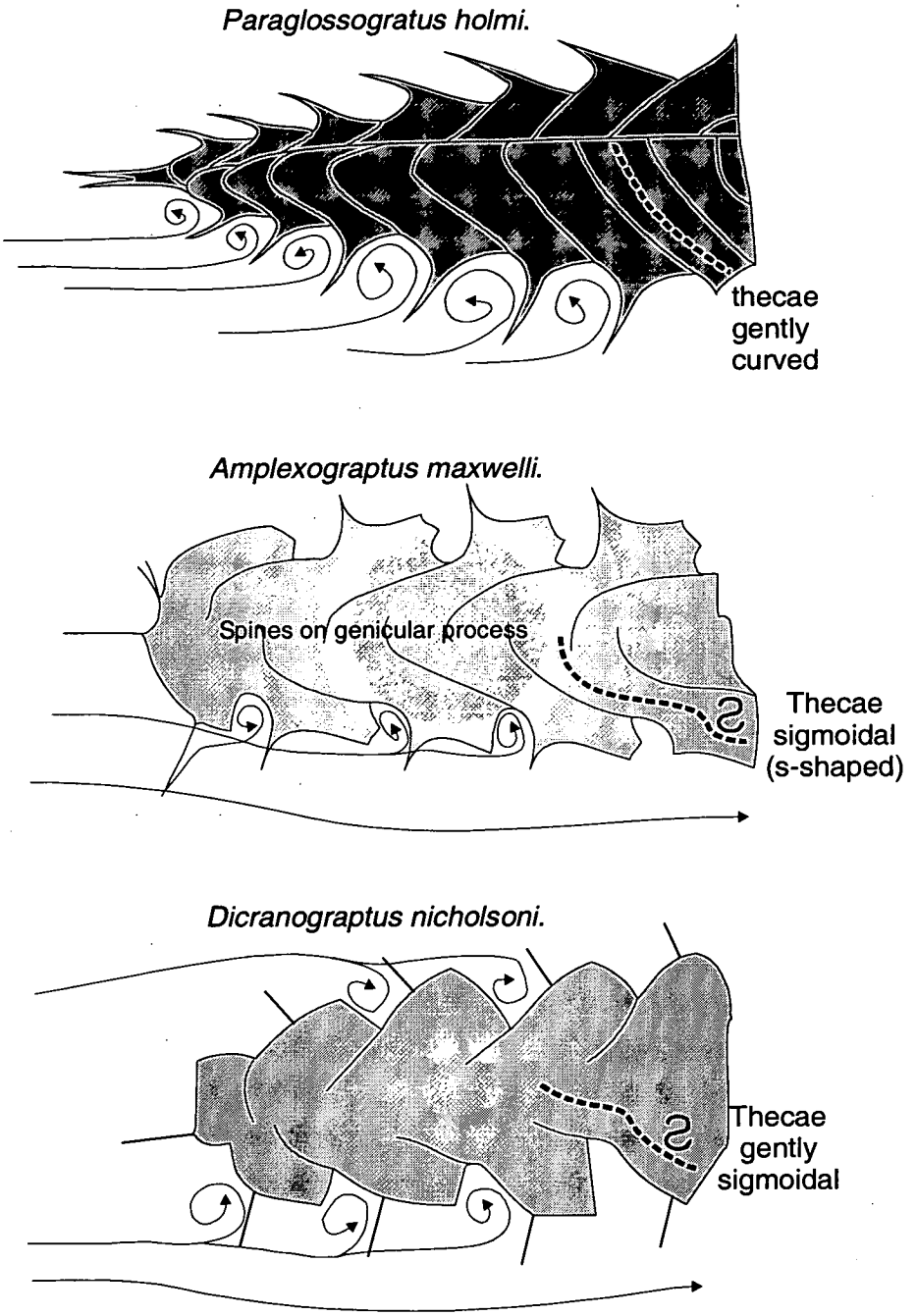

Figure 6.16: Different species exhibit varied degrees of thecal curvature, this affects the most efficient location for a thecal spine. The glossograptids and paraglossograptids, for example *P. holmi,* have straight to gently curved thecae, usually with a rutellum projecting from each thecal aperture. Many diplograptid species have strongly sigmoidal thecae, for example *Amplexograptus maxwelli*, whose spines are typically extend from the geniculum of these thecae. The biserial section of *Dicranograptus nicholsoni*, along with many diplograptid species, has gently sigmoidal thecae, the spines are located at the point at which the thecal wall becomes parallel to the stipe.

Laisograptus harknessi has paired spines projecting from the geniculum. These also would have formed vortices and, projecting away from each other out of the plane of the biserial colony, would have drawn flow to the rhabdosome from a much broader lateral area than a single spine.

Thecal spines and structures were also relatively common amongst the monograptids. Several species had hooded thecae (e.g. *M. praehercynicus*, *Saetograptus jaegeri* and *M. pridoliensis*), the hood (or process) forming from the dorsal edge of the thecae, over the thecal aperture, and projecting beyond the following theca. These hoods would have acted like the genicular processes, and spines, forming a vortex directly in the thecal aperture. In many species these hoods are only present on the proximal thecae (*S. jaegeri*), but these may reduce to a smaller process (*M. pridoliensis*) which, projecting beyond the main colony boundary, would have continued to form vortices and draw in flow along the entire graptolite. Spines are typically built on the thecal aperture (e.g. *M. chimera, Saetograptus fritschi linearis* (paired lateral spines) *Saetograptus jaegeri* (single spine from dorsal edge extending process)). These might have drawn in fresh particle-bearing water (laterally in the case of *Saetograptus fritschi linearis)* and formed vortices as described by Rickards *et al* (1998).

Multiple thecal spines would have been beneficial to the colony, particularly if more distal spines projected further from the rhabdosome body, drawing in fresh water along the colony. The spines would have interacted to produce numerous vortices bringing particle-bearing fluid, from beyond the rhabdosome surface, into the thecal apertures and directly to the zooids. The effective location of these spines was dependant on the thecal shape; a spine on the geniculum would have set up vortices in the apertures of strongly curved thecae, a spine at the thecal aperture would have formed vortices in the apertures of straight to gently curved thecae.

Conclusions:

- Multiple spines would interact to produce a pattern of vortices, which may have drawn fresh particle-bearing fluid along the entire spinose colony.
- The location at which a spine would have been most effective is dependent on the thecal morphology.

6.6. Investigating the function of anti-virgellar spines

6.6.1. Cambridge wind tunnel

Method: The *Amplexograptus maxwelli* base model was tested in the Cambridge wind tunnel with the three basic spine array patterns featuring anti-virgellar spines (see table 6.1). This experiment was intended to investigate how the anti-virgellar spines might function hydrodynamically, and how these spines might have interacted with thecal spines. The flow patterns observed were compared with the flow patterns produced by models lacking anti-virgellar spines (section 6.3.1).

The Cambridge wind tunnel was run at velocities between 0.5 and 0.7 m s^{-1} (Re's 5,000 - 8,000), which represent the minimum running velocities of the wind tunnel. Flow patterns are visualised using smoke streams, and these were photographed using a digital camera and processed to disc.

Results: The results are shown here as digital photographs of the smoke streams flowing over the models in the wind tunnel. The pictures are negative images in which streams of white smoke against a black background appear as streams of black smoke against a white background. Flow line interpretations have been drawn based on observations made during wind tunnel runs.

The thecal spines of *Amplexograptus maxwelli*-type and *Hustedograptus uplandicus*-type were observed to cause impacting smoke streams to extend along the spine towards the graptolite body (figure 6:17 and 6.18). The anti-virgellar spines had the same effect, drawing smoke along their length and onto the colony. With the completion of thecae 1^2 the anti-virgellar spines are largely overshadowed and appear to loose function, although an impacting smoke streamer is observed extending partially along the anti-virgella spine it is blocked by the boundary layer of $th1^2$.

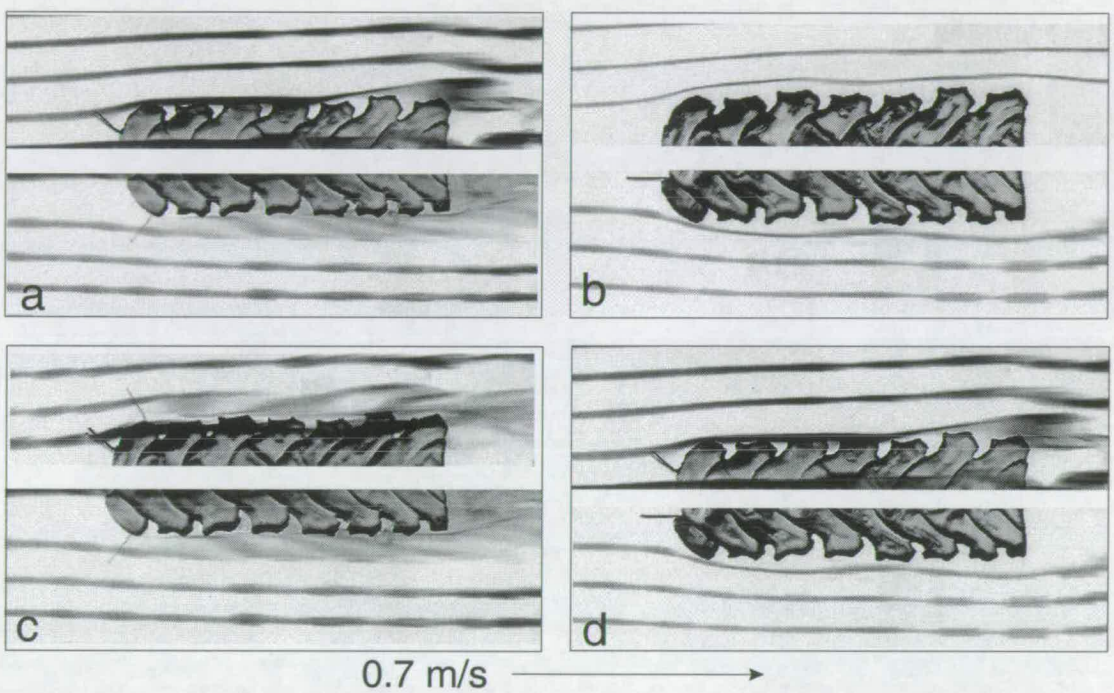

Figure 6.17: The anti-virgellar spines set: In the case of *Climacograptus pulchellus* (b. lacking proximal spines) a smoke stream can pass very close to the colony without running over the surface. Anti-virgellar spines expand the smoke-streamer up these spines towards the colony and onto the surface (a. *Amplexograptus maxwelli*, c. *Hustedograptus uplandicus and* d. *Glyptograptus typicalis*). An additional spine on $th1^1$ or $th1^2$ brings in smoke from an even wider area.

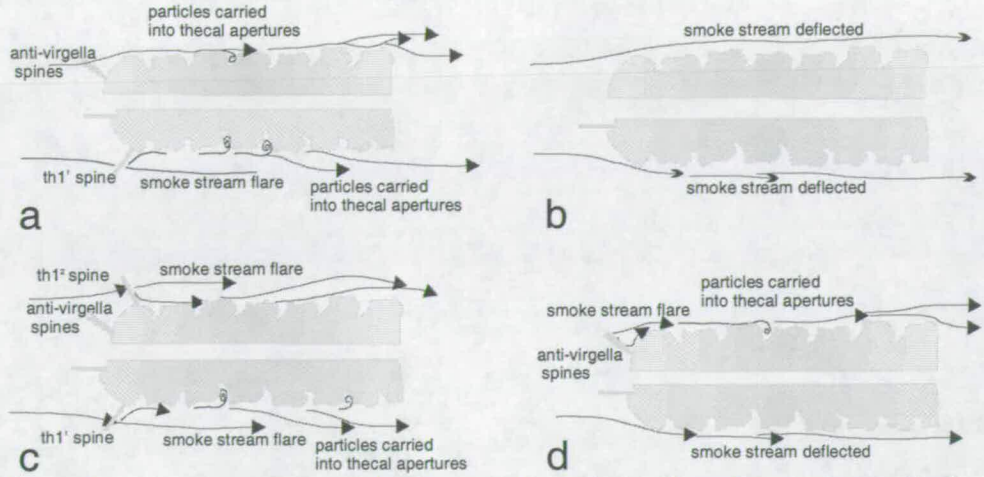

Figure 6.18: An interpretation of the flow over the anti-virgellar spine set observed in figure 6.17 based on observations made during testing.

Models of juvenile specimens were also used to investigate the hydrodynamic affect of anti-virgellar processes. At this juvenile stage the anti-virgellar spines or lappets are not overshadowed by th1^2 and are able to significantly draw impacting flow onto the rhabdosome surface. The paired lappets of the *Hustedograptus teretiusculus*-type model also caused mixing with surrounding airflow, spreading the smoke stream across the rhabdosome surface (figure 6.19 a and 6.20 a). These lappets reduce the separation holding the flow close to the colony over the acute angle of the sicula aperture lip (figure 6.19 and 6.20).

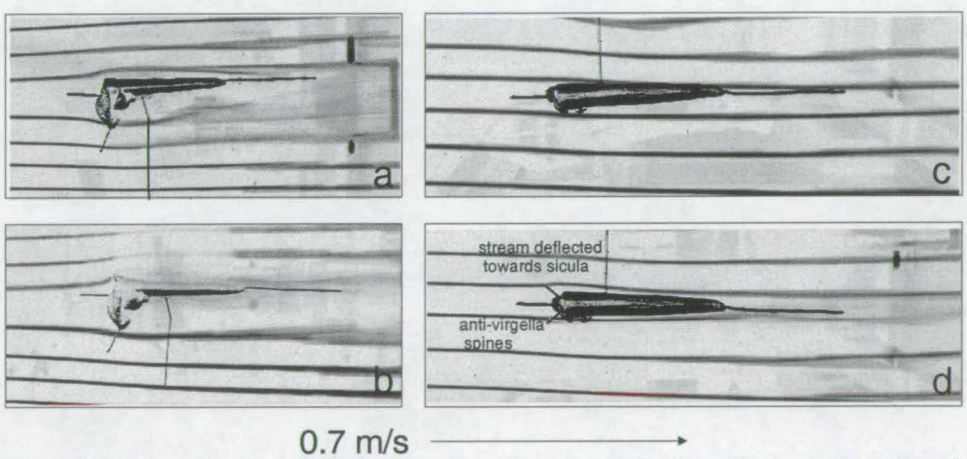

Figure 6.19: a. and c. Pseudoclimacograptus scharenbergi. b. Hustedograptus teretiusculus. d. Amplexograptus maxwelli.

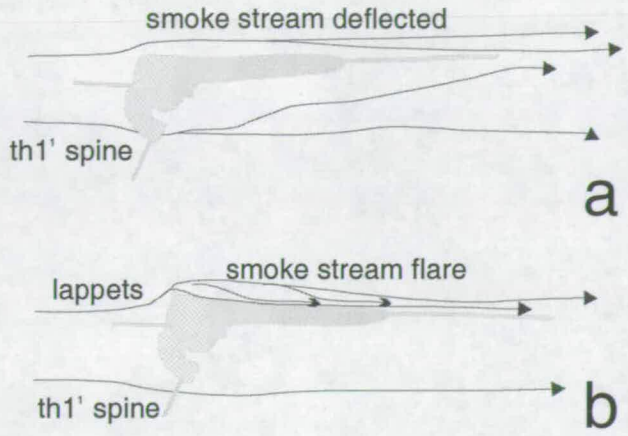

Figure 6.20: An interpretation of the flow over the anti-virgellar spine set observed in figure 6.19 based on observations made during testing.

The anti-virgellar spines would have been more significant during very early growth, when they projected more notably beyond the rhabdosome. Figure 6.19 (c & d) illustrates the flow pattern over the anti-virgellar spines from an orientation at right angles to previous images of these spines (figure 6.17 and 6.18). The anti-virgellar spines would have drawn the smoke up towards the colony. The lappets of *Hustedograptus teretiusculus* model (figure 6.19 and 6.20: b) caused impacting smoke streams to flare across the colony surface and prevents these streams being so widely deflected around the sharp sicula edge. Compare this to the *P. scharenbergi* model (figure 6.19and 6.20: a) lacking any ventral sicula structures.

Conclusions:

- Anti-virgellar spines would have prevented separation at the ventral edge of the sicula aperture.
- Impacting flow would have been drawn partially along the anti-virgellar spines to the colony surface.

6.6.2. Bristol wind tunnel

Method: The *Amplexograptus maxwelli* body-type was also run in the larger wind tunnel at the University of Bristol, which was able to run at low velocities (down to 0.1 m s^{-1}). Measurements were made using laser Doppler anemometry (LDA) (section 3.2.1). Data were processed using TECPLOT (version 7.0).

This investigation focused on the effect of the anti-virgellar spines. The anti-virgellar spines were investigated by comparing the flow over a juvenile graptolite, before the growth of any thecae on the ventral side of the colony (with and without the anti-virgellar spines), and the flow over a more mature colony (with and without anti-virgellar spines). Locations of observed planes are shown in figure 6.21.

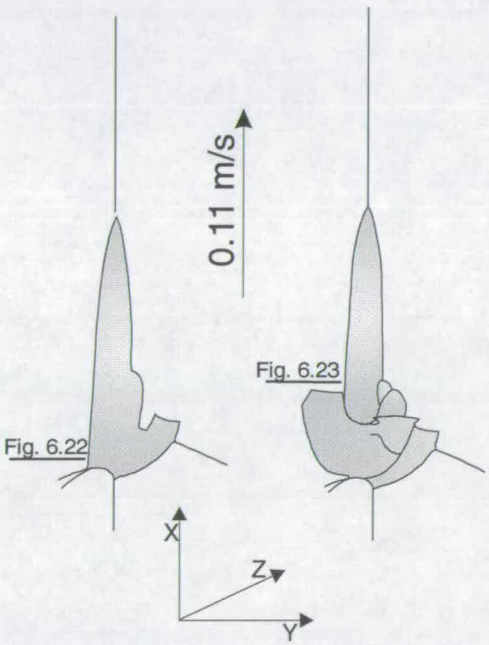

Figure 6.21: The *Amplexograptus maxwelli*-type body was modelled at two astogenetic stages. These were tested in the wind tunnel at the University of Bristol and flow through (and within) the marked planes was observed using LDA, and given here as figures 6.22 and 6.23.

Results: The results from this set of experiments are shown as contoured vector plots of a two-dimensional plane. The vectors represent the velocities of flow within the plane, and the contours represent velocity of flow through the plane. All the planes were measured perpendicular to the wind tunnel freestream flow (0.1 m/s), such that the major component of flow velocity is through the plane, and any within-plane velocities are disturbances caused by the presence of the model. The locations of the planes investigated are shown in figure 6.21.

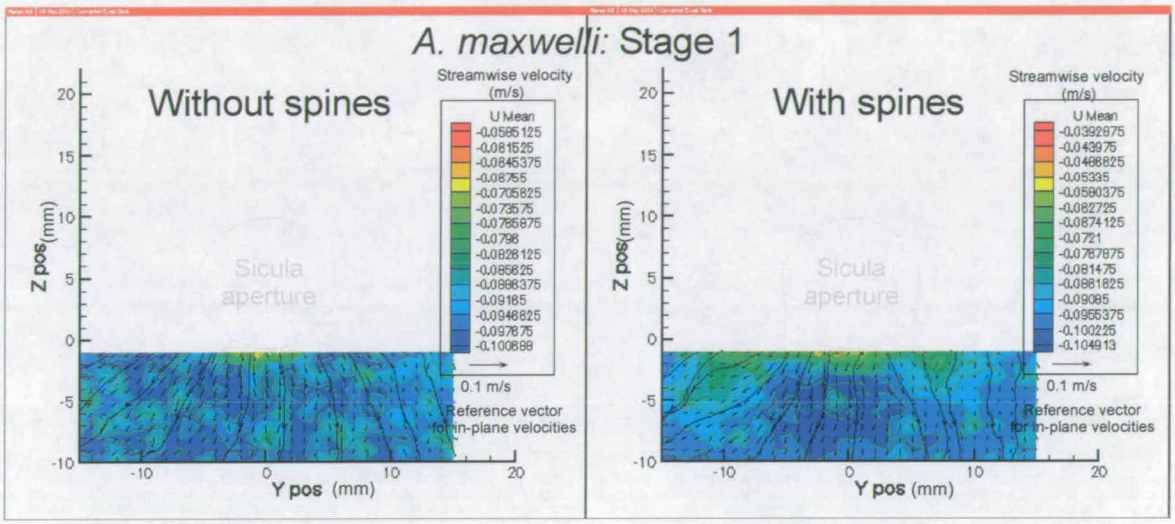

Figure 6.22: A vector plot of the flow through (and within) a plane just beyond the sicula aperture on the ventral side, the position of which is shown in figure 6.21, using the most juvenile model. The two plots represent the flow in the presence and absence of the anti-virgellar spines. The vectors, direction and length, represent in-plane velocities, direction and speed. The colour represents through-plane velocities. Streamtraces have been added to show how a particle would move through the plane. The second plot shows a pair of small low (through-plane) velocity areas lying in the shadow of the anti-virgellar spines which are absent in the first plot where the anti-virgellar spines are absent. The in-plane velocities show the airflow deflecting around the sicula edge, wide of the graptolite. The first plot (with anti-virgellar spines) has reduced flow away from the graptolite in the areas behind the spines.

A low (through-plane) velocity shadow of the anti-virgellar spines can be seen in the first ventral plane, directly behind the spines. Comparing the vector planes recorded in the presence and absence of the anti-virgellar spines, it can be observed that within these spine 'shadows' the in-plane velocities are reduced in comparison to the

stronger in-plane flow radiating away from the rhabdosome observed when the spines are absent (figure 6.22). The presence of anti-virgellar spines caused no significant difference to the flow through the second ventral planes, behind th1[2] (figure 6.23).

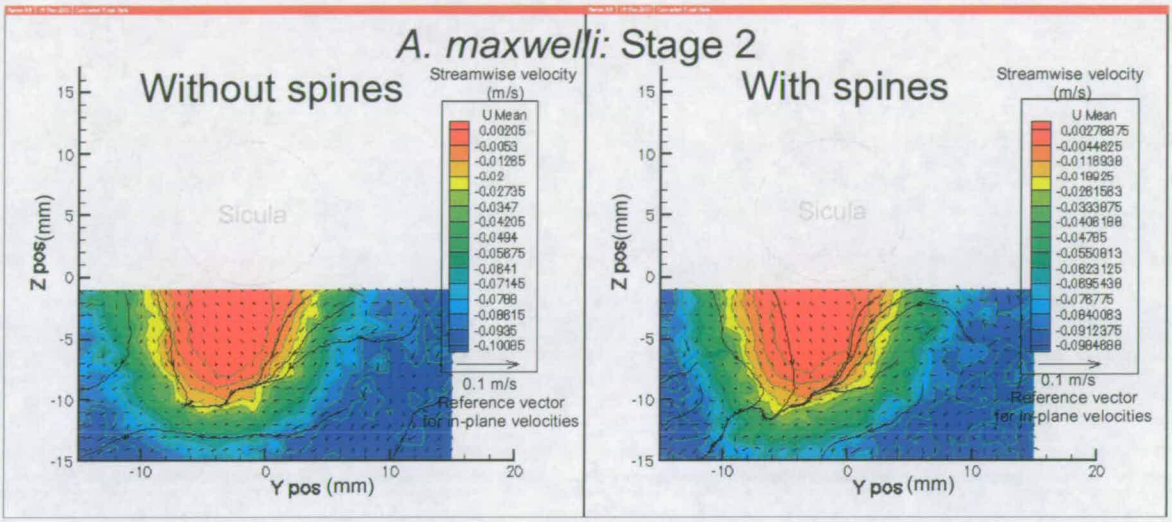

Figure 6.23: A vector plot of the flow through (and within) a plane behind the aperture behind th1[2], the position of which is shown in figure 6.21. The two plots represent the flow in the presence and absence of the anti-virgellar spines. The vectors, direction and length, represent in-plane velocities, direction and speed. The colour represents through-plane velocities. Streamtraces have been added to show how a particle would move through the plane. There is no significant difference between the two plots; the anti-virgellar spines appear to have little effect this far along the colony.

Conclusions:

- The anti-virgellar spines prevented separation at the ventral sicula edge and held the flow close to the rhabdosome surface over the sicula edge.
- The anti-virgellar spines had little impact on the flow beyond th1[2].

6.7. Investigating the function of a deflected virgella

6.7.1. Cambridge wind tunnel

Method: The *Climacograptus (Diplacanthus) spiniferus* base model was tested in the Cambridge wind tunnel with the two basic spine array patterns featuring a deflected virgella (see table 6.1). This experiment was intended to investigate how the deflected virgella spines might function hydrodynamically.

The wind tunnel was run at velocities between 0.5 and 0.7 m s^{-1} (Re's 5,000 - 8,000), which represent the minimum running velocities of the wind tunnel. Flow patterns are visualised using smoke streams, and these were photographed using a digital camera and processed to disc.

Results: The results are shown here as digital photographs of the smoke streams flowing over the models in the wind tunnel. The pictures are negative images in which streams of white smoke against a black background appear as streams of black smoke against a white background. Flow line interpretations have been drawn based on observations made during wind tunnel runs.

The flow observed over three different spine arrays, based on the *Climacograptus (Diplacanthus) spiniferus* base model, are shown in figure 6.24 and 6.25. The long deflected virgella (b. *G. brevis*-type) and balancing thecal spine (c. *C. (D.) spiniferus*-type) bring smoke to the colony, by extending impacting smoke streams along the spines, exactly as do the various proximal spines of the simple sicula and anti-virgella set. This extension along the virgella does not continue into the sicula aperture, it is blocked by interaction with the colony boundary layer.

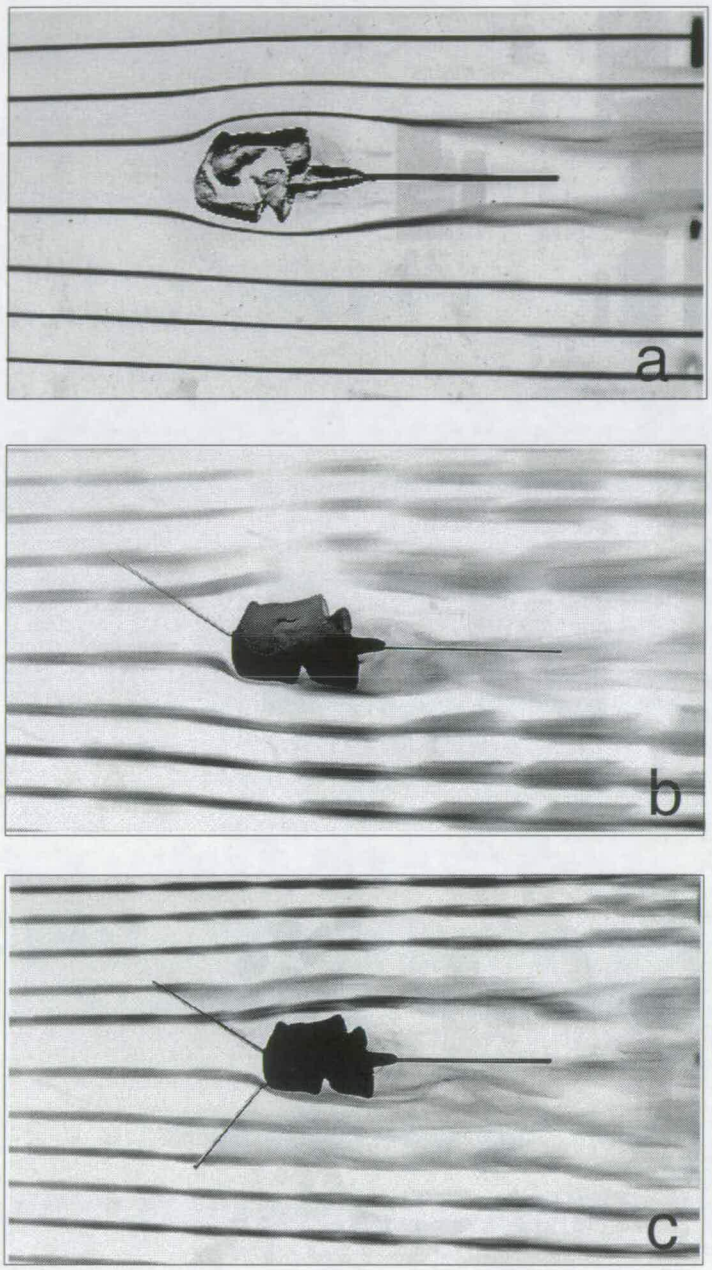

Figure 6.24: The deflected-sicula set: Without any proximal spines (a. no species), the smoke streams are easily deflected completely around the colony, and do not enter any of the thecal apertures. The presence of a deflected virgella (b. *Glyptograptus brevis*) and a balancing thecal spine (c. *Climacograptus (Diplacanthus) spiniferus*) brings these smoke streams onto the colony surface, as the smoke is flared along the spines.

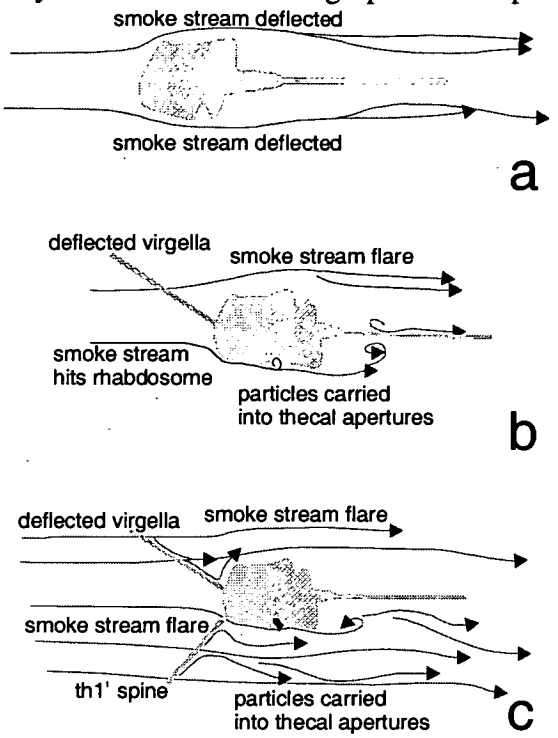

Figure 6.25: An interpretation of the flow over the deflected virgella spine set observed in figure 6.24 based on observations made during testing.

Without the deflected virgellar or thecal spine (figure 6.24 a and 6.25 b), the airborne smoke is carried around the rhabdosome and slips easily past the graptolite without touching the surface or flowing into thecal apertures.

Conclusions: The deflected virgella acted like a thecal spine drawing flow over the colony surface from a wider capture area.

6.7.2. Bristol wind tunnel

Method: The *Climacograptus (Diplacanthus) spiniferus* body-type models was also run in the larger wind tunnel at the University of Bristol, which was able to run at low velocities (down to 0.1 m s^{-1}). Measurements were made using laser Doppler anemometry (LDA) (section 3.2.1). Data are processed using TECPLOT (version 7.0).

This investigation focused on the effect of the deflected virgellar spine. The deflected virgella was investigated by comparing the flow over a juvenile graptolite, before the

growth of any thecae on the ventral side of the colony (with and without the virgellar spine). The flow through a plane in front of the sicula aperture (behind the virgellar spine) was observed.

Results: The results from this set of experiments are shown as contoured vector plots of a two-dimensional plane. The vectors represent the velocities of flow within the plane, and the contours represent velocity of flow through the plane. All the planes were measured perpendicular to the wind tunnel freestream flow (0.1 m/s), such that the major component of flow velocity is through the plane, and any within-plane velocities are disturbances caused by the presence of the model. The locations of the planes investigated are shown in figure 6.26.

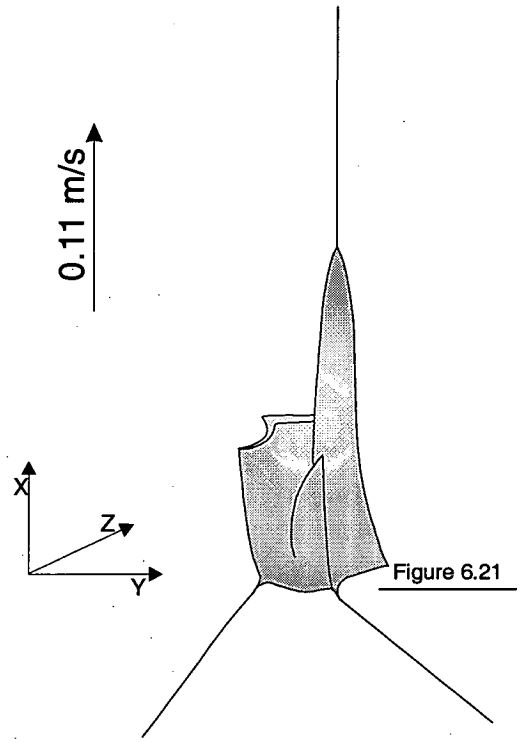

Figure 6.26: The *Climacograptus (Diplacanthus) spiniferus*-type body was modelled at an early astogenetic stages. These were tested in the wind tunnel at the University of Bristol and flow through (and within) the marked plane was observed using LDA, and presented here as figure 6.27.

A clear low (through-plane) velocity shadow is visible behind the deflected virgella (figure 6.27). Moving away from the base of the virgella this reduction in flow velocity lessens, as the plane lies further behind the spine, but a low velocity shadow is still distinguishable. The slowest through-plane velocities, in front of the sicular

growth of any thecae on the ventral side of the colony (with and without the virgellar spine). The flow through a plane in front of the sicula aperture (behind the virgellar spine) was observed.

Results: The results from this set of experiments are shown as contoured vector plots of a two-dimensional plane. The vectors represent the velocities of flow within the plane, and the contours represent velocity of flow through the plane. All the planes were measured perpendicular to the wind tunnel freestream flow (0.1 m/s), such that the major component of flow velocity is through the plane, and any within-plane velocities are disturbances caused by the presence of the model. The locations of the planes investigated are shown in figure 6.26.

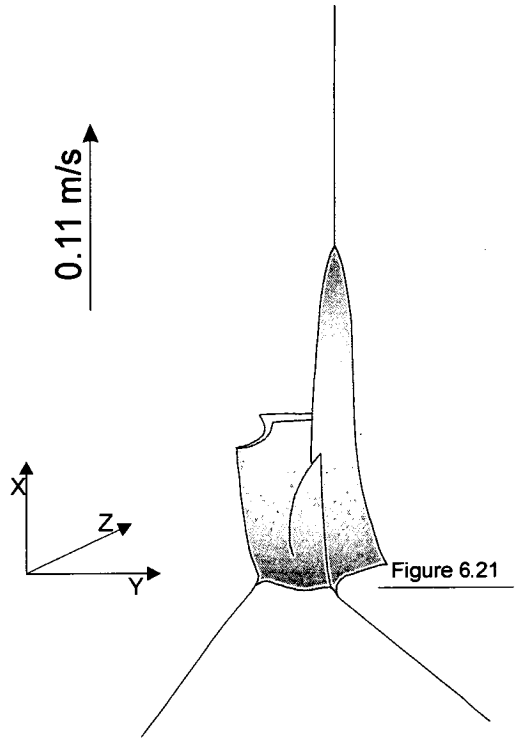

Figure 6.26: The *Climacograptus (Diplacanthus) spiniferus*-type body was modelled at an early astogenetic stages. These were tested in the wind tunnel at the University of Bristol and flow through (and within) the marked plane was observed using LDA, and presented here as figure 6.27.

A clear low (through-plane) velocity shadow is visible behind the deflected virgella (figure 6.27). Moving away from the base of the virgella this reduction in flow velocity lessens, as the plane lies further behind the spine, but a low velocity shadow is still distinguishable. The slowest through-plane velocities, in front of the sicular

through-plane velocities are not significantly slowed beyond approximately 5mm downstream distance from the spine (this corresponds to a distance of 0.2mm converted to the scale of a real graptolite).

The expanded smoke-streamer is not observed running up the spine in the LDA plane as it does not extend the entire length of the spine. The area of spine viewed is directly in front of sicula aperture and flare is deflected away before this.

Conclusions: The influence of a spine, to slow flow velocity along the colony, would have extended approximately 0.2mm downstream from the spine. However a proximal spine may have caused an alteration of the flow pattern which affected the entire colony beyond it.

6.8. Changes during astogeny?

Fossil and experimental evidence indicates that proximal spines had varying functional lifetimes. Some ceased to grow beyond the juvenile stages (e.g. the anti-virgella and thecal spines of *A. maxwelli* and *C. schaeferi*), others continued to develop throughout the lifetime of the colony (e.g. the proximal spines of *C. bicornis* and *C. diplacanthus)*. Continuing development implies continuing utility although this function may have changed as the colony matured.

It is clear that proximal spines must have functioned during the very early stages of colony life, since they were constructed at a time when the energy budget of the colony would have been most limited with only one or two zooids to support it. They appear to have been constructed rapidly, so as to function effectively as quickly as possible. If a spine or structure then ceased growth for the rest of the colony lifetime it is not clear whether it continued to serve a useful function.

That a structure completed its growth early in the colony lifetime does not necessarily imply short-term functionality. Wind tunnel experiments (section 6.3) have shown that a single spine built on the most proximal thecae could have brought particle-bearing flow onto the rhabdosome surface, and into all subsequent thecal

apertures along the entire colony. A larger spine was not required for continuing function as the colony matured.

In some cases the structure may have ceased to function. The anti-virgellar spines, of *A. maxwelli*, and particularly those of *C. schaeferi* (figure 6.28), become completely overshadowed by the construction of later thecae. Data collected by the LDA system in the Bristol wind tunnel has shown that the anti-virgellar spines made very little difference to flow beyond $th1^2$ (section 6.6.2). These spines could have continued to function only for the most proximal parts of the colony, bringing the impacting flow smoothly over ventral edge of the sicular aperture, but would have had little beneficial affect on the rest of the colony.

Many climacograptid species have prominent proximal spines (e.g. *C. diplacanthus, C. cruciformis* and *C. bicornis*). The basic spines were built with the first few thecae, and some reached their mature length during these juvenile stages. Other climacograptid spines continued to grow as the colony matured, sometimes adding membrane-like vanes and tubes to the structure. As a result the overall form might change considerably; for example the genicular spines of *Climacograptus cruciformis* (Vandenberg 1990) reached their final length when the colony was only 4mm long, whereas the virgella continued to grow, relatively dwarfing the pair of genicular spines.

If the function of these spines was purely to draw in fresh particle-bearing waters, a small spine would have continued to function for the entire colony length as it grew (c.f. *A. maxwelli* $th1^1$ spine), the spine would not have needed to be enlarged and expanded as is commonly observed from fossil specimens.

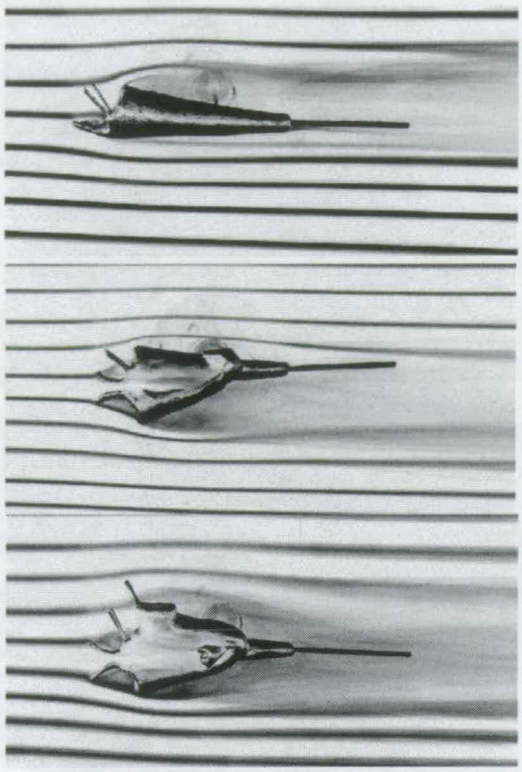

Figure 6.28: Three models representing different astogenistic stages of *Cryptograptus schaeferi*. The models are being tested in the Cambridge wind tunnel at a free-stream velocity of 0.5 ms^{-1}.

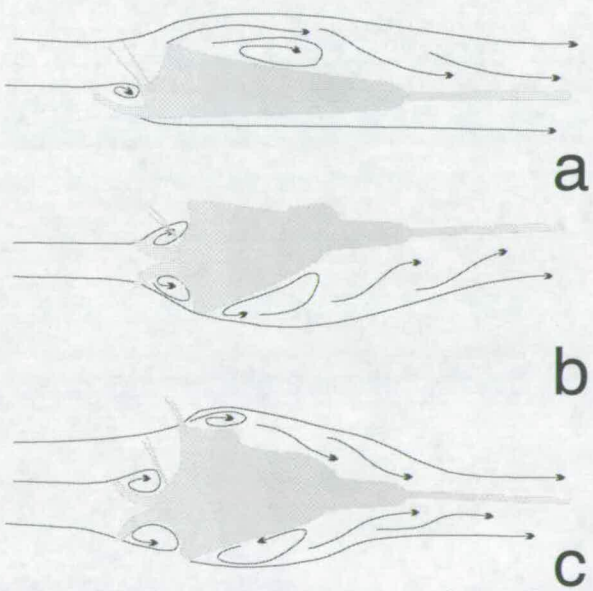

Figure 6.29: An interpretation of the flow over *Cryptograptus schaferi* observed in figure 6.28 based on observations made during testing.

The number of smoke particles attenuates as they are drawn along a spine, implying a maximum beneficial length (see section 6.4.2), and so unbounded growth would have represented a waste of the colonies' energy. Clearly a structure which continued to grow must have continued to have a vital function, as the energy budget of a graptolite colony would have been small and precious. It is likely that as the colony matured the proximal spine arrays developed other functions, in addition to food entrainment, but this function cannot be speculated on here.

The proximal spines of all species considered must have been functional at the time of their construction (or shortly after), the energy budget of a juvenile graptolite would have been too limited to allow excess building. These spines could have continued to bring particles to the rhabdosome surface throughout the life of the colony, at this juvenile length, provided they were not overshadowed by later colony growth (anti-virgellar spines). Some increase in length may have drawn in more flow, but spines which became greatly enlarged must have served another purpose as the colony developed.

6.9. The likely range of hydrodynamic function for proximal structures on scandent graptolites

These investigations have clearly indicated that proximal spines did have a significant affect on the hydrodynamics of the colony, and could have provided a beneficial function.

All the proximal spines investigated increased feeding efficiency by bringing water gathered from a larger cross sectional area (and hence more food as fresh particles were entrained along the spine) onto the graptolite surface than would have been encountered by a colony lacking proximal spines. Some (thecal spines and a large deflected virgella) increased the feeding efficiency for the entire colony in this way, while others (anti-virgellar spines) affected only a localised section. Some spines (anti-virgellar spines and the deflected virgella) also controlled the initial impact of

the flow with the colony, guiding it and potentially affecting the stability of the graptolite in the flow.

The proximal spines would have increased feeding efficiency by creating lateral currents, along the spine and onto the colony surface. These would have drawn fresh food-bearing water onto the surface, where it would have run into the thecal apertures for easy availability to the zooids. These projecting spines brought in water from a wider (cross-sectional) area than the colony would have encountered without the proximal spines. As a result a greater volume of water, and hence a greater volume of food particles, were sampled by the colony. Food particles impacting with the proximal spines would have become trapped in the newly forming boundary layer and carried onto the rhabdosome surface.

Why particles get trapped in the Boundary Layer: Frictional forces dictate that the fluid directly in contact with any surface is stationary with respect to that surface. The freely moving fluid (beyond the boundary layer) is moving at velocity U, with respect to the surface, so the fluid velocity must increase from zero to U across the boundary layer (this increase is parabolic) (figure 6.30). As a result successive 'sheets' of fluid through the boundary layer are moving at different velocities, and therefore moving with respect to each other (Vogel, 1981). This relative movement causes shear forces between the 'sheets' of fluid which will act on objects within the boundary layer.

A particle will experience greater fluid flow across the face farthest from the stationary surface than that closest to the surface. This difference will produce shear forces acting on the particle that may cause it to rotate and will tend to hold it within the boundary layer. There is a resulting lack of diffusion across the layer so that particles impacting with the proximal spines might have become trapped in the boundary layer of the spines as it formed and been carried within it up to the rhabdosome and to the thecal apertures.

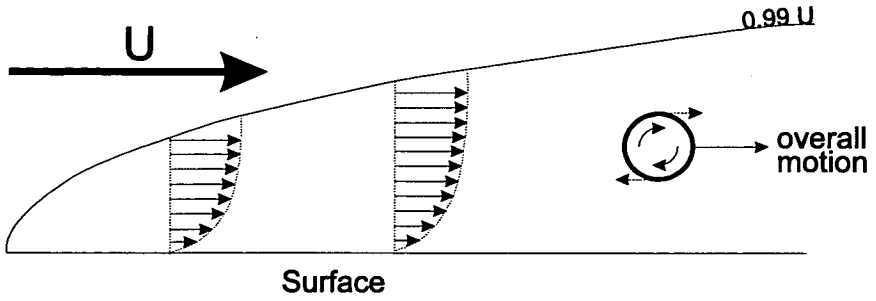

figure 6.30: The parabolic growth of the boundary layer over a surface is shown; highlighting two velocity profiles across the layer to demonstrate the rapid increase from zero at the surface to 0.99U (where U is the free flow velocity) which defines the limit of the boundary layer. The velocity difference between successive 'sheets' of fluid through the boundary produces sheer forces that will act on any particle within the layer.

Thecal spines: The angle of the thecal spines would have had a strong effect on the percentage of impacting smoke particles reaching the colony. If the spine was nearly parallel to the long axis of the colony the smoke-stream would have expanded easily along the spine, and the 'flare' effect would be very strong, but the spine could gather from only a small area. If the spine was nearly at right angles to the colony the smoke-stream would have expanded only slightly along the spine, and the 'flare' affect would be weak but the spine would gather from a large area. A spine at right angles to the colony would have produced no significant directional expansion of the smoke-streamers. The optimal spine angle for feeding efficiency depends on the exact nature of the relationship between the degree of smoke-stream expansion and angle of spine. This was investigated mathematically in section 6.4.2.

Some spines would have directly benefited the entire colony. It was observed that a spine on the geniculum of thecae 1^1 would have brought smoke into all subsequent thecal apertures not just that of thecae 1^1 (figure 6.2). Consequently only single thecal spines would have been required on the dorsal and ventral side of the colony, provided they are located on $th1^1$ and $th1^2$. The long deflected virgella (seen on *C. diplacnthus*) would also have brought smoke to all subsequent thecae, and would have increased feeding efficiency for the entire living colony (figure 6.24).

Anti-virgellar spines: Not all types of proximal spine could have had such a generalised affect on the colony. It was observed that the presence of anti-virgellar spines would have had very little affect on the flow beyond $th1^2$ (figure 6.23). A comparison of the flow observed over models of *C. pulchellus* type and *A. maxwelli* type showed that the anti-virgellar spines might have had a small effect on a particle-bearing flow, bringing it close enough to impact with the colony and into vortices in the thecal apertures. However this effect was very small as the anti-virgellar spines were almost entirely overshadowed by $th1^2$, and did not project significantly beyond it to widen the capture area.

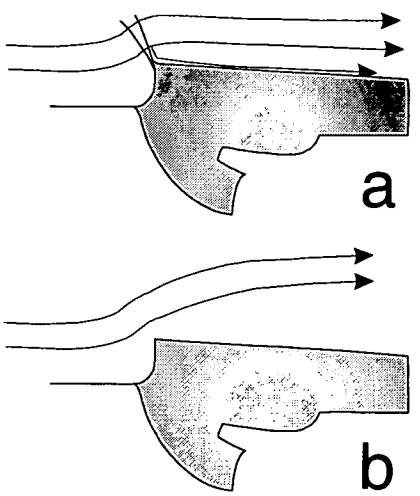

Figure 6.31: An interpretation of the flow over the leading edge of the sicula.
a. The presence of anti-virgellar spines holds the flow onto the rhabdosome surface over this edge, preventing separation.
b. Without anti-virgellar spines the flow is deflected away from the rhabdosome surface as it separates at the sharp edge of the sicula aperture.

More significantly it was also observed that anti-virgellar spines appear to have guided the flow over the sharp anti-virgellar edge of the sicula aperture, preventing separation. The flow would be held closer to the rhabdosome surface (figure 6.31) and the flow drawn laterally into the 'gap' behind the spines, where they had cut the flow. This would have helped bring food to the graptolite and may also have had a significant effect on stability. A flow impacting with a colony lacking anti-virgellar spines would be deflected violently away from the rhabdosome by the separation at

the ventral sicula edge (figure 6.17 and 6.19). Much reduced spines (in the form of lappets) could have also functioned for this purpose (*Hustedograptus teretiusculus*).

Deflected virgella: The deflected virgella would have brought flow in from a wide area as it projected far beyond the colony. However the virgella was perhaps not as efficient as a thecal spine for bringing the captured water to the surface, as the flow could not run directly up the spine to the rhabdsome. Smoke drawn along the spine would have been deflected by the sicular aperture (and colony boundary layer) as it approached the colony, and although some of the deflected flow would then impact with the ventral edge of the sicula and continue to flow over the colony surface, the rest would have been deflected beyond it. The virgella would have functioned, to some extent, to guide the flow over the sharp angle of the ventral sicula aperture (in comparison with the anti-virgellar spines); flow would have been deflected more violently by impact with sicula in the absence of the deflected virgella (figure 6.24).

The deflected virgella would also have produced a marked quiet zone directly in front of the sicular aperture. It is perhaps significant that the dimensions of this observed quiet zone were approximately 0.5mm by 0.5mm (figure 6.27), corresponding to the area of the model sicular aperture. The deflected-virgella therefore appears perfectly 'designed' to have protected the sicular aperture, preventing impact with fast moving flows. The presence of a simple virgella has also been observed to produce a similar quiet zone directly in front of the sicular aperture through wind tunnel experiments (using the Bristol wind tunnel and LDA system) by Rickards *et al* (1998).

Multiple spines: Multiple thecal spines (in either location) appear to have enhanced the drawing in of smoke-bearing air, although weakly, along the entire spinose length of the colony. This entrainment of air (or water as would have been the case for a living graptolite) would have been even more effective if distal spines projected beyond the proximal spines enabling them to gather from a wider area (e.g. *Paraglossograptus holmi*). The introduction of fresh food-bearing waters along the

length of a mature colony would have significantly improved the feeding efficiency of such a colony, preventing over-sampling of the same water body.

The spines would have interacted to produce numerous vortices bringing particle-bearing fluid, from beyond the rhabdosome surface, into the thecal apertures and directly to the zooids. The effective location of these spines was dependant on the thecal shape; a spine on the geniculum would have set up vortices in the apertures of strongly curved thecae, a spine at the thecal aperture would have formed vortices in the apertures of straight to gently curved thecae.

Orientation: Many of the models were tested in two orientations; virgella leading into the flow, and virgula leading into the flow. All the models pictured here are aligned with the virgella leading into the flow; this is the orientation indicated by the seawater tank experiments (section 5.3.1), and suggested by Rickards *et al* (1998) from their wind tunnel testing. In this orientation a single thecal spine on $th1^1$ and $th1^2$ may bring this flow into all subsequent thecal apertures along a mature colony. The anti-virgellar spines have limited values drawing in flow, but control the stability of very juvenile stages and guide the flow over the sharp ventral edge of the sicula. The deflected sicula of *C. diplacanthus,* and other climacograptids, also protects the sicular aperture, diverting and slowing impacting flow. This investigation supports the results of the seawater tank experiments (section 5.3.1), confirming a 'virgella leading' orientation. When the models were aligned with the virgula leading, the proximal spines (projecting at an angle from the thecae and sicula) trail with the flow. The flares produced by these spines would have tended to draw flow off the rhabdosome surface and away from the colony. A spine can only affect the flow pattern to the benefit of anything downstream or directly upstream of it, consequently arrays of proximal spines could have only drawn in food for the local proximal thecae, or added drag to the entire colony.

6.10. Conclusions

1. Spines were functional; they brought food to the surface (primarily the virgella and thecal spines) and stabilised the colony (primarily the anti-virgellar spines).
2. The influence of a spine, to slow flow velocity along the colony, extended approximately 0.2mm downstream from the spine. However a proximal spine may have caused an alteration of the flow pattern which affected the entire colony beyond it.
3. Multiple spines interacted to produce a pattern of vortices, which may have drawn fresh particle-bearing fluid along the entire spinose colony.
4. The location at which a spine would have been most effective depends on the thecal morphology.
5. Scandent colonies would have maintained a 'virgella first' orientation with respect to prevailing flow.
6. Growth of spines produced varied patterns, but the results are simple and similar for all patterns, suggesting a budgetary limitation and/or evolutionary limitations on design.
7. Care is required in attributing a taxonomic value to these functional structures.

6.11. Geological examples:

6.11.1. Real spine data:

Thecal spine function was investigated through simple mathematical modelling (section 6.4.2). This model attempted to predict an optimal spine length and angle for a spine whose function is to increase feeding efficiency by drawing fresh food-bearing fluid onto the rhabdosome surface. Too little real data could be 'plugged into' this model in order to make any precise predictions, but a comparison with real fossil angle and length data may determine if the model is reasonable.

Method:

The angles (to the scandent colony central line) and lengths of proximal spines were measured from illustrations of 284 specimens in peer-reviewed journals and monographs (appendices D and E: references section 9.2). These illustrations included both flattened and isolated specimens of 39 diplograptid species.

The results were grouped in a number of ways for analysis.

a. If all proximal spines had a similar function (for example to bring in more food-bearing flow and stabilise the colony) then similar spine angles would be expected to have been effective for all. Therefore initially the whole dataset was considered together and the mean and standard deviation of all spine data calculated.
b. The spinose diplograptid species can be divided into two basic spine array types. Type I: Those species with short thecal spines including those with anti-virgellar spines, e.g. *A. maxwelli*. Type II: Those with long proximal spines (typically proximal spines are fewer in number and may have continued to grow as the colony matures), this group includes those species with a deflected virgella, e.g. *C. diplacanthus*. The mean and standard deviation of spine angles and length were calculated for the two datasets.

c. The dataset was divided by species in order to look at variation of spine types. Reasonable similarity of values between spine types of different species would be expected if these spines had the same function.

Results: These data cannot be expected to provide reliable values for graptolite spine lengths or angles, as this study has too many inherent sources of error. These include drawing inaccuracies, the variable orientations of specimens and, more importantly, original specimens with broken and incomplete or distorted spines. Spine lengths observed represent a minimum value only, as long spines would have been more liable to break prior to burial; measured angles will be distributed around the 'real' value, as spines could be distorted to either larger or smaller angles. In both cases some natural variation of the living graptolite must be expected (section 4.2).

a. Entire data set:

The spine data gathered are plotted as a series of simple histograms (figure 6.32 and 6.33) illustrating the distribution of values for spine lengths and angles. Values for the mean and standard deviation of each spine are given in table 6.2.

Spine Location	Mean angle (degrees)	Standard deviation (angle)	Mean length (mm)	Standard deviation (length)
Virgella (deflected)	34.5	19.8	2.2	3.3
Anti-virgella	48.6	21.8	0.33	0.36
$th1^1$	66.6	19.4	0.86	2.4
$th1^2$	61.6	20.0	1.1	2.7
$th2^1$	78.2	13.3	0.24	0.12
$th2^2$	71.8	11.9	0.38	0.33
$th3^1$	79.6	15.2	0.19	0.085

Table 6.2: Combined spine data. Mean values and standard deviation are given for both angles and lengths. Original data in appendices D and E.

The histograms produced from the spine angle data reveal an approximately normal distribution for each spine type (figure 6.32). The histograms plotted using the spine length data are less clear revealing an approximately normal distribution for the anti-virgellar spines (centred around 0.3 mm), and a more random spread of values for the deflected virgella and thecal spines (figure 6.33). These histograms do feature a peak of values around 0.3 to 0.4 mm but these are followed by a number of specimens with considerably longer spines (up to 17 mm).

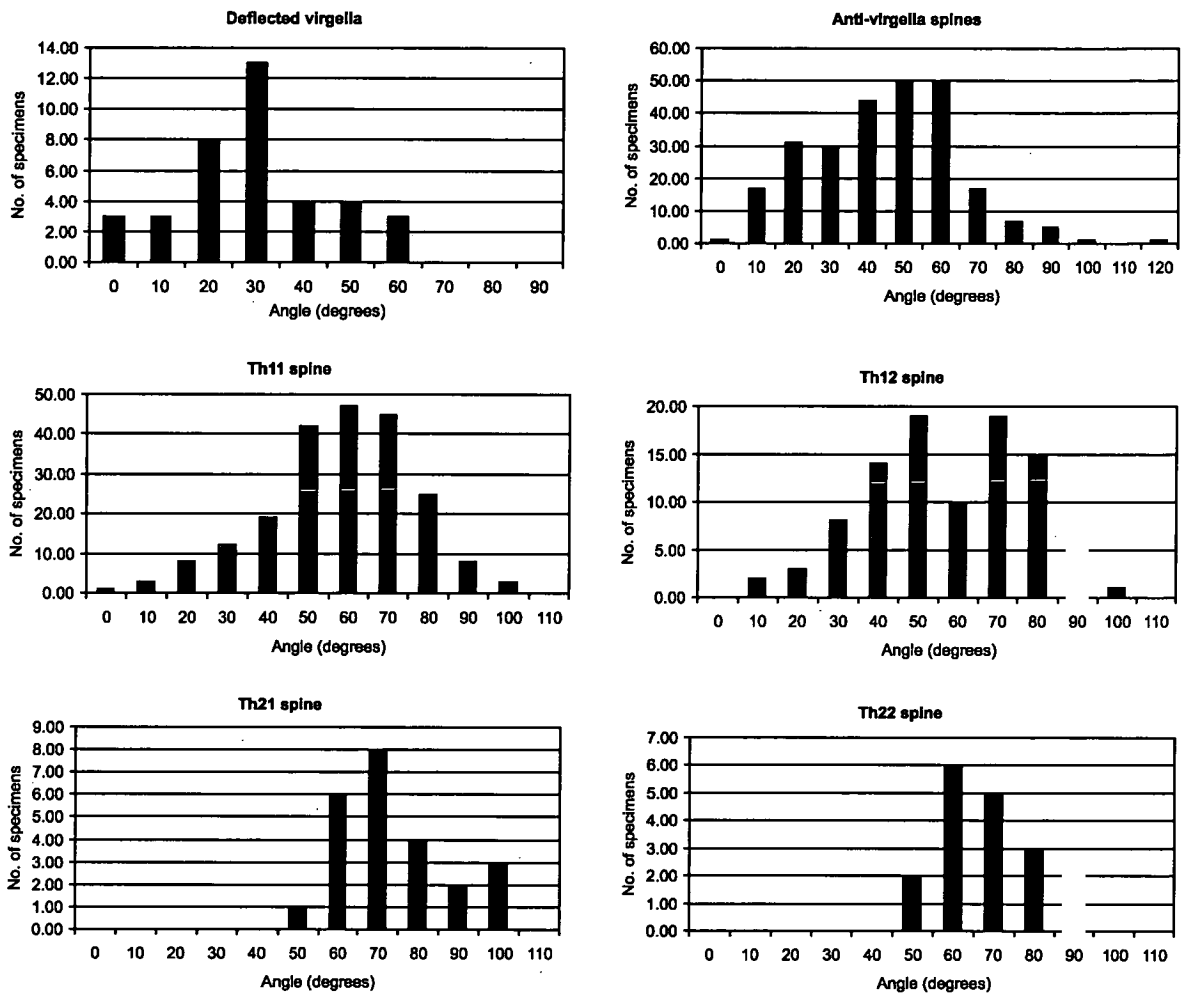

Figure 6.32: Histogram plots displaying the distribution of proximal spine angles; the data are divided by proximal spine type (deflected virgella, anti-virgellar spines and thecal spines). The measured angle is that between the spine and the central colony line. All six graphs describe a rough bell-shape indicating a near-normal distribution. More specimens are required for clearer results. Original data in appendices D and E.

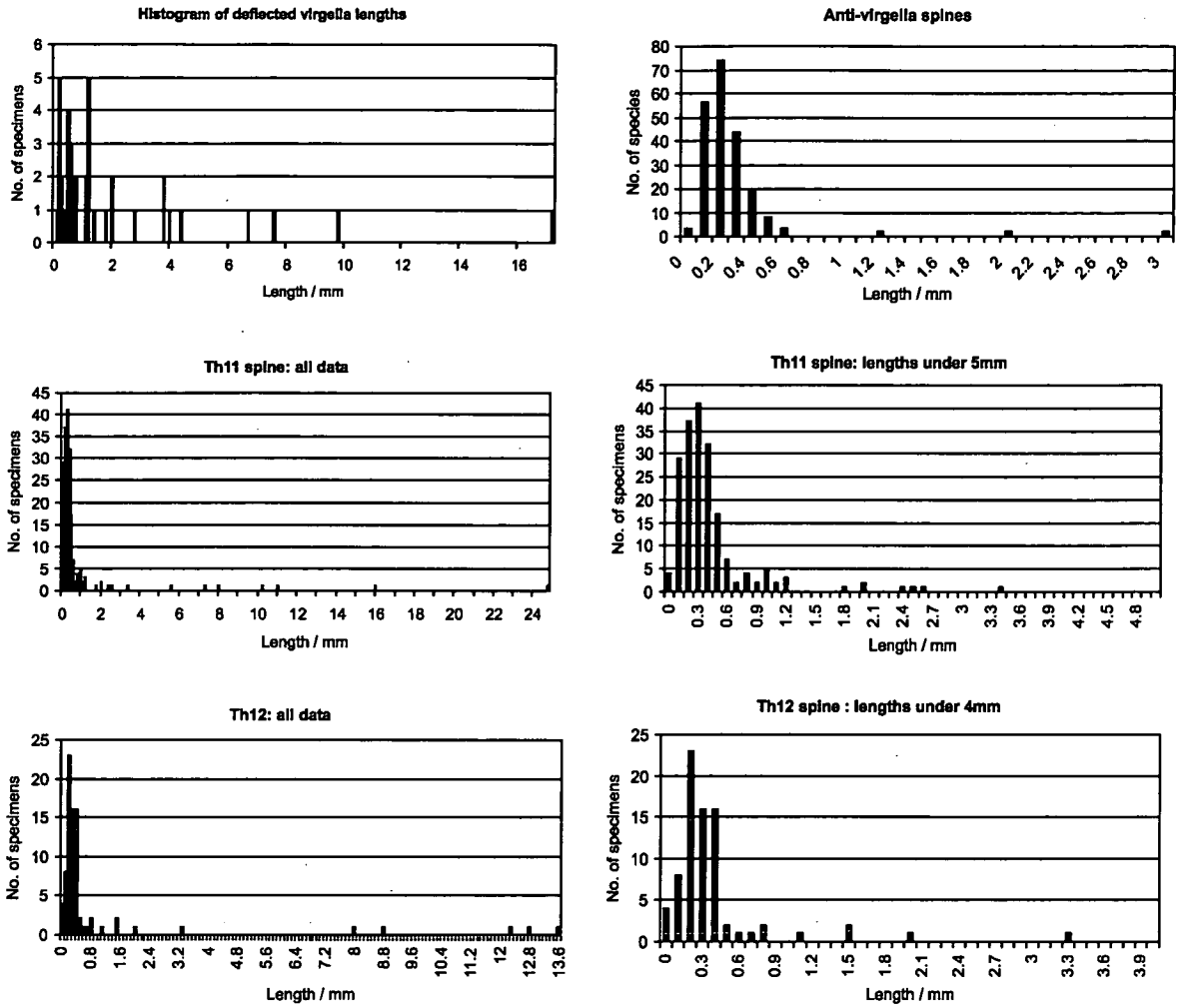

Figure 6.33: Histogram plots displaying the distribution of proximal spine lengths; the data are divided by proximal spine type (deflected virgella, anti-virgellar spines and thecal spines). Th11 and Th12 spine length are plotted twice (all data and those under 4mm only) to hightlighht the distribution of shorter spines. All graphs describe a rough bell-shape in the small length range indicating a near-normal distribution, however a few specimens exhibit much longer spines. More specimens are required for clearer results. Original data in appendices D and E.

If the purpose of anti-virgellar spines was to control orientation through increased drag (section 6.3.3) spines at a large angle (approaching 90°), offering the largest surface area to the flow, would be optimal. However the anti-virgellar spines measured projected at a lower angle to the colony than the thecal spines. It does not seem likely that the anti-virgellar spines had a strong function in drawing in fresh food-bearing water. As discussed previously (section 6.6.1) during the period when

the anti-virgellar spines might have functioned most effectively to draw in flow (before the construction of $th1^2$ which overshadowed them) there were no zooids on the ventral side of the colony to feed. However it was also shown that the anti-virgellar spines brought the flow around sharp ventral edge of sicula, holding it close to the colony surface.

b. Divide by type:

Despite the limitations of this investigation, due to taphonomic distortion and breakage, the data do appear to fall broadly into two sets (Type I and II).

Type I: short proximal thecal spines, may have anti-virgellar spines, cf. *A. maxwelli.*

Spine Location	Mean angle (degrees)	Standard deviation (angle)	Mean length (mm)	Standard deviation (length)
Anti-virgella	48.6	19.8	0.28	0.13
$th1^1$	72.4	15.8	0.33	0.17
$th1^2$	64.7	18.8	0.31	0.16
$th2^1$	78.2	13.3	0.23	0.12
$th2^2$	71.8	11.9	0.24	0.12
$th3^1$	79.6	15.2	0.21	0.12

Table 6.3: Type I spine data. Mean values and standard deviation are given for both angles and lengths. Note the decrease in thecal spine length distally. Original data in appendices D and E.

Type I spine data (antivirgellar spines, $th1^1$ and $th1^2$ spines) are plotted as a series of simple histograms (figure 6.34 and 6.35).

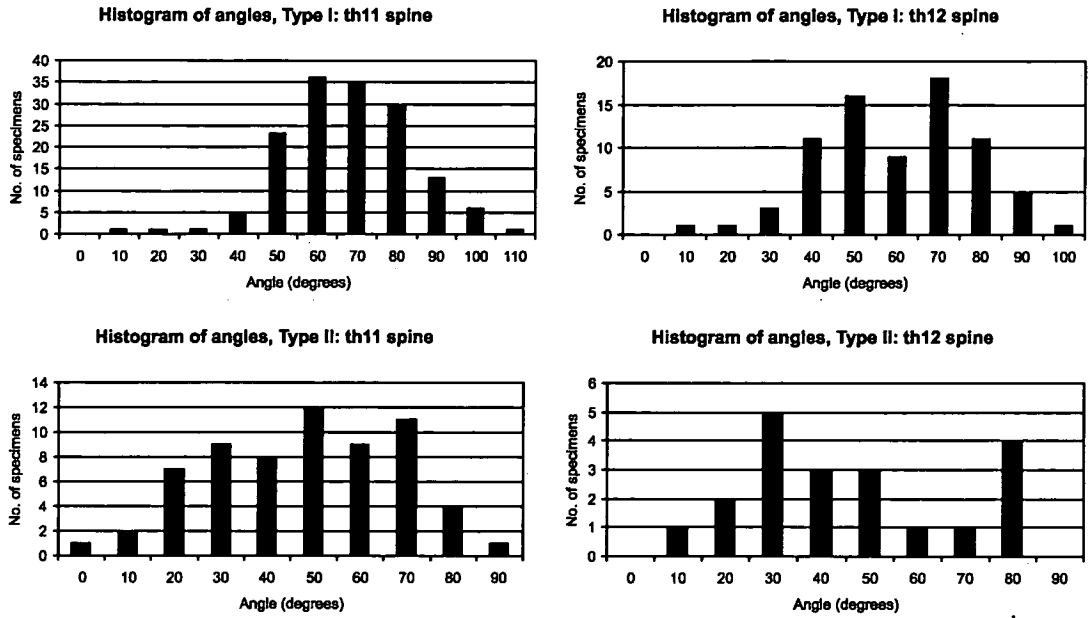

Figure 6.34: Histogram plots displaying the distribution of thecal proximal spine angles ($th1^1$ and $th1^2$). The data are divided by species 'Type' as described in the text. The angle is that measured between the spine and the central colony line. All four graphs describe a rough bell-shape indicating a near-normal distribution. More specimens are required for clearer results. Original data in appendices D and E.

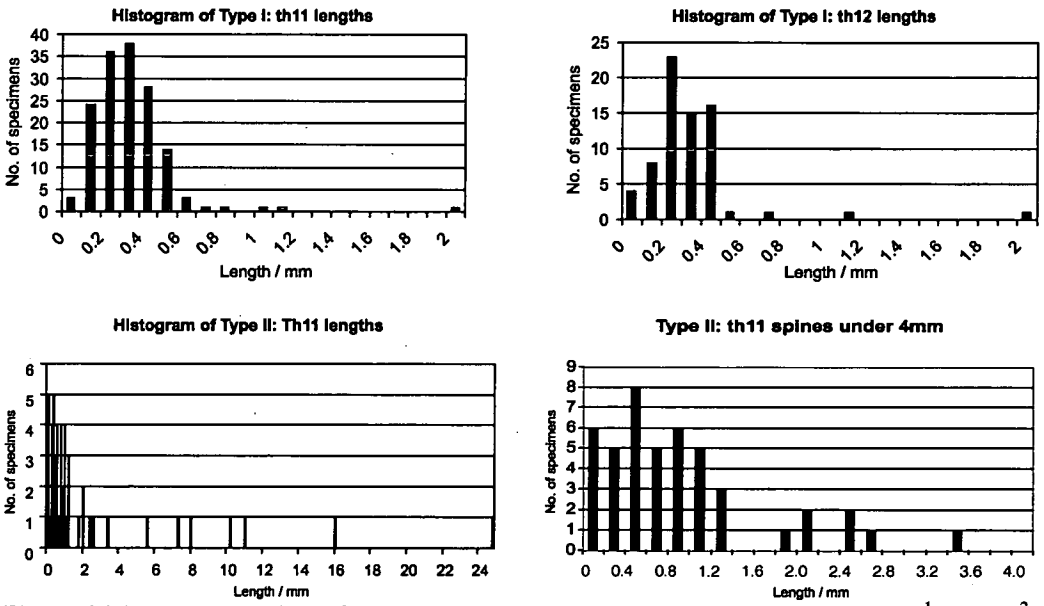

Figure 6.35: Histogram plots of the distribution of thecal proximal spine lengths ($th1^1$ and $th1^2$). Data are divided by species 'Type' as described in the text. The Type I graphs describe a rough bell-shape, with few specimens featuring longer spines. The distribution of Type II lengths is less clear where many specimens exhibit much longer spines. The Type II $th1^1$ spines are plotted twice: all data and just those under 4mm to highlight the distribution of shorter spines. Type II $th1^2$ spines are not plotted as there were too few specimens. Original data in appendices D and E.

Separated from the Type II data, the normal distribution of the Type I data becomes clearer. The thecal spines were typically approximately 0.2-0.35mm long, and projected at an angle approximately 65-80° from the colony central line (figure 6.34, 6.35 and table 6.3). The most proximal spines were typically longer than subsequent spines. Anti-virgellar spines were approximately 0.3mm long and projected at approximately 50° from the central colony line.

Type II: long thecal spines ($th1^1$ and $th1^2$), may have deflected virgella, cf. *C. diplacanthus*.

Spine Location	Mean angle (degrees)	Standard deviation (angle)	Mean length (mm)	Standard deviation (length)
Virgella (deflected)	34.5	15.5	2.12	3.23
$th1^1$	53.2	20.4	2.40	4.46
$th1^2$	50.8	21.1	4.47	5.10

Table 6.4: Type II spine data. Mean values and standard deviation are given for both angles and lengths. Original data in appendices D and E.

Type II spine data (delfected virgella, $th1^1$ and $th1^2$ spines) are plotted as a series of simple histograms (figure 6.34 and 6.35).

All Type II spines were typically longer, and showed much more variation than Type I spines (figure 6.35 and table 6.4). This is due to their continuing development throughout the life of the colony, in comparison with the type I spines which appear, fully formed, in the earliest growth stages. Specimens of different growth stages, within the same species, could feature spines of quite different lengths.

The deflected virgella data revealed an approximate normal distribution of angle centred around 35° (figure 6.34 and table 6.4). $Th1^1$ and $th1^2$ spine data also revealed an approximate normal distribution centred around 50-55° from the colony central

One important question is what advantage might these twisted forms have offered the graptolites? It is clear that the whole-colony rotation of the dicellograptid species would have increased the feeding paths of the individual zooids in the colony as described by Rigby and Rickards (Rigby and Rickards 1989, Rigby 1990). The oil tank experiments, in this study, have indicated that the twisted stipes experienced greater drag than the simple straight uniserial stipes. This is borne out by the wind tunnel observations showing a greater area of turbulent wake behind the twisted models than the simple model (figure 7.12 and 7.14 compared with figure 7.10). The increased drag of the twisted uniserial stipes (forming the distal half of the colony) caused a more rapid re-alignment of these models, in comparison with the simple dicranograptid model, when tested in the oil tank. In this case the twisted stipes are acting as a vane-bearing *nema*, providing increased drag without a substantial increase in mass. The twisted forms would have been more stable to turbulent flows, given that the stable orientation was with the proximal end leading, and might have allowed the colony to maintain this orientation with continued growth of the uniserial stipes.

7.8. Further study

A detailed study of the collagen mass distribution of graptolite colonies would be invaluable for refining these experiments. The volumetric distribution of collagen might be investigated serial sections of three-dimensional specimens. This study might then be extended to consider more dichograptid shapes, providing a stronger bridge to the experimental work of Rigby and Rickards (Rigby and Rickards 1989, Rigby 1990 and 1992).

Tests using isolated specimens in seawater would provide useful, and possibly more reliable, insight into the orientation and motion of these non-scandent colonies. A larger number of complete isolated specimens would be required. It would be particularly interesting to also test some of the spiralled forms.

line (figure 6.34 and table 6.4). The Type II spine angles showed more variation than the Type I spine angles; again this is due to their continuous development. Initially the Type II spine angles grow at greater angle to the colony central line, more comparable with the Type I spines, as the colony matures and growth of the spines continues they appear to 'droop' growing at an increasingly low angle to the colony.

The contrasting angles and lengths typical to the two types may represent a difference in the relative importance of various functions for these two groups: feeding efficiency, stability, or another unidentified function. The contrast is largely a result of the continuing growth and function (or changing function) of Type II spines. The change in angle of these spines with increasing growth and maturity might indicate that a new or changed function became increasingly important.

The Type II spines appear to have served a similar function in part to that of the Type I anti-virgellar spines (section 6.7.1), preventing separation of the flow from the colony as it impacts with the proximal end. The lower angle spine would have been better adapted for this purpose.

The mathematical budget model for thecal spines (section 6.4.2) predicted that, if thecal spines functioned primarily to increase feeding efficiency, then a small range (approximately 20°) of optimal spine angles would be expected. This study has indicated that the deflected virgella and th1^1 spine of Type II species might have functioned both to increase feeding efficiency and prevent separation when flow first impacted with the blunt proximal end of the colony. It would seem reasonable that the spines of these species would have been constructed at a compromise angle to optimise both these functions. The Type I species thecal spines are more likely to have functioned primarily to increase feeding efficiency, and the Type I data would make a more realistic comparison with the budget model.

The Type I data did show an abundance peak of spine angles for th1^1 and th1^2 between 50° to 70° (figure 6.34). This range of optimal angles is most comparable with the T4 model (figure 6.11), although the budget angles are too low. This

indicates that if feeding efficiency was the primary function of these thecal spines the relationship between expansion of impacting smoke-streamers and spine angle was more extreme than those used for the budget model. In order to realistically test the budget model (and feeding efficiency function) this relationship would need to be investigated further.

C. Divide by species:

The species data are presented as a series of bar charts illustrating the average spine angles and lengths for the array of each species. In many cases these values were calculated from only a few, or even one, specimen (figure 6.36 to 6.39).

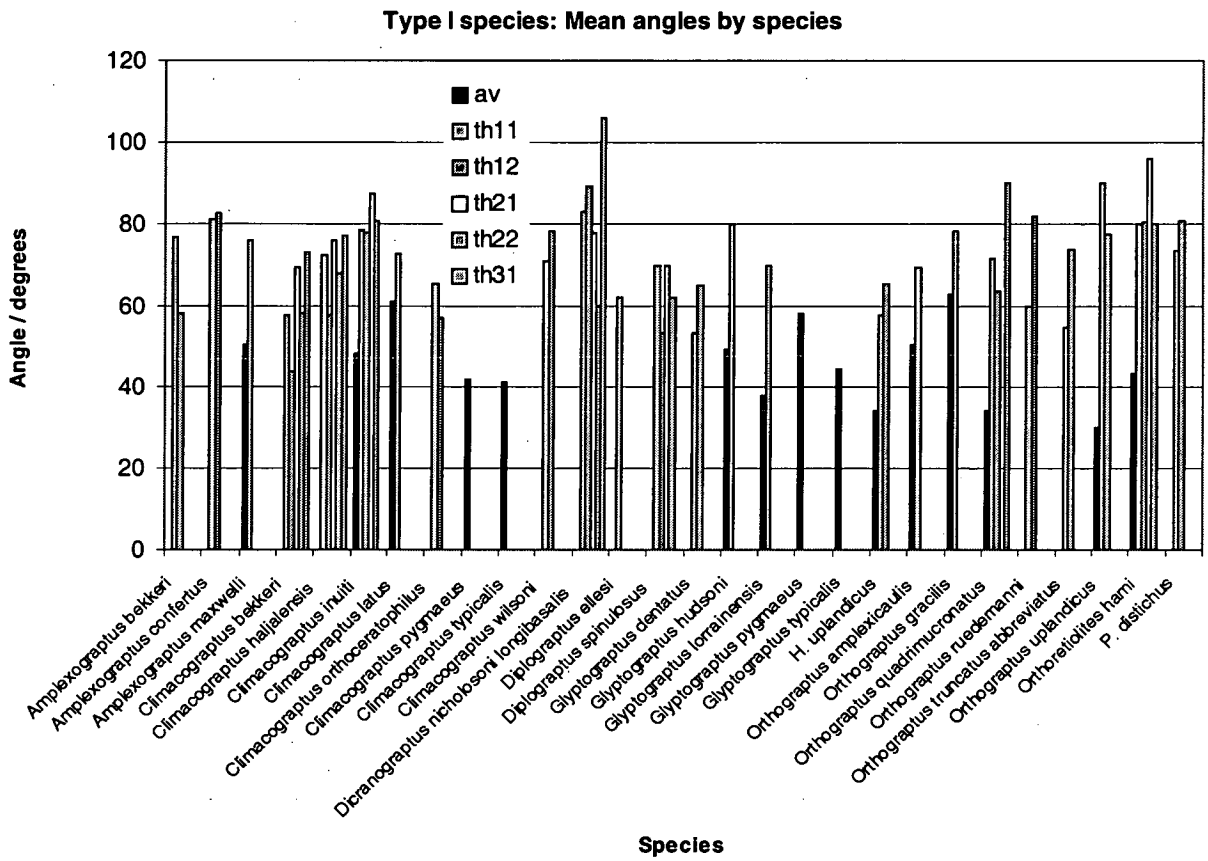

Figure 6.36: Type I species. The mean angles for each spine type (antivirgella spines (av) and thecal spines ($th1^1$ to $th3^1$)) are plotted for all type I species measured. Original data in appendices D and E.

The Type II species, as expected, show a much greater variation in angles and lengths. The Type I data shows a better continuity of angles and lengths between species. More specimens are required for significant results.

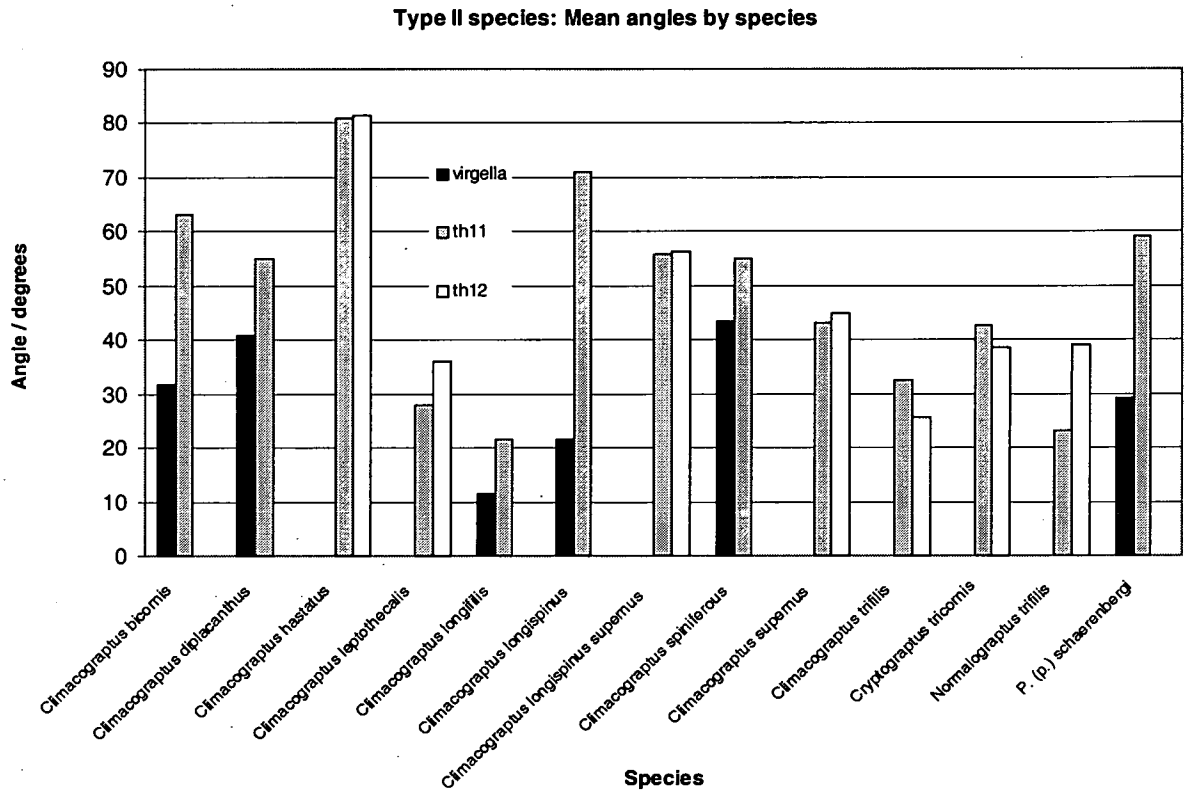

Figure 6.37: Type II species. The mean angles for each spine type (antivirgella spines (av) and thecal spines ($th1^1$ to $th1^2$)) are plotted for all type II species measured. Original data in appendices D and E.

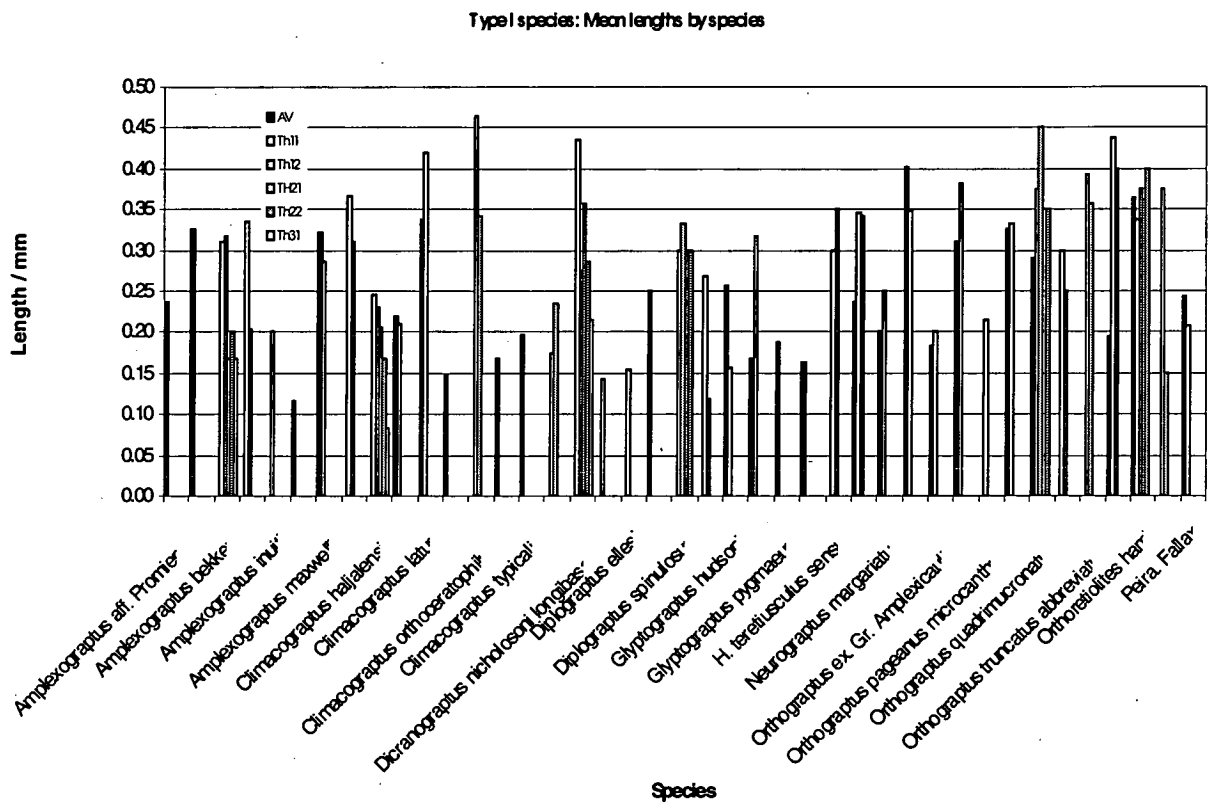

Figure 6.38: Type I species. The mean lengths for each spine type (antivirgella spines (av) and thecal spines ($th1^1$ to $th3^1$)) are plotted for all type I species measured. Original data in appendices D and E.

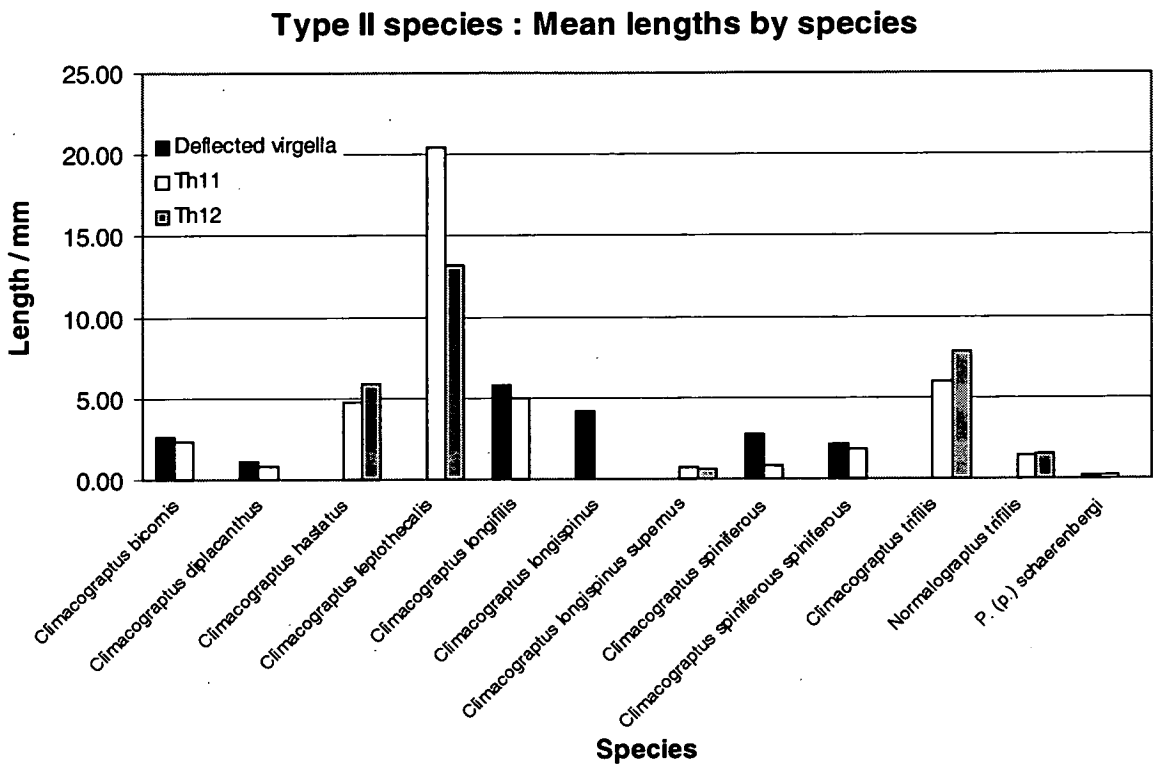

Figure 6.39: Type II species. The mean lengths for each spine type (antivirgella spines (av) and thecal spines ($th1^1$ to $th1^2$)) are plotted for all type II species measured. Original data in appendices D and E.

Conclusions:

- Graptolite species can be broadly divided into two types based on their proximal spine arrays.
- Type I species have an approximately normal distribution of lengths and angles within the error constraints of this study.
- Type II species are more variable due to the continuing development of these spines.
- Anti-virgella spine angles do not support a pure drag function. Prevention of separation seems to have been more important.
- The thecal spine angles of Type I species are consistent with the budget model for a feeding efficiency function, however this model needs to be more constrained for a true comparison.

6.11.2. The history of proximal spines:

In section 6.1.3 the distribution of proximal spines through the history of scandent graptolites was briefly discussed. This section attempts to quantify this pattern more clearly, looking at the relative proportion of diplograptid species with proximal spines to those without, and the apparent first and last appearances of different spine patterns.

A series of monographs from good faunas through the Ordovician to Early Silurian were considered. There was no single location at which a good fauna could be studied throughout this period, and a more accurate assessment would be obtained from a large fauna. This method also takes a more global view assuming that the pattern of introduction, abundance and abandonment of proximal spines was broadly congruent across the Palaeozoic world.

The faunas included are listed below:

Geological age of fauna	Location	Reference
late Tremadoc to early Llanvirn	Bohemia	B. Bouček 1973
late Llanvirn to Llandeilo	Oslo region	W.B.N. Berry 1964
Caradoc	Laggan Burn (Scotland)	O.M.B. Bulman 1947
Ashgill	Southern Scotland	S.H. Williams 1981
late Ashgill to Llandovery	Kazakhstan	M.K. Apollonov *et al* 1980
Llandovery	Southern Urals	T.N. Koren' & R.B. Rickards 1996

The earliest diplograptids, which appeared in the late Arenig to early Llanvirn, as described by Bulman (1963), were also considered although a complete fauna was not studied.

Results: The results are shown as a bar chart illustrating the relative abundance of diplograptid species in each fauna with isolated proximal thecal spines (limited to the first two thecae only), species featuring anti-virgellar spines and those with

spines on all thecae. Abundance is given as a percentage of the total number of diplograptid species in the fauna (figure 9.40).

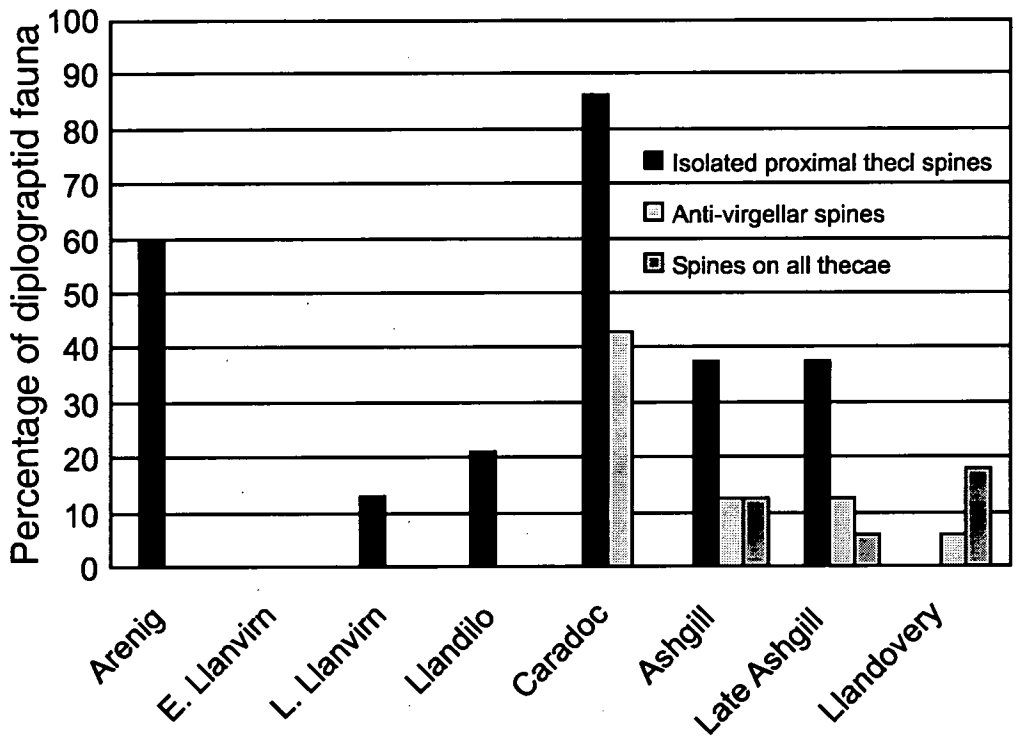

Figure 6.40: The graph shows the relative abundance of species with isolated proximal spines, anti-virgellar spines and multiple spines within the diplograptid contingent of each typical fauna. Species with both proximal spines and anti-virgellar spines are counted in both groups.

Sixty percent of the first diplograptid species (largely glyptograptids) which appeared in the late Arenig (described by Bulman (1963)) feature proximal thecal spines. These spines were all short, slender, sub-apertural and confined to $th1^1$ and $th1^2$ only.

By the early Llanvirn, diplograptids represented approximately 12% of graptoloid species. None of the biserial species observed in the Bohemian fauna (Bouček 1973) have proximal spines in addition to the virgella. However some of the spinose early glyptograptids, as described by Bulman (1947), have been found continuing into the Llanvirn in other locations: e.g. *G. austrodentatus oelandicus*, *G. shelvensis* and *Diplograptus ellesi*. This fauna would appear to indicate a diversification of non-spinose diplograptid species resulting in a lower relative abundance of those with proximal spines.

In the late Llanvirn to Llandeilo fauna of the Oslo region (Berry 1964) diplograptids represent 42% of species described, with the introduction of *Orthograptus* and *Amplexograptus* and expansion of the *Climacograptus*. Thirteen percent of the late Llanvirn diplograptid fauna of Oslo had proximal thecal spines; this increased in the Llandeilo to 21% of the diplograptid fauna. As in the Arenig these proximal spine-arrays were limited to short spines built onto th1[1] and th1[2] only.

The Caradoc was represented by the Laggan Burn fauna (Bulman 1947). Of the graptoloid species described, 50% are diplograptids, as they began to dominate the global fauna. The spine-arrays of older faunas featured short spines on the first two thecae only. However the Caradoc fauna appears to represent a radiation of proximal spine patterns. The Laggan burn fauna introduces species with anti-virgellar spines (*Diplograptus leptotheca*: paired antivirgella spines and a single spine on th1[1], *Orthograptus apiculatus*: paired antivirgella spines and single spines on th1[1] and th1[2]), representing approximately 43% of the diplograptid fauna. This Caradoc fauna also sees the introduction of species with considerably longer proximal spines (Type II as discussed in the previous section 6.11.1), such as *Climacograptus bicornis*, whose spines continued to grow as the colony matured. *Lasiograptus harknessi* marks the spread of thecal spines along the colony as it had anti-virgellar spines, single spines on th1[1] and th1[2], and paired spines built onto all subsequent thecae. In total 86% of the Laggan Burn Caradoc fauna featured proximal thecal spines.

The Ashgill fauna of Southern Scotland was described in the PhD thesis of Williams (1981). Fifty percent of the diplograptid species observed had proximal spines; 37.5% limited to the first two thecae only, 12.5% with spines on all thecae and anti-virgellar spines. The diversity of proximal spine patterns was apparently more limited than in the Caradoc with only four spine-array types represented: Long spines on th1[1] and th1[2], *Climacograptus longispinus supernus*; short spines on th1[1] and th1[2] only, *Climacograptus latus*; antivirgella spines and paired spines on all thecae, *Orthograptus quadrimucronatus*; and antivirgella spines with single spines on all

thecae, *Pacificograptus pacificus*. Thus the Ashgill fauna indicates a decline in both abundance and diversity of proximal spines.

The late Ashgill and Llandovery fauna of Kazakhstan records the further decline of proximal spines where approximately 37% of the Ashgill diplograptid fauna preserved featured proximal spines. Patterns represented included long spines on $th1^1$ and $th1^2$, *Climacograptus longispinus hvalross*; short spines on $th1^1$ and $th1^2$, *Glyptograptus posterus*; antivirgella spines with a single spine on $th1^1$, *Amplexograptus stukalinae*; and antivirgella spines with single spines on all thecae, *Pacificograptus pacificus pacificus*. The Llandovery of Kazakhstan saw the apparent total loss of anti-virgella and proximal spines.

Koren' and Rickards (1996) looked only at the biserials of the Southen Urals. Of the Southern Urals biserial species, 18% described had proximal spines that were rarely confined to the proximal end (e.g. *Normalograptus trifilis trifilis*). More spinose species featured spines on all thecae, often up to four projecting from the geniculum, often these spines formed part of a lacinia. Of the species described, 6% were believed to have had spines in the anti-virgella location, but this was either a single spine (which may have been a misidentified spine on $th1^1$) or multiple spines in addition to others on the sicula and along the entire colony.

Discussion: The data used are limited. Although the data came from 'good' faunas even these did not include a large total number of species. Consequently percentages are only approximate, and very sensitive to chance preservation. This investigation also assumes that faunal changes were global (apparently broadly the case with the history of proximal spines) but the precise times of appearance and abandonment may not have been concurrent. Such a study should be undertaken through a thorough plotting of the patterns of graptolite morphology globally throughout the Palaeozoic, however this would be a PhD project in itself and was not a realistic prospect within this study. This is merely a brief overview to provide some evidence for a pattern based on the presence and abundance of proximal spines throughout the Ordovician. The numbers produced are guidelines only.

Within these limitations the data gathered would seem to clearly indicate that proximal spines appeared with the first Arenig diplograptids, amongst which they were relatively common. These all featured the same pattern of proximal spines (short spines on th1[1] and th1[2]). As the diplograptids radiated through the Llanvirn these spines became relatively less common although some of the original Arenig species remained. The late Llanvirn to Caradoc saw a steady increase in the relative abundance of spinose species and the diversity of proximal spine combinations reaching a peak in the Caradoc when the majority of biserial species had proximal spines. The abundance and diversity of species with proximal spines then rapidly decreased again from the Ashgill to the Llandovery where such forms are relatively rare.

The abundance of species with anti-virgella spine pairs shows a similar, but reduced, pattern through the Ordovician. Anti-virgellar spines appear with peak abundance in the Caradoc, then declining in the Ashgill, and apparently completely absent by the Llandovery.

The typical biserial colony form changed through the Ordovician and was much more pointed in the Llandovery relative to older species. Perhaps graptolites with such pointed proximal ends did not require anti-virgellar spines to hold the flow on the rhabdosome surface, as there was little possibility for detachment with these forms. Did graptolites have particularly blunt or wide proximal ends in the Caradoc?

Environmental links: Many environmental factors changed and fluctuated throughout the Ordovician. It is impossible to establish causal links between any environmental events and diversity changes; at best correlation can be established and implications discussed.

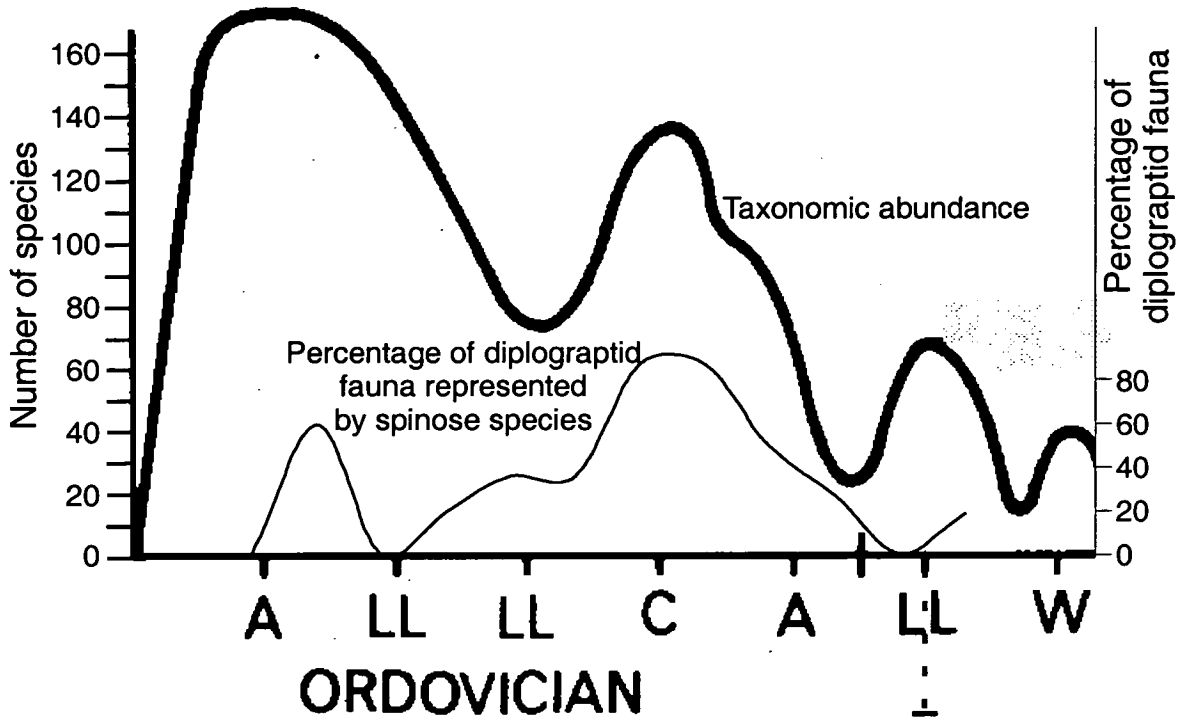

Figure 6.41: A comparison the total taxonomic abundance of graptolite species through the Ordovician (based on Koren' and Rickards 1979), plotted with the heavy line, with the abundance of spinose species (values are given by the percentage of the diplograptid fauna represented by spinose species), plotted with the feint line. Not to scale.

It is apparent that the peak diversity of species with proximal spines is concurrent with a period of high total graptolite diversity (figure 6.41). The pattern of total graptolite diversity through the Ordovician and Silurian comprises of a series of peaks. The earliest and largest diversity peak lies in the Arenig, followed by peaks of decreasing height in the Caradoc, Llandovery, Wenlock and Ludlow (Koren' and Rickards 1979).

$\delta^{18}O$ and $\delta^{13}C$ isotope signatures from Ordovician brachiopod shells (Patzkawsky *et al* 1997) indicate that overall global temperatures cooled throughout the Ordovician, towards the end-Ordovician glaciation, with a marked change from warm to cool conditions at the end of the Caradoc (Lavoie and Asselin 1998), and a corresponding increase in productivity and burial of organic matter depositing widespread black shales in the Caradoc. The Caradoc also saw a global sea-level high (Fortey 1984), which would have expanded shelf habitats, and was a probable factor in the

breakdown of provincialism (largely attributed to the closure of the Iaptus) also noted at this time.

The typical Palaeozoic superoligotrophic ocean conditions (Martin 1996) combined with the increased shelf area and warm seas would have generated an increase in the number and type of niches available to graptolites. Such an environment could trigger an increase in diversity with graptolite species filling specialist niches.

It is unrealistic to point to any single environmental factor as the cause of the peak diversity and abundance of spinose forms centred on the Caradoc; reasonable evidence is unobtainable. Proximal spines appeared with the earliest biserial graptolites, and clearly were not a later innovation of that group, but more likely a surviving, altered, character from a dichograptid ancestor. It could be suggested that the increasing abundance of species with proximal spines might be linked to the

As the end-Ordovician glaciation set in, with glacial maximum in the mid-Ashgill (*pacificus – extraordinarius* biozones), graptolite numbers dwindled and along with them those species with proximal spines. Possibly a result of the cooler temperatures, lower sealevel and increased nutrient availability in the late Ordovician (Martin 1995), dramatically reducing the available niches. This does not explain why Silurian graptolites did not feature proximal spines, post-recovery from the glaciation event. Possibly by unlucky chance no species with spines limited to the proximal end survived in order to re-radiate, or the niches previously occupied by these species were now more successfully filled by the new monograptid species.

Conclusions:

- Proximal thecal spines appeared with the earliest diplograptids in the Arenig.
- The broad abundance and diversity of thecal spines shows an increase towards a peak in the Caradoc, and subsequent decrease through the rest of the Ordovician.
- Anti-virgellar spines appeared in the Caradoc with a relatively high abundance, which then declined through the rest of the Ordovician.

- Silurian spinose graptolites tended to have much larger number of spines spread along the entire colony. Anti-virgellar spines were rarely present but tended to be either a single spine or part of a very spinose sicula.

6.12. Further study:

The work described in this chapter could be refined through a more detailed study of the relationship between spine angle and the expansion of an impacting smoke-streamer. Computer analysis of digital photographs taken with the spine at a wider range of angles might allow the shape of this relationship to be determined, which would provide the tighter constraints needed for a realistic model.

A more detailed study of global distribution of graptolite structures throughout their geological history would also be interesting, perhaps combined with a more thorough study of linked environmental changes throughout this time.

This study could be further extended to investigate a wider range of proximal structures including lacinia and ancora, and more unusual structures.

7. The possible hydrodynamics of simple two-stipe dichograptids.

7.1. Introduction:

This work has concentrated on the hydrodynamics of scandent graptolites. These typically had a simple stick-like form with a *nema* spine projecting from the distal end and a virgellar spine projecting from the proximal end.

The experiments described in the previous chapters have led to an improved understanding of the possible life orientations of graptolites, and have provided insight into possible functions for some of the common structures observed (the *nema* and secondary distal structures are discussed in chapter 5; proximal structures are investigated in chapter 6). The natural continuation of this project is to consider some of the other, non-scandent, graptolite colony forms, moving backwards through graptolite evolution towards the multiramous species, the hydrodynamics of which have been previously studied, particularly by Rigby and Rickards (Rigby and Rickards 1989, Rigby 1990).

This chapter takes a first look at the hydrodynamics of the simplest dichograptids: dicellograptids, didymograptids and dicranograptids. These are all forms with two uniserial stipes.

7.1.1. Previous study

There have been a number of discussions (largely published as small sections of papers covering wider topics) as to the form and mode of life of the didymograptids, dicellograptids and dicranograptids. These discussions have focussed mainly on species from these groups which exhibit twisted forms, and the impact of these shapes on the overall motion (and possible rotation) of the colony.

Most of this work has concentrated on the dicellograptids. Williams (1981) undertook a detailed study of the form of dicellograptid species, in order to refine taxonomy for correlation in the Upper Ordovician. This study involved construction of models for comparison with flattened fossils, using the method described by Briggs and Williams (1981) to investigate three-dimensional shape. In almost all cases dicellograptid species show stipe torsion (Williams 1981). This has been confirmed by the isolation of spiralled specimens. Williams was particularly concerned with this stipe torsion and the morphology of spiralled species. This investigation revealed that the two stipes of a dicellograptid colony always show the same sense of torsion, but this sense may be species dependent or equally mixed amongst the specimens of a single species. The observed stipe torsion is due to an openly spiralled form, about an axis passing through sicula; rarely a species shows no torsion (*D. forchhammeri*) and has simple, straight stipes lying in the same plane as the sicula.

Bulman (1964) first suggested a function for such spiralled forms when he compared the spiral shape of the monograptid *Cyrtograptus* with that of the umbrella sponge *Axoniderma*, which rotates in response to small currents. He suggested that similarly the spiral-shaped *Cyrtograptus* might have rotated as a result of the overall colony shape. Bulman then extended this comparison to other spiralled species: nemagraptids, dicellograptids, dicranograptids; would their shape have also caused rotation? He discussed *Dicranograptus furcatus bispiralis,* which has only a short biserial section branching into two spirally intertwined uniserial stipes, generating an overall colony form remarkably similar to that of *Dicellograptus caudatus* suggesting that this too may have rotated in the same manner.

This idea has been supported and extended a number of times. Williams (1981) pointed out that a spiralled form would clearly have had important implications for the mode of life of the colony. He suggested that if the colony rotated this shape would have increased feeding efficiency. *Dicranograptus ziczac* featured independently spiral arms that occasionally intertwined (Williams 1981). Williams predicted that a spiralled stipe would have provided maximum feeding efficiency if

the thecal apertures were situated on the outside of the spiral, and that this could also have aided floatation combined with auto-rotation as described by Kirk (1969).

Kirk (1969), outlining her theory of automobility, described how the feeding currents produced by the zooids in such a spiralled colony (particularly *Dicellograptus caudatus* and *Dicranograptus furcatus bispiralis*) would have resulted in strong rotation of the colony as it swam upwards. Although the didymograptids did not exhibit spiral colony forms Kirk suggested that directed feeding currents might have caused rotation of *Didymograptus extensus.* The conical shape of these colonies would have ensured feeding efficiency as each zooid would have exploited a different water mass as they rose and rotated.

Rigby and Rickards (1989) investigated the effects of colony form on their motion sinking through water through physical modelling experiments. These focused largely on many-branched dichograptid species, using real-scale models, and the majority were observed to rotate naturally. Smaller colonies were also modelled, including some two and four-branched forms, although this was not always possible at the correct scale. These experiments confirmed that spiralled dicellograptid colonies did rotate as they sank, and indicated that it was not the degree of thecal torsion (spiral form) but the degree of thecal offset around the stipe (in comparison with a twisted ribbon) which controlled this rotation. Rigby and Rickards' work linked rotation to feeding efficiency and included a mathematical model describing the increase in feeding path with rotation rate and colony size (Rigby 1990, 1992 and Rigby and Rickards 1989).

Williams (1981) and Bulman (1964) both assumed that the dicellograptid and dicranograptid colonies would have been orientated, as they are traditionally illustrated, with the proximal end leading as the colony sank or was carried by a current. This orientation was supported by the experimental work of Rigby (1990). Kirk also predicted that the proximal end would have led, although she typically illustrated these graptolites in an apparently opposite orientation as she suggested that the colony actively swam upwards. The conical shape of these two-stipe

dichograptid colonies would have represented a streamlined shape. Kirk (1969) described the development of the dicranograptid biserial section as streamlining the 'rocket form'.

Most dicellograptid species featured spines on the proximal thecae (Williams 1981), occasionally these became very developed in maturity (*Dicellograptus ornatus*), and other species had spines on many, or all, thecae (*Dicellograptus bispiralis bispiralis*). Williams (1981) did not postulate a specific function for these spines, but suggested that the weight of the spines, and additional thickening of the proximal thecae, would have made the colony 'bottom heavy', which might have enforced an orientation with the sicula apex directed vertically upwards (the traditional orientation).

7.2. This study

The following experiments attempted to investigate some of the functional interpretations that have been put forwards for these two-stiped dichograptids. Initially the question of orientation was tested following similar methods to the investigation of scandent colony orientation in chapter 5. Further experiments looked at the possible hydrodynamics of spiralled dicellograptid and dicranograptid species on which the literature has focused.

The use of isolated specimens was a successful method for the initial investigation of scandent orientation (section 5.3.1). Seawater tank tests using real specimens were also used as the starting point of this dichograptid study, although this was less successful due to the restricted number of complete specimens). The investigation is expanded with oil tank modelling and observations from the Cambridge wind tunnel (section 3.3.2 and 3.2.2).

The experiments investigated particular questions as follows:

- To what extent could the colony shape and weight distribution have controlled orientation?
- Did this change during astogeny?

- Did species with twisted stipes react differently to simpler (untwisted) colony shapes?
- What was the nature of the water flow patterns over these dichograptids in light of their probable orientations?

7.3. How did shape and weight distribution affect the orientation of two-stiped dichograptids?

7.3.1. Tests using real isolated specimens in seawater

It was hoped that an initial understanding might be gained from studying real isolated specimens, as had been the case for scandent specimens (section 5.3.1). Chemically isolated specimens were obtained from the Sedgwick museum, Cambridge, from Dr Barrie Rickards. These specimens were of the dichograptid species *Didymograptus formosus*. Numbers of specimens were very limited, and the majority were incomplete.

Experiment: These specimens were thoroughly washed in seawater, and then dropped into a tank of seawater at room temperature (as described previously: section 3.3.1 and 5.3.1). This experiment uses gravity as a proxy for a current. Each specimen was allowed to fall through the tank freely, and the sinking orientation was observed, and assumed comparable with orientation to a flow.

Each specimen was repeatedly dropped through the water until three consistent results were obtained. The angles of orientation were judged by eye, and can be considered accurate to ±5°.

Results: The majority of the *D. formosus* specimens sank with the sicula cone orientated vertically, the apex directed downwards. One specimen sank with the sicula cone horizontal, the two stipes arrayed horizontally on either side. A specimen that had only one stipe fell with the sicula cone directed upwards and the single stipe raised (table 7.1, figure 7.1).

Number of thecae	Horizontal or vertical	Angle (degrees: 0 = nema directed vertically upwards)	Comments.
2	v	175	No nema. Sank virgella up.
2.4	h	90	No nema. Sank with sicula lying horizontal.
2.5	v	180	No nema. Sank virgella up.
2.5	v	170	No nema. Sank virgella up.
4.2	v/h	45	Sank nema up. Specimen had one stipe only.

Table 7.1: Seawater tank results using five isolated specimens of *D. formosus*.

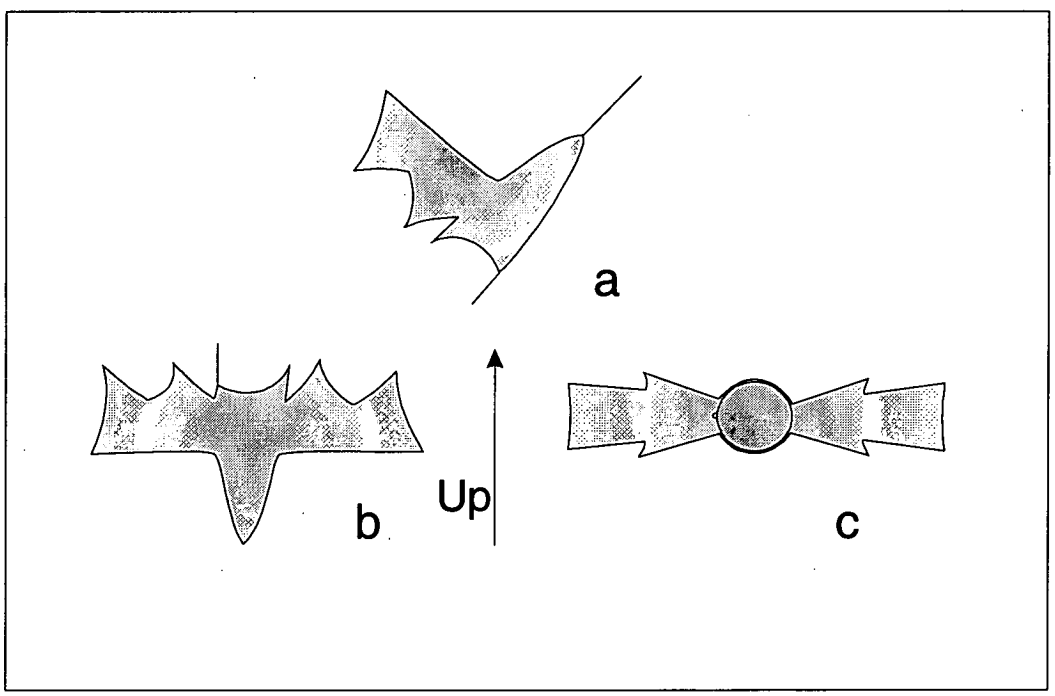

Figure 7.1: Observed orientations of isolated specimens of *D. formosus* sinking through seawater. a. angle = 45° b. angle = 180° c. angle = 90°.

Discussion: These results are not conclusive due to the low numbers, and incomplete nature of specimens tested (the majority of which were fragments from the proximal end of a mature colony).

The *D. formosus* specimens tested displayed some consistency in orientation, but the majority lacked a *nema*, which may have been expected to effect the sinking orientation. The sinking orientation of the asymmetric specimen was apparently affected by the presence of a *nema*, which was raised. However without testing a similar specimen lacking a *nema* this is not conclusive.

Tests using isolated specimens may suffer the same problem as early oil tank experiments (section 3.3.2). If the specimens are too flattened then they will act as an aerofoil, creating lift, and will sink horizontally as would a piece of paper through air. Tests using a much larger number of unflattened specimens, at a variety of growth stages would be required to drawn any real conclusions from this. More mature colonies, with a fully developed shape, are required to pass any judgement on the orientation and hydrodynamics of these dichograptid forms.

Conclusions: The tank experiments indicate that straight didymograptids (cf. *D. formosus*) may have orientated with the sicula apex directed into the flow and the stipes projecting at right angles.

These experiments were inconclusive. Further testing, using larger numbers of complete specimens, is required.

7.3.2. Oil tank tests using models

The testing of simplified models in a tank of oil is intended to compensate for the lack of isolated specimens available. These models are very simple and necessarily make a lot of assumptions about living graptolites. They do not take into account the finer details of shape and structure, and the distribution of weight throughout the colonies is unknown. However the basic effects of shape and weighting for a variety of graptolite forms can be investigated.

Experiment: Simple, wire and plasticine, models were tested to investigate the effects on orientation of different weighting patterns of dichograptid shapes. A simple U-shaped dicellograptid and didymograptid, and a Y-shaped dicranograptid

were tested initially (figure 7.2). The sinking orientations of models, representing a variety of colony shapes, were observed, and the effect of degree and location of weighting was investigated.

The probable weight distribution of the living species must be assumed. It is unlikely that the weight of a graptolite rhabdosome would have been distributed entirely evenly over the colony. Chemically isolated scandent graptolite specimens are commonly black / dark brown and opaque at the proximal end, which grades to a transparent honey colour towards the distal end. This is due to a variation in the thickness of collagen forming the colony walls, where the proximal end is reinforced with additional cortical layers of collagen bandages resulting in a concentration of colony mass (previously described in section 5.3.1). This study has largely assumed that other graptolite species also had a greater concentration of collagen, and consequently weight, at the proximal end. The non-scandent graptolites are slightly more complex but in the case of the dicellograptids and dicranograptids it has been assumed that there would have been a slight concentration of mass towards the sicula. This mass distribution is also put forward by Williams (1981), who suggested that the proximal spines and secondary thickening of dicellograptid proximal thecae would have made the rhabdosome 'bottom heavy', and might have had an effect on orientation. The dicranograptid biserial section would have required a greater concentration of collagen material, constructing twice as many thecae per unit length, than along the uniserial sections. Consequently there would have been a concentration of mass at the proximal parts of the colony. The didymograptid stipes expand rapidly away from the sicula. In this case it might be expected that although the sicula might be reinforced with more cortical layers, the wider distal ends of the stipes would have a greater mass of collagen material.

Results: Weighting did have a significant effect on the sinking orientation of the models, although in many cases no weighting was required to achieve a consistent orientation.

The dicranograptid model (figure 7.2 f), naturally weighted with a double thickness of wire along the biserial section, repeatedly sank with this biserial section leading.

A piece of bare straight wire (figure 7.2 e), with no additional weighting, sank with a horizontal orientation. Bending the same wire, even with if the resultant curve is very weak, forced a stable orientation. This curved wire (figure 7.2 d) represents a simple dicellograptid colony and when unweighted always sank 'concave up'. Adding a weight to the centre of the curved wire (figure 7.2 a and c) further enforced this orientation (table 7.2 and fig 7.3).

Adding weights to the distal ends of the curved wire (the didymograptid model; figure 7.2 b) reversed this orientation and it sinks 'convex up' (table 7.2 and fig 7.3).

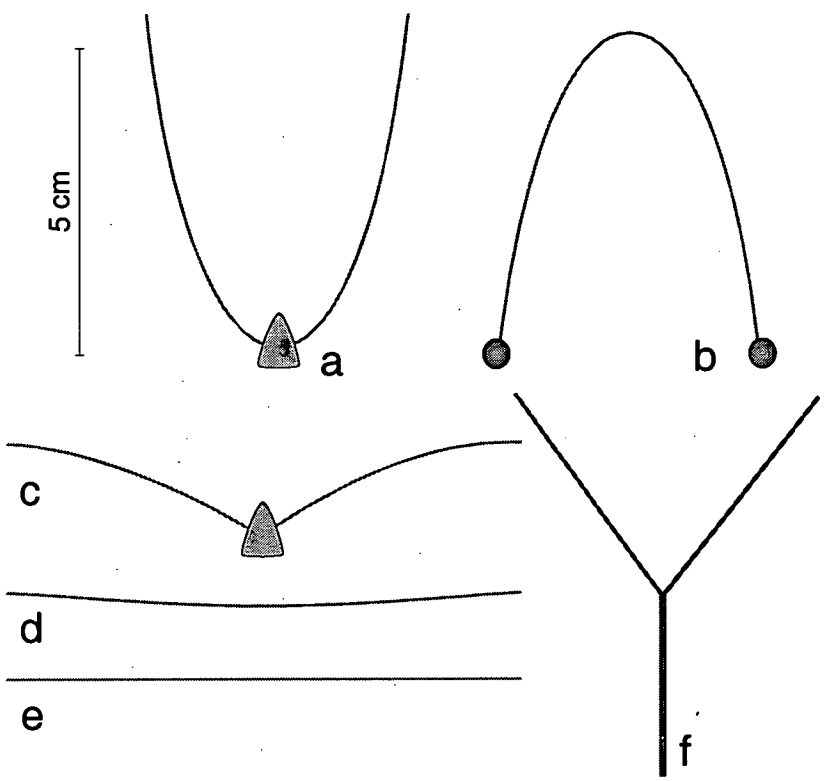

Figure 7.2: The two-stipe dichograptid test set. a. A strongly curved dicellograptid c.f. *D. moffatensis*. b. A didymograptid with robust distal stipe ends. c. An intermediate dicellograptid c.f. *D. elegans* d. A shallow dicellograptid c.f. *D. patulosus*. e. A straight, evenly weighted, colony (not an observed graptolite form). f. A simple dicranograptid c.f. *D. nicholsoni*.

Weight (g) and location (curved wire)	Final angle (degrees)	Rotation rate (degrees s^{-1})
0	0	0
0.56 central (fig. 7.2 a)	60	120
1.47 central (fig. 7.2 a)	80	198
0.56 ends (fig. 7.2 b)	-60	-88
1.47 ends (fig. 7.2 b)		-101
Straight wire (fig. 7.2 e)	0	0

Table 7.2: Oil tank test results using two-stipe dichograptid set (figure 7.2). Final angle given only if model settled to a stable sinking orientation. Rotation rate calculated from average sinking times / rotation times and angles. Complete data in appendix B.

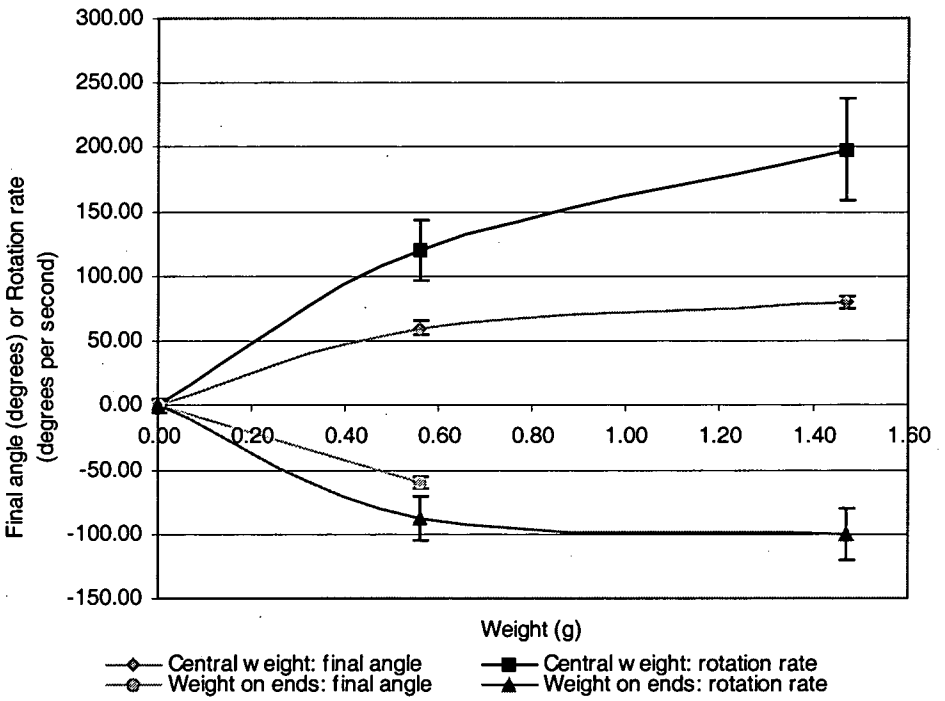

Figure 7.3: Rotation rates (and final angles when stable orientation observed) for curved dicellograptid (weight central) and didymograptid (weight on ends) models. Note opposite orientation observed for didymograptid models (∩ orientation). Greater weighting leads to faster rotation rates.

Conclusions:

- All species tested naturally align sicula apex directed down-flow / sicula aperture directed up-flow given the mass-distribution assumptions described.

- Colony shape could have been an important factor for controlling orientation (note the effect of simply curving the wire).
- Colony weight distribution was also very important for determining orientation.

7.4. Changes with astogeny

These experiments investigate how colony astogeny, resulting in morphological changes, might have affected the stable sinking orientation. As a dicranograptid colony continued to mature the uniserial stipes grew and increased their length relative to the (now fixed) biserial section. This changed the form of the colony from an Y-shape to an increasingly, uniserial stipe dominated, V-shape.

A series of models (figure 7.4) were constructed with an identical length of biserial section, followed by different lengths of uniserial stipes. These models were tested repeatedly in the oil tank until it was clear that a consistent orientation was observed.

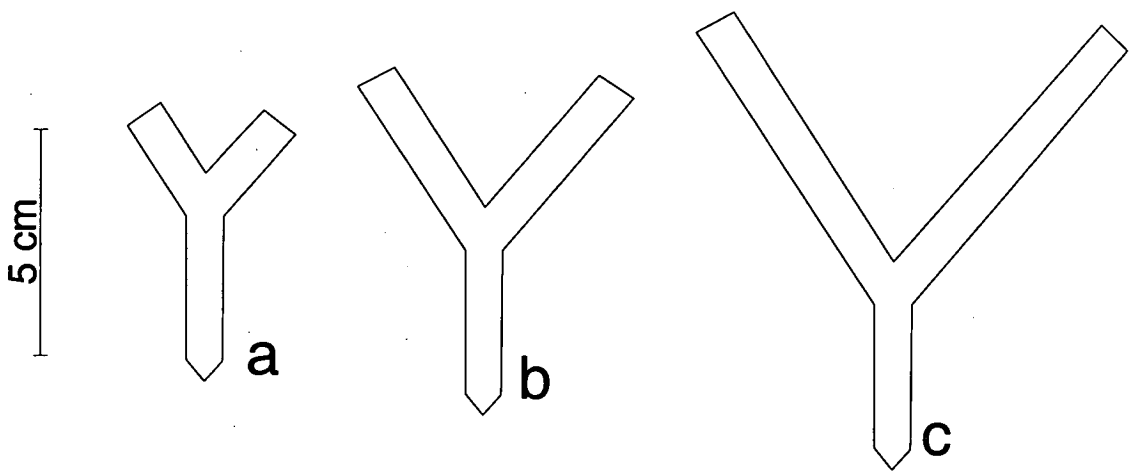

Figure 7.4: Simple wire models representing a dicranograptid colony (c.f. *D. nicholsoni*) at three astogenetic stages. The length of the biserial section is fixed but the uniserial lengths increase.

Results: The biserial section of the dicranograptid models was weighted, as described in section 7.3.2. The majority of the models sink in a near vertical Y orientation, with the denser biserial section leading. Only the model with the longest

uniserial stipes (figure 7.4 c) deviated from this, sinking with a more horizontal orientation (table 7.4 and fig. 7.5).

Uniserial arm length (cm)	Final angle (degrees)	Rotation rate (degrees s^{-1})
2.4	65	61
5.6	70	49
8.0	20	12

Table 7.3: Average oil tank results for astogenetic dicranograptid models (figure 7.4). Longer uniserial stipes leads to slower rotation rates and more horizontal stable sinking orientations. Complete data in appendix B.

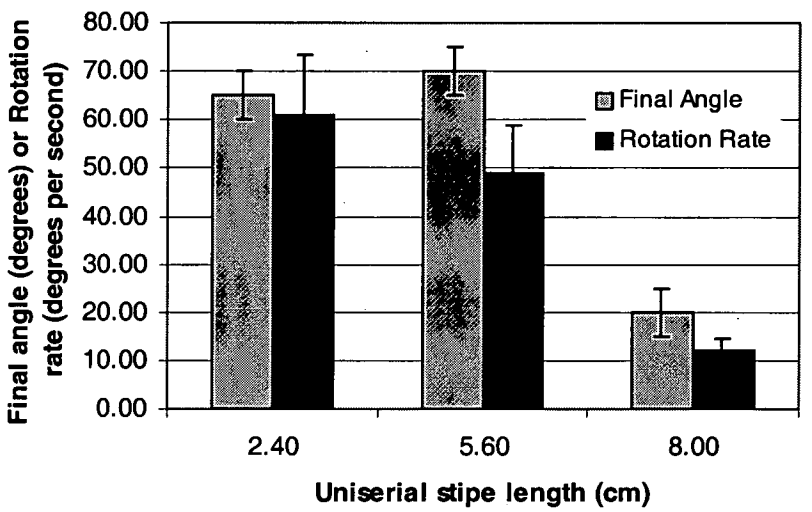

Figure 7.5: Average results of oil tanks tests showing angle of stable sinking orientation and rotation rate observed.

Conclusions:

- Dicranograptid species may have changed orientation with increasing maturity.

7.5. Did forms with twisted stipes react differently?

Both the dicellograptids and dicranograptids include species with twisted stipes. This experiment investigated what effect some of these twisted forms might have had on the stable sinking orientation and hydrodynamics of the graptolites.

The simple stipes of *Dicranograptus nicholsoni* were compared with the twisted stipes of species such as *Dicranograptus ziczac* and *Dicranograptus ramosus spinifer.*

A simple planar U-shaped dicellograptid model (cf. *Dicellograptus elegans*) was compared with that of a twisted form (e.g. *Dicellograptus caduceus*).

Results: Both dicranograptid models (figure 7.6 b and c) with twisted uniserial stipes (either with a simple ribbon twist about the stipe axis, or by spiralling the entire stipe) sank with the biserial section leading, as had been observed for the simple dicranograptid model (section 7.3.2). The twisted stipes appeared to enforce this orientation, causing the models to realign more rapidly to this vertical orientation (table 7.4 and figure 7.7). Twisting the Dicranograptid uniserial stipes also slowed the rate of sinking. The model with the spiral twisted stipes sank most slowly.

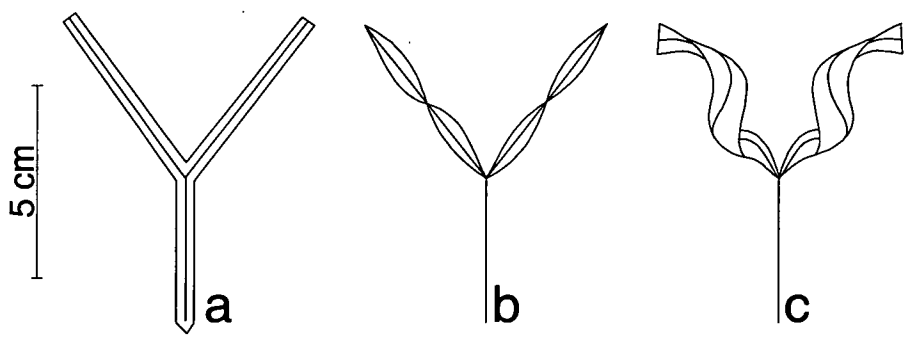

Figure 7.6: Dicranograptid models. a. A simple dicranograptid c.f. *D. nicholsoni.* b. A dicranograptid with uniserial stipes twisted about their axis (ribbon twist) c.f. *D. ramosus spinifer.* c. A dicranograptid with uniserial stipes openly spiralled about the stipe axis (spiral twist) c.f. *D. ziczac.*

Dicranograptid	Rotation rate (degrees s^{-1})	Sinking time (s)
D. nicholsoni	49	1.42
D. ramosus spinifer	51	1.48
D. ziczac	52	1.63

Table 7.4: Average results from oil tank experiments with dicranograptid models (figure 7.6). Calculated rotation rates and total sink times are given. Complete data given in appendix B. The sink time increases as the uniserial stipes become more twisted.

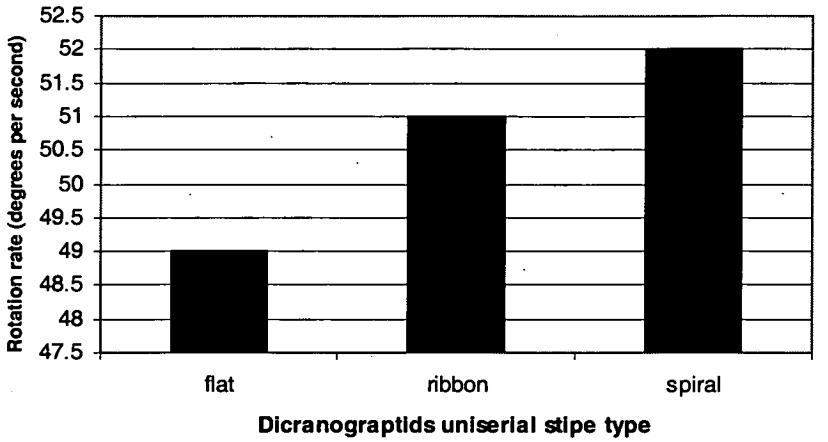

Figure 7.7: Average calculated rotation rates from oil tank experiments with dicranograptid models (figure 7.6). Note rotation rate increases slightly as the uniserial stipes become more twisted.

The dicellograptid model with curved wire stipes, twisting around one another in an open spiral to model (*Dicellograptus caduceus*; figure 7.8 b), rotated as it sank. When the spiralled model was released unweighted it sank with a horizontal orientation. The addition of a small weight to the centre point of the wire (where the sicula would have been located) caused the model to align vertically, allowing the rotation (table 7.5 and figure 7.9). Very little weight was required to enforce the orientation of the spiralled model in comparison to the untwisted model (table 7.5 and figure 7.9).

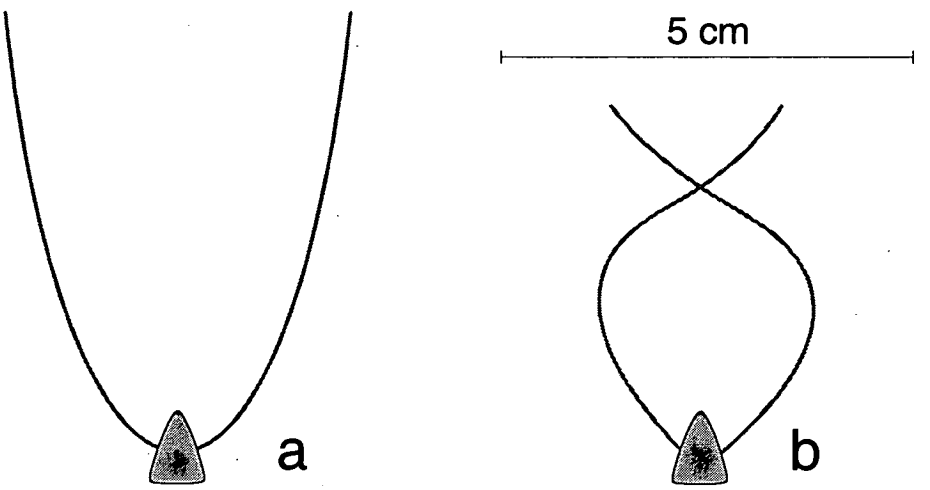

Figure 7.8: Dicellograptid models. a. A simple dicellograptid c.f. *D. elegans*. b. A twisted dicellograptid c.f. *D. caduceus*.

Dicellograptid	Final angle (degrees)	Rotation rate (degrees s^{-1})
D. elegans	60	120
D. caduceus	90	199

Table 7.5: Average stable sinking angles and rotation rates from oil tank experiments using dicellograptid models (figure 7.8). Complete data given in appendix B.

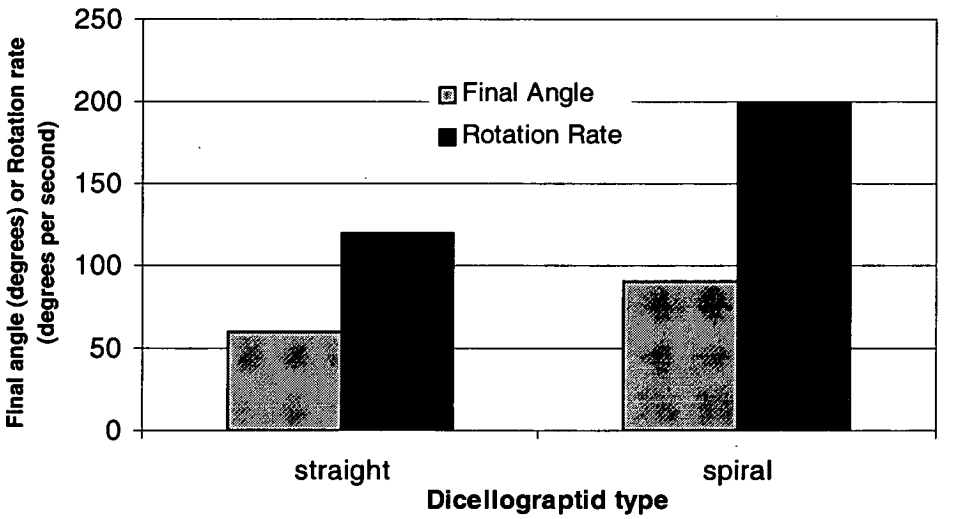

Figure 7.9: Average stable sinking angles and rotation rates from oil tank experiments using dicellograptid models (figure 7.8).

Conclusions:

- Twisted dicellograptids rotated under the influence of a flow.
- The twisted uniserial stipes of dicranograptid colonies enforces the colony orientation and increased drag, thus slowing the sink rate.

7.6. What was the nature of the water flow patterns over these dichograptids in light of their probable orientations?

Having observed the reactions of these simple dichograptid shapes to a fluid, they were further investigated using the Cambridge wind tunnel. The smoke streams and scaled up models allowed the flow interactions to be studied with more detail. These models do recreate the details of the graptolite shapes producing a more accurate flow pattern over the colony than was seen in the simple oil experiments.

Experiment: Models of a variety of two-stiped dichograptids were observed in the wind tunnel at Cambridge, Department of Engineering. The airflow patterns over the models were observed using streamers of paraffin smoke as described in section 3.2.2. The species modelled fell into three groups; dicranograptids, dicellograptids and didymograptids. These experiments focused on the interaction of the overall colony shape with the flow and the effect of variations with twisted stipes.

7.6.1. Dicranograptus

One Y-shaped, dicranograptid model was adapted to represent three forms: one with simple, straight uniserial stipes (c.f. *D. nicholsoni*), one with uniserial stipes twisted about the stipe axis (c.f. *D. ramosus spinifer*) and one with the uniserial stipes twisted into a spiral centred around the stipe axis (c.f. *D. ziczac*). The basic model was based on *Dicranograptus nicholsoni*, providing the thecal shapes and spacing. All three forms were tested in two orientations; with the biserial sections directed into the flow, and with the biserial section pointed directly down-flow.

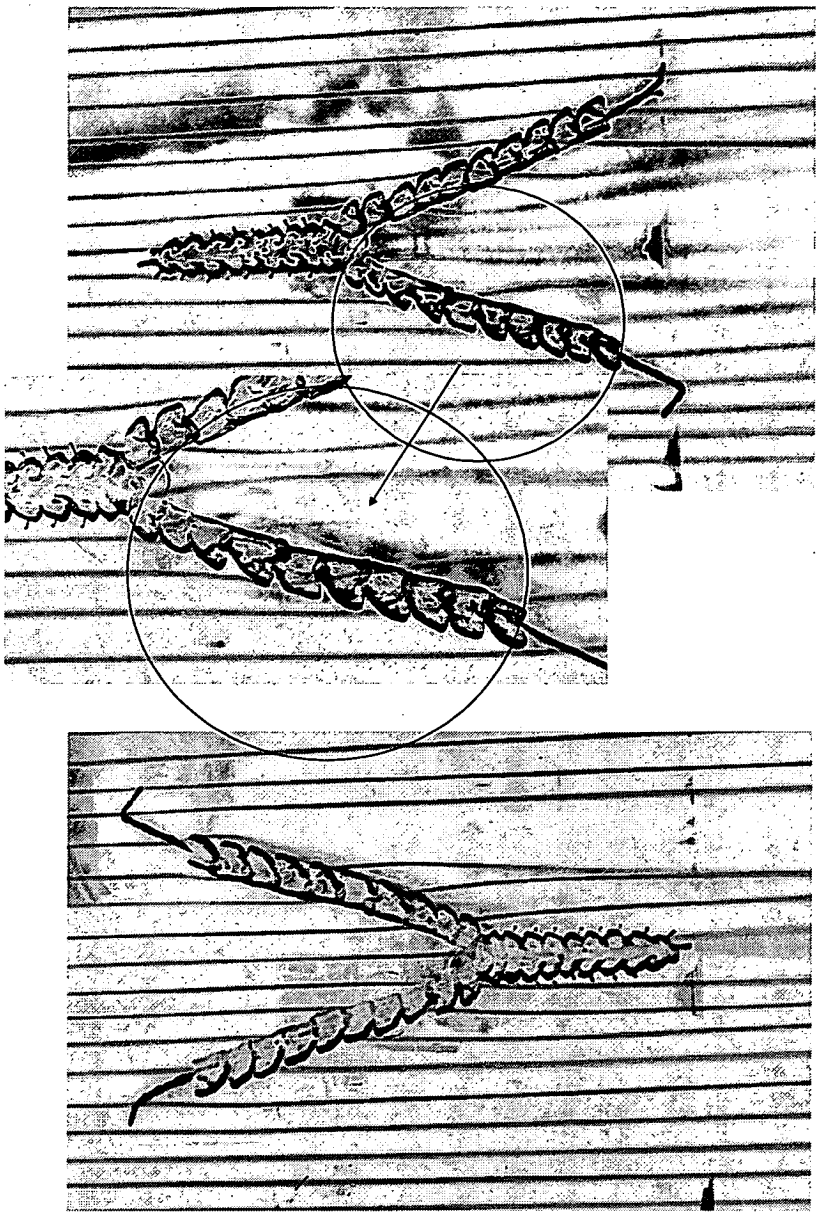

Figure 7.10: A model of the simple dicranograptid *D. nicholsoni* under observation in the Cambridge wind tunnel. The image is inverted such that the white smoke streamers against a black background appear as black smoke-streamers against a white background.

The top image shows the model in a flow running from proximal to distal end (as predicted by the oil tank experiments). Note the standing vortices forming in the thecal apertures of the biserial section, as discussed in section 6.5.

The centre image is an enlargement of one of the uniserial stipes. The flow may run into standing eddies in the thecal apertures, or may flow across the thecal aperture to the dorsal edge of the stipe.

The bottom image shows the same model run in the opposite orientation with the flow running from distal to proximal end. Standing eddies do not form in the thecal apertures.

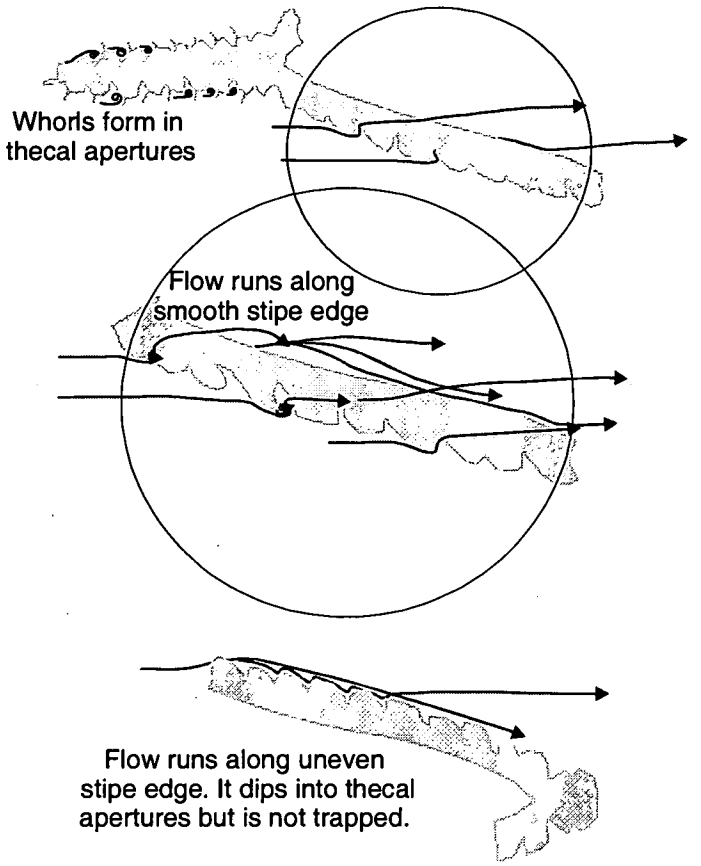

Figure 7.11: An interpretation of the flow patterns observed in figure 7.10, based on observations made during testing.

Images of the simple (straight stiped) model are shown in figure 7.10 and 7.11. The first two digital photographs (figure 7.10) show the model in a 'normal' orientation (the orientation predicted by the tank experiments with the biserial section directed up-flow). It can be observed that the thecal spines along the biserial section tap the passing flow and form small vortices in thecal apertures, trapping smoke particles. The majority of a smoke stream impacting with the ventral side of the uniserial stipe flows across the thecal apertures to the dorsal surface, a fraction runs along the ventral surface to the next theca where a smaller percentage will flow across this aperture to the dorsal edge. The smoke streams are drawn along the uniserial stipes and smoke-bearing flow is concentrated at the distal ends of these stipes. The airflow runs easily along the smooth dorsal edge of the uniserial stipe, where small-scale turbulence allows it to mix with other airflows.

The lower image (Figure 7.10) shows the model in reverse orientation. Impacting smoke streamers are able to run along the upper ventral surface, as the flow attempts to follow the uneven topography of the thecae it tends to skip over the surface, and does not flow directly across the apertures (figure 7.11). Flow in the wake of the stipes is drawn towards the trailing biserial section but no vortices are observed in the thecal apertures. In this orientation the upward-angled thecal spines would cause the flow to be drawn away from the colony.

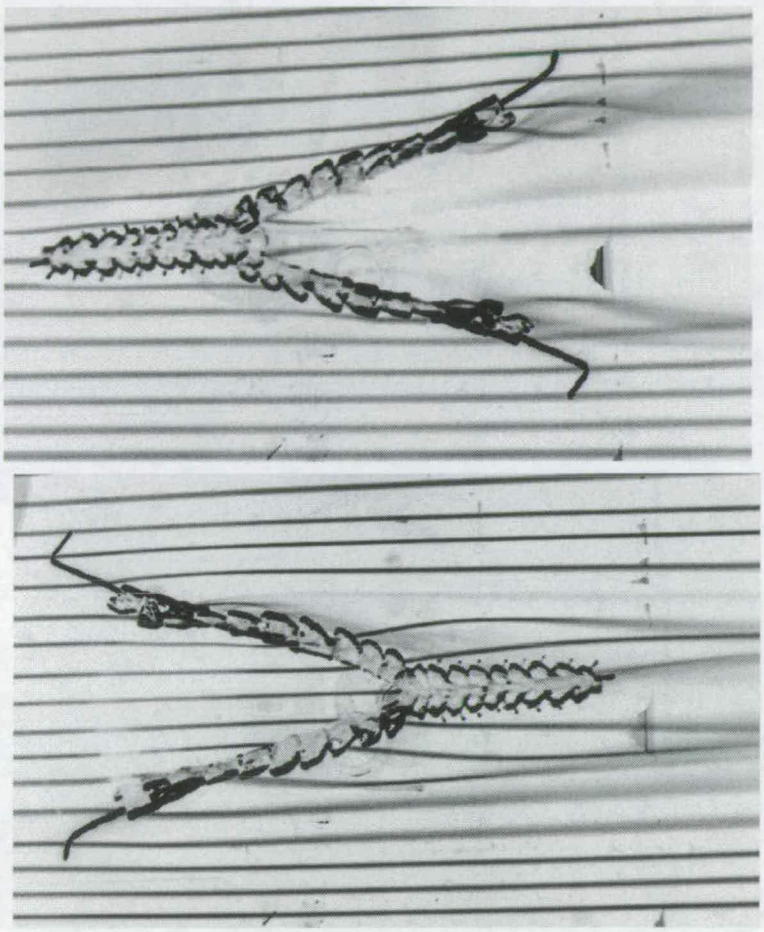

Figure 7.12: A model of the ribbon-twist dicranograptid *D. ramosus spinifer* under observation in the Cambridge wind tunnel. The image is inverted such that the white smoke streamers against a black background appear as black smoke-streamers against a white background.

The top image shows the model in a flow running from proximal to distal end (as predicted by the oil tank experiments). The flow follows the twists of the stipe. It may run into standing eddies in the thecal apertures, or may flow across the thecal aperture to the smooth dorsal edge of the stipe which it continues to run along.

The bottom image shows the same model run in the opposite orientation with the flow running from distal to proximal end. Standing eddies do not form in the thecal apertures.

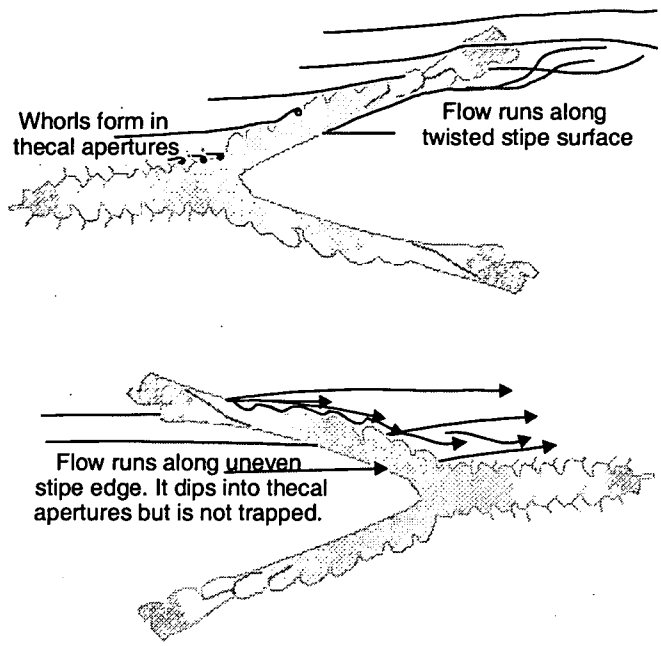

Figure 7.13: An interpretation of the flow patterns observed in figure 7.12, based on observations made during testing.

If the uniserial stipes are twisted around their axis (a 'ribbon twist' c.f. *D. ramosus spinifer*) the flow, running along the smooth dorsal surface of these stipes, also twists (figure 7.12, top image). Flows impacting with the ventral surface of the uniserial stipes pass across the thecal apertures to the dorsal surface (figure 7.13), and the smoke-bearing flow is possibly more strongly drawn outwards towards the ends of the stipes. Standing eddies form within the thecal apertures of the biserial portion as was observed when testing the simple model.

The model is also shown in reverse orientation (figure 7.12, lower image). The flow is drawn along the uniserial stipes, following the twist. The flow runs less successfully along the uneven ventral surface then the smooth dorsal surface (figure 7.13). In the wake of the uniserial stipes once again the flow is drawn towards the biserial section, but no vortices are formed in the thecal apertures.

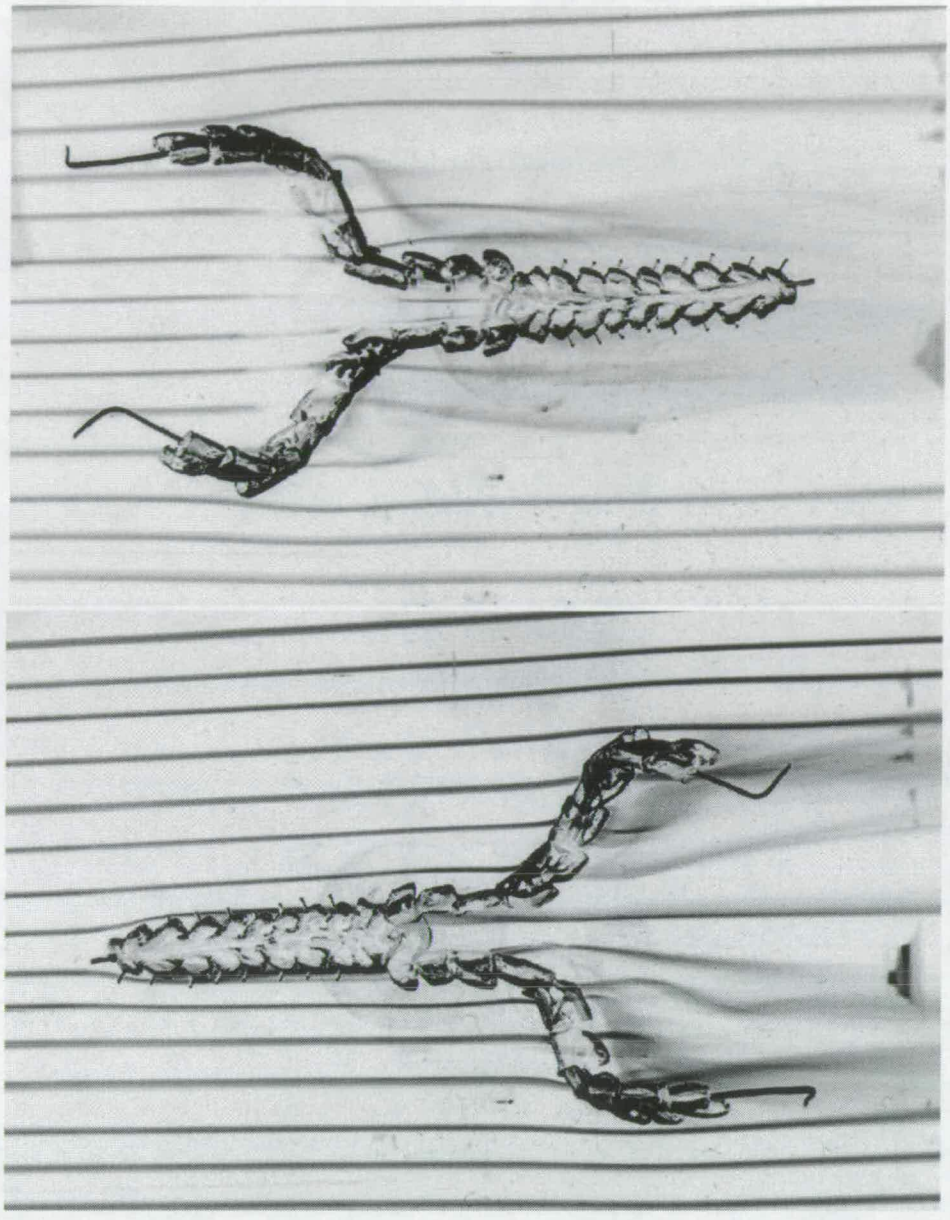

Figure 7.14: A model of the spiral-twist dicranograptid *D. ziczac* under observation in the Cambridge wind tunnel. The image is inverted such that the white smoke streamers against a black background appear as black smoke-streamers against a white background.

The lower image shows the model in a flow running from proximal to distal end (as predicted by the oil tank experiments). Standing vortices formed in the thecal apertures of the biserial section, as discussed in section 6.5, although they are too small to observe clearly in this image (see fig. 6.14). The flow follows the spiral shape of the uniserial stipes. Impacting smoke streamers are extended laterally along the spiral stipes until small-scale turbulent mixing with passing smoke-free air carries the smoke downstream. This produces the distinctive 'flare' affects behind the stipes.

The upper image shows the same model run in the opposite orientation with the flow running from distal to proximal end. Standing eddies do not form in the thecal apertures.

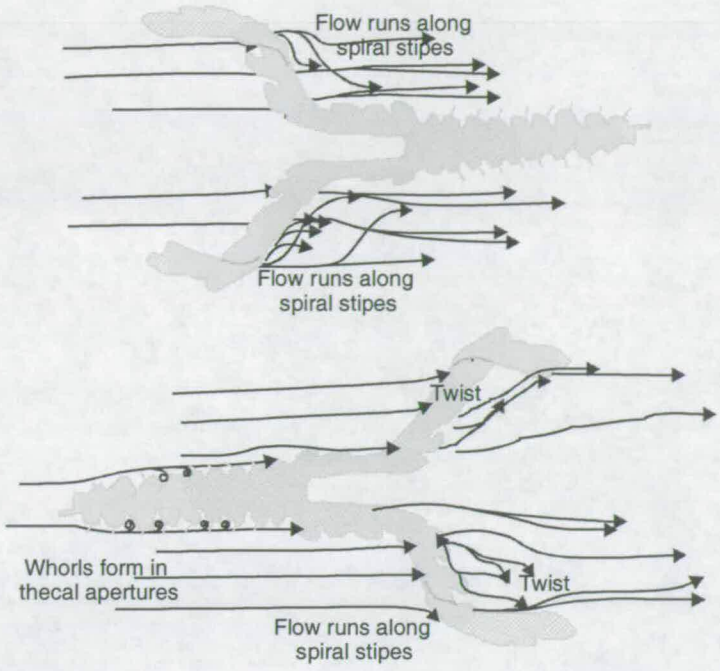

Figure 7.15: An interpretation of the flow patterns observed in figure 7.14, based on observations made during testing.

The model with spiral-twisted stipes (figure 7.14 and 7.15, cf. *D. ziczac*) produced similar flow patterns. When the model was tested in a 'normal' orientation (figure 7.14, lower image) impacting flow was drawn along the smooth dorsal edge of uniserial stipes, following the spiral. This draws the flow laterally out of its original plane of motion. As it runs along the dorsal surface the flow becomes increasingly turbulent and more mixing occurs with adjacent airflow.

In reverse orientation (figure 7.14 and 7.15, upper image) the smoke-bearing flow is drawn around the spiral shape of the uniserial stipes, exactly as it was in the normal orientation. This smoke-bearing flow is swept away from the colony, by small-scale turbulent mixing with passing airflow, before it reaches the biserial section.

7.6.2. *Dicellograptus*

Three dicellograptid models were constructed representing a simple straight-stiped form (*Dicellograptus elegans*) at two scales, and one representing a form in which the two stipes spiralled about one another (*Dicellograptus caduceus*). All models were tested in two orientations; once with the sicula aperture directed up-flow and again directed down-flow.

The simple model (cf. *D. elegans*) was initially tested in a 'normal' orientation to the flow, with the sicula aperture directed up-flow (figure 7.16 to 7.19). Flow impacting with the spines on $th1^1$ and $th1^2$ was drawn up the spine towards the colony surface, in the same manner as had been previously observed with the proximal thecal spines of biserial graptolites (section 6.3.1). This smoke-bearing flow was deflected around the lip of the thecal aperture and into a standing eddy (figure 7.16 and 7.17). Similar standing eddies also formed in front of the thecal apertures of the other proximal thecae. Flow impacting the thecae on the ventral face of the stipes runs up the stipe and is drawn laterally across the thecal apertures (and across the stipe to the smooth dorsal edge) intermittently forming vortices in the apertures of later thecae. In the initial wake of the colony (within the area bounded by the stipes) flow is either drawn laterally outwards towards the stipes, a concentration of smoke-bearing flow trailing off each stipe end (figure 7.16); or drawn inwards towards the sicula, another concentration of smoke-bearing flow can be observed trailing off the sicula apex. Some small-scale turbulent mixing occurs between the smoke streamers and smoke-free airflow, the streamers become blurred and indistinct.

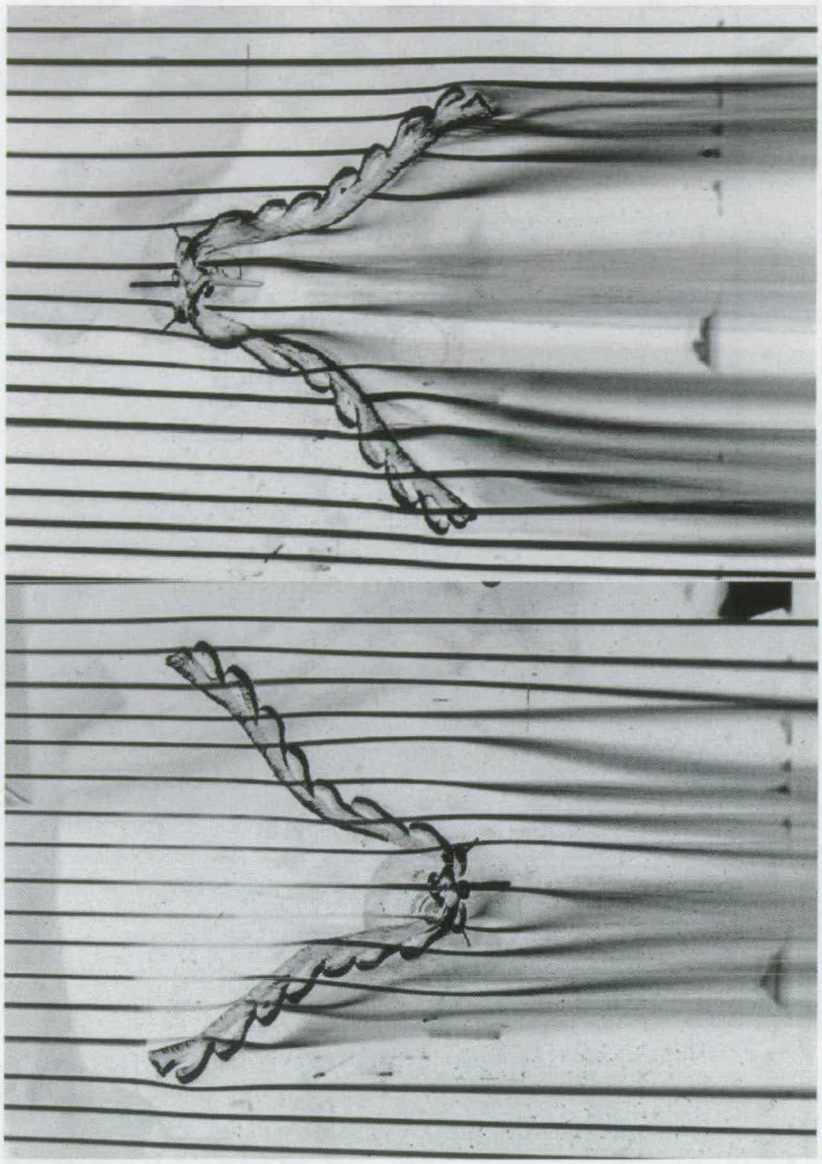

Figure 7.16: A model of the simple dicellograptid *D. elegans* under observation in the Cambridge wind tunnel. The image is inverted such that the white smoke streamers against a black background appear as black smoke-streamers against a white background.

The upper image shows the model in a flow running from proximal to distal end (as predicted by the oil tank experiments). Smoke streamers impacting with the thecal spines are extended along the spine towards the proximal thecae. Smoke streamers impacting the rest of the colony flow across the thecal apertures to the smooth dorsal side of the stipes, here the flow is drawn laterally outwards along the trailing stipes. A concentration of smoke-bearing flow is observed flowing off the two distal stipes ends.

The lower image shows the same model run in the opposite orientation with the flow running from distal to proximal end. The flow detaches behind the colony and it drawn inwards.

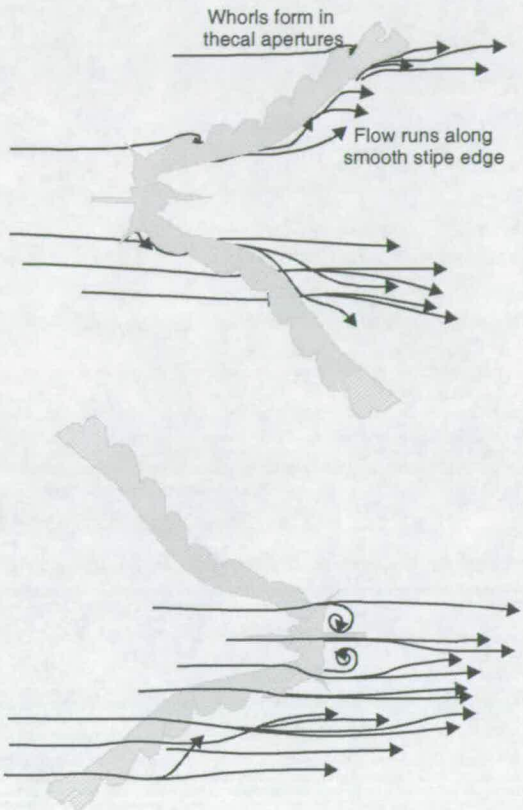

Figure 7.17: An interpretation of the flow patterns observed in figure 7.16, based on observations made during testing.

In reverse orientation (figure 7.16 to 7.19) flow impacting the smooth dorsal stipe surfaces tends to flow along and around the stipe to the ventral surface, passing across the thecal apertures. In the wake of the colony the smoke-bearing flow which had been following the stipe is swept downstream mixing with smoke-free airflow in the small-scale turbulence.

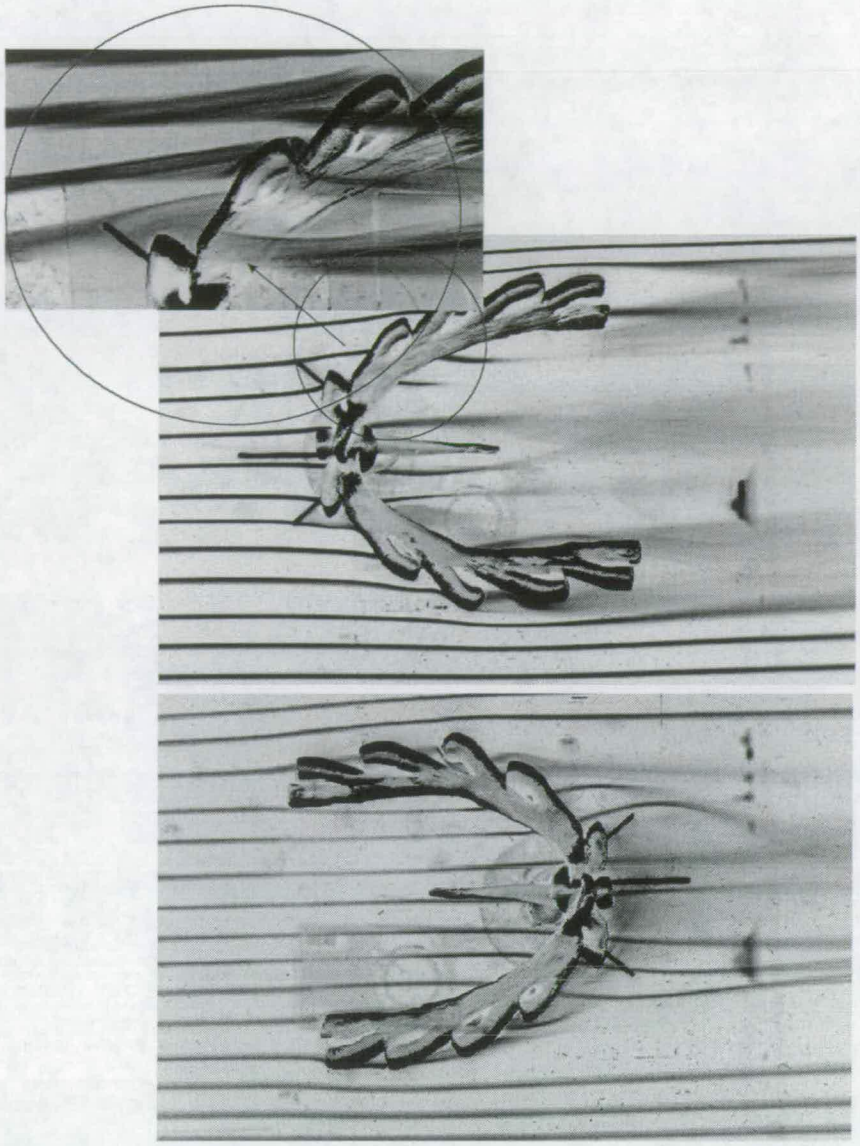

Figure 7.18: A model of the simple dicellograptid *D. elegans* under observation in the Cambridge wind tunnel. The image is inverted such that the white smoke streamers against a black background appear as black smoke-streamers against a white background.

The central image shows the model in a flow running from proximal to distal end (as predicted by the oil tank experiments). Smoke streamers impacting with the thecal spines are extended along the spine towards the proximal thecae. Smoke streamers impacting the rest of the colony flow across the thecal apertures to the smooth dorsal side of the stipes, here the flow is drawn laterally outwards towards along the trailing stipes. A concentration of smoke-bearing flow is observed flowing off the two distal stipes ends.

The upper image shows an enlargement of the proximal thecae of one stipe with vortices forming in the early thecal apertures.

The lower image shows the same model run in the opposite orientation with the flow running from distal to proximal end. The flow detaches behind the colony and it drawn inwards.

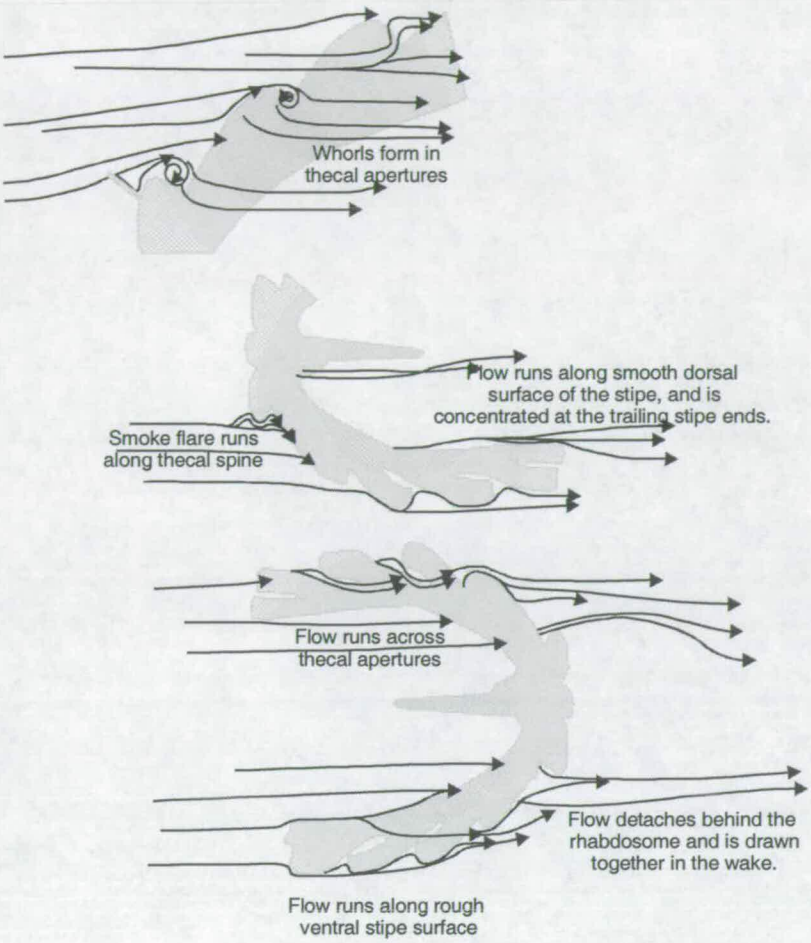

Figure 7.19: An interpretation of the flow patterns observed in figure 7.18, based on observations made during testing.

The twisted dicellograptid model (cf. *D. caduceus*) produced broadly similar flow patterns (figure 7.20 and 7.21). However flow impacting with the twisted stipes would then follow their spiral form, resulting in a net rotation of the airflow. Smoke-bearing air can be observed flowing the spiral along the smooth dorsal surface of the stipe (figure 7.20, upper image), small-scale turbulence causes mixing with passing airflow which sweeps some of the smoke downstream away from the stipe. This apparent flare of smoke becomes taller further around the spiral as more smoke streams impact the stipe and are drawn along the surface.

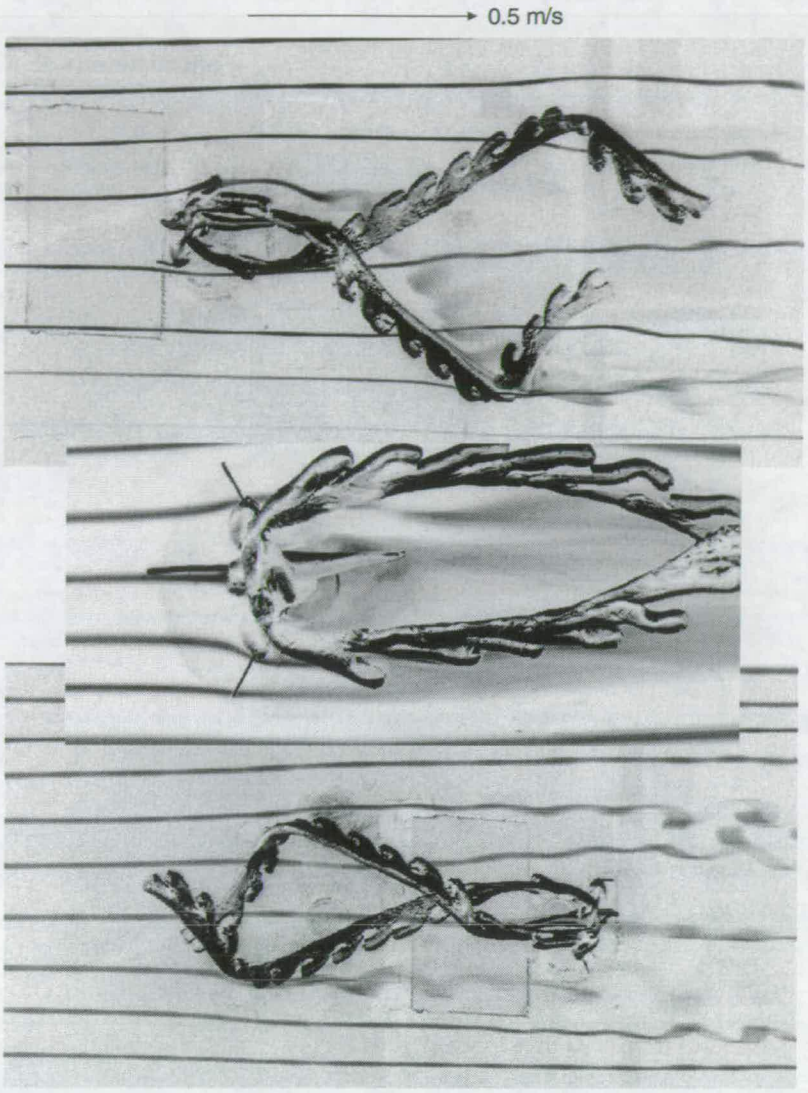

Figure 7.20: A model of the spiralled dicellograptid *D. caduceus* under observation in the Cambridge wind tunnel. The image is inverted such that the white smoke streamers against a black background appear as black smoke-streamers against a white background.

The upper image shows the model in a flow running from proximal to distal end (as predicted by the oil tank experiments). This results in a net rotation of the flow. Impacting smoke-bearing flow is drawn laterally along the smooth dorsal side of the stipes until small-scale turbulence results in mixing with passing smoke-free airflow, and the smoke is swept downstream. This produces the distinctive 'flare' affects behind the stipes.

The central image shows an enlargement of the proximal section of the colony with a standing eddy in the aperture of the most proximal thecae.

The lower image shows the same model run in the opposite orientation with the flow running from distal to proximal end. The flow is less inclined to follow the spiral shape of the colony in this orientation.

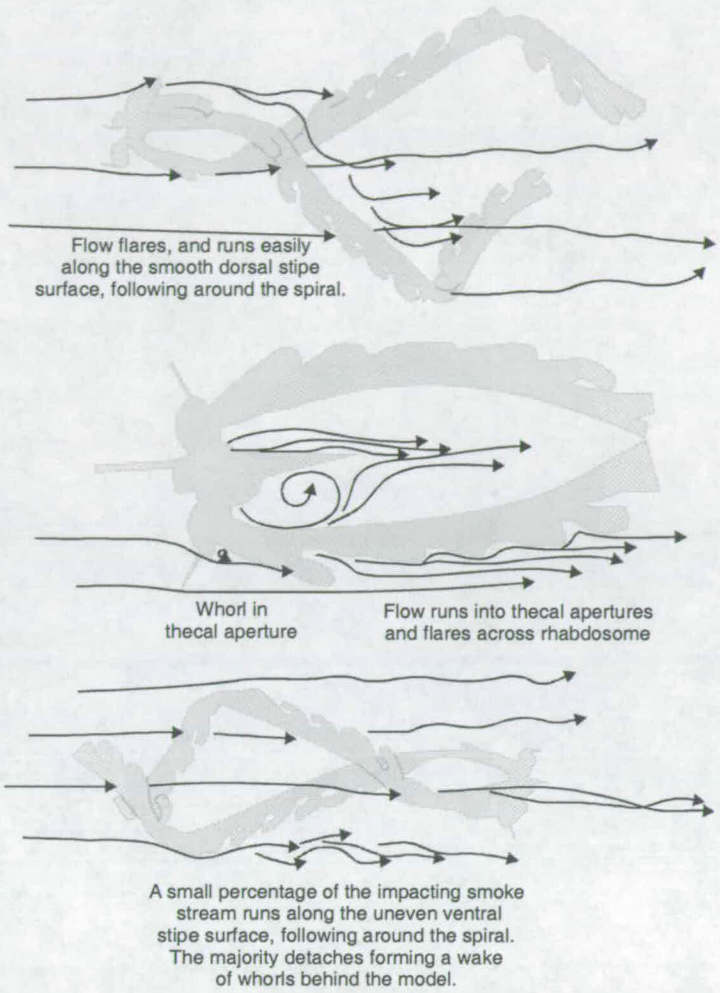

Figure 7.21: An interpretation of the flow patterns observed in figure 7.20, based on observations made during testing.

In reverse orientation only a small percentage of the flow impacting the stipes flows along the spiral, the majority detaches and forms a large turbulent wake (figure 7.20, lower image).

7.6.3. *Didymograptus*

A simple pendant didymograptid was also tested (*Didymograptus muchisoni*). Once again this model was run in two orientations; once with the sicula aperture directed up-flow and again directed down-flow.

The model is shown in 'normal' (upper image) and 'reverse' (lower image) alignment in figure 7.22 and 7.23. When aligned 'normally' (sicula apex directed down-flow) a smoke stream impacting with the thecae, on the inner surface of the U-shaped colony, flows along this inner stipe surface, forming vortices in the thecal apertures which feed the flow across the stipe to the smooth outer surface via the inter-thecal troughs. This smoke-bearing flow is then drawn laterally along the smooth stipe surface, towards the sicula. Small-scale turbulence causes mixing with air flowing around the colony and the smoke-bearing air is swept downstream. The lateral drawing of flow towards the sicula results in a concentration of smoke-bearing flow trailing off the sicula apex.

In reverse orientation (sicula apex directed up-flow) the flow impacting smoke streamers flow around the smooth outer stipe surface, forming a small turbulent wake beyond. Some of the flow is drawn around the stipe, but very little reaches the inner stipe surface and the thecal apertures.

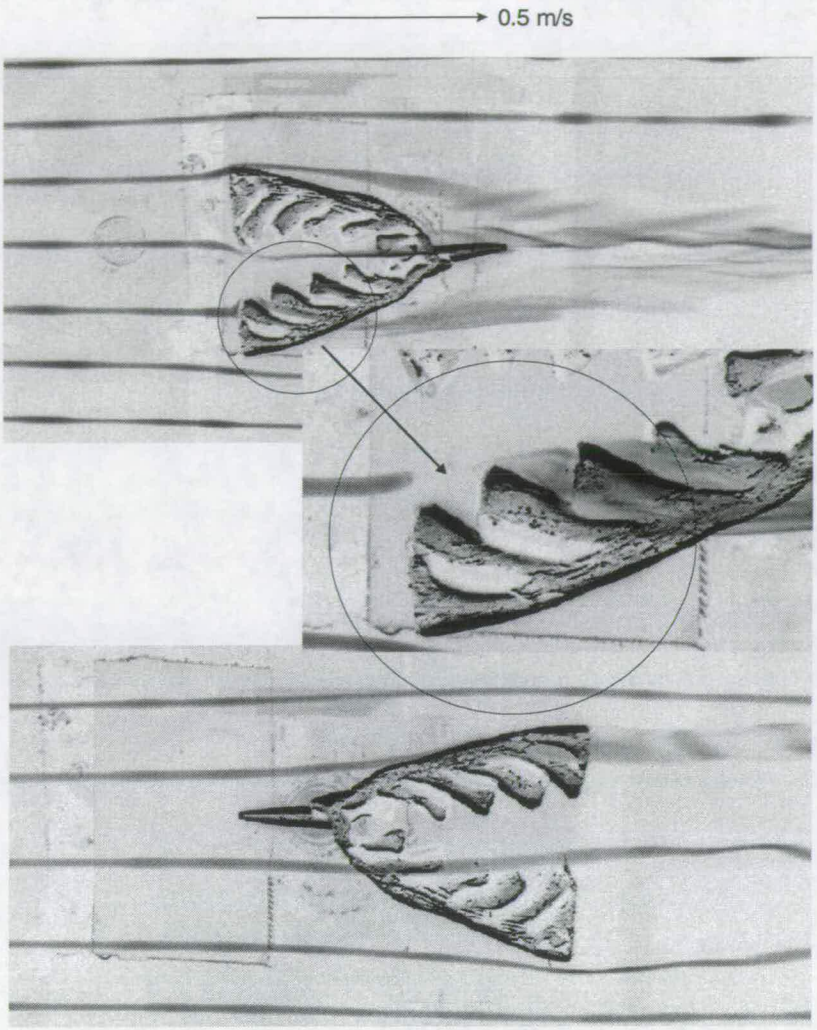

Figure 7.22: A model of the didymograptid, *D. murchisoni* under observation in the Cambridge wind tunnel. The image is inverted such that the white smoke streamers against a black background appear as black smoke-streamers against a white background.

The upper image shows the model in a flow running from distal to proximal end (as predicted by the oil tank experiments). Impacting smoke flows into standing eddies in the thecal apertures and across the stipe to the smooth dorsal edge. The flow is drawn along the dorsal side of the stipes towards the sicula from which trails a concentration of smoke.

The central image shows an enlargement of one of the stipes. Vortices form in the thecal apertures.

The lower image shows the same model run in the opposite orientation with the flow running from proximal to distal end. Impacting flow runs along the smooth dorsal stipe edge until it trails off the distal end. Some smoke-bearing flow runs to the ventral side of the stipe but little new fluid is brought into the area between the stipes.

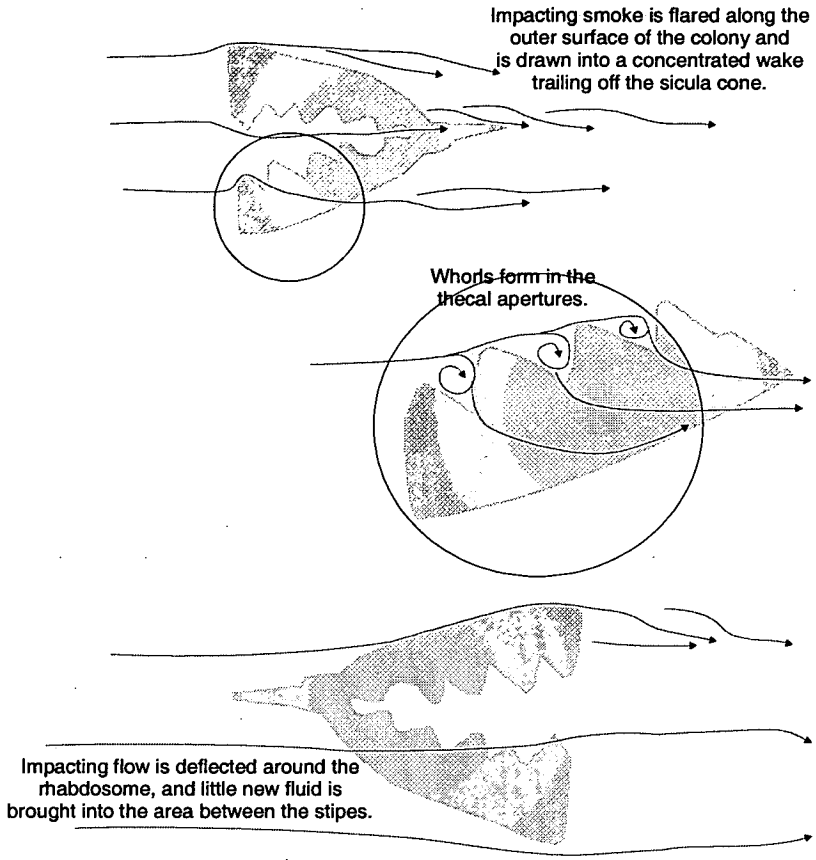

Figure 7.23: An interpretation of the flow patterns observed in figure 7.22, based on observations made during testing.

Discussion: When the models were tested in a 'normal' orientation vortices were observed forming in thecal apertures. This was particularly observed in the case of the biserial section of dicranograptid species (cf. biserial experiments, section 6.5), the proximal thecae of dicellograptid species and the distal thecae of the didymograptid model. These vortices could have been beneficial to the colony, bringing a supply of food particles into the thecal apertures where it might easily be tapped by a zooid in the theca. These vortices were not formed when the models were run in a reverse orientation. Running the didymograptid model in the wind tunnel in a reverse orientation resulted in large quiet zone, with reduced smoke particle concentration, between the stipe. This would not represent a good scenario for feeding zooids, with no supply of new food particles being brought to the thecae.

The flow over the twisted stipes of *Dicellograptus caduceus*, *Dicranograptus ziczac* and *Dicranograptus ramosus spinifer* was drawn laterally around the twist of these stipes, resulting in a net rotation of the flow. It is uncertain what affect this may have had on the colony orientation and motion as the models are fixed in the wind tunnel. However the twisted models all produced a larger wake than their simple counterparts implying that these species would have experienced more drag.

Conclusions:

- The flow patterns over the models of all species appear to be more coherent, and beneficial to the colony, when the model is in a 'normal' orientation.
- Twisted and spiralled stipes produced a corresponding rotation of the flow over them.
- The models of twisted species produced larger turbulent wakes than the simple models.

7.7. The likely range of hydrodynamic function for simple two-stipe dichograptid colony shapes

Basic orientation:

All lines of evidence, both the experimental study here and the previous work of others, points to a life orientation with the sicula cone directed down-flow for all three dichograptid genera considered (dicellograptids, dicranograptids and didymograptids). It is impossible to prove that this was the true orientation for these species, however it can be suggested as the most likely possibility.

This study gathered evidence from two main sources; oil tank experiments using simplified models (sections 7.3.2 to 7.5), and wind tunnel observations using more detailed models (section 7.6). The investigation using real isolated fossils (section 7.3.1) was not reliable due to the low numbers, and poor quality, of specimens available.

The models used in the oil tank tests were not accurate reconstructions of graptolite specimens in detail; instead they merely represent the broad colony shape. They have shown that this overall shape can have a significant effect on the orientation and motion of the model in a fluid. In many cases it was the effects of differential weighting that had the greatest effect on the orientation of a model, however the shape alone might control orientation (e.g. the curved wire representing a simple dicellograptid: section 7.3.2) or cause the model to rotate (twisted dicellograptid: section 7.5).

The oil tank experiments relied on assumptions about the differential weighting of graptolite colony shapes. The weight distribution assumed by the dicranograptid model seems reasonable, as a biserial stipe section would contain more collagen than the same length of unserial stipe. The simple dicellograptid model (a curved wire) was not weighted, and only a little additional weight was required to cause the spiralled model to sink with the proximal end leading, allowing it to rotate. The case for weighting the distal ends of the didymograptid model is less certain, and consequently the 'convex up' orientations predicted are more uncertain. If the weight were concentrated towards the centre of the colony (at the sicula) it would sink in the opposite orientation, 'concave up'. The development of a three-part vane at the proximal end of mature *Didymograptus murchisoni* specimens, noted by Rickards and Khashogji (2000), would tend to support a 'convex up' orientation. Such an addition would significantly increase the surface area of the proximal end without greatly increasing the mass, the scandent colony model (section 5.6.2) showed that such an addition would tend to preferentially rotate the vane into the trailing position. With no extant planktonic graptolite species it is impossible to determine what the life mass distribution of these graptolites would have been.

The wind tunnel observations provided more evidence in agreement with the orientations predicted by the oil tank experiments. The flow patterns produced when these models were tested in a 'normal' orientation to the flow (i.e. the orientation predicted by the oil tank experiments) appeared to generate feeding opportunities for

the colonies. The smoke-bearing flow (a proxy for food particles) was observed running into standing eddies in the thecal apertures of all three genera. The flow was typically then drawn along the stipes bringing food to the entire colony. Conversely the flow patterns produced when the colonies were tested in a 'reverse' orientation the flow (i.e. an orientation 180° from that predicted by the oil tank experiments) did not appear to provide any advantage to the colony. Standing eddies were not formed in any of the thecal apertures, and the flow typically detached from the colony towards the proximal end drawing the smoke bearing flow away from the colony. In the case of the didymograptid model (figure 7.22 and 7.23) the colony shape in a reverse orientation protected the thecal apertures, forming a quite zone between the stipes into which little (or no) new smoke-bearing flow was introduced. Although such a quite zone might have offered some advantages to the zooids it would have ultimately led to a food depletion unless the zooids travelled to the external edges of the colony to feed.

Changes with development:

All the orientations predicted by the models tested in the oil tank have the sicula directed into the flow. This is the same orientation as that predicted for scandent species (section 5.3.1). In the earliest growth stages, before a dichograptid colony had assumed it's characteristic shape, the *nema* is likely to have served to maintain this orientation to a flow. As the colony matured and its characteristic shape emerged this would have become increasingly important for controlling the colony orientation. The *nema* did not grow with the colony.

The oil tank experiments also indicated that the orientations of dicranograptid species might have changed as the colony matured and grew (section 7.4). Lengthening the uniserial stipes on the dicranograptid model eventually caused it to assume a horizontal orientation. In order to retain the initial alignment, with the biserial section directed into the flow, the weight of this biserial section would have needed to increase with growth. It is uncertain whether this might have happened.

Twisted species:

The dicellograptid and dicranograptid genera included a number of species with twisted stipes. Examples of these were investigated in both the oil tank and the wind tunnel.

The oil tank experiments indicated that the twisted dicellograptid species were likely to have rotated as they sank, given that they sank with the proximal end leading. The simple dicellograptid model did not sink but this was probably a result of the over simplicity of the model, which did not include any thecal torsion about the stipe axis. The experimental study of Rigby and Rickards (Rigby and Rickards 1989, Rigby 1990), using less detailed models, suggested that this stipe torsion would have been enough to cause rotation of the entire colony. A colony lacking such stipe torsion would not have rotated. The wind tunnel observations, using detailed models, indicated that the spiralled stipes induced a corresponding rotation of the flow. It is a natural assumption that this would have caused the colony rotation observed in the oil tank where the model was free to move.

The twisted and spiralled uniserial stipes of the dicranograptid species (*D. ziczac* and *D. ramosus spinifer*) tested also produced a corresponding rotation of the airflow in the wind tunnel. However no rotation was observed when the simple models of these species were tested in the oil tank. The two spiralled stipes of these species are often observed to haven been quite separate from each other (see *D. ziz zac*, Plate XXV, Elles and Wood 1901-1918). The independent spiralling of these stipes is discussed by Williams (1981) who comments that this would prevent autorotation as described by Kirk (1969). Similarly the independence of the two spirals would have prevented the set up of a strong central rotation of the flow over the rhabdosome which might have carried the whole colony around.

One important question is what advantage might these twisted forms have offered the graptolites? It is clear that the whole-colony rotation of the dicellograptid species would have increased the feeding paths of the individual zooids in the colony as described by Rigby and Rickards (Rigby and Rickards 1989, Rigby 1990). The oil tank experiments, in this study, have indicated that the twisted stipes experienced greater drag than the simple straight uniserial stipes. This is borne out by the wind tunnel observations showing a greater area of turbulent wake behind the twisted models than the simple model (figure 7.12 and 7.14 compared with figure 7.10). The increased drag of the twisted uniserial stipes (forming the distal half of the colony) caused a more rapid re-alignment of these models, in comparison with the simple dicranograptid model, when tested in the oil tank. In this case the twisted stipes are acting as a vane-bearing *nema*, providing increased drag without a substantial increase in mass. The twisted forms would have been more stable to turbulent flows, given that the stable orientation was with the proximal end leading, and might have allowed the colony to maintain this orientation with continued growth of the uniserial stipes.

7.8. Further study

A detailed study of the collagen mass distribution of graptolite colonies would be invaluable for refining these experiments. The volumetric distribution of collagen might be investigated serial sections of three-dimensional specimens. This study might then be extended to consider more dichograptid shapes, providing a stronger bridge to the experimental work of Rigby and Rickards (Rigby and Rickards 1989, Rigby 1990 and 1992).

Tests using isolated specimens in seawater would provide useful, and possibly more reliable, insight into the orientation and motion of these non-scandent colonies. A larger number of complete isolated specimens would be required. It would be particularly interesting to also test some of the spiralled forms.

Another obvious line of investigation would be a more detailed look at the changing hydrodynamics of the colony through astogeny using a larger series of models. This study could consider both the early development as the overall colony form takes shape and later development as this shape alters with maturity.

8. Synthesis and Conclusions

This study has identified a number of common graptolite structures and morphologies that might have served a hydrodynamic purpose. The physical modelling has provided evidence for scandent graptolite orientations and suggested functions for vanes and a variety of proximal spines. Mathematical modelling has extended understanding of how these structures functioned and provided predictions regarding optimal morphologies which have been examined in the light of fossil evidence. The understanding gained from these investigations can now be applied to the hydrodynamic analysis of untested species.

The implications of this study can be considered on two levels; the impact of these findings on interpretations of the hydrodynamics of specific graptolite morphologies, as well as the wider implications regarding interpretations of taxonomy, ocean environment and evolution of the graptoloids. It is no longer necessary to test each graptolite species before drawing conclusions about hydrodynamic function. The hydrodynamic response of a variety of graptolite species is discussed here in the light of this study. A synthesis of the experimental results described in chapters 5 to 7 is used to predict the orientation and fluid-flow patterns over untested colonies. The impact of this study on the broader issues of taxonomy, oceanography and evolution is then briefly considered, and opportunities for further work put forward.

8.1. Hydrodynamic principles derived from this study:

8.1.1. Regarding orientation

- Scandent graptolites typically orientated to a flow with the sicula aperture directed up-flow.
- This was true regardless of thecal shape, but may not have been if the colony bore a very long virgella.
- The nema or virgula served as a device for orientation control.
- The mass distribution of the colony was a major factor in controlling orientation. For an alignment with the sicula aperture directed up-flow, the colonies centre of mass would have been located towards the proximal end (where the periderm is thicker).
- A longer virgula would have had a stronger controlling effect on orientation.
- Although taphonomic breakage often results in non-preservation, both diplograptids and monograptids are likely to have had a significant virgular length in comparison to the thecal-bearing section. The virgular length would have increased to maintain this ratio as the colony matured.
- The introduction of a vane structure would also have enforced colony orientation by increasing the surface area of the distal end without significantly increasing the mass.
- Colonies with a robust thecal-bearing portion (with a high drag) would have required a longer or more robust (or vane-bearing) virgula to enforce orientation.
- Vanes would not have caused rotation of the colony, about the sicular axis, when orientated with the flow.
- Three-part and twisted vanes would have been more affective than a flat vane (not seen) as they would always present a large surface area to the flow.

- Multiple virgular spines would also have acted as an effective vane structure.
- A relatively consistent orientation to the prevailing flow would have been beneficial to the colony. This would have allowed greater sophistication of graptolite hydrodynamic structures given that the flow direction relative to these would have also been consistent.
- With the scandent colony orientated to the flow such that the sicula aperture was directed up flow, any structures at the proximal end (i.e. spines) would have affected the flow over the entire colony.

8.1.2. Regarding spines

- Both thecal spines and deflected virgellar spines might have increased feeding efficiency by sampling, and drawing in, seawater from a wider cross-sectional area.
- Low angled spines would have drawn a greater percentage of particles carried in an impacting flow towards the rhabdosome. However a low angled spine would not have sampled the flow from a wide area.
- Longer spines would have sampled from a greater area but only to the point at which any particles captured at the tip of the spine were all swept by small-scale turbulent mixing with passing flow before they could reach the rhabdosome surface.
- A short spine on each of the proximal thecae ($th1^1$ and $th1^2$) would have been sufficient to bring particles from flows impacting the spine into standing eddies in all subsequent thecal apertures.
- Spines on successive thecae would have drawn in flow weakly along the entire spine-bearing colony section.
- The optimal location for thecal spines was dependent on the shape of the thecae.
- Thecal spines and genicular processes controlled the formation of (and fixed the location of) standing eddies in the thecal apertures.

- The overshadowing of the anti-virgellar spines by th1^2 prevented their significantly increasing feeding efficiency.
- The anti-virgellar spines prevented separation of the flow over the sharp angle of the sicular aperture ventral edge, holding the flow closer to the surface of the colony. This may have affected the stability of the colony.
- The deflected virgellar might also have prevented separation of the flow.
- Proximal spines affected the orientation of juvenile colonies producing unbalanced drag.
- Proximal spine arrays can be divided into two types (I and II).
- The proximal spines of type I graptolites reveal an optimal angle of 60-70° and length of 0.3-0.4 mm for thecal spines, and an optimal angle of 50° and length of 0.3 mm for anti-virgellar spines.
- The proximal spines of type II graptolites continued to grow as the colony matured indicating that these spines served a function in addition to increasing feeding efficiency.

8.1.3. Regarding two-stipe dichograptids

- Colony shape and weight distribution significantly controlled orientation.
- Physical modelling has indicated that dicranograptids, didymograptids and dicellograptids might all have orientated with the sicular aperture directed up-flow.
- This orientation may have changed as astogeny altered the overall morphology and mass distribution of the colony.
- Dicellograptid species with twisted stipes would have rotated around the axis of the sicular cone.
- The twisted stipes of some dicranograptid species would have enforced orientation and drag, but would not have caused rotation of the colony about the sicular axis.

8.2. Hydrodynamic interpretations of untested graptolite species

Using the results of this study it is now possible to say a lot more about the hydrodynamics and potential function of specific graptolite morphologies. Given here are hydrodynamic interpretations of a number of graptolite species exhibiting a variety of morphologies.

8.2.1. Species examples

Pseudoclimacograptus scharenbergi

Description: This graptolite exhibits a narrow rhabdosome (1-1.5mm wide) with a circular cross-section and a long, thin virgula (preserved virgula length observed 1.7 times length of thecal-bearing portion on a mature colony). Juvenile specimens have a simple virgula, whereas more mature specimens constructed a three-part vane.

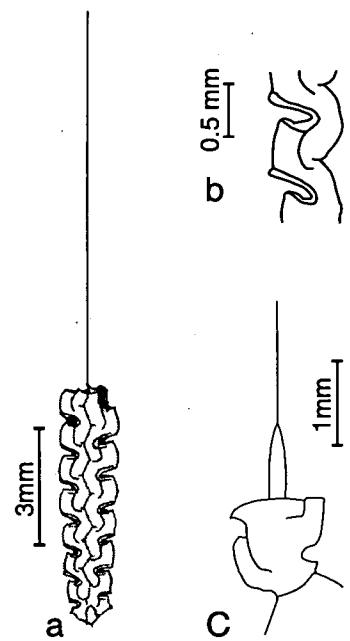

Figure 8.1: *Pseudoclimacograptus scharenbergi*. Schematic drawings based on Elles and Wood (1901-1918) and Bulman (1970). a. Whole mature specimen with long virgula. b. genicular lip c. proximal end with slightly deflected virgella and th1[1] spine.

The virgella is weakly deflected across the sicula aperture. Th1[1] bears a single, Type I (section 6.11.1), spine. Thecae are strongly sigmoidal with a genicular lip. Figure 8.1, based on Elles and Wood (1901-1918) and Bulman (1970).

Interpretation: The rhabdosome, despite having a near-circular cross-section, was very narrow and secondary structures would not have been required on the virgula of juvenile specimens in order for it to function as a stabiliser and orientation control device. The length of the virgula in comparison to that of the thecal-bearing portion would have enforced this orientation (section 5.6.2), with the proximal end facing into any ambient current. As the colony matured the virgular length was not sufficient to enforce orientation and a vane was constructed to increase the virgular surface area.

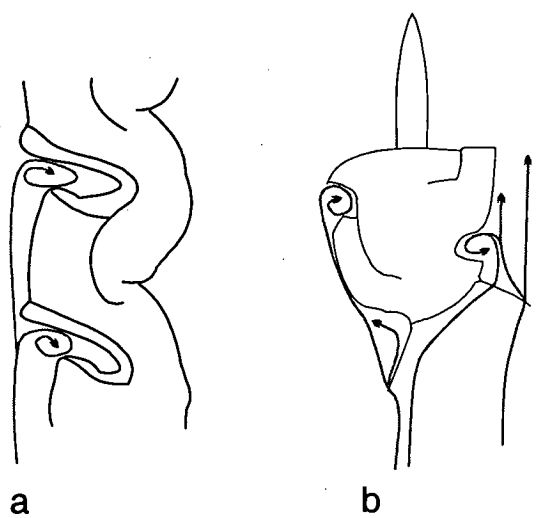

Figure 9.2: An interpretation of fluid flow over *Pseudoclimacograptus scharenbergi.* a. The genicular lip acts like a short spine encouraging vortex formation in the thecal apertures. b. The slightly deflected virgella protects the sicula aperture and prevents seperation of the flow. The thecal spine (th1[1]) draws in flow laterally.

The orientation maintained by the virgula, with the proximal end directed up-flow, would have ensured that the proximal spines encountered the flow first. The th1[1] spine would have drawn in food-bearing water, from a wider area than would have been sampled without such a spine, improving feeding efficiency (section 6.3). The weakly deflected virgella protected the sicula aperture (figure 9.2). The formation of a boundary layer on this spine would have deflected the flow away from the sicula

aperture as suggested by Rickards *et al* (1998) and Melchin (1998). The virgellar spine would have also helped prevent separation as the flow initially impacted the colony (section 6.7). Both the virgella and th1[1] spine would have continued to function in this manner as the colony matured, provided that the virgula lengthened to maintain orientation.

The genicular lip would have acted in the same manner as a short thecal spine (figure 9.2), aiding the formation of standing eddies in the thecal apertures (section 6.5).

Petalolithus folium

Description: The petalograptids have a distinctive pointed proximal end, with the rhabdosome flaring rapidly to approximately to 5mm in the case of *P. folium*, and an exaggerated rectangular cross-section.

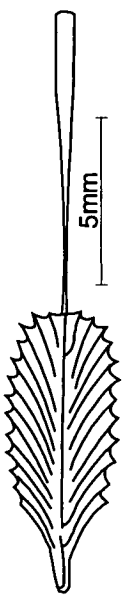

Figure 9.5: *Petalolithus folium*. Schematic drawing based on Elles and Wood (1901-1918) and Bulman (1970).

The tubular virgula flares to a narrow vane 0.5 to 1mm wide. The colony lacks proximal spines beyond the virgella. Thecae are long and straight with a large overlap. Figure 9.5, based on Elles and Wood (1901-1918) and Bulman (1970).

Interpretation: Despite the predictions of the mathematical *nema* model (section 5.6.2), that a flat colony shape would have only required a narrow virgula, it was argued in section 5.6.2 that graptolites such as *Petalolithus* might have required a vane. The substantial surface area resulting from the exaggerated rectangular cross-section thecal-bearing colony section, even when orientated with the large surface parallel to the flow, would have added considerably to the drag of this section. The increased drag represented by the large surface area of *P. folium* would have been counterbalanced by the presence of the vane, reinforcing virgular function.

The virgula would have maintained an orientation with the pointed proximal end directed into the flow. The streamlined morphology of the swept-back, straight thecae, would have prevented detachment of the flow on impact with the colony (figure 9.6), reducing the requirement for anti-virgella and low angle spines (section 6.6).

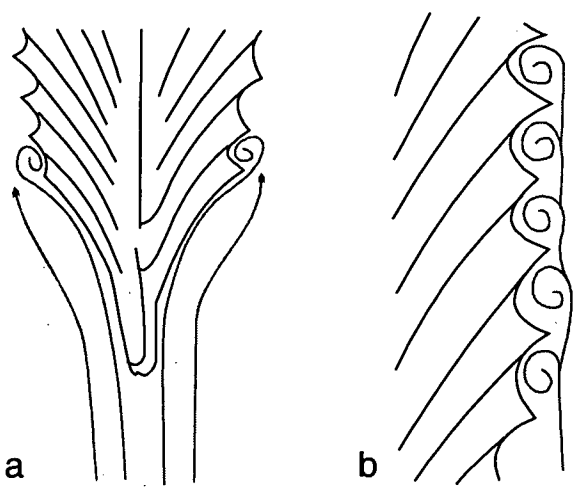

Figure 9.6: An interpretation of the flow over *Petalolithus folium*. a. The flow slips smoothly over the pointed proximal end of the colony without separation on impact with the thecae. b. The stepped edge of the overlapping straight thecae naturally forms standing eddies in the thecal apertures.

Vortices would have formed naturally in the simple, stepped, thecal apertures without the aid of thecal spines (figure 9.6).

Hallograptus mucronatus nobilis

Description: *H. mucronatus nobilis* has a broad (5mm wide, minus spines), very spinose rhabdosome. The virgula exhibits secondary structures, which might have formed a twisted vane. Thecae are geniculate, with a short, inwardly inclined, supragenicular wall, and pairs of long (2-3mm) spines located on the geniculum. The sicula has spines additional to the virgella in the anti-virgella location. The colony also displays scopulae, septal processes that project at right angles to the thecae. Figure 9.7, based on Elles and Wood (1901-1918) and Bulman (1970).

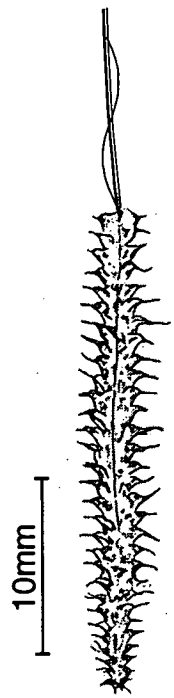

Figure 9.7: *Hallograptus mucronatus nobilis*. Schematic drawing based on Elles and Wood (1901-1918) and Bulman (1970).

Interpretation: The vane would have reinforced the orientation control exerted by the virgula as the large surface area of the broad colony, plus thecal spines, resisted it (section 5.5, 5.6.2 and 5.9.3). These thecal spines would have brought food-bearing flow to the colony form a wide area, along the entire length of the colony (section 6.5) (figure 9.8). Paired spines, directed away from each other, would also have

drawn flow to the colony laterally. The location of the thecal spines, on the geniculum of the thecae would have ensured that standing eddies ran into the thecal apertures (section 6.5).

The anti-virgellar spines would have prevented separation of the flow over the blunt ventral edge of the sicula (section 6.6), holding food-bearing flow closer to the surface, and aiding the stability of the colony in the orientation dictated by the vane-bearing virgula (figure 9.8).

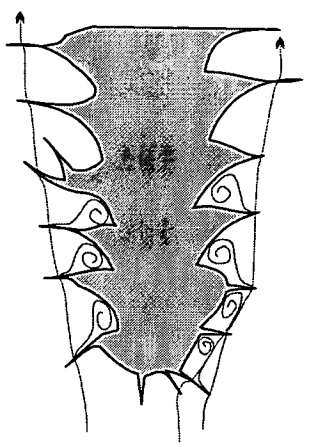

Figure 9.8: An interpretation of the flow over *Hallograptus mucronatus nobilis*. The anti-virgellar spines prevent separation of the flow over the sharp sicula edge. The thecal spines weakly draw in flow laterally along the entire colony length and dictate the location of standing eddies in front of the thecal apertures.

Dicellograptus furcatus bispiralis

Description: *D. furcatus bispiralis* has two uniserial stipes, reclined with distinct clockwise torsion resulting in the two stipes spiralling about one another to form a narrow open spiral about the axis of the sicula cone (1mm wide at proximal end expanding to 2mm wide after two twists: widths do not include spines). Thecae are strongly sigmoidal, bearing long (0.5-1.5mm), single, spines on the genuiculum for the entire length of the uniserial stipes. Figure 9.9, based on Bulman (1970).

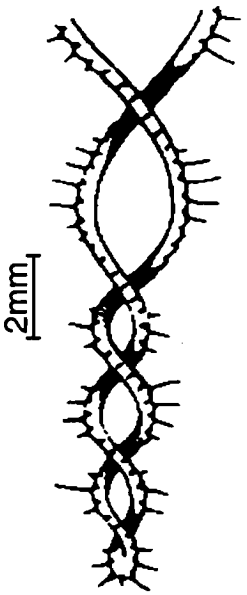

Figure 9.9: *Dicellograptus furcatus bispiralis*. Schematic drawing based on Bulman (1970).

Interpretation: The spiral colony form would have caused rotation of the colony, around the axis of the sicula cone, as flow was drawn laterally around the spiralled stipes (section 7.6.2) (figure 9.10). The long thecal spines might have increased the drag of the colony and slowed this rotation but this possibility has not been investigated in this study.

The thecal spines would have drawn fresh flow laterally into the spiral colony (9.10). These spines would also have controlled vortex formation, producing standing eddies which ran into the sigmoidal thecal apertures facilitating feeding for a zooid inhabiting the thecae (section 6.5).

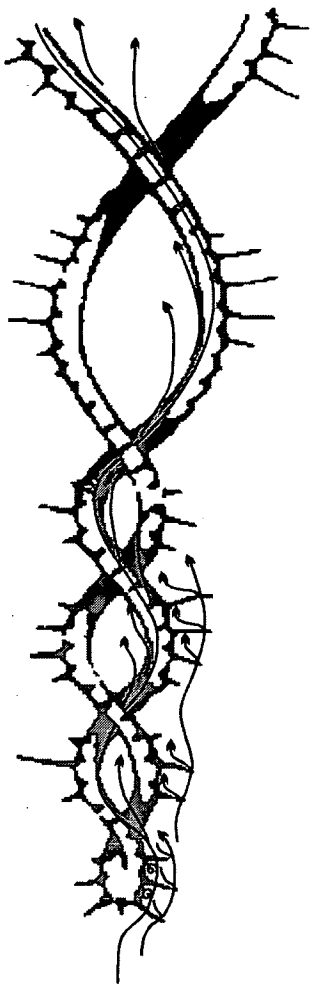

Figure 9.10: An interpretation of the flow over *Dicellograptus furcatus bispiralis*. The flow would follow the spiral shape of the uniserial stipes, causing a net rotation of the colony. The thecal spines weakly draw flow laterally towards the rhabdosome, gathering from a wider area.

Saetograptus frischi linearis

Description: The proximal end of *Saetograptus frischi linearis* exhibits ventral curvature due to a sicula with a marked apertural flare. The overall form of the rhabdosome is that of a straight monograptid. The rhabdosome widens distally to 1.5mm (minus spines). The proximal end bears a distinct, slightly ventrally directed, virgella (0.4mm) and single, dorsally directed, anti-virgella spine. Thecae are simple and straight, bearing paired apertural spines for the entire length of the colony. These spines originate from the dorsolateral edges of the aperture. The robust virgula extends far beyond the thecal-bearing portion (preserved virgular length observed at

equal length of thecal-bearing portion on a mature colony). Figure 9.11, based on Yuan-dang and Lenz (1997).

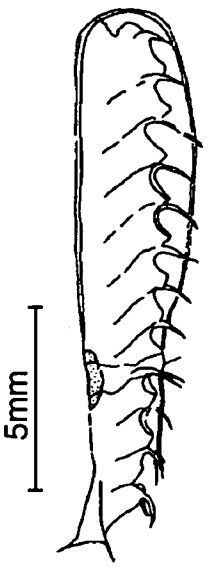

Figure 9.11: *Saetograptus frischi linearis*. Schematic drawing based on Zang and Lenz (1997). The long virgular spine has been deformed, probably through taphonomic processes, and is bent back along the thecal-bearing colony length.

Interpretation: The colony was fairly narrow, but the abundant, sturdy, spines would have increased the drag of the thecal-bearing portion, which was balanced by a long, robust virgula in order to reinforce orientation control (section 5.6.2).

The thecal spines would have drawn in fresh flow along the length of the colony (section 6.5), and would also have controlled vortex location such that standing eddies will form in the thecal apertures (section 6.5) (figure 9.12). Paired apertural spines, directed slight outwards from the plane of the colony, might also have brought flow in laterally.

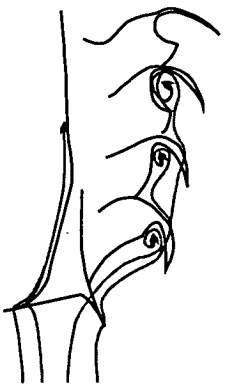

Figure 9.12: An interpretation of the flow over *Saetograptus frischi linearis*. The anti-virgellar spine stabilises the colony by preventing separation of the flow over the flared dorsal edge of the sicula aperture. The thecal spines encourage vortex formation in the thecal apertures and draw flow laterally towards the colony.

The anti-virgella spine would have prevented detachment as the flow impacted with the sharp dorsal edge of the flared sicula (section 6.6) (figure 9.12). This would have held the flow onto the surface of the rhabdosome and stabilised the colony.

Climacograptus lanceolatus

Description: The rhabdosome of *C. lanceolatus* widens gradually from the proximal end to a maximum width of approximately 2.5mm, and has an oval to rectangular cross-section. The proximal end exhibits Type II (section 6.11.1) spines with a distinct deflected virgella spine and thecal spine on the geniculum of $th1^1$ (both initially 1-1.5mm long). With increasing maturity the virgella spine extends with a marked bend at approximately 0.8-1.5mm from its origin. These spines are arranged asymmetrically with the virgella spine directed more proximally. This spine reachs up to 25mm long and is typically longer than the thecal-bearing colony. The thecal spine lengthens only slightly up to 2mm long. Thecae are strongly geniculate. Figure 9.3, based on Vandenberg (1990).

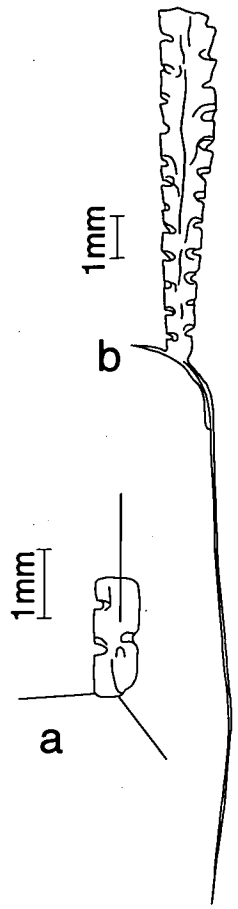

Figure 9.3: *Climacograptus lanceolatus.* Schematic drawings based on Vandenberg (1990). a. A juvenile specimen showing deflected virgella and th1[1] spine of equivalent length. b. A mature specimen with an enlarged virgella. Note the bend in the virgella spine changing its angle to the colony central line.

Interpretation: The virgula and any associated structures, of *C. lanceolatus* are not well known. The rhabdosome is fairly narrow such that additional virgula thickening and reinforcement might not have been necessary to maintain and control colony orientation provided the virgula were of reasonable length (section 5.6.2). As the virgella spine lengthens dramatically with maturity this is likely to have become a significant factor affecting the orientation. Marked thickening of the proximal end is noted, and the increasing asymmetry of mass distribution along the colony would have helped maintain a virgella up-stream orientation (section 5.4). As the virgella became longer than the thecal-bearing section of the colony (figure 9.3 b) then this

may have taken over the orientation control of the colony, dictating a reverse orientation (section 5.3.1). The combination of a very long virgella and virgula was not tested as part of this study.

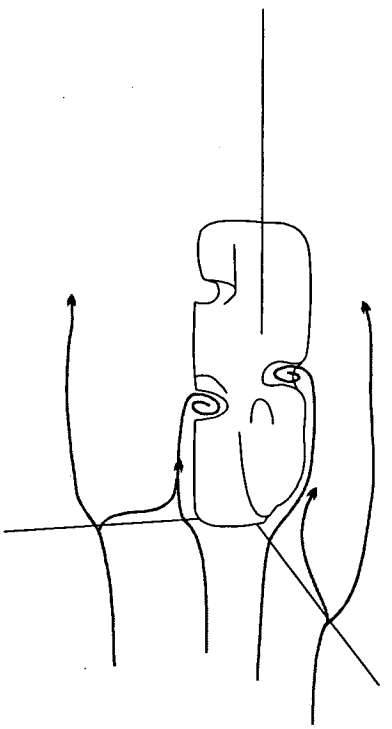

Figure 9.4: An interpretation of the flow over an early growth stage of *Climacograptus lanceolatus*. The deflected virgella prevents separation over sicula aperture, both the virgella and the spine on th1[1] draw flow onto the rhabdosome for a wide area.

Initially it is assumed that the virgula would have maintained an orientation with the proximal end directed into the flow, such that the proximal spines would have encountered the flow first. These spines would both have drawn flow from a wider area to the colony surface (figure 9.4), increasing feeding efficiency (section 6.3 and 6.7). The deflected virgella particularly might also have had a significant effect on the stability of the colony, preventing separation of the flow over the sharp ventral edge of the sicula (section 6.7) (figure 9.4). As the length of these spines increased with maturity the orientation of the colony might have changed. If the colony maintained its initial orientation, with the sicula aperture directed into the flow, then these spines would have continued to function as stabilisers and increasing the feeding efficiency, additional length was not required as the colony matures. This increasing growth indicates that these spines had another function that was becoming

significant to the colony. The virgella bent as it lengthened, changing its overall angle from the colony. This is a common feature of Type II spines (section 6.11.1). This new angle was probably optimal for the unknown function dictating the increasing length of the spine.

This example illustrates that although this study has allowed hydrodynamic interpretations of many graptolite morphologies and structures, beyond those initially modelled, these predictions will ultimately be limited by problems of taphonomy. Species that are poorly preserved, lacking detailed information about the virgula or proximal end, will not allow a complete analysis of the likely hydrodynamics of the graptolite.

8.3. Wider implications

This study has wider implications beyond the direct ramifications regarding the hydrodynamic interpretation of a range of graptolite structures and morphologies. Potentially the results of the hydrodynamic investigations included in this study could also influence interpretations of taxonomy, graptolite ecology and evolution.

8.3.1. Taxonomy

Care should be taken when basing taxonomy on structures of known function. Although these structures may still be valuable for taxonomic analysis it is important to be aware of their function and the possibility of convergent evolution.

Fortey and Cooper (1986) outlined a phylogenetic classification of graptoloids in which structures constructed early in astogeny are given more weight. These features were considered more significant as they may alter subsequent development of the colony and have a greater resultant affect, on the colony morphology as a whole, than features constructed later in development. Consequently this phylogeny relies heavily on the morphology of the sicula and proximal end. This includes deflected siculae, anti-virgellar spines and thecal spines; features which were investigated hydrodynamicaly as part of this study (chapter 6).

The investigation of these structures revealed that all could have had functional implications. These spinose structures were relatively simple to construct, and very similar arrangements might have arisen in separate lineages, as a result of convergent evolution due to the same environmental pressures, thus weakening their use as taxonomic indicators. However different spine arrays were shown to have similar functions (i.e. an *A. maxwelli* type spine array and an *C. (D.) spiniferus* type spine array might both increase feeding efficiency), implying that these solutions were not unique, reducing the risk of convergent evolution.

8.3.2. Oceanography

Originally it was hoped that better understanding of the hydrodynamic functional morphology of graptolites might allow links to be made between shape and oceanic environment. This study has suggested functions for a number of common graptolite shapes and structures, but these have tended to be quite universal.

It has been shown that all types of proximal spines might have increased feeding efficiency, whilst some could also have had an effect on stability, indicating that perhaps these structures might have been linked to low nutrient waters or turbulent conditions. Superoligotrophic conditions were typical of the Cambrian to Devonian, encompassing the entire graptolite range. The Caradoc, when proximal spines were most abundant (section 6.11.2), also represented a period of high sea level and relatively warm waters which might have triggered speciation. The diversity of spinose forms would have filled the abundant specialist niches created by the flooded continents. The decline of spinose species diversity through the Ashgill may have resulted from the loss of many of these niches with a fall in sealevel, a transition to cooler conditions and potentially a eutrophic episode in the late Ordovician (Martin 1995).

The fact that the different spine arrays, including those featuring a deflected virgella, have all been shown to increase feeding efficiency reduces their potential as environmental indicators. It appears that all these arrays were different evolutionary solutions to the same problem, triggered by needs common to almost all graptolites. The occurrence of any particular spine array type could not be used to predict different environmental conditions.

8.3.3. Evolution

The brief study of representative Ordovician faunas (section 6.11.2) indicated that the Caradoc represented an acme for the proximal hydrodynamic features identified in chapter 6. This period represented an apparent peak in overall species diversity and abundance (Koren' and Rickards 1979), with graptolites taking advantage of increased feeding efficiencies through spinose forms. Diversity abruptly dropped with the end Ordovician extinction, potentially linked to the onset of glaciation at this time. The post-glacial recovery fauna, although initially dominated by normalograptid biserials, the fauna was then taken over by monograptid forms that largely lacked proximal spines beyond the virgella. There are a few examples of monograptids with a single anti-virgella spine (for example *Saetograptus fristchi linearis*) and many examples of species with spine-bearing and hooked thecae. A small number of spinose biserial species appeared representing a change towards species with either no spines beyond the virgella (for example, *Glyptograptus auritus*), or those with a mass of spines (for example, *Hirsuitograptus villosus*). Did this represent a loss of genetic information, regarding the hydrodynamic proximal spine arrays observed throughout the Ordovician, over the end-Ordovician glaciation?

The monograptids had many representative species with hooked or spine-bearing thecae. These spines would also have increased feeding efficiency (section 6.5 and Rickards *et al* 1998). The spines of these monograptid species were not limited to the first two thecae as had been the case for many Ordovician biserial species. With

examples of spines on both the thecae and in the anti-virgellar location it does not seem likely that monograptids were unable to build proximal spine arrays, rather that they were not sufficiently beneficial to the colony. The development of curved species would have had a dramatic affect on the flow patterns over the rhabdosome and spines concentrated in a proximal location may no longer have been appropriate or effective (except possibly for very early growth stages).

The previously distinctively spinose glossograptids also appear to have undergone a reduction in spinosity during the early Silurian, evolving forms such as *Rogercooperia* (Sherwin and Rickards 2000). This might indicate that there was some broader advantage to not building spines at this time. Many Silurian biserial species had pointed proximal ends, particularly the large number of *Petalolithus* species (*P. folium*, *P. minor* etc.), which would have presented a streamlined shape to the flow, preventing separation without the requirement of anti-virgella spines.

The major argument for loss of spines may return to the provision of specialist niches. Mid-Ordovician proximal spines may have been a response to the creation of specialist niches created by a warm, low-nutrient, environment. Post-glacial recovery these niches may have no longer existed, or may simply have been preferentially filled by new monograptid species (including spinose and hooked species) which would have restrained the re-radiation of the proximal-spined diplograptids.

These trends can be observed at Dob's Linn (Williams1981) where abundant specimens can be collected across the Ordovician-Silurian boundary. Many species featuring proximal spine arrays can be collected below the boundary, such as *O. abbreviatus* (Type I spines: section 6.11.1), *C. longispinus supernus* (Type II spines: section 6.11.1) and *P. pacificus*. Several species of both straight (*D. anceps*) and twisted (*D. complexus*) dicellograptids are also relatively abundant. Fossil abundance drops off at the Ordovician – Silurian boundary only to return with a few non-spinose biserial species (for example, *C. normalis* and *C. extraordinarius*), and a total lack of dicellograptid species. The biserial species surviving and re-radiating

after the extinction event all exhibited relatively streamlined, pointed, proximal ends in comparison with the spinose species observed lower down in the series. These Silurian biserials would not have required low-angle proximal spines to prevent flow separation on impact with the colony. Specimens of *C. trifilis* appearing within the Silurian section confirm that some genetic instructions regarding proximal spines did survive the extinction.

It appears that the dramatic loss of species with proximal spine arrays (anti-virgellar spines and thecal spines restricted to $th1^1$ and $th1^2$) was probably not a result of lost genetic information over the end-Ordovician extinction. Silurian graptolites were capable of building these structures but given new competitive conditions, and more streamlined proximal ends, these structures were no longer of sufficient benefit to the colony to justify the initial outlay of constructing them.

8.4. Areas for further study

This study has indicated many areas for further study as this is a relatively new field and much remains to be investigated. Three areas are highlighted here:

- The distribution of colony mass, which has been revealed to be a key factor controlling colony orientation.
- The hydrodynamics of monograptid species, a large and significant group of species which has been largely untapped here.
- Dichograptid early development, a opportunity to link this work with that of Rigby and Rickards (Rigby and Rickards 1989, Rigby 1990).

8.4.1. Mass distribution of real graptolites

One of the key factors, controlling colony orientation, identified by this study, was the distribution of mass along the colony (section 5.4 and 7.3.2). There is little

information regarding the distribution of mass along scandent colonies, although it has largely been assumed that the mass would have been concentrated at the proximal end. The mass distribution assumed for dichograptid colonies was even more speculative.

Graptolite colonies could have altered their mass distribution by adding additional layers of cortical tissue to controlled sections of the rhabdosome. Additional cortical tissue is observed at the proximal ends of many scandent specimens. These specimens are proximally opaque due to the density of tissue, changing to a translucent honey tissue as the collagen walls thin distally. The mass-distribution of the two-stipe dichograptid colonies is less certain, and it has been shown that changes in the mass distribution could have reversed orientations (section 7.3.2).

A more accurate understanding of the detailed mass distribution of all these colony types might be gained though detailed SEM investigations using isolated specimens and serial sections. Given more reliable data the mathematical model (section 5.6.2) might be refined to make more detailed predictions and those regarding more complex shapes.

8.4.2. Monograptids

This study has concentrated on scandent colonies, but the subject of monograptid species was largely untapped. Although these investigations have led to some understanding of the hydrodynamic response of a straight monograptid colony, little can be said about the abundant and diverse curved species.

Some implications for monograptid hydrodynamics can be taken from this study. Straight monograptids would react to the influence of a virgula in the same manner as a diplograptid (section 5.6.2), in fact the isolated specimens tested were monograptids (section 5.3.2 and 5.7). Wind tunnel studies have shown that there is

little flow interaction between the two rows of thecae along a biserial colony, and as such a single row of thecae along a uniserial colony would have reacted to form the same flow patterns. There was a fundamental similarity of form between the basic structures (spines) and their locations (thecal, anti-virgella, distal virgula) of diplograptid and straight monograptid colonies.

The curved monograptids remain an unknown quantity. Their curvature ranged from gently curved forms such as *Bohemograptus bohemicus bohemicus* to the more spiralled *M. turriculatus* and cyrtograptid species. During very early astogeny these graptolites would have appeared, and reacted, little different from juvenile straight monograptids. The early growth stages of isolated cyrtograptids sank with the same orientation as those of *M. priodon* (section 5.7). These juveniles would have been, under the same hydrodynamic influences, comparable to straight monograptids and diplograptids.

As the colony matured, and its characteristic shape became apparent, the curvature would have had a significant effect on the colony orientation. It is not reasonable to assume an orientation for these species with the virgula directed directly down-flow, in which the proximal end would have encountered the flow first. A different orientation would imply some other part of the colony would have acted as the leading edge, and would have significant ramifications of the optimal location and angles for functional structures.

The orientations of these colonies, moving towards the horizontally disposed cyrtograptids (Rigby 1990, Rigby and Rickards 1989), could be investigated through more accurate modelling techniques. The mass distribution along real colony specimens could be investigated (through serial sections and SEM work) and this information used to build a correctly weighted model. Such a model could more reliably predict stable orientations taking into account the interaction of both colony morphology and mass distribution. These orientations could then be used as a basis

for wind tunnel investigations of the interactions of the flow with curved monograptid morphologies.

8.4.3. Dichograptid early development

Experimental work with isolated specimens has indicated that the early growth stages of all planktonic graptoloids might be expected have common hydrodynamic responses, with the nema (or sicula cone) acting as a stabiliser. As the colony shape developed the more mature morphology might have become the more significant factor controlling colony orientation. This was particularly true of dichograptids in which stipe orientation and torsion have been shown to have a significant affect on colony orientation and movement (Rigby 1990). The limited experimental work modelling dichograptids within this study has also indicated that the orientation and movement of dichograptids might have changed as they matured (section 7.4).

9. References

9.1. Main text references.

Apollonov, M.K. *et al.* 1980. *The Ordovician-Silurian boundary in Kazakhstan* <<Nauka>> Kazakh SSR Publishing House. Ed. M.K. Apollonov, S.M. Bandaletov and I.F. Nikitin. 299p.

Bates, D.E.B. and Kirk, N.H. 1985. Graptolites, a fossil case-history of evolution from sessile colonial animals to automobile superindividuals. *Proceedings of The Royal Society of London* **228**, 207 – 224.

Berry, W.B.N. 1964. The middle Ordovician of the Oslo region, Norway. No. 16. Graptolites of the Ogygiocaris series. *Norsk Geologisk Tidsskrift* **44**, 61 – 170.

Briggs, D.E.G. Kear, A.J., Baas, M. *et al.* 1995. Decay and composition of the hemichordate *Rhabdopleura*: implications for the taphonomy of graptolites. *Lethaia* **28**, 15 – 23.

Bouček, B. 1973. *Lower Ordovician graptolites of Bohemia.* Publishing house of the Czechoslovak Academy of Sciences. 185p.

Bulman, O.M.B. 1931. On the graptolites prepared by Holm. 1. Certain 'diprianidion'graptoites and their development. *Arkiv för Zoologi.* Band **24A** no. 8, 1 - 46.

Bulman, O.M.B. 1944 - 1947. A monograph of the Caradoc (Balclathie) Graptolites from limestones in Laggan Burn Ayrshire. London. *Palaeontological Society (monograph).*

Bulman, O.M.B. 1963. On *Glyptograptus dentatus* and some allied species. Palaeontology **6**, 665 – 689.

Bulman, O.M.B.1964. Lower Palaeozoic Plankton. *Quarterly Journal of the Geological Society of London* **120**, 455 – 476.

Bulman, O.M.B. 1970. *Treatise on Invertibrate Palaeontology : part V.* Geological Society of America. University of Kansas, 163p.

Briggs, D.E.G. and Williams, S.H. 1981. The restoration of flattened fossils. *Lethaia* **14**, 157 – 164.

Carruthers, W. 1868. A revision of the British Graptolites. *Geological Magazine* **5**, 64 – 74.

Cooper, R.A. Fortey, R.A., Lindholm, K. 1991. Latitudinal and depth zonation of early Ordovician graptolites. *Lethaia* **24**, 199 – 218.

Cooper, R.A. and Fortey, R.A. 1983. Development of the graptolite rhabdosome. *Alcheringa* **7**, 201 – 221.

Cox, I. 1933. On *Climacograptus inuiti* sp. nov. and its development. *Geological Magazine*. **70**, 1-18.

Crowther, P.R. 1981. The fine structure of graptolite periderm. *Special papers in Palaeontology* **26**, 119p.

Crowther, P.R. and Rickards, R.B. 1977. Cortical bandages and the graptoloid zooid. *Geology and Palaeontology.* **11**, 9 – 46.

Dilly, P.N. 1993. *Cephalodiscus graptolitoides* sp.nov.: a living graptolite? *Journal of Zoology* **229**, 69-78

Drain, L.E. 1980. *The Laser Doppler technique.* Wiley and Sons, London and New York, 214p.

Elles, G.L. and Wood, E.M.R. 1901 - 1918. *A monograph of British Graptolites.* Edited by C. Lapworth. London : Printed for the Palaeontographical Society, 122p.

Emlet, R.B. and Strathman, R.R. 1985. Gravity, Drag, and Feeding Currents of Small Zooplankton. *Science* **228**, 1016 – 1017.

Finney, S. 1978. Mode of life of planktonic graptolites: floatation structure in Ordovician *Dicellograptus sp. Palaeobiology* **5**, 31-39.

Finney, S. and Berry, W.B.N. 1997. New perspectives on graptolite distributions and their use as indicators of platform margin dynamics. *Geology* **25**, 919 – 922.

Fortey, R. A. 1984. Global earlier Ordovician transgressions and regressions and their biological implications. In Bruton, D.L. *Aspects of the Ordovician System.* Palaeontological contributions from the University of Oslo No. **295**. Universitetsforlaget.

Fortey, R. A. and Cooper, R. A. 1986. A phylogenetic classification of the graptoloids. *Palaeontology* **29**, 631 - 654.

Gentile, L.F., Nowell Donovan, R. and Finney, S.C. 1984. Orientated graptolites as paleocurrent indicators in the lower Viola Springs Formation (Ordovician) in the Arbuckle Mountains and Criner Hills, Oaklahoma. *Oaklahoma Geological Survey.* **44**, 121 – 126.

Gutierrez-Marco, J. C. and Lenz, A. C. 1998. Graptolite synrhabdosomes: biological or taphonomic entities? *Paleobiology* **24**, 37-48.

Hutt, J. 1973. The development of *Clonograptus tenellus* and *Adelograptus hunnebergensis.* Lethia **7**, 79-92.

Jenkins, C.J. 1997. Fine scale structures important for hydrodynamics. *Alcheringa.* in press

Keble, R.A. and Harris, W.J. 1934. Graptolites of Victoria: new species and additional records. *Memoir of the National Museum, Melbourne* **8**, 199 – 218.

Kirk, N. 1969. Some thoughts on the ecology, mode of life and evolution of the Graptolithina. *Proceedings of the Geological Society, London* **1659**, 273 – 292.

Kirk, N. 1972. More thoughts on the automobility of the graptolites. *Journal of the Geological Society* **128**, 127 – 133.

Koren', T.N. and Rickards, R.B. 1979. Extinction of the graptolites in Harris A.L., Holland C.H. and Leake B.E. (eds.) *The Caledonides of the British Isles, reviewed.* Geological Society of London, Special publication **8**, 457 - 466.

Koren', T.N. and Rickards, R.B. 1996. Taxonomy and evolution of Llandovery biserial graptoloids from the Southern Urals, Western Kazakhstan. *Special papers in Palaeontology* **54**, 1 – 103.

Kozlowska-Dawidziuk, A.1997. retiolitid graptoloite *spinogratus* from Poland and it's membrane structures. *Acta Palaeontologica Polonica.* **42**, 391 – 412.

Kozlowski, R. 1971. Early development stages and the mode of life of graptolites. *Acta Palaeontologica polonica* **16**, 313 – 343.

Lapworth, C. 1897. Die Lebensweise der graptolinthen In Eber die Lenenweise fossiler Meeresthiere. z. dtsch. geol. Ges. (ed Walter, J.), 238 – 258.

Lavoie, D. and E. Asselin. 1998. Upper Ordovician facies in the Lac Saint-Jean outlier, Quebec (eastern Canada): palaeoenvironmental significance for Late Ordovician oceanography. *Sedimentology* **45**, 817 – 832.

Loydell, D. and J. Zalasiewicz. 1998. Predation on graptolites. New evidence from the Silurian of Wales. *Palaeontology* **41**, 423 – 429.

Maletz, J. and Mitchell, C.E. 1996. Evolution and Phylogenetic classification of the Glossograpidae and Arienigraptidae (Graptioloidea): new data and remaining questions. *Journal of Paleontology* **70**, 641 – 655.

Martin, R.E. 1995. Cyclic and secular variation in microfossil biomineralization – clues to the biogeochemical evolution of phanerozoic oceans. *Global and Planetary Change* **11**, 1 – 23.

Martin, R.E. 1996. Secular increase in nutrient levels throughout the phanerozoic: Implications for productivity, biomass, and diversity of the marine biosphere. *Palaios* **11**, 209 – 219.

Melchin, M.J. 1998. Morphology and phylogeny of some early 'diplograptid' genera from Cornwallis Island, Arctic Canada. *Palaeontology* **41**, 263 - 315.

Melchin, M.J. 1998. A hydrodynamic function of the graptolite virgella. *Sixth International Graptolite Conference + 1998 Field meeting of the IUGS subcommision on Silurian stratigraphy*. 218-219

Melchin, M. J. and DeMont, M. E. 1995. Possible propulsion modes in Graptoloidea: a new model for graptoloid locomotion. *Palaeobiology* **21**, 110 – 120.

Melchin,M. and Doucek, K.M. 1996. Modelling flow patterns in conical dendroid graptolites. *Lethaia* **29**, 39-46.

Mitchell, C.E. 1987. Evolution and Phylogenetic classification of the Diplograptacea. *Palaeontology* **30**, 353 – 405.

Mitchell, C. E. and K. J. Carle. 1986. The nematularium of *Pseudoclimacograptus scharenbergi* (Lapworth) and its secretion. *Palaeontology* **29**, 373 – 390.

Palmer, D.C. 1986. The montypic 'population' accompanying the lectotype of *Saetograptus variens* (Wood 1900). From Huges,C.P. & Rickards,R.B. (eds) *Palaeocecology and Biostratigraphy of Graptolites, Geological Society Special Publication* **20**, 249-259.

Patzkawsky *et al.* 1997. Late middle Ordovician environmental change and extinction: Harbinger of the late Ordovician or continuation of Cambrian patterns? *Geology* **25**, 911 – 914.

Ruedemann, R. 1947. Graptolites of North America. *Memories of the Geological Association of America* **19**, 1 – 652.

Rickards, R.B. 1975. Palaeoecology of the graptolinitha, an extinct class of the phylum hemichordata. *Biological Review* **50**, 397 – 436.

Rickards, R.B. 1979. Early evolution of graptolites and related groups. In House,M.R. (ed.) The Origin of Major Invertebrate Groups. *Sytematics Association Special Publication* **12**, 431-441.

Rickards, R.B. 1996. The graptolite nema: problem to all our solutions. *Geological Magazine* **133**, 343 – 346.

Rickards, R.B and Crowther P.R. 1979. New observations on the mode of life, evolution and ultrastructure of graptolites. *Systematics Association Special Publication* **11**, 397-410.

Rickards, R. B. and M. S. Khashogji. 2000. The tuning fork graptoloid, *Didymograptus murchisoni* (Beck, 1839). *Transactions of the Royal Society of Edinburgh – Earth Sciences*. **90**, 173 – 187.

Rickards, R.B., Rigby, S., Rickards, J. *et al.* 1998. Fluid dynamics of the graptolite rhabdosome recorded by Laser Doppler Anemometry. *Palaeontology* **41**, 737-752.

Rickards, R.B. and Stait, B.A. 1984. *Psigraptus*, its classification, evolution and zooid. Alcheringa **8**, 101 – 111.

Rigby, S. and Rickards, R.B. 1989. New evidence for the life habit of graptolites from physical modelling. *Palaeobiology* **15**, 402 – 413.

Rigby, S. 1990. PhD thesis. Graptoloid form and function. Unpublished, University of Cambridge, 226p.

Rigby, S. 1991. Feeding strategies in graptolites. *Palaeontology* **34**, 797 – 813.

Rigby, S. 1992. Graptoloid feeding efficiency, rotation and astogeny. *Lethaia* **25**, 51 – 68.

Rigby, S. 1994. Hemichordate skeletal growth:shared patterns in *Rhabdopleura* and graptoloids. *Lethaia* **27**, 317 – 324.

Rigby, S. and P. N. Dilly. 1993. Growth-rates of petrobranchs and the life-span of graptolites. *Palaeobiology* **19**, 459 – 475.

Rigby, S. & Sudbury, M 1995. Graptolite ontogeny and the size of the graptolite zooid. *Geological Magazine* **132**, 427 – 433.

Riva, J. 1976. *Climacograptus Bicornis Bicornis* (Hall) it's ancestor and likely descendants. pp.589 - 619 in Bassett, M.G. *The Ordovician System: proceedings of a Palaeontological Association Symposium, Birmingham, September 1974.* University of Wales Press & National Museum of Wales, 696p.

Riva, J. F. 1994. Yutagraptus mantuanus Riva in Rickards 1994, a pendent xiphograprid from the Lower Ordovician of Utah. In: Chen, Xu, B. D.,

Erdtmann and Ni Yu-nan (eds.): *Graptolite Research Today*, Nanjing University Press: 1-13.

Schleiger, N.W. 1968. Orientation distribution patterns of graptolite rhabdosomes from Ordovician sediments in central Victoria, Australia. *Journal of Sedimentary Petrology*. **38**, 462 – 472.

Sherwin, L. and Rickards, R.B. 2000. *Rogercooperia*, a new genus of Ordovician glossograptid graptolite from Southern Scotland and New South Wales, Australia. *Scottish Journal of Geology* **36**, 159 – 164.

Strickler, J. Rudi. 1981. Calanoid Copepods, feeding currents, and the role of gravity. *Science* **218**, 158 – 160.

Underwood C.J. Interstipe webbing in the Silurian graptolite *Cyrtograptus murchisoni. Palaeontology* **38**, 619 - 625.

Urbanek, A. 1976. The problem of graptolite affinities in the light of ultrastructural studies on peridermal derivatives in pterobranchs. *Acta Palaeont Polonica.* **21**, 3 – 36.

Vandenberg, A.H.M. 1990. The ancestry of Climacograptus spiniferus Ruedemann. *Alcheringa* **14**, 39 – 51.

Vogel, S. 1981. *Life in moving fluids: the physical biology of flow.* Willard Grant Press, 467p.

Walker, M 1953. The development of a diplograptid from the Platteville limestone. *Geological Magazine* **90**, 1 - 16.

Williams, S.H. 1981. Upper Ordovician and Lowest Silurian Graptolite Biostratigraphy. Unpublished PhD thesis, University of Cambridge.

Williams, S.H. 1981. Form and mode of life of *Dicellograptus* (Graptolithina). *Geological Magazine*. **118**, 401 – 408.

Williams, S.H.1994. revision and definition of the *C. wilsoni* graptolitezone (middle Ordovician) of southen Scotland.*Transactions of the Royal Society Edinburgh - Earth Sciences* **85**, 143 – 157.

Williams, S.H. & Stevens R.K. 1998. The Lower Ordovician (Arenig) graptolites of the Cow Head Group, western Newfoundland. *Palaeontographica Canadiana*. **5**, 1 – 167.

Zang, Yuan-dang & Lenz, A.C.1997. Uppermost Wenlock and Ludlow graptolites from Southen Yunnan China. *Canadian Journal of Earth Sciences* **34**, 1220 – 1238.

9.2. Data references for appendices C – E.

Bjerreskov, M. 1981. Silurian Graptolites from Washington Land, Western North Greenland. *Gørnlands Geologiske Undersøgelse* **142**. 58p.

Buchroithener, M, Jaeger, H. and Holzer, H.L. 1978. Das gemeinsame Vorkommen von Graptolinthen und Conodonten in einem Ludlow – Profil des Synklinoriums von Feixa – Castellás – Esphent (Zentralpyrenäen, Prov. Lerida, Sponien).*Mitt. Österr. Geol. Ges.* **68**, 39 – 49.

Bulman, O.M.B. 1931. On the graptolites prepared by Holm. 1. Certain 'diprianidion'graptoites and their development. *Arkiv för Zoologi*. Band **24A** no. 8, 1 - 46.

Bulman, O.M.B. 1931. On the graptolites prepared by Holm. 1. Certain 'diprianidion'graptoites and their development. *Arkiv för Zoologi*. Band **24A** no. 9, 1 – 29.

Bulman, O.M.B. 1934. . *Report on a collection of graptolites from the Charchq series of Chinese Turkistan*. The Sino-Swedish Expedition. Publication 4.

Bulman, O.M.B. 1964. Lower Palaeozoic Plankton. *Quarterly Journal of the Geological Society of London* **120**, 455 – 476.

Clark, T.H. and Srachen, I. 1955. Log of the Sengion well, Southern Quebec. *Bulletin of the Geological Society of America* **66**, 685 – 698.

Cox, I. 1933. On *Climacograptud inuiti* sp. nov. and its development. *Geological Magazine* **70**, 1 – 19.

Cuerda, A.J. 1974. Monograpten aus dem Ludlow Boliviens. *N. Jb. – Geol. Paläont. Mh.* **6**, 321 – 335.

Dover, J.H. 1980. Ordovician and Silurian Phi Kappa and Trail Creek Formations, Pioneer Mountains, Central Idaho – Stratiographic and structural revisions and new data on graptolite faunas. *Geological Survey Professional Paper* **1090**, 54p.

Eisenack, A. 1959. Einige Mittleilungen Űber Graptolithen. Neues Jb. Geol. U. Paläont. **107**, 253 – 260.

Finney, S.C. 1986. Graptolite biofacies and correlation of eustatic subsidence, and tectonic events in the Middle to Upper Ordovician of North America. *Palaios* **1**, 435 – 461.

Finney, S.C., Gentile, L.F. and Asbery, R. 1984. The Viola springs formation (Ordovician) of Oaklahoms, a heaven for graptolite specialists. *Oklahoma Geological Survey* **44**, 116 – 120.

Garret, M.J. and Rickards, R.B. 1984. Graptolite biostratigraphy of early land plants from Victoria, Australia. *Proceedings of the Yorkshire Geological Society* **44**, 377 – 384.

Gutiérrez-Marco, J.C. et al. 1999. Gratolites de la Biozona de Coronograptus cyphus (Rhuddaniense: Silúro inferior) en el área del Montseny (Cadenas Coasteras Catalonas, noreste de España). *Temas Geologica – Mineros I.T.G.E.* **26**, 618 – 622.

Herr, S.R. 1971. Regeneration and growth abnormalities in *Orthograptus quadrimucronatus* from the Ordovician Maquoketa Formation of Iowa. *Journal of Paleontology* **45**, 628 – 632.

Jackson, D.E. 1971. Development of *Glyptograptus hudsoni* sp. nov. from Southampton Island, North-West territories, Canada. *Palaeontology* **14**, 478 – 486.

Jackson, D.E. 1973. *Amplexograptus* and *Glyptograptus* isolated from Ordovician limestones in Manitoba. Bulletin - *Geological Society of Canada* **222**, 1 – 18.

Jaeger, H. 1964. Monograptus hercynicus in de Westsudeten und das Alter der Westsudeten und das Alter der Westsudeten-Hauptfaltung, Teil I. *Geologie Jahrgang B. Heft* **3**, 249 – 277.

Jaeger, H. 1983. Unterdevonische Graptolithen aus Burma und zu vergleichende Formen. *Jahrbuch der Geologischen Bundesanstalt Wien* **126**, 245 – 257.

Jaanussan, V. 1995. Confacies differentiation and upper middle Ordovician correlation in the Baltoscandian basin. *Proceedings of the Estonian Academy of Science – Geology* **44**, 73 – 86.

Jenkins, C.J., Kidd, P.R. and Mills, K.J. 1982. Upper Ordovician graptolites from the Wagona beds near Batemans Bay, New South Wales. *Journal of the Geological Society of Australia* **29**, 367 – 373.

Jerzmoński, J. 1955. Nowe stanowisko graptolitów w górach kaczawskich. *Instytut geologiczny biuletyn* **95**, 169 – 176.

Ji-jin, L. and Han-jun, C. 1988.Graptolites from Nancheng formation at Liangshan, Hanzhang of Shaanxi. *Acta Palaeontologica Sinca* **27**, 164 – 178.

Kirk, N.H. 1975. More thoughts on the construction and functioning of the rhabdosome in the Graptoloidea in the light of their ultrastructure. *University college of Wales Aberystwyth Department of geology Publications.* **7**, 1 – 24.

Koren', T.N. 1971. The zones of *Monograptus hercynicus* and *Monograptus falcarius* in Pai-khoi. *Lethaia* **4**, 235 – 248.

Legrand, P. 1976. Contribution a l'etude des graptolites du llandoverin inferiur de l'oued in djerane. *De Bulletin de la Société d'Histoire Naturelle de l'Afrique du Nord* **67**, 141 – 190.

Lenz, A.C. 1982. Llandoverian Grapolites of the Northen Canadian Cordillera: Petalograptus, Cephalograptus, Rhaphidograptus, Dimorphograptus, Retiolitidae and Monograptids. *Life Sciences Contributions Royal Ontario Museum* **130**, 154p.

Lenz, A.C. and Xu, C. 1985. Middle to Upper Ordovician graptolite biostratigraphy of Peel River and other areas of the Northern Canadian Cordillera. *Canadian journal of Earth Sciences* **22**, 227 – 239.

Melchin, M.J. 1986. Upper Ordovician graptolites from the cape Phillips Formation, Canadian Arctic Islands. *Bulletin of the Geological Society of Denmark* **33**, 191 – 202.

Mihajlovic, M. 1974. Silurki Graptoliti Istočne srbije. *Bulletin du Muséum d'histoire naturelle (Belgrade). Série A* **29**.

Mitchell, C.E. 1986. Morphometric studies of *Climacograptus* (Hall) and the phylogenetic significance of astogeny. *Geological Society special publication* **20**, 119 – 129.

Mitchell, C.E. and Bergstrom, S.M. 1977. Three-dimensionally preserved Richmondian graptolites from southwestern Ohio and the graptolite correlation of the North American Upper Ordovician standard. *Boll. Soc. Palaeont. Italia* **16**, 257 – 270.

Mu, A.T., Lee, C.K. and Geh, M.Y. 1960. Ordovician graptolites from Xinjiang (Sinkiang). *Acta Palaeontologica Sinica* **8**, 28 – 39.

Mu, A.T., Lee, C.K., Geh, M.Y. and Yin, G.H. 1962. Graptolites of Chilianshan in *Geology of Chilianshan. Paleontology* **4**, fasc 2.

Müller, A.H. and Schauer, M. 1969. Uber Schwebeeninrichtungen bei Diplograptidae (Graptolintjina) aus dem Silur. *Freiberger Forschungshefie* **245**, 5 – 26.

Münch, A. 1952. *Die Graptolinthen aus dem anstehenden Gotlandium Deutschlands und der tschecoslowakei.* Schriftenreihe der geologischen institute der univesitaten Berlin **7**, 1 - 157.

Öfversigt, A. 1882. Skånes Graptoliter af sven axel tullberg. *Afhandlingar och uppsater* **50**.

Palmer, D. 1970. *Monograptus ludensis* zone graptolites from the Devilsbit Mountain district, Tipperary. *Scientific Proceedings of the Royal Dublin Society series A.* **3**, 335 – 342.

Piçarra, J.M. et al. 1995. Characterization of the *Parakidograptus accuminatus* graptolite biozone in the Silurian of the Barrancosregion (Ossa Morena Zone, S. Portugal).

Rickards, R.B. and Palmer, D.C. 1977. Early Ludlow monograptids with Devonian morphological affinities. *Lethaia* **10**, 59 – 70.

Skevington, D. 1960. A new variety of *Orthoretiolites Hami* Whittington (Oaklahoma). *Palaeontology* **2**, 226 – 235.

Skevington, D. 1970. A lower Llanvirn graptolite fauna from the Skiddaw Slates, Westmorland. *Proceedings of the Yorkshire Geological Society* **37**, 395 – 444.

Skevington, D. and Paris, F. 1975. Les graptolithes de la formation de Saint-Grmain-sur-ille (Ordovician supérieur du Massif Armorican). *Bulletin de la Société de Geologie de France* **7**, 260 - 266.

Skwarko, S.K. 1974. Some Ordovician graptolites from the Canning Basin, Western Australia,2: Graptolites from the Goldwyer No.1 well. *Bulletin of the Bureau of Mineral Resources* **150**, 43 - 56.

Štorch, P. 1982. Ordovician – Silurian boundary in the northernmost past of the Prague Basin (Barrandian, Bohemia). *Věstník Ústředního ústavu geologického* **57**, 231 – 236.

Strachen, I. 1954. The structure and development of *Peiragraptus fallax*, gen. et sp. nov. A new graptolite from the Ordovician of Canada. *Geological Magazine* **41**, 509 – 513.

Strachen, I. 1959. Graptolites from the the Ludibundus Beds (Middle Ordovician) of Tvären, Sweden. *Publications from the Palaeontological Institution of the university of Uppsala* **23**, 48 – 68.

Sudbury, M. 1957. Diplograptus spinulosus sp. nov., from the Ordovician of Syria. *Geological Magazine* **94**, 503 – 506.

Teller, L. 1964. Graptolite fauna and stratigraphy of the Ludlovian deposits of the Chelm borehole, E. Poland. *Studia Geologica Polonica* **13**, 88p.

Törnquist, L.S.V. 1897. On the diplograptidae and heteroprionidae of the scanian rastrites beds. *Särtryck of kongl fysiogr sällskapets I lund handlingar ny följd* **8**.

Underwood, C.J., Deynoux, M., Ghienne, J.F. 1998. High palaeolatitude (Hodh, Mauritania) recovery of graptolite faunas after the Hirnantian (end

Ordovician) extinction event. *Paleogeography, Paleoclimatology, Palaeoecology* **142**, 91 – 105.

Walters, M. 1977. Middle and Upper Ordovician graptolites from the St. Lawrence lowlands, Quebec, Canada. *Canadian Journal of Earth Sciences* **14**, 932 – 952.

Williams, S.H. 1994. Revision and definition of the *C. wilsoni* graptolite zone (Middle Ordovician) of Southern Scotland. *Transactions of the Royal Society of Edinburgh: Earth Sciences* **85**, 143 – 157.

Xiaofeng, W. and Zhaogui, Y. 1984. Early Devonian graptolite faunas from Yulin, Guangxi. *Dizhi Lunping* **30**, 416 – 424.

Xu, C. 1982. Early Ordovician *Exiograptus* and *Glyptograptus* from Xingon, N. Guangxi and the origin of biserial axonophorus graptolites. *Acta Palaeotologica Sinca* **21**, 505 – 514.

Xu, C. 1983. Silurian Graptolites from Southern Shaanxi and Northern Sichuan with special reference to classification of monograptidae. *Palaeontologia Sincta* **166**, 1 – 102.

A. Seawater tank data.

List of abbreviations. v: vertical. h: horizontal. n: nema. vi: virgella. th: thecae.

Early growth stages

Complete specimens

Early Growth Stages	Specimen number	No. of thecae	vertical or horizontal	Comments	Average angle (degrees: 0
1	3.7	0	v	n up	0
2	3.9	0	v	Angled to v - slow turn. See align n first into horizontal current.	0
3	3.4	0	v	n up	0
4	3.19	0	v	n up	0
5	5.20	0	v	n up - n long	0
6	1.13	0	v	n up	0
7	3.22	0	v	n up - curved n. n vert.	15
8	3.6	0	h	n down. n curved	100
9	3.8	0.01	v	n up - slow response	0
10	1.12	0.01	v	n up	10
11	3.15	0.01	v	n up	15
12	4.8	0.25	v	n up th down	0
13	4.10	0.25	v	n up very vertical	0
14	4.3	0.25	v	n up th up?	10
15	4.13	0.25	v	n up - n vert but bent.	15
16	2.10	0.3	v	n up	10
17	3.20	0.4	v	Slight angle. n up - th up – nema deflected?	10
18	3.25	0.5	v	n up	0
19	2.15	0.5	v	n up th down	10
20	3.24	0.5	v	n up th down	10
21	3.26 / 4.1	0.5	v	n up. th up - slow alignment.	10
22	1.8	0.5	v	n up	15
23	3.5	0.6	v	n up th down	10
24	2.4	0.8	v	n up - th down	10
25	2.7	0.9	v	n up	10
26	1.15	0.95	v	n up - th down	10
27	1.5	1	v	n up	0
28	1.6?	1	v	n up	0
29	3.18	1	v	Very v. n up	0
30	3.23	1	v	n up th down	10
31	3.17	1	v	n up - angle due to curved nema. n vertical	15

Specimens without a *nema*

Early Growth Stages	Specimen number	No. of thecae	vertical or horizontal	Comments	Average angle (degrees: 0 = nema
1	5.21	0	v	vi up	180
2	3.2	0	v - h	vi up	180
3	5.13	0.2	v	vi down	0
4	4.15	0.25	v	vi down th up	0
5	5.9	0.5	v	vi down very v.	0
6	4.9	0.75	v	vi up th up?	170
7	5.10	0.75	v/h	Angled to near h. vi up	100
8	5.19	0.75	v	vi up	180
9	3.14	1	v	vi up.	180
10	3.21	1	v	vi up - distal end missing.	130

Straight thecae

Complete specimens

Straight Monograptids	Specimen number	No. of thecae	vertical or horizontal	Comments	Average angle (degrees: 0 = nema vertical)
1	4.14	1	v	n up	0
2	4.16	1	v	n up th down	5
3	1.10	1.1	v	n up	0
4	1.14	1.1	v	n up - slight angle th down	10
5	2.9	1.2	v to h	n up - th up.	55
6	2.11	1.2	v	n up - th down	10
7	1.3	1.2	v	n up.	45
8	4.5	1.2	v/h	Nema vert - but bent so main nr. h	0
9	4.7	1.3	v	n up th down - rapid alignment	10
10	5.18	1.3	v	n up - very v. rapid alignment.	0
11	5.11	1.4	v	Very v - n up (long n) – rapid alignment	0
12	5.12	1.5	v	n up th down. slow alignment	0
13	2.14	1.75	v	n up	0
14	2.2	2	v	n up	10
15	5.2	2	h	Angled to h - th side to down	90
16	5.4	2.2	h	nr h - n up th down	90
17	5.5	2.3	v	Very v - n up	0
18	3.10	2.5	v	n up th down - slight angle	10
19	5.17	3	v	n up - very v. rapid alignment	0
20	1.2	3.5	h	n up	50
21	4.21	4	h	nr. H - v up th up	100
22	5.3	4	h	dist up th side to down	85
23	3.3	4	h	n up th down	80
24	2.16	5	h	n up th down	70

Specimens without a *nema*

Straight Monograptids	Specimen number	No. of thecae	vertical or horizontal	Comments	Average angle (degrees: 0 = nema vertical)
1	1.4	1	h	vi down - steep angle	100
2	5.16	1.2	h	nr. h - vi up th up	110
3	2.19 / 3.1	2	h	vi up th up	100
4	4.2	2	v/h	Angled - varied. vi down	135
5	5.15	2.5	v	vi up	180
6	3.12	2.9	h	Angled - vi up th down	140
7	4.4	3	v	nr. Vert vi up th up?	170
8	2.13	3.5	h	on side. vi up	100
9	2.6	3.5	v	vi up - th down	160
10	2.3	3.5	v	vi up	180
11	1.16/2.1	4	h - v	vi up	110
12	4.12	4.4	v	vi up th up	170
13	2.5	4.5	v	vi up	170
14	4.23	5	h	vi up th down - n broken very short	90
15	5.8	5	h	Angled - vi up th up – slow alignment	140
16	1.9	5.5	h	Proximal end up	80

Specimens without a virgella

Straight Monograptids	Specimen number	No. of thecae	vertical or horizontal	Comments	Average angle (degrees: 0 = nema vertical)
1	1.1	3.75	h	n up	60
2	4.17	1.5	v	n up th down - slow alignment	10

Hooked thecae

Complete specimens

Hooked monograptids	Specimen number	No. of thecae	vertical or horizontal	Comments	Average angle (degrees: 0 = nema vertical)
1	4.6	0.75	v	n up th down	0
2	1.7	1	v	n up	0
3	5.6	1.5	v	n up n-vi line vert. Th down	5
4	3.16	0.9	v	n up th down to near h.	10
5	4.19	1	v	n up. th up	10
6	2.17	2	v	n up th down	10
7	5.1	1.5	h	Angled - n up th side/up - n and vi short.	50
8	4.18	3	v/h	Angled to near h – th down. n up	50
9	1.11	2	h	n up th down	75
10	2.8	2	v / h	n up th down	80

Specimens without a *nema*

Hooked monograptids	Specimen number	No. of thecae	vertical or horizontal	Comments	Average angle (degrees: 0 = nema vertical)
1	5.7	1	h	th side vi down	85
2	5.14	1	v	vi up	180

Specimens without a virgella

Hooked monograptids	Specimen number	No. of thecae	vertical or horizontal	Comments	Average angle (degrees: 0 = nema vertical)
1	3.13	1	h	angled - n up th down	50

Dicellograptids

D. formosus	Specimen number	No. of thecae	vertical or horizontal	Comments	Average angle (degrees: 0 = nema vertical)
1	a5	2	v	no nema – vi up	175
2	a1	2.4	h	no nema – sicula lies horizontal	90
3	a2	2.5	v	no nema – vi up	180
4	a3	2.5	v	no nema – vi up	170
5	a4	4.2	v/h	n up – one stipe only	45

B. Oil tank data

Nema length

Experiment	**1.00**		**3.00**		**2.00**		**4.00**		**5.00**		**6.00**	
Nema Length / cm	0.00		2.60		4.50		6.30		9.20		12.80	
Sink times / s	0.83	Rotation time / s	0.89	Rotation time / s	0.64	Rotation time / s	0.64	Rotation time / s	0.69	Rotation time / s	0.63	Rotation time / s
	0.80	---	0.90	too quick	0.69	0.25	0.86	0.49	0.69	Still rotating	0.75	Still rotating
	0.84		0.83		0.67	0.32	0.72	0.49	0.63		0.74	
	0.76		0.42		0.64	0.33	0.70	0.37	0.63		0.71	
	0.60		0.72		0.67	0.29	0.64	0.55	0.63		0.66	
	0.71		0.97		0.67	0.26	0.64	0.61	0.67		0.65	
	0.69		0.67		0.77		0.49		0.61		0.77	
	0.64		0.77		0.66		0.61		0.78		0.63	
	0.71		0.83		0.66		0.63		0.75		0.79	
	0.77		0.67		0.67		0.66		0.84		0.69	
Average	0.74		0.77		0.67	0.29	0.66	0.50	0.69		0.70	
Standard deviation	0.08		0.16		0.04	0.04	0.09	0.09	0.08		0.06	
Angle	0.00		30.00		60.00		65.00		55.00		45.00	
Rotation Rate	---		---		206.90		129.48		79.48		64.10	

Experiment	4.00		7.00		8.00	
weight / g	0.94	Rotation time / s	0.68	Rotation time / s	0.26	Rotation time / s
Sink times / s	0.64	0.49	0.57	0.62	1.24	0.95
	0.86	0.49	0.75	0.67	1.47	1.17
	0.72	0.37	0.67	0.61	1.08	0.72
	0.70	0.55	0.61	0.55	1.13	0.84
	0.64	0.61	0.68	0.57	1.20	0.73
	0.64		0.75		1.47	
	0.49		0.71		1.30	
	0.61		0.59		1.23	
	0.63		0.67		1.21	
	0.66		0.73		1.27	
Average	0.66	0.50	0.67	0.60	1.26	0.88
Standard deviation	0.09	0.09	0.06	0.05	0.13	0.19
Angle	65.00		60.00		25.00	
Rotation Rate	129.48		99.34		28.34	

Vane types

Experiment	**7.00**		**10.00**		**12.00**		**13.00**		**14.00**	
Vane type	**no vane**	Rotation time / s	**twisted vane**	Rotation time / s	**3-part vane**	Rotation time / s	**flat vane**	Rotation time / s	**threads**	Rotation time / s
Sink times / s	0.57	0.62	0.83	0.58	0.90	0.53	0.71	0.55	0.99	0.73
	0.75	0.67	0.74	0.61	0.70	0.53	0.63	0.45	0.77	0.56
	0.67	0.61	0.65	0.47	0.78	0.49	0.91	0.46	1.11	0.58
	0.61	0.55	0.67	0.53	0.00	0.50	0.79	0.48	1.16	0.52
	0.68	0.57	0.67	0.48	0.88	0.63	0.94	0.41	1.09	0.54
	0.75		0.79		0.81		0.84		1.13	
	0.71		0.70		0.74		0.79		0.93	
	0.59		0.79		0.56		0.73		1.09	
	0.67		0.69		0.77		0.83		1.18	
	0.73		0.69		0.93		0.84		1.19	
					0.82					
Average	0.67	0.60	0.72	0.53	0.71	0.54	0.80	0.47	1.06	0.59
Standard deviation	0.06	0.05	0.06	0.06	0.27	0.06	0.09	0.05	0.13	0.08
Angle	60.00		70.00		75.00		65.00		85.00	
Rotation Rate	99.34		131.09		139.93		138.30		145.05	

Vanes and weighting

Experiment	**9.00**		**10.00**		**11.00**	
Weight / g	0.94	Rotation time / s	0.68	Rotation time / s	0.26	Rotation time / s
Sink times / s	0.70	Still rotating	0.83	0.58	0.97	0.69
(Twisted vane)	0.67		0.74	0.61	1.01	0.58
	0.80		0.65	0.47	0.96	0.73
	0.70		0.67	0.53	1.09	0.71
	0.71		0.67	0.48	0.97	0.67
	0.57		0.79		1.02	
	0.66		0.70		0.93	
	0.83		0.79		1.00	
	0.67		0.69		0.96	
	0.66		0.69		0.87	
Average	0.70		0.72	0.53	0.98	0.68
Standard deviation	0.07		0.06	0.06	0.06	0.06
Angle	75.00		70.00		65.00	
Rotation Rate	107.60		131.09		96.15	

Weight distribution

Experiment	4.00		15.00		16.00		17.00		18.00		19.00	
Weight Distribution	**fat cone**	Rotation time / s	**fat reverse cone**	Rotation time / s	**sphere**	Rotation time / s	**cylinder**	Rotation time / s	**long cone**	Rotation time / s	**long reverse cone**	Rotation time / s
Sink time / s	0.64	0.49	0.62	Still rotating	0.75	Still rotating	0.88	0.56	1.13	too quick	0.83	0.53
	0.86	0.49	0.54		0.66		0.83	0.49	1.16		0.80	0.47
	0.72	0.37	0.64		0.61		0.80	0.42	0.93		0.73	0.58
	0.70	0.55	0.66		0.64		0.87	0.54	0.94		0.78	0.91
	0.64	0.61	0.57		0.61		0.81	0.53	1.19		0.73	0.44
	0.64		0.64		0.67		0.69		1.18		0.83	
	0.49		0.58		0.59		0.74		1.14		0.84	
	0.61		0.54		0.63		0.79		0.92		0.70	
	0.63		0.54		0.58		0.68		1.03		0.83	
	0.66		0.69		0.58		0.93		1.19		0.90	
Average	0.66	0.50	0.60		0.63		0.80	0.51	1.08		0.80	0.59
Standard deviation	0.09	0.09	0.06		0.05		0.08	0.06	0.11		0.06	0.19
Angle	65.00		70.00		70.00		30.00		10.00		40.00	
Rotation Rate	129.48		116.28		110.76		59.06				68.26	

Experiment	20.00		21.00		22.00		23.00		24.00		26.00	
weight / shape	**U-curve no weight**	Rotation time / s	**0.56 central**	Rotation time / s	**1.47 central**	Rotation time / s	**0.56 ends**	Rotation time / s	**1.47 ends**	Rotation time / s	**Straight no weight**	Rotation time / s
Sink time / s	1.77	---	0.99	0.60	0.74	0.36	1.12	0.57	0.84	Still rotating	1.57	---
	1.63		0.91	0.51	0.58	0.36	1.22	0.59	0.77		1.78	
	1.77		0.91	0.45	0.67	0.43	1.07	0.73	0.64		1.75	
	1.59		0.98	0.46	0.65	0.45	1.04	0.71	0.72		1.74	
	1.35		0.86	0.49	0.56	0.42	1.16	0.80	0.76		1.80	
	1.47		1.09		0.64		0.93		0.79		1.49	
	1.58		1.05		0.59		1.03		1.01		1.59	
	1.34		1.09		0.74		0.93		1.02		1.75	
	1.63		1.07		0.65		0.99		0.89		1.73	
	1.54		1.02		0.59		0.87		0.99		1.69	
Average	1.57		1.00	0.50	0.64	0.40	1.04	0.68	0.84		1.69	
Standard deviation	0.15		0.08	0.06	0.06	0.04	0.11	0.10	0.13		0.10	
Angle	0.00		60.00		80.00		-60.00		-85.00		0.00	
Rotation Rate	0.00		119.52		198.02		-88.24		-100.83		0.00	

Experiment	21.00		25.00	
Dicellograptid shape	straight	Rotation time / s	spiral	Rotation time / s
Sink time / s	0.99	0.60	0.96	0.49
	0.91	0.51	0.98	0.37
	0.91	0.45	0.83	0.47
	0.98	0.46	1.05	0.46
	0.86	0.49	1.17	0.47
	1.09		1.09	
	1.05		0.83	
	1.09		0.92	
	1.07		0.88	
	1.02		0.93	
Average	1.00	0.50	0.96	0.45
Standard deviation	0.08	0.06	0.11	0.05
Angle	60.00		90.00	
Rotation Rate	119.52		199.12	

Experiment	**28.00**		**27.00**		**29.00**	
Uniserial stipe length / cm	**2.40**	Rotation time / s	**5.60**	Rotation time / s	**8.00**	Rotation time / s
Sink time / s	1.40	0.89	1.51	Still rotating	2.52	1.55
	1.34	1.09	1.36		2.55	1.87
	1.82	1.24	1.47		2.62	1.81
	1.56	1.02	1.41		2.19	1.67
	1.42	1.07	1.24		2.29	1.74
	1.27		1.37		2.31	
	1.21		1.65		2.70	
	1.43		1.25		2.09	
	1.16		1.68		2.73	
	1.30		1.25		2.33	
Average	1.39	1.06	1.42		2.43	1.73
Standard deviation	0.19	0.13	0.16		0.22	0.12
Angle	65.00		70.00		20.00	
Rotation Rate	61.21		49.33		11.57	

Experiment	27.00		30.00		31.00	
Dicranograptid type	**flat**	Rotation time / s	**ribbon**	Rotation time / s	**spiral**	Rotation time / s
Sink time / s	1.51	Still rotating	1.37	Still rotating	1.88	Still rotating
	1.36		1.56		1.68	
	1.47		1.44		1.49	
	1.41		1.47		1.84	
	1.24		1.57		1.46	
	1.37		1.58		1.57	
	1.65		1.59		1.86	
	1.25		1.47		1.46	
	1.68		1.39		1.41	
	1.25		1.37		1.69	
Average	1.42		1.48		1.63	
Standard deviation	0.16		0.09		0.18	
Angle	70.00		75.00		85.00	
Rotation Rate	49.33		50.64		52.02	

C. Relative virgula length data

Diplograptid data

Reference	Species	Colony (mm)	Virgula (mm)	Virgella (mm)	virgula/ colony
Jaanusson 1995	*Amplexograptus baltoscandicus*	66	13	5	0.20
Mu 1962	*Amplexograptus confertus*	18	13	2	0.72
Mu 1962	*Amplexograptus modicellus*	30.5	24		0.79
Jackson 1973	*Amplexograptus sp. Indet.*	47	35	2	0.74
A.Munch 1952.	*C. kirstei*	8	1		0.13
A.Munch 1952.	*C. kirstei*	8	2		0.25
A.Munch 1952.	*Ceph. Cometa*	14	3		0.21
A.Munch 1952.	*Ceph. Tuberlariformis*	60	30	1	0.50
A.Munch 1952.	*Ceph. Tuberlariformis*	48	15		0.31
Bulman 1964	*Ceph. tuburlariformis*	22	20		0.91
Nomen Nudum 1983	*Climacograptus affinis*	105	57		0.54
Bulman 1964	*Climacograptus angustatus*	43	16	2	0.37
Nomen Nudum 1983	*Climacograptus brevis brevis*	41	13	4	0.32
Nomen Nudum 1983	*Climacograptus brevis cf. Strictus*	38	30	5	0.79
Nomen Nudum 1983	*Climacograptus caudatus*	97	6	58	0.06
Walters 1977	*Climacograptus cf. Augustus*	19	24	4	1.26
Bulman 1934	*Climacograptus cf. Uniformis*	51	44	11	0.86
A.Munch 1952.	*Climacograptus citocrescens*	20	19	5	0.95
Kirk 1975	*Climacograptus diplacanthus*	44	42	38	0.95
Ji-jin & Han-jun 1988	*Climacograptus hastatus*	68	50	6	0.74
Cox 1933	*Climacograptus inuiti*	74	55	15	0.74
Ji-jin & Han-jun 1988	*Climacograptus leptothecalis*	109	8	3	0.07
Ji-jin & Han-jun 1988	*Climacograptus leptothecalis*	59	18	2	0.31
Storch 1982	*Climacograptus longifilis*	45	10	23	0.22
A.Munch 1952.	*Climacograptus medius*	32	11	37	0.34
A.Munch 1952.	*Climacograptus medius*	26	35	6	1.35
Leonn Tornquist 1897	*Climacograptus medius*	27	23	9	0.85

Reference	Species	Colony (mm)	Virgula (mm)	Virgella (mm)	virgula/ colony
Leonn Tornquist 1897	*Climacograptus medius*	8	11	8	1.38
Legrand 1977	*Climacograptus normalis*	41	34	5	0.83
Kirk 1975	*Climacograptus orthoceratophilus*	61	25	21	0.41
Bulman 1964	*Climacograptus parvus*	28	43		1.54
Mitchell 1986	*Climacograptus pygmaeus*	30	10	2.5	0.33
Mitchell 1986	*Climacograptus pygmaeus*	21	10	2.5	0.48
Finney 1986	*Climacograptus pygmaeus*	33	15	4	0.45
A.Munch 1952.	*Climacograptus rectangularis*	68		26	0.00
A.Munch 1952.	*Climacograptus rectangularis*	74	16	14	0.22
A.Munch 1952.	*Climacograptus resurectus*	36	6		0.17
A.Munch 1952.	*Climacograptus scalaris*	32	6	2	0.19
A.Munch 1952.	*Climacograptus scalaris*	15	10	2	0.67
A.Munch 1952.	*Climacograptus scalaris*	5	10	1	2.00
A.Munch 1952.	*Climacograptus scalaris normalis*	62	4	6	0.06
A.Munch 1952.	*Climacograptus scalaris normalis*	74	5	1	0.07
A.Munch 1952.	*Climacograptus scalaris normalis*	51	11	4	0.22
Nomen Nudum 1983	*Climacograptus spiniferus*	67	3	86	0.04
Finney 1986	*Climacograptus spiniferus*	1.5	10	9	6.67
Nomen Nudum 1983	*Climacograptus spiniferus spiniferus*	57	2	14	0.04
Nomen Nudum 1983	*Climacograptus spiniferus spiniferus*	18	2	7	0.11
Bulman 1964	*Climacograptus styloideus*	45	31		0.69
A.Munch 1952.	*Climacograptus supernus*	13	5		0.38
A.Munch 1952.	*Climacograptus supernus*	19	3		0.16
A.Munch 1952.	*Climacograptus tornquesti*	29		11	0.00
A.Munch 1952.	*Climacograptus tornquesti*	35		28	0.00
A.Munch 1952.	*Climacograptus trifilis*	26	4		0.15
Bulman 1964	*Climacograptus tubuliferus*	26	31.5		1.21
Lenz & Xu 1985	*Climacograptus tubuliferus*	69	55	2	0.80

Reference	Species	Colony (mm)	Virgula (mm)	Virgella (mm)	virgula/ colony
Legrand 1976	*Climacograptus venustus*	63	24	81	0.38
A.Munch 1952.	*Cyst boerneri*	12	11		0.92
A.Munch 1952.	*Cyst. Cystiferus*	32	20		0.63
A.Munch 1952.	*Cyst. Diplocystiferus*	44	35		0.80
A.Munch 1952.	*Cyst. Grandis*	85	32		0.38
A.Munch 1952.	*Cyst. Hydromedusae*	30	40		1.33
A.Munch 1952.	*Cyst. Laasiae*	19	21		1.11
A.Munch 1952.	*Cyst. Longbicornis*	13	11		0.85
A.Munch 1952.	*Cyst. Longecystiferus*	21	58		2.76
A.Munch 1952.	*Cyst. Munchi*	38	20		0.53
A.Munch 1952.	*Cyst. Speciosus*	31	9		0.29
Storch 1982	*Cystograptus vesiculosus*	62	62		1.00
Gutierrez-Marco *et al* 1999	*Cystograptus vesiculosus*	50	89		1.78
A.Munch 1952.	*Diplagarptus cf. Modestus*	55	10	2	0.18
A.Munch 1952.	*Diplagarptus cf. Modestus*	43	2		0.05
A.Munch 1952.	*Diplagraptus modestus diminutus*	26	2		0.08
A.Munch 1952.	*Diplagraptus modestus diminutus*	26	2		0.08
A.Munch 1952.	*Diplagraptus modestus parrulus*	5	2	3	0.40
A.Munch 1952.	*Diplagraptus modestus parrulus*	4.5	1.5	0.5	0.33
A.Munch 1952.	*Diplagraptus modestus transversus*	50	4	3	0.08
A.Munch 1952.	*Diplagraptus thuringiacus*	31.5	12.5	9	0.40
A.Munch 1952.	*Diplagraptus thuringiacus*	46	2	7	0.04
A.Munch 1952.	*Diplagraptus thuringiacus*	53	18	6	0.34
A.Munch 1952.	*Diplograptus (Ak.) acuminatus praecedens*	31	17		0.55
A.Munch 1952.	*Diplograptus (Ak.) acuminatus praecedens*	23	2		0.09

Reference	Species	Colony (mm)	Virgula (mm)	Virgella (mm)	virgula/ colony
A.Munch 1952.	*Diplograptus (Ak.) acuminatus praecedens*	16	18		1.13
Bulman 1964	*Diplograptus decoratus*	54	13.5		0.25
Eisenack 1959	*Diplograptus gracilis*	52	21	17	0.40
Bulman 1964	*Diplograptus multidens*	58	17		0.29
Leonn Tornquist 1897	*Diplograptus palmeus*	15	36		2.40
Sudbury 1957	*Diplograptus spinulosus*	18	12		0.67
Xu 1983	*Diplograptus tcherskyi variatus*	85	36		0.42
Xu 1983	*Diplograptus tortithecatus*	37	44	5	1.19
Xu 1983	*Diplograptus tortithecatus*	51	21	7	0.41
Xu 1982	*Exigraptus clavus*	24	28		1.17
Xu 1982	*Exigraptus globosus*	16	12		0.75
Xu 1982	*Exigraptus uniformis*	31	45		1.45
Bulman 1964	*Glossograptus ciliatus*	15	17		1.13
Bulman 1964	*Glossograptus ciliatus douglasi*	17	32		1.88
Xu 1982	*Glyptograptus dentatus pusillus*	50	26	14	0.52
Walters 1977	*Glyptograptus lorrainensis*	65	5		0.08
Xu 1982	*Glyptograptus pilus*	37	25		0.68
Xu 1982	*Glyptograptus pilus*	67	33		0.49
Xu 1982	*Glyptograptus pilus*	47	46		0.98
Xu 1982	*Glyptograptus pilus fluctus*	29	34		1.17
A.Munch 1952.	*Glyptograptus serratus*	39	13		0.33
Xu 1982	*Glyptograptus shelvensis variabilis*	24	52		2.17
A.Munch 1952.	*Glyptograptus sinuatus*	16	1	2.5	0.06
A.Munch 1952.	*Glyptograptus tamariscus*	61	16		0.26
Bulman 1964	*Glyptogratus dentatus appendiculatus*	28	29.5		1.05
Bulman 1964	*Hallogarptus mucranatus nobilis*	19	18		0.95
Bulman 1964	*Isograptus gibberulus*	9	31		3.44

Reference	Species	Colony (mm)	Virgula (mm)	Virgella (mm)	virgula/ colony
Dover 1980.	*Isograptus victoriae victoriae*	58	78		1.34
Xiaofeng & Zhaogui 1984	*Nemograptus hercynicus*	69	10		0.14
Xiaofeng & Zhaogui 1984	*Nemograptus hercynicus*	65	9	1.5	0.14
Gutierrez-Marco et al 1999	*Neodiplograptus thuringiacus*	59	26	17	0.44
Underwood et al 1998	*Normalograptus miserabilis*	21	32.5	3.2	1.55
Lenz & Xu 1985	*Orthograptus apiculatus*	38	30	3	0.79
A.Munch 1952.	*Orthograptus bellulus*	30		22	0.00
A.Munch 1952.	*Orthograptus bellulus*	29	3	23	0.10
Xu 1982	*Orthograptus curviseptatus*	25	17		0.68
Lenz & Xu 1985	*orthograptus expansus*	41.5	43		1.04
Kirk 1975	*Orthograptus gracilis*	74	37	35	0.50
A.Munch 1952.	*Orthograptus insectiformis*	27	27		1.00
Nomen Nudum 1983	*Orthograptus n.sp.*	57	10	4	0.18
Nomen Nudum 1983	*Orthograptus quadrimucronatus*	61	19	11	0.31
Nomen Nudum 1983	*Orthograptus quadrimucronatus*	111	6	1.5	0.05
A.Munch 1952.	*Orthograptus raiculatus*	29	1		0.03
A.Munch 1952.	*Orthograptus raiculatus*	13	1		0.08
Walters 1977	*Orthograptus ruedemanni*	35	9	5	0.26
Walters 1977	*Orthograptus ruedemanni*	46	19	1.5	0.41
Nomen Nudum 1983	*Orthograptus ruedemanni*	49	11	1	0.22
A.Munch 1952.	*Orthograptus tridens*	114	13		0.11
A.Munch 1952.	*Orthograptus truncatus abbrevians*	21	5		0.24
A.Munch 1952.	*Orthograptus vesiculosus*	43	27		0.63
A.Munch 1952.	*Orthograptus vesiculosus*	81	7		0.09
Bulman 1964	*Orthograptus vesiculosus*	78	56		0.72
A.Munch 1952.	*Orthograptus vesiculosus juncus*	34	18		0.53
A.Munch 1952.	*Orthograptus vesiculosus penna*	51	7		0.14
Muller & Schouer 1969	*Orthograptus vesiculus*	134	111		0.83

Reference	Species	Colony (mm)	Virgula (mm)	Virgella (mm)	virgula/ colony
Muller & Schouer 1969	*Orthograptus vesiculus*	101	84		0.83
Muller & Schouer 1969	*Orthograptus vesiculus*	108	113		1.05
Skevington 1960	*Orthoretiolites hami*	35	15	9	0.43
Skevington 1960	*Orthoretiolites hami*	34	30	11	0.88
A.Munch 1952.	*Pa. C. hughesi*	27	2.5	1	0.09
A.Munch 1952.	*Pa. C. hughesi*	16	10	0.5	0.63
A.Munch 1952.	*Pa. C. hughesi*	13	5	0.5	0.38
Mu 1962	*Paraglossograptus intermedius longispina*	47	30	4	0.64
Mu 1962	*Paraglossograptus tricornis distincta*	39		2	0.00
Mu 1962	*Paraglossograptus tricornis major*	57	53	5	0.93
Mu 1962	*Paraglossograptus typicalis*	36	25		0.69
Mu 1962	*Paraglossograptus typicalis*	18	25		1.39
Mu 1962	*Paraglossograptus typicalis*	10	29	4	2.90
Bjerreskov 1981	*Petalograptus ? Conicus*	43.5	53.5	1	1.23
A.Munch 1952.	*Petalograptus altissimus*	36	8		0.22
A.Munch 1952.	*petalograptus altissimus*	49	2	1	0.04
Boucek & Pribyl 1941	*Petalograptus cf. Palmeus*	19	21	6	1.11
Boucek & Pribyl 1941	*Petalograptus cf. Palmeus*	35	7		0.20
Boucek & Pribyl 1941	*Petalograptus cf. Palmeus*	25	20		0.80
Lenz 1982	*Petalograptus cf. Palmeus clavatus*	48	69	1.5	1.44
Muller & Schouer 1969	*Petalograptus cf. Tenuis*	79	121	6	1.53
Muller & Schouer 1969	*Petalograptus cf. Tenuis*	65	96	4	1.48
A.Munch 1952.	*Petalograptus conicus*	21	6		0.29
A.Munch 1952.	*Petalograptus conicus*	19	5		0.26
A.Munch 1952.	*Petalograptus elongatus*	40	9		0.23
A.Munch 1952.	*Petalograptus elongatus*	37	7		0.19
Boucek & Pribyl 1941	*Petalograptus elongatus*	93	24		0.26

Reference	Species	Colony (mm)	Virgula (mm)	Virgella (mm)	virgula/ colony
Muller & Schouer 1969	*Petalograptus elongatus*	81	124		1.53
Xu 1983	*Petalograptus elongatus*	49	54	1	1.10
Xu 1983	*Petalograptus elongatus*	68.5	49	1	0.72
Lenz 1982	*Petalograptus elongatus*	81	47	4	0.58
A.Munch 1952.	*Petalograptus elongatus linearis*	28	4	1	0.14
A.Munch 1952.	*Petalograptus folium*	35	53		1.51
Muller & Schouer 1969	*Petalograptus folium*	62	62		1.00
Xu 1983	*Petalograptus fusiformis*	46	19		0.41
Xu 1983	*Petalograptus fusiformis*	59	35		0.59
Xu 1983	*Petalograptus fusiformis*	63	38		0.60
A.Munch 1952.	*Petalograptus giganteus*	45	7		0.16
A.Munch 1952.	*Petalograptus giganteus*	41	8		0.20
Xu 1983	*Petalograptus globosus*	19	12		0.63
A.Munch 1952.	*Petalograptus hispanicus*	17	10	2	0.59
Boucek & Pribyl 1941	*Petalograptus hispanicus*	35	33		0.94
Xu 1983	*Petalograptus hispanicus*	33	42		1.27
A.Munch 1952.	*Petalograptus intermedius*	29	4		0.14
A.Munch 1952.	*Petalograptus minor*	12.5	7		0.56
A.Munch 1952.	*Petalograptus ovato-elongatus*	16	7		0.44
A.Munch 1952.	*Petalograptus ovato-elongatus*	32	53		1.66
A.Munch 1952.	*Petalograptus ovatus*	8	4		0.50
A.Munch 1952.	*Petalograptus ovatus*	13	5	1.5	0.38
A.Munch 1952.	*Petalograptus ovatus*	14	4	0.5	0.29
Boucek & Pribyl 1941	*Petalograptus ovatus*	19	21	6	1.11
Boucek & Pribyl 1941	*Petalograptus paalmeus clavatus*	82.5	22	0.5	0.27
A.Munch 1952.	*Petalograptus palmeus*	29	21		0.72
A.Munch 1952.	*Petalograptus palmeus*	34	19		0.56
A.Munch 1952.	*Petalograptus palmeus clavatus*	35	10		0.29

Reference	Species	Colony (mm)	Virgula (mm)	Virgella (mm)	virgula/ colony
Muller & Schouer 1969	*Petalograptus palmeus clavatus*	120	124	4	1.03
A.Munch 1952.	*Petalograptus palmeus ellesi*	27	4		0.15
Boucek & Pribyl 1941	*Petalograptus palmeus palmeus*	67	47.5		0.71
Muller & Schouer 1969	*Petalograptus palmeus palmeus*	81	80		0.99
Muller & Schouer 1969	*Petalograptus palmeus palmeus*	65	46		0.71
A.Munch 1952.	*Petalograptus palmeus posthumus*	18	2		0.11
A.Munch 1952.	*Petalograptus palmeus posthumus*	16.5	2		0.12
A.Munch 1952.	*Petalograptus praecedens*	16	5.5	1	0.34
A.Munch 1952.	*Petalograptus praecedens*	22	9		0.41
A.Munch 1952.	*Petalograptus praecursor*	19	4.5		0.24
A.Munch 1952.	*Petalograptus primulus*	35	5		0.14
Bulman 1964	*Petalograptus sp.*	16	21	1	1.31
Bulman 1964	*Petalograptus speciosus*	25	38	1	1.52
A.Munch 1952.	*Petalograptus tenuis*	21.5	9	1	0.42
Muller & Schouer 1969	*Petalograptus tenuis*	70	161	3	2.30
Muller & Schouer 1969	*Petalograptus tenuis*	73	121	5	1.66
Muller & Schouer 1969	*Petalograptus tenuis*	73	122		1.67
A.Munch 1952.	*Ps. C. extremus*	12	4.5		0.38
A.Munch 1952.	*Ps. C. extremus*	8.5	8	1	0.94
A.Munch 1952.	*Ps. C. extremus*	7	5	1	0.71
A.Munch 1952.	*Ps. C. minutus*	10	2	0.5	0.20
Mu 1962	*Pseudoclimacograptus qilianshanensis*	15	11	0.5	0.73
Mu 1962	*Pseudoclimacograptus qilianshanensis*	13	18		1.38
Mu 1962	*Pseudoclimacograptus qilianshanensis tenuis*	39	26	4.5	0.67
Bulman 1964	*Pseudoclimacograptus scharenbergi*	50	18		0.36
Elles & Wood 1901-1918	*Climacograptus scalaris*	29	4		0.14
Elles & Wood 1901-1918	*Climacograptus scalaris*	27	14		0.52

Reference	Species	Colony (mm)	Virgula (mm)	Virgella (mm)	virgula/ colony
Elles & Wood 1901-1918	*Climacograptus medius*	31	5		0.16
Elles & Wood 1901-1918	*Climacograptus medius*	30	3		0.10
Elles & Wood 1901-1918	*Climacograptus medius*	17	9		0.53
Elles & Wood 1901-1918	*Climacograptus medius*	7	10		1.43
Elles & Wood 1901-1918	*Climacograptus rectangularis*	36	4		0.11
Elles & Wood 1901-1918	*Climacograptus minimus*	12	4		0.33
Elles & Wood 1901-1918	*Climacograptus minimus*	19	6		0.32
Elles & Wood 1901-1918	*Climacograptus minimus*	18	2		0.11
Elles & Wood 1901-1918	*Climacograptus minimus*	18	5		0.28
Elles & Wood 1901-1918	*Climacograptus latus*	20	6		0.30
Elles & Wood 1901-1918	*Climacograptus antiquus*	31	17		0.55
Elles & Wood 1901-1918	*Climacograptus antiquus*	30	14		0.47
Elles & Wood 1901-1918	*Climacograptus antiquus linneatus*	42	9		0.21
Elles & Wood 1901-1918	*Climacograptus antiquus linneatus*	37	19		0.51
Elles & Wood 1901-1918	*Climacograptus antiquus bursifer*	36	14		0.39
Elles & Wood 1901-1918	*Climacograptus caudatus*	21	17		0.81
Elles & Wood 1901-1918	*Climacograptus tubiferus*	37	18		0.49
Elles & Wood 1901-1918	*Climacograptus tubiferus*	40	12		0.30
Elles & Wood 1901-1918	*Climacograptus tubiferus*	27	17		0.63
Elles & Wood 1901-1918	*Climacograptus tubiferus*	37	16		0.43
Elles & Wood 1901-1918	*Climacograptus styloideus*	54	7		0.13
Elles & Wood 1901-1918	*Climacograptus styloideus*	30	19		0.63
Elles & Wood 1901-1918	*Climacograptus styloideus*	41	7		0.17
Elles & Wood 1901-1918	*Climacograptus styloideus*	37	10		0.27
Elles & Wood 1901-1918	*Climacograptus scharenbergi*	35	4		0.11
Elles & Wood 1901-1918	*Climacograptus scharenbergi*	30	5		0.17
Elles & Wood 1901-1918	*Climacograptus scharenbergi*	16	27		1.69
Elles & Wood 1901-1918	*Orthograptus quadrimucranatus*	51	5.5		0.11

Reference	Species	Colony (mm)	Virgula (mm)	Virgella (mm)	virgula/ colony
Elles & Wood 1901-1918	*Orthograptus quadrimucranatus*	53	3		0.06
Elles & Wood 1901-1918	*Orthograptus pageanus*	40	42		1.05
Elles & Wood 1901-1918	*Orthograptus pageanus*	13	14		1.08
Elles & Wood 1901-1918	*Orthograptus pageanus*	11	7		0.64
Elles & Wood 1901-1918	*Orthograptus pageanus micracanthus*	28	12		0.43
Elles & Wood 1901-1918	*Orthograptus pageanus micracanthus*	28	5		0.18
Elles & Wood 1901-1918	*Orthograptus pageanus micracanthus*	23	5		0.22
Elles & Wood 1901-1918	*Orthograptus pageanus abnormispinosus*	20	17.5		0.88
Elles & Wood 1901-1918	*Orthograptus pageanus abnormispinosus*	23	16		0.70
Elles & Wood 1901-1918	*Orthograptus whitfieldi*	21	13		0.62
Elles & Wood 1901-1918	*Orthograptus whitfieldi*	21	16		0.76
Elles & Wood 1901-1918	*Orthograptus vesiculosus*	51	37		0.73
Elles & Wood 1901-1918	*Orthograptus vesiculosus*	27	31		1.15
Elles & Wood 1901-1918	*Orthograptus vesiculosus penna*	19	32.5		1.71
Elles & Wood 1901-1918	*Orthograptus calcaratus*	70	22		0.31
Elles & Wood 1901-1918	*Orthograptus calcaratus*	64	10		0.16
Elles & Wood 1901-1918	*Orthograptus calcaratus basilicus*	66	17		0.26
Elles & Wood 1901-1918	*Orthograptus calcaratus basilicus*	54	8		0.15
Elles & Wood 1901-1918	*Orthograptus calcaratus basilicus*	56	23		0.41
Elles & Wood 1901-1918	*Orthograptus calcaratus basilicus*	42	21		0.50
Elles & Wood 1901-1918	*Orthograptus calcaratus tenuicornis*	19	25		1.32
Elles & Wood 1901-1918	*Orthograptus calcaratus tenuicornis*	47	12		0.26
Elles & Wood 1901-1918	*Orthograptus calcaratus vulgatus*	47	20		0.43
Elles & Wood 1901-1918	*Orthograptus calcaratus vulgatus*	61	25		0.41
Elles & Wood 1901-1918	*G. teretiusculus siccatus*	6	3		0.50
Elles & Wood 1901-1918	*Mesograptus faliaceus*	28	6		0.21

Reference	Species	Colony (mm)	Virgula (mm)	Virgella (mm)	virgula/ colony
Elles & Wood 1901-1918	*M. multidens compactus*	53	16		0.30
Elles & Wood 1901-1918	*M. multidens compactus*	24	9		0.38
Elles & Wood 1901-1918	*M. multidens compactus*	28	9		0.32
Elles & Wood 1901-1918	*M. multidens compactus*	27	21		0.78
Elles & Wood 1901-1918	*M. multidens compactus*	28	5		0.18
Elles & Wood 1901-1918	*Amplexograptus perexcoratus*	16	3		0.19
Elles & Wood 1901-1918	*Amplexograptus perexcoratus*	21	7		0.33
Elles & Wood 1901-1918	*Amplexograptus coelatus*	21	11		0.52
Elles & Wood 1901-1918	*Amplexograptus confertus*	6	4		0.67
Elles & Wood 1901-1918	*Petalograptus palmeus*	13	42		3.23
Elles & Wood 1901-1918	*Petalograptus palmeus*	15	21		1.40
Elles & Wood 1901-1918	*Petalograptus palmeus latus*	22	6		0.27
Elles & Wood 1901-1918	*Petalograptus palmeus tenuis*	10	4		0.40
Elles & Wood 1901-1918	*Petalograptus palmeus tenuis*	8	4		0.50
Elles & Wood 1901-1918	*Petalograptus palmeus tenuis*	5	5		1.00
Elles & Wood 1901-1918	*Petalograptus palmeus ovato-elongatus*	13	4		0.31
Elles & Wood 1901-1918	*Petalograptus folium*	19	8		0.42
Elles & Wood 1901-1918	*Cephalograptus tubulariformis*	14	15		1.07
Elles & Wood 1901-1918	*Crytograptus tricornis*	36	6		0.17
Elles & Wood 1901-1918	*Crytograptus antennarius*	14	9		0.64
Elles & Wood 1901-1918	*Crytograptus antennarius*	15.5	8		0.52
Elles & Wood 1901-1918	*Crytograptus antennarius*	21	13		0.62
Elles & Wood 1901-1918	*Crytograptus antennarius*	7	11		1.57
Elles & Wood 1901-1918	*Crytograptus hopkinsoni*	17	4		0.24
Elles & Wood 1901-1918	*Crytograptus hopkinsoni*	17	12		0.71
Elles & Wood 1901-1918	*Petalograptus phylloides*	3	2		0.67
Elles & Wood 1901-1918	*Petalograptus phylloides*	2.5	2		0.80

Reference	Species	Colony (mm)	Virgula (mm)	Virgella (mm)	virgula/ colony
Elles & Wood 1901-1918	*G. hincksii*	19	17.5		0.92
Elles & Wood 1901-1918	*G. hincksii*	15	12		0.80
Elles & Wood 1901-1918	*G. hincksii*	23	6		0.26
Elles & Wood 1901-1918	*G. hincksii*	5	3		0.60
Elles & Wood 1901-1918	*G. hincksii*	18	28		1.56
Elles & Wood 1901-1918	*G. hincksii*	19	19		1.00
Elles & Wood 1901-1918	*G. hincksii fimbriatus*	9	3		0.33
Elles & Wood 1901-1918	*G. acanthus*	14	3		0.21
Elles & Wood 1901-1918	*G. armatus*	9	9		1.00
Elles & Wood 1901-1918	*G. armatus*	8.5	12		1.41
Elles & Wood 1901-1918	*G. armatus*	9	5		0.56
Elles & Wood 1901-1918	*Hallograptus mucranatus*	45	4		0.09
Elles & Wood 1901-1918	*Hallograptus mucranatus bimucranatus*	33	4		0.12
Elles & Wood 1901-1918	*Hallograptus mucranatus nobilis*	66	13		0.20
Elles & Wood 1901-1918	*Hallograptus mucranatus inutilis*	8	4		0.50
Elles & Wood 1901-1918	*Thysanograptus retusus*	14	4		0.29
Elles & Wood 1901-1918	*Thysanograptus retusus*	15	4		0.27
Elles & Wood 1901-1918	*Dimorphograptus elongatus*	30	25		0.83
Bulman 1932	*Climacograptus orthoceratophilus*	29	45		1.55
Bulman 1932	*Climacograptus orthoceratophilus*	98	10		0.10
Bulman 1932	*Climacograptus sp.*	45	11		0.24
Bulman 1932	*Climacograptus sp.*	43	56		1.30
Bulman 1932	*Climacograptus sp.*	28.5	18		0.63
Bulman 1932	*Climacograptus diplacantus*	28	32		1.14
Bulman 1932	*Climacograptus diplacantus*	22.5	25		1.11
Bulman 1932	*Climacograptus schaerenbergi*	23	8		0.35

Reference	Species	Colony (mm)	Virgula (mm)	Virgella (mm)	virgula/ colony
Bulman 1932	*Climacograptus schaerenbergi*	30	13		0.43
Bulman 1932	*Climacograptus schaerenbergi*	50	6		0.12
Bulman 1932	*Climacograptus schaerenbergi*	27	11		0.41
Bulman 1932	*Climacograptus schaerenbergi*	26	14		0.54
Bulman 1932	*Climacograptus schaerenbergi*	39	13		0.33
Bulman 1932	*Climacograptus haljalensis*	55	30		0.55
Bulman 1932	*Laisograptus hysterix*	32	11		0.34
Bulman 1932	*Laisograptus hysterix*	46	9		0.20
Bulman 1932	*Laisograptus hysterix*	30	17		0.57
Mitchell 1987	*Paraclimacograptus innotatus obesus*	23	16		0.70
Mitchell 1987	*Climacograptus (diplacanthograptus) spiniferus*	78	24		0.31
Mitchell 1987	*Climacograptus (climacograptus) caudatus*	36	16		0.44
Mitchell 1987	*Prolasiograptus haplus*	26	13.5		0.52
Mitchell 1987	*Pseudoclimacograptus (Archiclimacograptus) luperus*	36	35		0.97
Mitchell 1987	*Undulograptus paradoxus*	26	26		1.00
Mitchell 1987	*Eoglyptograptus dentatus sensu*	111	27		0.24
Mitchell 1987	*Hustedograptus uplandicus*	32.5	11		0.34
Mitchell 1987	*Hustedograptus teretiusculus sensu*	22.5	33		1.47
Mitchell 1987	*Dicranograptus nicholsoni longibasalis*	30	25		0.83
Hughes, Rickards & Williams 1980	*Glyptograptus sp.*	43	35		0.81
Hughes, Rickards & Williams 1980	*Glossograptus sp.*	45	15		0.33
Hughes, Rickards & Williams 1980	*Glossograptus sp.*	76	35		0.46

Reference	Species	Colony (mm)	Virgula (mm)	Virgella (mm)	virgula/ colony
WBN Berry	*Glyptograptus persculptus*	41	21		0.51
Brussa, Toro & Ortega 1996	*Climacograptus normalis*	75	52		0.69
Brussa, Toro & Ortega 1996	*Pseudoclimacograptus (Climacograptus) cingolani*	32	6.5		0.20
Brussa, Toro & Ortega 1996	*Glyptograptus persculptus*	27	6.5		0.24

Monograptid data

Reference	Species	Colony (mm)	Virgula (mm)	Virgella (mm)	virgula/ colony
Xiaofeng & Zhaogui 1984	*Monograptus aequabilis*	49	4.5	1	0.09
Xiaofeng & Zhaogui 1984	*Monograptus aequabilis*	29	8	1	0.28
Jackson 1971	*Monograptus aequabilus notoaequabilis*	61	29	0.5	0.48
Cuerda 1974	*Monograptus argebtius*	32	13	1.5	0.41
Palmer 1970	*Monograptus auctus*	120	24	4	0.20
Palmer 1970	*Monograptus auctus*	36	7	3	0.19
Jaeger 1964	*Monograptus chimeara*	34	13	1.5	0.38
Ofversigt 1982	*Monograptus colonus*	55	9		0.16
Ofversigt 1982	*Monograptus cultellus*	8	4		0.50
Ofversigt 1982	*Monograptus cultellus*	24	9		0.38
Buchroithner et al 1978	*Monograptus dubius*	72	10	1	0.14
Buchroithner et al 1978	*Monograptus dubius*	107	37		0.35
Ofversigt 1982	*Monograptus dubius*	58	16	4	0.28
Van Phuc 1998	*Monograptus hercynicus*	49	8		0.16
Palmer 1970	*Monograptus ludensis*	139	67	3	0.48
Palmer 1970	*Monograptus ludensis*	83.5	55	3.5	0.66
Palmer 1970	*Monograptus ludensis*	41	33		0.80
Xiaofeng & Zhaogui 1984	*Monograptus microdon microdon*	23	4	0.5	0.17
Rickards & Palmer 1977	*Monograptus sp.*	72	64	1	0.89
Jaeger 1983	*Monograptus telleri*	106	16		0.15
Ofversigt 1982	*Monograptus uncinatus*	46	9		0.20
Garret & Rickards 1984	*Monograptus uncinatus uncinatus*	52	14	1	0.27
Jerzmonski 1955	*Monograptus varieans pumilus*	41	16	2	0.39
Teller 1964	*Monoograptus angustidens*	93.5	19	3	0.20
Mihajlovic 1974	*Pristiograptus dubius*	39	18		0.46
Mihajlovic 1974	*Pristiograptus graciosus*	53	15		0.28

Reference	Species	Colony (mm)	Virgula (mm)	Virgella (mm)	virgula/ colony
Teller 1964	*Pristograptus aduncus*	59	20	3	0.34
Cuerda 1974	*Pristograptus aff. Jaegeri*	24	6	0.5	0.25
Teller 1964	*Pristograptus bugensius*	69.5	14	5	0.20
Teller 1964	*Pristograptus cheimensis*	105.5	10	3	0.09
Teller 1964	*Pristograptus ex. Gr. Dubius*	96	24	3	0.25
Teller 1964	*Pristograptus samsonowiczi*	42	6	1.5	0.14
Teller 1964	*Pristograptus varus*	69	25	4	0.36
Teller 1964	*Pristograptus varus*	63	21	5	0.33
Elles & Wood 1901-1918	*Monograptus vulgaris*	46	2		0.04
Elles & Wood 1901-1918	*M. compactus*	38	3		0.08
Elles & Wood 1901-1918	*M. compactus*	36	4		0.11
Elles & Wood 1901-1918	*M. chimaera*	21.5	3		0.14
Elles & Wood 1901-1918	*M. c. semispinosus*	22	3		0.14
Elles & Wood 1901-1918	*M. c. semispinosus*	18	5		0.28
Elles & Wood 1901-1918	*M. c. Salweyi*	12.5	2		0.16
Elles & Wood 1901-1918	*M. c. Salweyi*	13	3		0.23
Elles & Wood 1901-1918	*M. varians*	26	13		0.50
Elles & Wood 1901-1918	*M. varians*	23	10		0.43
Elles & Wood 1901-1918	*M. leintwardienesis*	7.5	1		0.13
Elles & Wood 1901-1918	*M. leintwardienesis*	13.5	1		0.07
Elles & Wood 1901-1918	*M. l. incipiens*	10	1.5		0.15
Elles & Wood 1901-1918	*M. uncinatus micropama*	17	2		0.12
Elles & Wood 1901-1918	*M. uncinatus micropama*	21	2		0.10
Elles & Wood 1901-1918	*M. halli*	30	1.5		0.05
Zhang & Lenz 1997	*Colonograptus praedeubeli*	25	29		1.16
Zhang & Lenz 1997	*Colonograptus praedeubeli*	71	23		0.32
Zhang & Lenz 1997	*Colonograptus praedeubeli*	40	16		0.40
Zhang & Lenz 1997	*Colonograptus praedeubeli*	42	10		0.24

Reference	Species	Colony (mm)	Virgula (mm)	Virgella (mm)	virgula/ colony
Zhang & Lenz 1997	*Colonograptus praedeubeli*	25	16		0.64
Zhang & Lenz 1997	*Saetograptus fritschi linearis*	37	12		0.32
Zhang & Lenz 1997	*Saetograptus fritschi linearis*	62	8		0.13
Zhang & Lenz 1997	*Saetograptus lentwardinensis*	91	22		0.24
Zhang & Lenz 1997	*Saetograptus lentwardinensis*	70	12		0.17
Zhang & Lenz 1997	*Saetograptus chimaera*	12.9	16		1.24
Zhang & Lenz 1997	*Pseudomonoclimacis dalejensis*	24	8		0.33
Zhang & Lenz 1997	*Pseudomonoclimacis dalejensis*	20	4.5		0.23
Garratt & Rickards 1987	*Monograptus thomasi*	60	16		0.27
Palmer 1986	*Saetograptus varians*	18	20		1.11
Palmer 1986	*Saetograptus varians*	20.5	28		1.37
Palmer 1986	*Saetograptus varians*	19	30		1.58
Palmer 1986	*Saetograptus varians*	23	19		0.83
Palmer 1986	*Saetograptus varians*	21	33		1.57
Palmer 1986	*Saetograptus varians*	26	45		1.73
Palmer 1986	*Saetograptus varians*	28	23		0.82
Palmer 1986	*Saetograptus varians*	32	31		0.97
Palmer 1986	*Saetograptus varians*	33	52		1.58
Palmer 1986	*Saetograptus varians*	36	51		1.42
Palmer 1986	*Saetograptus varians*	37	26		0.70
Palmer 1986	*Saetograptus varians*	42	31		0.74
Palmer 1986	*Saetograptus varians*	33	41		1.24
Palmer 1986	*Saetograptus varians*	36	33		0.92
Palmer 1986	*Saetograptus varians*	42	37		0.88
Palmer 1986	*Saetograptus varians*	46	37		0.80
Rickards, Holland & Serpagli	*Monograptus praebercynicus*	35	10		0.29

Reference	Species	Colony (mm)	Virgula (mm)	Virgella (mm)	virgula/ colony
Rickards & Wright 1997 (Barnby hill)	*Pristograptus dubius cf. frequens*	81	5		0.06
Rickards & Wright 1997 (zonation)	*Pristograptus jaegeri*	77	9		0.12
Rickards & Wright 1997 (zonation)		80	7		0.09
Rickards & Wright 1997 (zonation)		67	32		0.48
Rickards & Wright 1997 (zonation)		36	12		0.33
Rickards & Wright 1997 (zonation)	*Pristograptus dubius*	92	15		0.16
Rickards & Wright 1997 (zonation)	*Monograptus ludensis*	98	9		0.09
Rickards & Wright 1997 (zonation)		26.5	4		0.15
Rickards & Wright 1997 (zonation)	*Monograptus sp.*	68	7		0.10
Rickards & Wright 1997 (zonation)	*Lobograptus sherrardae*	90	15		0.17

D. Real spine angles (degrees)

Reference	Figure	Species	virgella	av	av	th1[1]	th1[2]	th2[1]	th2[2]	th3[1]	th3[2]
Jackson 1973		*Amplexograptus aff. Promiens*		39	23						
Joanusson 1995		*Amplexograptus baltoscandius*		59	50						
Mitchell 1987	10A	*Amplexograptus bekkeri*				77					
Mitchell 1987	10B	*Amplexograptus bekkeri*				79					
Mitchell 1987	10D	*Amplexograptus bekkeri*				62	70				
Mitchell 1987	10E	*Amplexograptus bekkeri*				82	59				
Mitchell 1987	10F	*Amplexograptus bekkeri*				86	53				
Mitchell 1987	10G	*Amplexograptus bekkeri*				72	50				
Mitchell 1987	10H	*Amplexograptus bekkeri*				79					
Strachen 1959		*Amplexograptus bekkeri*				66	39	71	54	76	
Strachen 1959		*Amplexograptus bekkeri*				49	48	68	62	70	
Skwarko 1974		*Amplexograptus confertus*				102					
Skwarko 1974		*Amplexograptus confertus*				79	75				
Skwarko 1974		*Amplexograptus confertus*					79				
Skwarko 1974		*Amplexograptus confertus*					90				
Skwarko 1974		*Amplexograptus confertus*				60	77				
Skwarko 1974		*Amplexograptus confertus*				89	93				
Skwarko 1974		*Amplexograptus confertus*				93					
Skwarko 1974		*Amplexograptus confertus*				65					
Jackson 1973		*Amplexograptus inuiti*				50					
Mitchell 1987	9E	*Amplexograptus leptotheca*		49	37	73					
Finney 1986		*Amplexograptus maxwelli*		65	40	76					
Finney 1986		*Amplexograptus maxwelli*		48	48						
Walters 1977		*Amplexograptus sp.*				76	59				

Reference	Figure	Species	virgella	av	av	th1[1]	th1[2]	th2[1]	th2[2]	th3[1]	th3[2]
Finney 1986		*Amplexograptus sp. Aff. maxwelli*		56	56	52					
Jackson 1973		*Amplexograptus sp. Indet*		42	47						
Mitchell 1987	6J	*Climacograptus bicornis*	39			59					
Mitchell 1987	6O	*Climacograptus bicornis*				82					
Mitchell 1987	6L	*Climacograptus bicornis*				77	80				
Mitchell 1987	6P	*Climacograptus bicornis*				73					
Finney *et al* 1984		*Climacograptus bicornis*	18			75					
Finney 1986		*Climacograptus bicornis*				75					
Williams 1994		*Climacograptus bicornis*	37			51					
Williams 1994		*Climacograptus bicornis*	35			42					
Williams 1994		*Climacograptus bicornis*	29			35					
Bulman 1931	Fig III 1	*Climacograptus diplacanthus*	26			47					
Bulman 1931	6	*Climacograptus diplacanthus*	34			60					
Bulman 1931	7	*Climacograptus diplacanthus*	42			47					
Bulman 1931	14	*Climacograptus diplacanthus*	33			56					
Bulman 1931	16	*Climacograptus diplacanthus*	39			36					
Bulman 1931	19	*Climacograptus diplacanthus*	38			50					
Kirk 1975		*Climacograptus diplacanthus*	42			34					
AT Mu et al 1960		*Climacograptus diplacanthus*	41			58					
AT Mu et al 1960		*Climacograptus diplacanthus*	36			65					
AT Mu et al 1960		*Climacograptus diplacanthus*	51			48					
AT Mu et al 1960		*Climacograptus diplacanthus*	50			78					
AT Mu et al 1960		*Climacograptus diplacanthus*	59			81					
Bulman 1931	Fig. II 18	*Climacograptus haljalensis*				85	73				
Bulman 1931	20	*Climacograptus haljalensis*				58	49	72			

Reference	Figure	Species	virgella	av	av	th1[1]	th1[2]	th2[1]	th2[2]	th3[1]	th3[2]
Bulman 1931	21	*Climacograptus haljalensis*				56	49	84	61		
Bulman 1931	22	*Climacograptus haljalensis*				101	84	73	74		
Bulman 1931	23	*Climacograptus haljalensis*					44	73	66	77	
Bulman 1931	26	*Climacograptus haljalensis*				52	50	85	62		
Bulman 1931	27	*Climacograptus haljalensis*				82	84	69	74		
Bulman 1931	30	*Climacograptus haljalensis*				71		88			
Bulman 1931	32	*Climacograptus haljalensis*				74	45	90			
Bulman 1931	33	*Climacograptus haljalensis*				83	60	70	70		
Bulman 1932		*Climacograptus haljalensis*				86	64				
Bulman 1932		*Climacograptus haljalensis*				61	40	65			
Bulman 1932		*Climacograptus haljalensis*				60	50	68			
Jenkins et al 1982		*Climacograptus hastatus*				98	84				
Ji-jin & Han-jun 1988		*Climacograptus hastatus*				78	85				
Ji-jin & Han-jun 1988		*Climacograptus hastatus*				67	75				
Walters 1977		*Climacograptus inuiti*				67	103	102	86		
Walters 1977		*Climacograptus inuiti*				61	53	73	76		
Cox 1933		*Climacograptus inuiti*		35	35	89					
Cox 1933		*Climacograptus inuiti*		27	40	97					
Cox 1933		*Climacograptus inuiti*		62	56						
Cox 1933		*Climacograptus inuiti*		68	44						
Cox 1933		*Climacograptus inuiti*		70	46						
Cox 1933		*Climacograptus inuiti*		57	38	80					
Melchin 1986		*Climacograptus latus*		69	69	55					
Melchin 1986		*Climacograptus latus*		60	60	86					
Melchin 1986		*Climacograptus latus*				67					

Reference	Figure	Species	virgella	av	av	th1[1]	th1[2]	th2[1]	th2[2]	th3[1]	th3[2]
Melchin 1986		*Climacograptus latus*		65	65	87					
Melchin 1986		*Climacograptus latus*		49	49	68					
Ji-jin & Han-jun 1988		*Climacograptus leptothecalis*				28	32				
Ji-jin & Han-jun 1988		*Climacograptus leptothecalis*				28	40				
Munch 1952		*Climacograptus longifilis*	8			10					
Munch 1952		*Climacograptus longifilis*	4			10					
Storch 1982		*Climacograptus longifilis*	20			57					
Storch 1982		*Climacograptus longifilis*	14			9					
Jenkins et al 1982		*Climacograptus longispinus*	22			71					
Jenkins et al 1982		*Climacograptus longispinus*	36			85					
Jenkins et al 1982		*Climacograptus longispinus*	7			57					
Melchin 1986		*Climacograptus longispinus supernus*				50					
Melchin 1986		*Climacograptus longispinus supernus*				74	55				
Melchin 1986		*Climacograptus longispinus supernus*				50	65				
Melchin 1986		*Climacograptus longispinus supernus*				49	49				
Finney 1986		*Climacograptus manitouliensis*		42	42						
Bulman 1931	Fig IV 15	*Climacograptus orthoceratophilus*				67					
Bulman 1931	17	*Climacograptus orthoceratophilus*				55	51				
Bulman 1931	18	*Climacograptus orthoceratophilus*				69					
Bulman 1931	19	*Climacograptus orthoceratophilus*				54					
Bulman 1931	22	*Climacograptus orthoceratophilus*				70	56				

Reference	Figure	Species	virgella	av	av	th1[1]	th1[2]	th2[1]	th2[2]	th3[1]	th3[2]
Bulman 1931	23	*Climacograptus orthoceratophilus*					42				
Bulman 1931	25	*Climacograptus orthoceratophilus*					59				
Bulman 1931	26	*Climacograptus orthoceratophilus*				65	79				
Bulman 1931	Fig V 1	*Climacograptus orthoceratophilus*				73	50				
Bulman 1931	3	*Climacograptus orthoceratophilus*				61	41				
Bulman 1931	4	*Climacograptus orthoceratophilus*				77	63				
Kirk 1975		*Climacograptus orthoceratophilus*				59	51				
Bulman 1932		*Climacograptus orthoceratophilus*				70					
Bulman 1932		*Climacograptus orthoceratophilus*				85	75				
Bulman 1932		*Climacograptus orthoceratophilus*					58				
Bulman 1932		*Climacograptus orthoceratophilus*				47	56				
Mitchell 1986		*Climacograptus pygmaeus*		40	40						
Mitchell 1986		*Climacograptus pygmaeus*		37	32						
Mitchell 1986		*Climacograptus pygmaeus*		55	55						
Mitchell 1986		*Climacograptus pygmaeus*		45	48						
Mitchell 1986		*Climacograptus pygmaeus*		20	20						
Mitchell 1986		*Climacograptus pygmaeus*		51	38						
Finney 1986		*Climacograptus pygmaeus*		52	52						
Munch 1952		*Climacograptus resurectus*				22	12				
Bulman 1931	22	*Climacograptus sp.*		72	39						
Bulman 1931	28	*Climacograptus sp.*				73	83				
Bulman 1931	29	*Climacograptus sp.*				65	75				
Bulman 1931	30	*Climacograptus sp.*				93	79				
Bulman 1931	31	*Climacograptus sp.*				89	93				
Mitchell 1987	7G	*Climacograptus spiniferous*	65			69					

Reference	Figure	Species	virgella	av	av	th1[1]	th1[2]	th2[1]	th2[2]	th3[1]	th3[2]
Mitchell 1987	7I	*Climacograptus spiniferous*	26			65					
Mitchell 1987	7K	*Climacograptus spiniferous*	33			36					
Finney et al 1984		*Climacograptus spiniferous*	33			46					
Nomen Nudem 1983		*Climacograptus spiniferous*	39			56					
Finney 1986		*Climacograptus spiniferous*	67			69					
Finney 1986		*Climacograptus spiniferous*	40			40					
Clark & Strachen 1955		*Climacograptus spiniferous*	13			22					
Nomen Nudem 1983		*Climacograptus spiniferous spiniferous*	55			74					
Nomen Nudem 1983		*Climacograptus spiniferous spiniferous*	62			74					
Munch 1952		*Climacograptus supernus*				47	37				
Munch 1952		*Climacograptus supernus*				39	53				
Munch 1952		*Climacograptus trifilis*				39	34				
Storch 1982		*Climacograptus trifilis*				30	19				
Storch 1982		*Climacograptus trifilis*				28	24				
Munch 1952		*Climacograptus tuberculatus*				39	39				
Finney et al 1984		*Climacograptus typicalis*		27	27						
Mitchell 1986		*Climacograptus typicalis*		34	50						
Mitchell 1986		*Climacograptus typicalis*		84	21						
Mitchell 1986		*Climacograptus typicalis*		23	14						
Mitchell 1986		*Climacograptus typicalis*		30	39						
Mitchell 1986		*Climacograptus typicalis*		48	20						
Mitchell 1986		*Climacograptus typicalis*		90	90						
Mitchell 1986		*Climacograptus typicalis*		59	61						

Reference	Figure	Species	virgella	av	av	th1[1]	th1[2]	th2[1]	th2[2]	th3[1]	th3[2]
Mitchell 1986		*Climacograptus typicalis*		55	32						
Mitchell 1986		*Climacograptus typicalis*		26	26						
Mitchell 1986		*Climacograptus typicalis*		37	37						
Mitchell 1986		*Climacograptus typicalis*		43	24						
Bulman 1932		*Climacograptus typicalis*		50	42						
Bulman 1932		*Climacograptus typicalis*		56	49						
Bulman 1932		*Climacograptus typicalis*		68	55						
Bulman 1932		*Climacograptus typicalis*		27	34						
Bulman 1932		*Climacograptus typicalis*		11	10						
Bulman 1932		*Climacograptus typicalis*		45	28						
Williams 1994		*Climacograptus wilsoni*				75					
Williams 1994		*Climacograptus wilsoni*				63	65				
Williams 1994		*Climacograptus wilsoni*				59	81				
Williams 1994		*Climacograptus wilsoni*				86	89				
Bulman 1934		*Cryptograptus tricornis*				61	55				
Munch 1952		*Cystograptus tricornis*				24	22				
Mitchell 1987	2H	*Dicranograptus nicholosoni longibasalis*				81					
Mitchell 1987	2R	*Dicranograptus nicholosoni longibasalis*				93	95				
Finney 1986		*Dicranograptus nicholsoni longibasalis*				75	84	78	60	106	
Skevington & Paris 1975		*Diplograptus ?fastigatus*				75					
Skevington 1970		*Diplograptus ellesi*				75					

Reference	Figure	Species	virgella	av	av	th1[1]	th1[2]	th2[1]	th2[2]	th3[1]	th3[2]
Skevington 1970		*Diplograptus ellesi*				53					
Skevington 1970		*Diplograptus ellesi*				58					
Clark & Strachen 1955		*Diplograptus molestus*		52	52	44					
Walters 1977		*Diplograptus sp.*				69	34				
Sudbury 1957		*Diplograptus spinulosus*				58	40	67			
Sudbury 1957		*Diplograptus spinulosus*				70	41	65	62		
Sudbury 1957		*Diplograptus spinulosus*				81	79	77			
C. Xu 1983		*Diplograptus tortithecatus*				59	59				
Finney 1986		*Glyptograptus cf. Teretiusculus*				83	68				
Skevington 1970		*Glyptograptus dentatus*				62	44				
Skevington 1970		*Glyptograptus dentatus*				44	86				
Jackson 1971		*Glyptograptus hudsoni*		52	62						
Jackson 1971		*Glyptograptus hudsoni*		61	61						
Jackson 1971		*Glyptograptus hudsoni*		21	29						
Jackson 1971		*Glyptograptus hudsoni*		72	72	79					
Jackson 1971		*Glyptograptus hudsoni*		17	17	78					
Jackson 1971		*Glyptograptus hudsoni*		63	63	83					
Mitchell 1987	8L	*Glyptograptus Inuiti*		52	54	90					
Walters 1977		*Glyptograptus lorrainensis*		58	58	78					
Walters 1977		*Glyptograptus lorrainensis*		66	66	62					
Walters 1977		*Glyptograptus lorrainensis*		26	26	69					
Mitchell & Bergstroim 1977		*Glyptograptus lorrainensis anacanthus*		13	37						
Mitchell & Bergstroim 1977		*Glyptograptus lorrainensis anacanthus*		23	23						

Reference	Figure	Species	virgella	av	av	th1[1]	th1[2]	th2[1]	th2[2]	th3[1]	th3[2]
Mitchell & Bergstroim 1977		*Glyptograptus lorrainensis anacanthus*		29	29						
Mitchell 1987	8A	*Glyptograptus pygmaeus*		59	59						
Mitchell 1987	8B	*Glyptograptus pygmaeus*		47	47						
Mitchell 1987	8C	*Glyptograptus pygmaeus*		47	47						
Mitchell 1987	8D	*Glyptograptus pygmaeus*		66	66						
Mitchell 1987	8H	*Glyptograptus pygmaeus*		87	87						
Mitchell 1987	8O	*Glyptograptus pygmaeus*		58	43						
Mitchell 1987	8P	*Glyptograptus pygmaeus*		53	46						
Mitchell 1987	8G	*Glyptograptus typicalis*		82	23						
Mitchell 1987	8N	*Glyptograptus typicalis*		49	23						
Mitchell 1987	2L	*H. teretiusculus sensu*				57	53				
Mitchell 1987	2A	*H. uplandicus*		64	36	59	63				
Mitchell 1987	2E	*H. uplandicus*		29	29						
Mitchell 1987	2F	*H. uplandicus*		49	28	65	60				
Mitchell 1987	2G	*H. uplandicus*		22	22	65	73				
Mitchell 1987	2K	*H. uplandicus*		40	19	42					
Walters 1977		*Neurograptus margariatus*		53	53	76	70	54	76	69	69
Picarra 1995		*Normalograptus trifilis*				22	40				
Picarra 1995		*Normalograptus trifilis*				24	38				
Finney 1986		*Orthograptus amplexicaulis*		68	68	68					
Finney 1986		*Orthograptus amplexicaulis*		67	50	79					
Williams 1994		*Orthograptus ex. Gr. Amplexicaulis*		47	25						
Williams 1994		*Orthograptus ex. Gr. Amplexicaulis*		18	18	80					
Williams 1994		*Orthograptus ex. Gr. Amplexicaulis*				61					

Reference	Figure	Species	virgella	av	av	th1[1]	th1[2]	th2[1]	th2[2]	th3[1]	th3[2]
Williams 1994		*Orthograptus ex. Gr. Amplexicaulis*		78	65	60					
Eisenack 1959		*Orthograptus gracilis*		74	65	95					
Bulman 1931	Fig VII 1	*Orthograptus gracilis*		81	15	92					
Bulman 1931	2	*Orthograptus gracilis*		80	27	88					
Bulman 1931	3	*Orthograptus gracilis*		54	49	71					
Bulman 1931	4	*Orthograptus gracilis*		101	53	86					
Bulman 1931	6	*Orthograptus gracilis*		65	64						
Bulman 1931	8	*Orthograptus gracilis*		61	30	74					
Bulman 1931	10	*Orthograptus gracilis*		64	63	76					
Bulman 1931	11	*Orthograptus gracilis*		53	53	78					
Bulman 1931	22	*Orthograptus gracilis*		106	70	85					
Bulman 1931	Fig VI 21	*Orthograptus gracilis*		58	58						
Bulman 1931	22	*Orthograptus gracilis*		72	24						
Bulman 1931	25	*Orthograptus gracilis*		127	64	62					
Bulman 1931	27	*Orthograptus gracilis*		93	67	65					
Bulman 1931	28	*Orthograptus gracilis*		55	49	90					
Bulman 1931	29	*Orthograptus gracilis*		69	45						
Bulman 1931	30	*Orthograptus gracilis*		67	67	108					
Bulman 1931	31	*Orthograptus gracilis*		78	70	67					
Bulman 1931	32	*Orthograptus gracilis*		72	52						
Bulman 1931	34	*Orthograptus gracilis*		71	62	68					
Bulman 1931	35	*Orthograptus gracilis*		63	50	93					
Bulman 1931	12	*Orthograptus gracilis*		68	52	66					
Bulman 1931	16	*Orthograptus gracilis*		64	62	61					
Bulman 1931	17	*Orthograptus gracilis*		65	47	59					

Reference	Figure	Species	virgella	av	av	th1[1]	th1[2]	th2[1]	th2[2]	th3[1]	th3[2]
Bulman 1931	18	*Orthograptus gracilis*		72	70	82					
Bulman 1931	22	*Orthograptus gracilis*				87					
Kirk 1975		*Orthograptus gracilis*		48	73	70					
Bulman 1932		*Orthograptus gracilis*		79	24	84					
Bulman 1932		*Orthograptus gracilis*		82	70	63					
Bulman 1932		*Orthograptus gracilis*		57	49	77					
Bulman 1932		*Orthograptus gracilis*		66	66	109					
Skevington & Paris 1975		*Orthograptus pageanus microcanthus*				84					
Mitchell 1987	9A	*Orthograptus quadrimucronatus*		8	30	84					
Mitchell 1987	9D	*Orthograptus quadrimucronatus*		14	12	98					
Mitchell 1987	9F	*Orthograptus quadrimucronatus*		14	14	58					
Mitchell 1987	9G	*Orthograptus quadrimucronatus*		40	54	76					
Finney *et al* 1984		*Orthograptus quadrimucronatus*		27	32		77		90		
Nomen Nudem 1983		*Orthograptus quadrimucronatus*		14	14	57	79				
Herr 1971		*Orthograptus quadrimucronatus*		93	39	58					
Herr 1971		*Orthograptus quadrimucronatus*		59	31		34				
Herr 1971		*Orthograptus quadrimucronatus*		54	57	70					
Herr 1971		*Orthograptus quadrimucronatus*		38	38						
Walters 1977		*Orthograptus ruedemanni*				17					
Walters 1977		*Orthograptus ruedemanni*				54					
Walters 1977		*Orthograptus ruedemanni*				67	76				
Nomen Nudem 1983		*Orthograptus ruedemanni*				102	88				
Clark & Strachen 1955		*Orthograptus sp. Cf. pageanus microcanthus*		56	56	82					

Reference	Figure	Species	virgella	av	av	th1[1]	th1[2]	th2[1]	th2[2]	th3[1]	th3[2]
Clark & Strachen 1955		*Orthograptus sp. Cf. Peosta*				78					
Clark & Strachen 1955		*Orthograptus sp. Cf. Peosta*		50	50	91					
Munch 1952		*Orthograptus tridens*				34	23				
Skevington & Paris 1975		*Orthograptus truncatus abbreviatus*				59	61				
Skevington & Paris 1975		*Orthograptus truncatus abbreviatus*				50	87				
Strachen 1959		*Orthograptus uplandicus*		45	24	90	72				
Strachen 1959		*Orthograptus uplandicus*		25	25	90	83				
Skevington 1960		*Orthoretiolites hami*		38	38	104	70	105	87		
Skevington 1960		*Orthoretiolites hami*		42	34	66	76	82	84		
Skevington 1960		*Orthoretiolites hami*		63	39	80	86	104	58		
Skevington 1960		*Orthoretiolites hami*		66	42						
Skevington 1960		*Orthoretiolites hami*		40	29						
Skevington 1960		*Orthoretiolites hami*		49	38	70	90	93	91		
Mitchell 1987	6D	*P. (p.) schaerenbergi*	24			55					
Mitchell 1987	6E	*P. (p.) schaerenbergi*	27			74					
Mitchell 1987	6F	*P. (p.) schaerenbergi*	39			69					
Mitchell 1987	6G	*P. (p.) schaerenbergi*	27			59					
Mitchell 1987	6I	*P. (p.) schaerenbergi*				38					
Mitchell 1987	2O	*P. distichus*				66					
Mitchell 1987	2P	*P. distichus*				81	81				

Reference	Figure	Species	virgella	av	av	th1[1]	th1[2]	th2[1]	th2[2]	th3[1]	th3[2]
AT Mu 1962		*Paraglossograptus tricornis distincta*				62	60				
Strachan 1954		*Peira. Fallax*		65	29	110					
Strachan 1954		*Peira. Fallax*		65	65						
Strachan 1954		*Peira. Fallax*		28	18	81					
Strachan 1954		*Peira. Fallax*		64	25	62					
		Mean	**34.5**		**48.6**	**66.6**	**61.6**	**78.2**	**71.8**	**79.6**	**69.0**
		Standard deviation	15.5		19.8	19.4	20.0	13.3	11.9	15.2	

E. Real spine lengths (mm)

Reference	Figure	Species	virgella	av	av	th1[1]	th1[2]	th2[1]	th2[2]	th3[1]
Walters 1977		*Diplograptus sp.*				0.20	0.30			
Mitchell 1987	10A	*Amplexograptus bekkeri*				0.19				
Mitchell 1987	10B	*Amplexograptus bekkeri*				0.23				
Mitchell 1987	10D	*Amplexograptus bekkeri*				0.38	0.35			
Mitchell 1987	10E	*Amplexograptus bekkeri*				0.38	0.23			
Mitchell 1987	10F	*Amplexograptus bekkeri*				0.50	0.50			
Mitchell 1987	10G	*Amplexograptus bekkeri*				0.38	0.42			
Mitchell 1987	10H	*Amplexograptus bekkeri*				0.35				
Mitchell 1987	9E	*Amplexograptus leptotheca*		0.12	0.12	0.46				
Skwarko 1974		*Amplexograptus confertus*				0.14				
Skwarko 1974		*Amplexograptus confertus*				0.32	0.38	$2x10^{-4}$		
Skwarko 1974		*Amplexograptus confertus*								
Skwarko 1974		*Amplexograptus confertus*								
Skwarko 1974		*Amplexograptus confertus*				0.31	0.19			
Skwarko 1974		*Amplexograptus confertus*				0.22	0.22			
Skwarko 1974		*Amplexograptus confertus*				0.36				
Skwarko 1974		*Amplexograptus confertus*				0.45				
Walters 1977		*Amplexograptus sp.*				0.40	0.40			
Mitchell 1987	6J	*C. (C.) bicornis*	0.51			0.34				
Mitchell 1987	6O	*C. (C.) bicornis*	0.89			0.63				
Mitchell 1987	6L	*C. (C.) bicornis*	0.26			0.17	0.31			
Mitchell 1987	6P	*C. (C.) bicornis*	0.23			0.09				
Bulman 1931	Fig III 1	*C. diplacanthus*	1.29			1.00				
Bulman 1931	6	*C. diplacanthus*	1.29			0.50				
Bulman 1931	7	*C. diplacanthus*	1.21			1.07				
Bulman 1931	14	*C. diplacanthus*	1.21			0.50				
Bulman 1931	16	*C. diplacanthus*	1.18			0.91				
Bulman 1931	19	*C. diplacanthus*	0.79			0.86				
Bulman 1931	Fig. II 18	*C. haljalensis*				0.23	0.09			

Reference	Figure	Species	virgella	av	av	th1[1]	th1[2]	th2[1]	th2[2]	th3[1]
Bulman 1931	20	*C. haljalensis*				0.23	0.27	0.27		
Bulman 1931	21	*C. haljalensis*				0.29	0.29	0.29	0.21	
Bulman 1931	22	*C. haljalensis*				0.25	0.25	0.17	0.17	
Bulman 1931	23	*C. haljalensis*					0.17	0.08	0.17	0.08
Bulman 1931	26	*C. haljalensis*				0.29	0.29	0.29	0.21	
Bulman 1931	27	*C. haljalensis*				0.25	0.25	0.25	0.17	
Bulman 1931	30	*C. haljalensis*				0.25		0.11		
Bulman 1931	32	*C. haljalensis*				0.18	0.18	0.14		
Bulman 1931	33	*C. haljalensis*				0.18	0.18	0.11	0.07	
Bulman 1931	Fig IV 15	*C. orthoceratophilus*				0.39				
Bulman 1931	17	*C. orthoceratophilus*				0.32	0.29			
Bulman 1931	18	*C. orthoceratophilus*				0.46				
Bulman 1931	19	*C. orthoceratophilus*				0.36				
Bulman 1931	22	*C. orthoceratophilus*				0.35	0.30			
Bulman 1931	23	*C. orthoceratophilus*					0.29			
Bulman 1931	25	*C. orthoceratophilus*					0.36			
Bulman 1931	26	*C. orthoceratophilus*				0.29	0.43			
Bulman 1931	Fig V 1	*C. orthoceratophilus*				0.27	0.32			
Bulman 1931	3	*C. orthoceratophilus*				0.43	0.21			
Bulman 1931	4	*C. orthoceratophilus*				0.43	0.29			
Mitchell 1987	7G	*C.(D.) spiniferous*	0.53			0.47				
Mitchell 1987	7I	*C.(D.) spiniferous*	0.40			0.43				
Mitchell 1987	7K	*C.(D.) spiniferous*	0.66			0.38				
Finney et al 1984		*Climacograptus bicornis*	1.10			2.50				
Jenkins et al 1982		*Climacograptus hastatus*				0.71	0.86			
Walters 1977		*Climacograptus inuiti*				0.15	0.30	0.05	0.15	
Walters 1977		*Climacograptus inuiti*				0.10	0.05	0.05	0.10	
Munch 1952		*Climacograptus longifilis*								
Munch 1952		*Climacograptus longifilis*								

Reference	Figure	Species	virgella	av	av	th1[1]	th1[2]	th2[1]	th2[2]	th3[1]
Storch 1982		*Climacograptus longifilis*	4.00			2.67				
Storch 1982		*Climacograptus longifilis*	7.67			7.33				
Jenkins et al 1982		*Climacograptus longispinus*	3.86							
Jenkins et al 1982		*Climacograptus longispinus*	1.86							
Jenkins et al 1982		*Climacograptus longispinus*	6.71							
Munch 1952		*Climacograptus resurectus*								
Bulman 1931	22	*Climacograptus sp.*		0.07	0.36					
Bulman 1931	28	*Climacograptus sp.*				0.36	0.36			
Bulman 1931	29	*Climacograptus sp.*				0.29	0.21			
Bulman 1931	30	*Climacograptus sp.*				0.21	0.43			
Bulman 1931	31	*Climacograptus sp.*				0.43	0.21			
Finney et al 1984		*Climacograptus spiniferous*	0.50			0.80				
Nomen Nudem 1983		*Climacograptus spiniferous*	17.20			1.00				
Nomen Nudem 1983		*Climacograptus spiniferous spiniferous*	2.80			2.40				
Nomen Nudem 1983		*Climacograptus spiniferous spiniferous*	1.40			1.20				
Munch 1952		*Climacograptus supernus*								
Munch 1952		*Climacograptus supernus*								
Munch 1952		*Climacograptus trifilis*								
Storch 1982		*Climacograptus trifilis*				11.0	12.3			
Storch 1982		*Climacograptus trifilis*				1.00	3.33			
Munch 1952		*Climacograptus tuberculatus*								
Finney et al 1984		*Climacograptus typicalis*		0.10						
Bulman 1934		*Cryptograptus tricornis*								
Munch 1952		*Cystograptus tricornis*								
Bulman 1931	Fig VII 1	*Orthograptus gracilis*		0.41	0.32	0.45				
Bulman 1931	2	*Orthograptus gracilis*		0.36	0.32	0.45				
Bulman 1931	3	*Orthograptus gracilis*		0.27	0.32	0.45				

Reference	Figure	Species	virgella	av	av	th1[1]	th1[2]	th2[1]	th2[2]	th3[1]
Bulman 1931	4	*Orthograptus gracilis*		0.18	0.45	0.68				
Bulman 1931	6	*Orthograptus gracilis*		0.36	0.36					
Bulman 1931	8	*Orthograptus gracilis*		0.59	0.45	0.55				
Bulman 1931	10	*Orthograptus gracilis*		0.45	0.55	0.55				
Bulman 1931	11	*Orthograptus gracilis*		0.55		0.50				
Bulman 1931	22	*Orthograptus gracilis*		0.23	0.14	0.23				
Bulman 1931	Fig VI 21	*Orthograptus gracilis*		0.27	0.18					
Bulman 1931	22	*Orthograptus gracilis*		0.32	0.27					
Bulman 1931	25	*Orthograptus gracilis*		0.18	0.27	0.27				
Bulman 1931	27	*Orthograptus gracilis*		0.18	0.27	0.41				
Bulman 1931	28	*Orthograptus gracilis*		0.27	0.41	0.41				
Bulman 1931	29	*Orthograptus gracilis*		0.23	0.09					
Bulman 1931	30	*Orthograptus gracilis*		0.36		0.36				
Bulman 1931	31	*Orthograptus gracilis*		0.09	0.14	0.23				
Bulman 1931	32	*Orthograptus gracilis*		0.41	0.14					
Bulman 1931	34	*Orthograptus gracilis*		0.23	0.23	0.36				
Bulman 1931	35	*Orthograptus gracilis*		0.27	0.36	0.50				
Bulman 1931	12	*Orthograptus gracilis*		0.25	0.34	0.38				
Bulman 1931	16	*Orthograptus gracilis*		0.50	0.30	0.50				
Bulman 1931	17	*Orthograptus gracilis*		0.40	0.30	0.50				
Bulman 1931	18	*Orthograptus gracilis*		0.33	0.33	0.11				
Bulman 1931	22	*Orthograptus gracilis*				0.59				
Mitchell 1987	2H	*D. nicholosoni longibasalis*				0.50				
Mitchell 1987	2R	*D. nicholosoni longibasalis*				0.56	0.33			
Skevington & Paris 1975		*Diplograptus ?fastigatus*				0.14				
C. Xu 1983		*Diplograptus tortithecatus*				1.17	1.17			
Mitchell 1987	8L	*G. Inuiti*		0.31	0.27	0.31				
Mitchell 1987	8A	*G. pygmaeus*		0.15						

Reference	Figure	Species	virgella	av	av	th1[1]	th1[2]	th2[1]	th2[2]	th3[1]
Mitchell 1987	8B	*G. pygmaeus*		0.15						
Mitchell 1987	8C	*G. pygmaeus*		0.19						
Mitchell 1987	8D	*G. pygmaeus*		0.19	0.15					
Mitchell 1987	8H	*G. pygmaeus*								
Mitchell 1987	8O	*G. pygmaeus*		0.23	0.19					
Mitchell 1987	8P	*G. pygmaeus*		0.23	0.19					
Mitchell 1987	8G	*G. typicalis*		0.15	0.15					
Mitchell 1987	8N	*G. typicalis*		0.15	0.19					
Walters 1977		*Glyptograptus lorrainensis*		0.20	0.20	0.30				
Walters 1977		*Glyptograptus lorrainensis*		0.15	0.15	0.25				
Walters 1977		*Glyptograptus lorrainensis*		0.15	0.15	0.40				
Mitchell & Bergstroim 1977		*Glyptograptus lorrainensis anacanthus*		2.20	2.40					
Mitchell & Bergstroim 1977		*Glyptograptus lorrainensis anacanthus*		3.00	3.00					
Mitchell & Bergstroim 1977		*Glyptograptus lorrainensis anacanthus*		1.20	1.20					
Mitchell 1987	2L	*H. teretiusculus sensu*				0.30	0.35			
Mitchell 1987	2A	*H. uplandicus*		0.20	0.15	0.30	0.15			
Mitchell 1987	2E	*H. uplandicus*		0.30						
Mitchell 1987	2F	*H. uplandicus*		0.30	0.25	0.40	0.40			
Mitchell 1987	2G	*H. uplandicus*		0.29		0.29	0.48			
Mitchell 1987	2K	*H. uplandicus*		0.20	0.20	0.40				
Walters 1977		*Neurograptus margariatus*		0.20	0.20	0.25		0.30	0.20	0.40
Mitchell 1987	9A	*O. quadrimucronatus*		0.35	0.19	0.31				
Mitchell 1987	9D	*O. quadrimucronatus*		0.38	0.38	0.42				
Mitchell 1987	9F	*O. quadrimucronatus*		0.31		0.27				
Mitchell 1987	9G	*O. quadrimucronatus*		0.33	0.33	0.33				

Reference	Figure	Species	virgella	av	av	th1[1]	th1[2]	th2[1]	th2[2]	th3[1]
Skevington & Paris 1975		*Orthograptus pageanus microcanthus*				0.21				
Finney et al 1984		*Orthograptus quadrimucronatus*		0.20	0.25		0.70		0.35	
Nomen Nudem 1983		*Orthograptus quadrimucronatus*		0.30		0.30	0.20			
Walters 1977		*Orthograptus ruedemanni*				0.30				
Walters 1977		*Orthograptus ruedemanni*				0.30				
Walters 1977		*Orthograptus ruedemanni*				0.20	0.20			
Nomen Nudem 1983		*Orthograptus ruedemanni*				0.40	0.30			
Munch 1952		*Orthograptus tridens*								
Skevington & Paris 1975		*Orthograptus truncatus abbreviatus*				0.36	0.29			
Skevington & Paris 1975		*Orthograptus truncatus abbreviatus*				0.43	0.43			
Mitchell 1987	6D	*P. (p.) schaerenbergi*	0.34			0.23				
Mitchell 1987	6E	*P. (p.) schaerenbergi*	0.20			0.14				
Mitchell 1987	6F	*P. (p.) schaerenbergi*	0.31			0.14				
Mitchell 1987	6G	*P. (p.) schaerenbergi*	0.20			0.14				
Mitchell 1987	6I	*P. (p.) schaerenbergi*	0.11			0.11				
Mitchell 1987	2O	*P. distichus*				0.35				
Mitchell 1987	2P	*P. distichus*				0.40	0.15			
Jackson 1973		*Amplexograptus aff. Promiens*		0.26	0.21					
Joanusson 1995		*Amplexograptus baltoscandius*		0.30	0.35					
Strachen 1959		*Amplexograptus bekkeri*				0.27	0.33	0.20	0.23	0.20
Strachen 1959		*Amplexograptus bekkeri*				0.10	0.07	0.13	0.17	0.13
Jackson 1973		*Amplexograptus inuiti*				0.20				
Finney 1986		*Amplexograptus maxwelli*		0.29	0.29	0.29				
Finney 1986		*Amplexograptus maxwelli*		0.36	0.36					
Finney 1986		*Amplexograptus sp. Aff. maxwelli*		0.43	0.43	0.57				
Jackson 1973		*Amplexograptus sp. Indet*		0.18	0.18					

Reference	Figure	Species	virgella	av	av	th1[1]	th1[2]	th2[1]	th2[2]	th3[1]
Finney 1986		*Climacograptus bicornis*				1.14				
Williams 1994		*Climacograptus bicornis*	4.40							
Williams 1994		*Climacograptus bicornis*	9.80			10.2				
Williams 1994		*Climacograptus bicornis*	3.80			3.40				
AT Mu et al 1960		*Climacograptus diplacanthus*	1.20			1.20				
AT Mu et al 1960		*Climacograptus diplacanthus*	2.00			1.20				
AT Mu et al 1960		*Climacograptus diplacanthus*	0.60			0.60				
AT Mu et al 1960		*Climacograptus diplacanthus*	0.70			0.40				
AT Mu et al 1960		*Climacograptus diplacanthus*	0.50			0.40				
Bulman 1932		*Climacograptus haljalensis*				0.25	0.16			
Bulman 1932		*Climacograptus haljalensis*				0.32	0.27	0.18		
Bulman 1932		*Climacograptus haljalensis*				0.25	0.36	0.36		
Ji-jin & Han-jun 1988		*Climacograptus hastatus*				5.60	8.00			
Ji-jin & Han-jun 1988		*Climacograptus hastatus*				8.00	8.80			
Cox 1933		*Climacograptus inuiti*		0.13	0.13	0.13				
Cox 1933		*Climacograptus inuiti*		0.26	0.18	0.16				
Cox 1933		*Climacograptus inuiti*		0.20	0.22					
Cox 1933		*Climacograptus inuiti*		0.17	0.24					
Cox 1933		*Climacograptus inuiti*		0.20	0.22					
Cox 1933		*Climacograptus inuiti*		0.24	0.29	0.26				
Melchin 1986		*Climacograptus latus*		0.60	0.60	0.80				
Melchin 1986		*Climacograptus latus*		0.20	0.20	0.30				
Melchin 1986		*Climacograptus latus*				0.40				
Melchin 1986		*Climacograptus latus*		0.25	0.25	0.30				
Melchin 1986		*Climacograptus latus*		0.30	0.30	0.30				
Ji-jin & Han-jun 1988		*Climacograptus leptothecalis*				24.8	12.8			
Ji-jin & Han-jun 1988		*Climacograptus leptothecalis*				16.0	13.6			
Melchin 1986		*Climacograptus longispinus supernus*				0.90				

Reference	Figure	Species	virgella	av	av	th1[1]	th1[2]	th2[1]	th2[2]	th3[1]
Melchin 1986		*Climacograptus longispinus supernus*				0.50	0.50			
Melchin 1986		*Climacograptus longispinus supernus*				0.80	0.80			
Melchin 1986		*Climacograptus longispinus supernus*				0.60	0.60			
Finney 1986		*Climacograptus manitouliensis*		0.15	0.15					
Bulman 1932		*Climacograptus orthoceratophilus*				0.66				
Bulman 1932		*Climacograptus orthoceratophilus*				0.44	0.22			
Bulman 1932		*Climacograptus orthoceratophilus*					0.38			
Bulman 1932		*Climacograptus orthoceratophilus*				0.30	0.43			
Finney 1986		*Climacograptus pygmaeus*		0.17	0.17					
Finney 1986		*Climacograptus spiniferous*	0.64			0.64				
Finney 1986		*Climacograptus spiniferous*	0.28			0.39				
Clark & Strachen 1955		*Climacograptus spiniferous*	2.00			2.00				
Bulman 1932		*Climacograptus typicalis*		0.20	0.20					
Bulman 1932		*Climacograptus typicalis*		0.18	0.18					
Bulman 1932		*Climacograptus typicalis*		0.14	0.14					
Bulman 1932		*Climacograptus typicalis*		0.18	0.18					
Bulman 1932		*Climacograptus typicalis*		0.29	0.29					
Bulman 1932		*Climacograptus typicalis*		0.29						
Williams 1994		*Climacograptus wilsoni*				0.10				
Williams 1994		*Climacograptus wilsoni*				0.30	0.25			
Williams 1994		*Climacograptus wilsoni*				0.20	0.20			
Williams 1994		*Climacograptus wilsoni*				0.10	0.25			

Reference	Figure	Species	virgella	av	av	th1[1]	th1[2]	th2[1]	th2[2]	th3[1]
Finney 1986		*Dicranograptus nicholsoni longibasalis*				0.25	0.21	0.36	0.29	0.21
Skevington 1970		*Diplograptus ellesi*				0.14				
Skevington 1970		*Diplograptus ellesi*				0.18				
Skevington 1970		*Diplograptus ellesi*				0.14				
Eisenack 1959		*Orthograptus gracilis*		0.60	0.25	0.65				
Clark & Strachen 1955		*Diplograptus molestus*		0.25	0.25	1.00				
Sudbury 1957		*Diplograptus spinulosus*				0.40	0.40	0.40		
Sudbury 1957		*Diplograptus spinulosus*				0.30	0.40	0.30	0.30	
Sudbury 1957		*Diplograptus spinulosus*				0.20	0.20	0.20		
Finney 1986		*Glyptograptus cf. Teretiusculus*				0.29	0.48			
Skevington 1970		*Glyptograptus dentatus*				0.08	0.16			
Skevington 1970		*Glyptograptus dentatus*				0.45	0.08			
Jackson 1971		*Glyptograptus hudsoni*		0.27	0.32					
Jackson 1971		*Glyptograptus hudsoni*		0.30	0.30					
Jackson 1971		*Glyptograptus hudsoni*		0.21	0.21					
Jackson 1971		*Glyptograptus hudsoni*		0.31	0.31	0.13				
Jackson 1971		*Glyptograptus hudsoni*		0.17	0.17	0.11				
Jackson 1971		*Glyptograptus hudsoni*		0.25	0.25	0.23				
Picarra 1995		*Normalograptus trifilis*				0.88	1.50			
Picarra 1995		*Normalograptus trifilis*				1.88	1.50			
Finney 1986		*Orthograptus amplexicaulis*		0.33	0.33	0.28				
Finney 1986		*Orthograptus amplexicaulis*		0.50	0.44	0.42				
Williams 1994		*Orthograptus ex. Gr. Amplexicaulis*		0.25	0.25					
Williams 1994		*Orthograptus ex. Gr. Amplexicaulis*		0.10	0.10	0.10				

Reference	Figure	Species	virgella	av	av	th1[1]	th1[2]	th2[1]	th2[2]	th3[1]
Williams 1994		*Orthograptus ex. Gr. Amplexicaulis*				0.20				
Williams 1994		*Orthograptus ex. Gr. Amplexicaulis*		0.20	0.20	0.30				
Kirk 1975		*Orthograptus gracilis*		0.20	0.30	0.08				
Bulman 1932		*Orthograptus gracilis*		0.33	0.40	0.17				
Bulman 1932		*Orthograptus gracilis*		0.17	0.18	0.10				
Bulman 1932		*Orthograptus gracilis*		0.33	0.33	0.07				
Herr 1971		*Orthograptus quadrimucronatus*		0.40	0.27	0.33				
Herr 1971		*Orthograptus quadrimucronatus*		0.53	0.40	0.53				
Herr 1971		*Orthograptus quadrimucronatus*		0.17	0.13	0.33				
Herr 1971		*Orthograptus quadrimucronatus*		0.27	0.27					
Clark & Strachen 1955		*Orthograptus sp. Cf. pageanus microcanthus*		0.50	0.50	0.50				
Clark & Strachen 1955		*Orthograptus sp. Cf. Peosta*				0.50				
Clark & Strachen 1955		*Orthograptus sp. Cf. Peosta*		1.00	1.00	0.75				
Strachen 1959		*Orthograptus uplandicus*		0.23	0.15	0.48	0.40			
Strachen 1959		*Orthograptus uplandicus*		0.20	0.20	0.40	0.40			
Skevington 1960		*Orthoretiolites hami*		0.25	0.25	0.45	0.40	0.40	0.30	
Skevington 1960		*Orthoretiolites hami*		0.35	0.35	0.15	0.40	0.25	0.30	
Skevington 1960		*Orthoretiolites hami*		0.40	0.40	0.40	0.40	0.40	0.50	
Skevington 1960		*Orthoretiolites hami*		0.43	0.46					
Skevington 1960		*Orthoretiolites hami*		0.34	0.43					
Skevington 1960		*Orthoretiolites hami*		0.35	0.35	0.35	0.30	0.40	0.50	
AT Mu 1962		*Paraglossograptus tricornis distincta*				2.00	2.00			
Strachan 1954		*Peira. Fallax*		0.25	0.30	0.13				
Strachan 1954		*Peira. Fallax*		0.25	0.20					
Strachan 1954		*Peira. Fallax*		0.15	0.15	0.15				
Strachan 1954		*Peira. Fallax*		0.45	0.20	0.35				
		Mean	**2.17**			**0.86**	**1.04**	**0.23**	**0.24**	**0.21**
		Standard deviation	3.30			2.43	2.63	0.12	0.12	0.12